Measurement and Mathematical Modelling of Endoplasmic Reticulum Stress in Human Adipocytes

by

Alice Margaret Murphy, BSc Hons

A thesis submitted in partial fulfilment of the requirements for the degree of

Doctor of Philosophy in Engineering

University of Warwick, Department of Engineering

May 2018

Table of Contents

Abbreviations

(β-ME)	β-mercaptoethanol
AIC	Akaike information criterion
ATF4	Activating transcription factor 4
ATF6	Activating transcription factor 6
ATP	Adenosine triphosphate
AUC	Area under curve
BAD	Bcl-2-associated death promoter
BAT	Brown adipose tissue
BE	Broccoli extract
BIC	Bayesian information criterion
BiP	Binding immunoglobulin protein
BMI	Body mass index
BSA	Bovine serum albumin
CER	Ceramides
CHOP	C/EBP homologous protein
Con	Control
DAG	Diacylglycerols
DMEM	Dulbecco's modified eagle medium
DMSO	Dimethyl sulfoxide
DNA	Deoxyribose nucleic acid
DTT	Dithiotheritol
ECAR	Extracellular acidification rate
ECL	Enhanced chemiluminescence
ECL+	Enhanced chemiluminescence plus
EDTA	Ethylenediaminetetraacetic acid (EDTA)
eIF2α	Alpha subunit of eukaryotic translation initiation factor-2
eIF2β	Beta subunit of eukaryotic translation initiation factor-2
ER	Endoplasmic reticulum
ERAD	Endoplasmic reticulum-associated protein degradation

ERO1	Endoplasmic reticulum oxireductin 1
ETC	Electron transport chain
FCCP	Carbonyl cyanide p-trifluoromethoxyl-phenylhydrazone
FFA	Free fatty acid
GADD34	Growth arrest and DNA damage-inducible 34
GDP	Guanosine diphosphate
GLUT4	Glucose transporter 4
GSH	Glutathione
GSSG	Glutathione disulphide
GTP	Guanosine triphosphate
H_2O_2	Hydrogen peroxide
HbA_{1C}	Haemoglobin A_{1C}
HDL	High density lipoprotein
HMG-CoA reductase	3-hydroxy-3-methyl-glutaryl-coenzyme A reductase
HPV-E7	Human papillomavirus E7
Hr	Hour
hTERT	Human telomerase reverse transcriptase
IBMX	Isobutylmethylxanthine
IRE1α	Alpha subunit of inositol-requiring enzyme-1
IRS-1	Insulin receptor substrate 1
JNK	c-Jun N terminal kinase
LPS	Lipopolysaccharide
MAM	Mitochondrial associated membrane
MFN	Mitofusin
MPTP	Mitochondrial permeability pore
mRNA	Messenger ribonucleic acid
mtDNA	Mitochondrial deoxyribose nucleic acid
Na3VO4	Sodium vanadate
NaF	Sodium fluoride
NF-κB	Nuclear factor kappa-light-chain-enhancer of activated B cells

NHS	National Health Service
Nrf2	Nuclear factor erythroid 2-related 2
OCR	Oxygen consumption rate
ODE	Ordinary differential equation
OGTT	Oral glucose tolerance test
Oligo	Oligomycin
ORF	Open reading frame
ORO	Oil Red-O
ox-LDL	Oxidised low density lipoprotein
p50ATF6	N-terminal fragment of activating transcription factor 6
p58IPK	Protein kinase inhibitor p58
PARL	Presenillin-associated rhomboid-like protein
PBS	Phosphate buffered saline
PBS-T	Phosphate buffered saline-tween
PDI	Protein disulphide isomerase
P-eIF2α	Phosphorylated alpha subunit of eukaryotic translation initiation factor-2
PERK	Protein kinase RNA-like endoplasmic reticulum kinase
P-IRE1α	Phosphorylated alpha subunit of inositol-requiring enzyme-1
PK/PD	Pharmacokinetic/pharmacodynamic
qRT-PCR	Quantitative real-time polymerase chain reaction
RIPA	Radioimmunoprecipitation assay buffer
RNA	Ribonucleic acid
RNS	Reactive nitrogen species
ROS	Reactive oxygen species
RSS	Residual sum of squares
SAT	Subcutaneous adipose tissue
SE	Standard error of the mean
SERCA	Sarcoplasmic/endoplasmic reticulum Ca^{2+}/ATPase
SERP1	Stress-associated endoplasmic reticulum protein 1
SOD	Superoxide dismutase

sp-XBP1	Spliced X-box binding protein-1
T2DM	Type 2 diabetes mellitus
TA	Translation attenuation
Tun	Tunicamycin
UPR	Unfolded protein response
u-XBP1	Unspliced X-box binding protein-1
VAT	Visceral adipose tissue
WAT	White adipose tissue
WHO	World Health Organisation

List of Tables

List of Figures

Acknowledgements

I would like to thank several people and organisations who made this thesis possible through continued help, support, collaboration and funding.

Firstly, I would like to thank my academic supervisors, Professor Philip McTernan and Professor Michael Chappell, for giving me the opportunity to undertake this research and for their valuable advice and support throughout.

I would also like to thank Dr. Guy Barker and his team for providing the freeze dried broccoli powder and for their contribution to the transcriptomics analysis.

I am extremely grateful to the Engineering and Physical Sciences Research Council (EPSRC), who provided the funding for this research to be carried out.

This research was improved through valuable discussions with my colleagues in the Diabetes Research Team, who also provided encouragement and laughter when it was most needed. Thank you so much Sahar, Laura, Anoud, Lucia, Jinus, Farah, Adaikala, Philip V. and Phil M. for making this PhD so much more enjoyable.

I am grateful to everyone at Banbury Canoe Club for keeping me sane throughout my PhD, and to Matt, Sophie, Siobhan, Heather and Rachel for your help with proof-reading.

Finally, I would like to thank my family; in particular my mum, Melanie Murphy, but also my dad, Heather, Rachel and Padraig for their love and support.

Declaration

This thesis is submitted to the University of Warwick in support of my application for the degree of Doctor of Philosophy. It has been composed by myself and has not been submitted in any previous application for any degree.

The work presented (including data generated and data analysis) was carried out by the author except in the cases outlined below:

List of Data Provided and/or Analysis Carried out by Collaborators:

- Transcriptomics analysis, including the assessment of RNA quality, the creation of libraries of template molecules, the sequencing of the libraries and the analysis of data, was carried out by Dr. Guy Barker's team.

List of Publications

Parts of this thesis have been published as reviewed abstracts and presented as posters or oral presentations by the author:

1. **Murphy AM**, Azharian S, Tripathi G, Barker G, Chappell M, PG McTernan. A Systems Approach to ER Stress Pathway Dynamics Reveals the Impact of Freeze Dried Broccoli. American Diabetes Association, Orlando, June 2018. Poster
2. **Murphy AM**, Tripathi G, Barker G, Chappell M, PG McTernan. The Power of Broccoli Superfood: Measuring and Modelling ER Stress in Human Adipocytes. American Diabetes Association, San Diego, June 2017. Poster.
3. **Murphy AM**, Tripathi G, Barker G, Chappell M, PG McTernan, Broccoli extract improves tunicamycin-induced endoplasmic reticulum stress over time in

differentiated human preadipocyte cells. Warwick Engineering Postgraduate Symposium, Warwick University, April 2017. ***Oral Presentation – Awarded best oral presentation in Biomedical Engineering category***

4. **Murphy AM**, Tripathi G, Barker G, Chappell M, PG McTernan. A mathematical model of the endoplasmic reticulum stress response. BITE Network meeting, Warwick University, March 2017. ***Oral Presentation***
5. **Murphy AM**, Tripathi G, Barker G, Chappell M, PG McTernan. Superfood 'Freeze Dried Broccoli Extract' to the rescue of the mitochondrial inefficiency in human mature adipocytes. Trilateral Workshop 'Enhancing physiological understanding of exercise and obesity: designing personalised intervention strategies', South Africa, February 2017. Poster.
6. **Murphy AM**, Tripathi G, Barker G, Chappell M, McTernan PG. Superfood Freeze Dried Broccoli Extract Relieves ER stress and mitochondrial inefficiency in human mature adipocytes, UK Adipose Tissue Discussion Group, Oxford, Dec 2016. Poster.
7. **Murphy AM**, Tripathi G, Barker G, Chappell M, McTernan PG. Freeze dried broccoli extract relieves ER stress and mitochondrial inefficiency in differentiated human pre-adipocyte cells. British Endocrine Society Conference, Nov 2016, Brighton. Poster.
8. **Murphy AM**, Tripathi G, Barker G, Esparza-Franco MA, Chappell M, McTernan PG. Broccoli extract improves Tunicamycin induced Endoplasmic Reticulum Stress and Mitochondrial inefficiency in differentiated human pre-adipocyte cells. 7th World Congress on Targeting Mitochondria, Berlin, Oct 2016. Poster.

9. Jackisch L, Martinez de la Escalera L, **Murphy AM**, McTernan PG, Randeva H, Tripathi G. ER stress mediates mitochondrial dysfunction in human adipocytes which is exacerbated in obesity. 7th World Congress on Targeting Mitochondria, Berlin Oct 2016. ***Oral Presentation***
10. **Murphy AM**, Tripathi G, Barker G, Chappell M, McTernan PG. Broccoli extract improves tunicamycin induced endoplasmic reticulum stress and mitochondrial inefficiency in human pre-adipocyte cells. Warwick Engineering Postgraduate Symposium, Warwick University, April 2016. Poster.
11. **Murphy AM**, Tripathi G, Barker G, Esparza Franco A, Chappell M, PG McTernan. Superfood 'Freeze Dried Broccoli' reduced tunicamycin induced cellular damage in mature human adipocytes. Medical Science Festival, Leicester, April 2016. Poster.
12. **Murphy AM**, Tripathi G, Barker G, Chappell M, McTernan PG Broccoli extract improves Tunicamycin induced Endoplasmic Reticulum Stress and Mitochondrial inefficiency in differentiated human pre-adipocyte cells. Keystone Meeting, Alberta, Canada, Feb 2016. Poster.

Abstract

Obesity is the single biggest risk factor for type 2 diabetes mellitus (T2DM). Weight gain chronically induces endoplasmic reticulum (ER) stress in adipocytes, which activates the unfolded protein response (UPR) and leads to inflammation and insulin resistance. Therefore, investigating ways to combat inflammation through ER stress may reduce obesity mediated T2DM. One candidate to improve metabolic health may be cruciferous vegetables, such as broccoli, known to reduce inflammation and the risk of various cancers. Mathematical modelling may be a useful tool in order to identify how time and other factors may impact the UPR, however little experimental time series data exist to support the parameterisation and validation process. The aim was therefore to determine whether perturbation of human adipocytes with tunicamycin and broccoli extract can lead to significant changes in the UPR over time, deriving a novel mathematical model to characterise the relevant components of the UPR. Chub-S7 pre-adipocyte cells were grown, differentiated and treated with broccoli extract, tunicamycin, or a combination of the two (17 time points over 72 hours). Western blotting and qRT-PCR were used to assess ER stress markers, whilst the influence of broccoli on other cellular functions was analysed through appropriate assays. A qualitatively realistic mathematical model of part of the UPR was developed using nonlinear ordinary differential equations (ODEs), utilising experimental time series data for parameterisation and validation. The time series data identified novel expression profiles of proteins involved in the UPR, and highlighted that broccoli extract could significantly reduce the impact of tunicamycin on ER stress over time ($p<0.05$), as well as reactive oxygen species (ROS) ($p<0.05$) and mitochondrial dysfunction ($p<0.05$). These findings identify that broccoli extract appears to reduce the impact of tunicamycin on human adipocytes, and highlight the importance of modelling changes within the UPR to understand its response over time.

Thesis Outline

This thesis explores the UPR through systems biology and laboratory techniques with an aim to develop a mathematical model of the process and to investigate factors that stimulate and protect against ER stress. This is important as the UPR is activated when cells are under stress, which occurs in many diseases and is one of the prominent links between obesity and T2DM. As such, developing a mathematical model of the UPR in order to better understand its pathway dynamics, as well as investigating dietary factors that may protect against its activation, may provide an insight as to how the risk of T2DM may be reduced in obese patients. Previous researchers have developed mathematical models of the UPR, however these often lacked biological experimental data in the parameterisation and validation process. Dietary factors such as broccoli have not been well studied in their potential role of preventing UPR activation, and this thesis therefore provides a novel insight into how a broccoli extract may impact on the link between obesity and T2DM.

As such, the hypothesis and research aims for this thesis are as follows:

Broccoli, in the form of freeze dried broccoli powder, protects adipocytes against ER stress induced by tunicamycin. Time series data from this research will aid in the construction of a mathematical model characterising the unfolded protein response.

Research Aims:

1. To create a mathematical model of a pathway in the unfolded protein response using experimental time series data.
2. To study ER stress in more detail by analysing how the expression of key ER stress proteins varies over time following treatment with tunicamycin.

3. To investigate the potential protective effects of broccoli against ER stress in adipocytes.
4. To examine the effects of broccoli on other mechanisms that also contribute to metabolic disease, such as ROS and mitochondrial dysfunction.

A brief overview of how these aims can be met is described below:

Chapter 2 summarises relevant background information on obesity, adipose tissue and related metabolic diseases, as well as mathematical modelling of the ER stress pathway to understand its dynamics. The first half of this chapter leads the reader from the consequences of obesity and type 2 diabetes mellitus to endoplasmic reticulum stress and other cellular mechanisms which may be altered by the addition of a broccoli extract. The focus on the second half of this chapter is primarily on the process of creating a mathematical model of a biological response, culminating in a review of previous models of the unfolded protein response.

Chapter 3 highlights the importance of continuously considering complexity when developing a model of a biological pathway and outlines an initial model of the unfolded protein response. This chapter utilised standard laboratory techniques including cell culture and Western blotting to gather data that was used to parameterise the initial model. This provided important information as to which time points may be relevant to study in order to gain more information about the expression patterns of proteins involved in the unfolded protein response.

Chapter 4 expands on the model developed in Chapter 3, extending the model to include further components of the unfolded protein response. Further to this, more biological insight was gained into the expression profiles of proteins involved in the

unfolded protein response through carrying out a comprehensive time series analysis, studying 17 time points with the Western blot technique. These data were also used to parameterise and validate the developed mathematical model.

Chapter 5 investigates whether a freeze dried broccoli extract impacts the unfolded protein response that has been chemically induced in adipocytes. Studying time series data provided information on which specific components of the unfolded protein response may be most affected by the addition of a broccoli extract and how this may impact endoplasmic reticulum stress experienced by an adipocyte.

The final results chapter, Chapter 6, studies how a broccoli extract may impact other cellular mechanisms related to ER stress that are also associated with the development of insulin resistance, such as mitochondrial dysfunction and reactive oxygen species. Further to this, transcriptomics analysis revealed a potential mechanism of action for the broccoli extract.

Conclusions of this body of work, including limitations and future work, are discussed in Chapter 7 which provides a detailed overview of the work and how it may impact in the real world.

CHAPTER 1:

BACKGROUND

1.1 Obesity, Adipose Tissue and Metabolic Disease

1.1.1 Adipose Tissue Heterogeneity

Obesity is described by the World Health Organisation (WHO) as an abnormal or excessive fat accumulation that may impair health (World Health Organisation 2017). There are two broad categories that fat, or adipose tissue, in mammals can be divided into: brown adipose tissue (BAT) and white adipose tissue (WAT) (Figure 1.1.1.1). These two types of adipose tissue have different functions: BAT is specialised in the dissipation of energy through the production of heat, whilst WAT stores excess energy as triglycerides (Saely, Geiger *et al*. 2012). BAT plays an important role in body thermogenesis and is uniquely responsible for classical non-shivering thermogenesis, a form of heat production activated when an organism is in need of extra heat, *e.g.* postnatally, during entry into a febrile state, and during arousal from hibernation (Cannon and Nedergaard 2004). In response to certain conditions, such as chronic cold exposure and exercise, adipocyte 'browning' can occur in which brown-like adipocytes appear in white adipose depots. These cells are known as 'beige', or 'brite' adipocytes and their production is associated with increased energy expenditure, decreased body weight and increased insulin sensitivity (Wu, Boström et al. 2012, Kajimura, Spiegelman et al. 2015, Sidossis and Kajimura 2015).

There is a high proportion of metabolically active BAT in new-borns, however this proportion decreases with age and despite human adults having some metabolically active BAT, WAT comprises the vast majority of human adipose tissue. WAT expansion occurs during obesity, which is the main risk factor for several metabolic

disorders and will therefore be considered in more detail in this thesis. The distribution of BAT and WAT depots in humans is demonstrated in Figure 1.1.1.1.

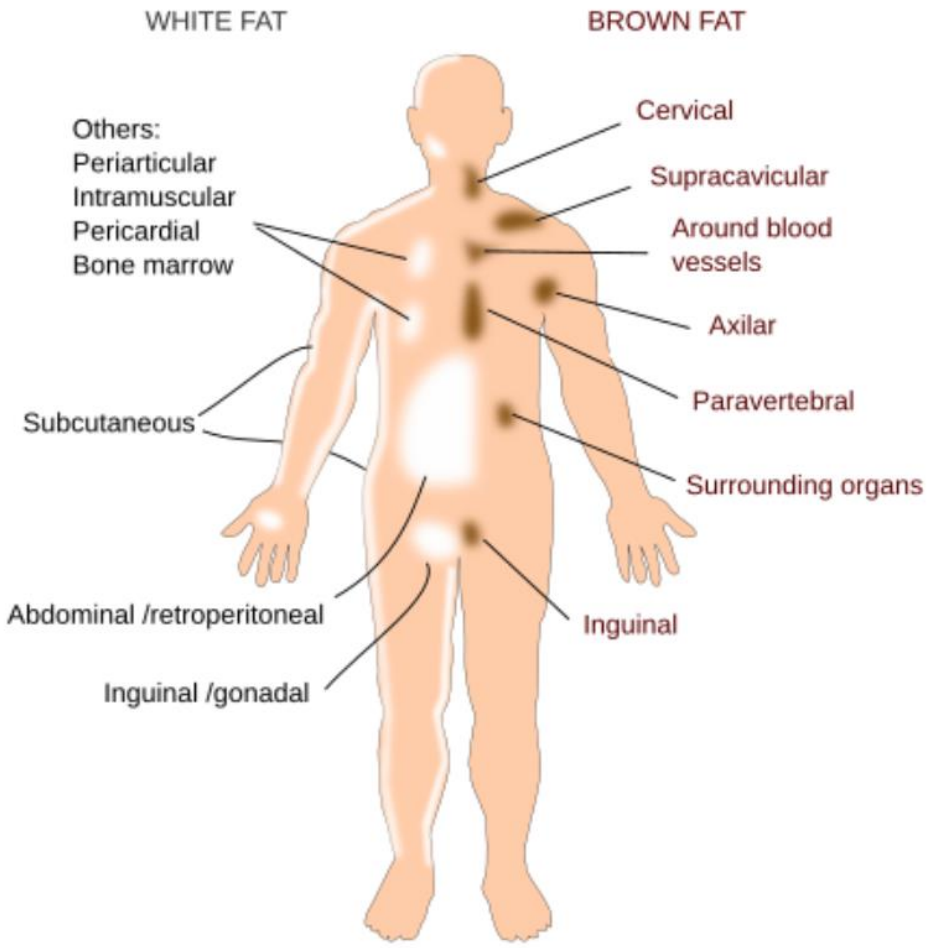

Figure 1.1.1.1 Distribution of adipose tissue: Mammalian adipose tissue is distributed throughout the body in distinct depots. White adipose tissue depots store excess energy as triglycerides, while brown adipose tissue depots dissipate energy through the production of heat. Figure from (Pacheco, Garcia *et al*. 2018).

Within the body there are distinct regional depots of WAT which differ in structural organisation, cellular size, and biological function, and it is the distribution of fat between these depots that can influence the risk of different metabolic disorders (Bjørndal, Burri *et al*. 2011). The two main WAT depots are subcutaneous adipose

tissue (SAT) and visceral adipose tissue (VAT). SAT, which makes up about 85% of all body fat, is found just beneath the skin and functions as both an energy reserve and padding for the body (Frayn and Karpe 2014). VAT is stored deeper within the abdominal cavity and surrounds a number of internal organs, including the liver, pancreas and intestines. The distribution of fat throughout the different depots seems to be more important than the total adipose tissue mass in contributing to the risk of developing obesity-associated diseases (Bjørndal, Burri *et al*. 2011). VAT accumulation has a much higher association with an adverse metabolic, dyslipidemic and atherogenic obesity phenotype, whilst SAT accumulation is more benign (Neeland, Ayers *et al*. 2013).

This variation in contribution to obesity-associated diseases by fat depots outlines one of the limitations of the body mass index (BMI), the most commonly used measure for identifying obesity, which is calculated based on the weight and height of a subject. Although it is intended to estimate body fat percentage, it does not differentiate between muscle mass and fat mass, nor between SAT and VAT. BMI is calculated by dividing a subject's weight (W, kg) by the square of their height (h, m^2) using the following equation (Nuttall 2015):

$$BMI = \frac{W}{h^2} \ (kgm^{-2})$$

This formula was developed nearly 200 years ago and despite its limitations is still widely used for the preliminary diagnosis of obesity due to its simplicity, safety and minimal cost (De Lorenzo, Soldati *et al*. 2016). There are six classifications defined by BMI value, which range from underweight (<18.5kg/m^2) to class III obesity (≥ 40.0kg/m^2) (Table 1.1.1.2) (World Health Organisation 2017) . However, there is

much debate about where the limits to each classification should lie, and other measures such as waist circumference are often used to complement BMI estimates (World Health Organisation 2017).

BMI (kg/m^2)	Classification
<18.5	Underweight
18.5 – 24.9	Normal Weight
25.0 – 29.9	Overweight
30.0 – 34.9	Class I Obesity
35.0 – 39.9	Class II Obesity
≥40.0	Class III Obesity

Table 1.1.1.2 BMI Classifications: Body mass index (BMI) measurements, calculated by dividing a subject's weight by the square of their height, and their corresponding weight classification (World Health Organisation 2017).

1.1.2 Risk Factors for Obesity

There are many factors that can contribute to the risk of developing obesity, including calorie intake, physical exercise, medical conditions, prescription drugs, and socio-demographic factors (Rosiek, Maciejewska *et al*. 2015). One of the major risk factors for obesity is an unhealthy diet which is described by WHO not just as an individual problem, but as a societal problem (World Health Organisation 2017). Despite the advice of WHO to eat more fruit, vegetables, legumes, nuts and grains and to cut down on salt, sugar and fats, people often ignore this advice or follow diets that are not necessarily supported by scientific evidence. Although this has led to an increase in obesity in the general population, there are also socio-demographic

factors that affect the risk of developing obesity. For instance, women have a higher adiposity relative to men, yet men are more likely to develop metabolic disorders. This is attributed to men having more VAT distributed in their central region, leading to an 'apple-shaped' body which carries greater risk. Women, however, are characterised by less VAT and more SAT, especially in their lower body, creating a 'pear-shaped' body (White and Tchoukalova 2014). This is true until the menopause where VAT increases from between 5-8% of the total body fat to 15-20% (Karvonen-Gutierrez and Kim 2016). This varied fat distribution between genders explains the difference in the risk of developing obesity-related disorders between the two groups. The redistribution of adipose depots in postmenopausal women, resulting in increased VAT, has also been attributed to increased risk of obesity related diseases (Atapattu 2015).

Ethnicity also contributes to the risk of obesity, with stark differences between ethnic groups observed from childhood (Falconer, Park *et al*. 2014). In the UK, Black African, Black Caribbean and South Asian children are more likely to be overweight or obese than White children (Zilanawala, Davis-Kean *et al*. 2015). Although socioeconomic, cultural and family routine factors, as well as maternal BMI, may contribute to this disparity, after adjustment for these factors Black Caribbean children were found to have a higher chance of developing obesity and Pakistani children were less likely to develop obesity in the UK, as demonstrated in Figure 1.1.2 (Zilanawala, Davis-Kean *et al*. 2015). The reasons behind these findings are unknown, however one possible explanation is altered WAT function in different ethnicities, which has been extensively documented (Araneta and Barrett-Connor 2005, Rahman, Temple *et al*. 2009, Staiano, Broyles *et al*. 2013).

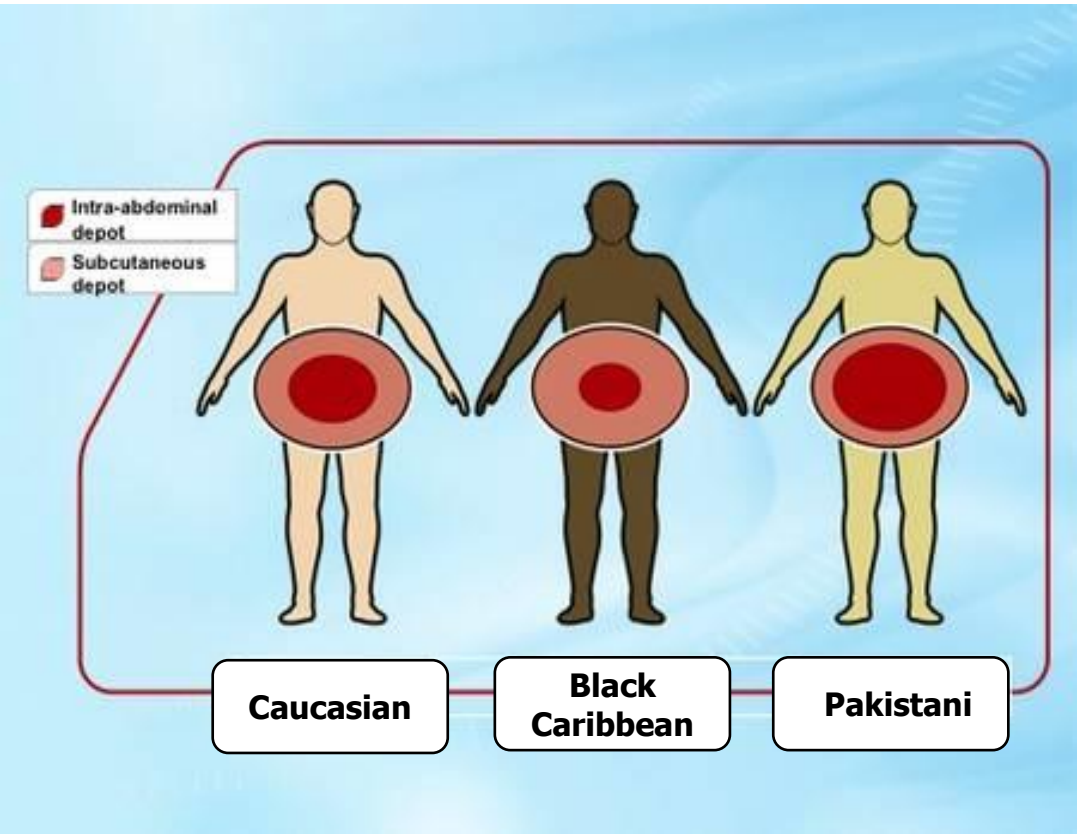

Figure 1.1.2 Contribution of Ethnicity to Risk of Obesity: Ethnicity can contribute to obesity risk. In the UK, Black Caribbean children were more likely to develop obesity than Caucasians, whilst Pakistani children were less likely to develop the condition (Zilanawala, Davis-Kean *et al*. 2015). *Figure adapted from* (My Healthy Waist 2018).

1.1.3 Adipose Tissue Function

Obese patients have increased amounts of adipose tissue, which, despite initially being thought of as metabolically inert, is now recognised as a highly active metabolic and endocrine organ that secretes a variety of adipokines to fulfil its function (Goossens 2008). In conditions of obesity, the adipose tissue is remodelled through changes to the number and/or size of adipocytes which creates a dysfunctional form of adipose tissue (Choe, Huh *et al*. 2016). This dysfunctional adipose tissue, which has larger adipocytes, has been shown to favour expressing pro-inflammatory factors compared to smaller, metabolically normal adipocytes (Skurk, Alberti-Huber *et al*. 2007). This contributes to the chronic low grade inflammation that is present in obesity and is involved in the pathogenesis of many chronic diseases, including T2DM, for which obesity is the single biggest risk factor (Ye 2014, diabetes.co.uk 2017). There are many factors that contribute to this chronic inflammation, with glucose, lipids and inflammatory insults, such as gut-derived factors, all exacerbating the problem (Collier, Dossett *et al*. 2008, van Diepen, Berbée *et al*. 2013, Schedlowski, Engler *et al*. 2014, Ye 2014). This can lead to insulin resistance, a state where cells become less sensitive to insulin, causing the body to increase its production. Over time, this can develop into T2DM due to the body's inability to produce enough insulin to induce the required response from cells.

1.1.4 Diagnosis of Type 2 Diabetes Mellitus

Diabetes mellitus is a condition defined by chronic hyperglycaemia (high circulating glucose levels) caused by insufficient insulin signalling. Diabetes mellitus can be separated into three main groups depending on the specific mechanism causing the disease: (i) type 1 diabetes mellitus, resulting from the inability of the pancreas to produce enough insulin; (ii) type 2 diabetes mellitus, whereby cells fail to respond sufficiently to insulin, often followed by a lack of insulin production; (iii) gestational diabetes mellitus, occurring when pregnant women develop high blood sugar levels. As of 2016, almost 3.6 million people in the UK have been diagnosed with diabetes, with a further 1 million people suspected to have undiagnosed T2DM (Diabetes UK 2016). It is a major public health problem that has been described as a global epidemic, with the prevalence of T2DM expected to double within the next 20 years (Marín-Peñalver, Martín-Timón *et al*. 2016).

In order to diagnose type 2 diabetes mellitus (T2DM), plasma glucose levels are measured to confirm chronic hyperglycaemia. Following WHO guidelines, patients are diagnosed as diabetic if their fasted plasma glucose levels are above 7.0 mmol/L (126 mg/dl) or if 2 hours post a 75g oral glucose tolerance test (OGTT) their plasma glucose is above 11.1 mmol/L (200 mg/dl) (World Health Organisation and International Diabetes Federation 2006). Normal blood glucose levels are defined as a fasting plasma glucose level of <6.1 mmol/L (<110 mg/dl) and a 2hr value of < 7.8 mmol/L (<140 mg/dl) in the OGTT. Borderline T2DM (neither T2DM nor normal blood glucose levels) is defined as falling between the normal and diabetic values, and is also known as an impaired fasting glucose state (Seino, Nanjo *et al*. 2010) (Table

1.1.4). Haemoglobin A_{1c} (HbA_{1c}) levels are also used to diagnose and monitor diabetic status. HbA_{1c} is produced in the blood in response to haemoglobin being exposed to plasma glucose, and it is seen as the gold standard for assessing glycaemic control in people who are already diagnosed. This is due to it reflecting the average plasma glucose level over the previous 2-3 months in a single measurement, as well as the fact that it can be performed at any time of day and does not require any special preparation such as fasting (World Health Organisation and International Diabetes Federation 2006). HbA_{1c} levels of 6.5% or over indicate diabetes, levels of 6.0% - 6.4% suggest impaired glucose regulation, or prediabetes, whilst levels lower than 6.0% are considered non-diabetic according to WHO guidelines (World Health Organisation 2011).

	Plasma Glucose Levels (mmol/L)	
Diagnosis	**Fasted**	**2hrs Post Oral Glucose Tolerance Test**
Non-Diabetic	< 6.1	< 7.8
Borderline Diabetic	6.1 - 7.0	7.8 - 11.1
Diabetic	> 7.0	> 11.1

Table 1.1.4 Plasma Glucose Levels and their Corresponding Diabetes Status: In order to diagnose Type 2 Diabetes Mellitus, plasma glucose levels are measured following fasting, as well as 2 hours post an oral glucose tolerance test. Patients are diagnosed using the glucose levels and diabetic categories above (World Health Organisation 2011).

1.1.5 Co-Morbidities of T2DM

There are many comorbidities associated with T2DM. The biggest comorbidity of T2DM is obesity, which not only increases the risk of developing T2DM, but also increases the risk of cardiovascular comorbidities, limits patients' ability to engage in physical activity and increases insulin resistance (American Association of Clinical Endocrinologists). T2DM is also linked to dyslipidaemia, whereby the body experiences decreased levels of high density lipoprotein (HDL) and increased levels of triglycerides, along with postprandial lipemia (a high concentration of emulsified fat in the blood) (Goldberg 2001). This can lead to accelerated macrovascular disease in T2DM patients, and may ultimately lead to heart attack, stroke and other conditions involving the heart and circulation (Tseng, Tseng *et al*. 2012). These conditions can also be exacerbated by hypertension, of which at least 67% of T2DM sufferers have, or are being treated for (American Association of Clinical Endocrinologists). Other comorbidities of T2DM include retinopathy, chronic kidney disease, cardiovascular disease, and non-alcoholic fatty liver disease (American Association of Clinical Endocrinologists , Cusi 2016). It is largely due to these comorbidities that the cost of treating diabetes and its complications is so high, at nearly £14 billion per year, or 10-15% of the annual NHS budget (diabetes.co.uk 2017).

1.1.6 Treatment of T2DM

It is important to treat T2DM effectively, and subjects must avoid states of hyperglycaemia (high blood sugar levels) and hypoglycaemia (low blood sugar levels) in order to reduce pathophysiology and severe side effects of such states. Adequate control of blood sugar levels reduces the risk and severity of the associated comorbidities and can prevent the accumulation of ketones in the blood, which can induce diabetic coma if left untreated. There are several ways of controlling T2DM, ranging from diet to surgery. Lifestyle changes are recommended for all sufferers of T2DM, as losing weight can help to improve insulin sensitivity and make diabetes easier to manage (diabetes.co.uk 2017). Altering dietary intake and physical exercise are usually the first steps in the treatment of T2DM as they are the two main determinants of weight (Marín-Peñalver, Martín-Timón *et al*. 2016). The dietary aspects that are recommended not only contribute to the control of blood glucose levels, but can also contribute to improved blood pressure, lipid profile, sleep quality, depression and quality of life related to health (Marín-Peñalver, Martín-Timón *et al*. 2016). It has been proposed that patients suffering from T2DM should have a reduced calorie intake of 500-1000kcal below their calorie needs in order to reduce weight and improve their insulin sensitivity (Gargallo Fernández Manuel, Breton Lesmes *et al*. 2012). It is important for T2DM patients to consider the source of their calorie intake as well as the calorie count itself. For instance, although it is the total amount of carbohydrate consumed that has the strongest influence on glycaemic response, it is preferable that the intake of carbohydrates comes from vegetables, fruits, whole grains, legumes and dairy products as opposed to sources that contain added fats, sugars or sodium (Gray 2000 [Updated 2015]). It is also recommended

for people with diabetes to consume at least the amount of fibre and whole grains that is recommended for the general public. A high fibre diet promotes early satiety, may be less caloric, lower in fat and added sugars, and may therefore help to combat obesity and prevent the risk of heart disease and colon cancer (Gray 2000 [Updated 2015]).

As well as lifestyle changes, many pharmacological agents are available to aid the control of T2DM (Olokoba, Obateru *et al*. 2012). The most common drug that is prescribed is Metformin, which reduces hepatic glucose production and absorption of glucose from the gastrointestinal tract, as well as increasing insulin uptake in the periphery, thereby improving insulin sensitivity (Tran, Zielinski *et al*. 2015). Metformin's high efficacy, low hypoglycaemia risk, and potential for weight loss make it a popular drug choice for both patients and doctors. Other drugs are available that treat T2DM in a variety of ways, including slowing carbohydrate digestion, assisting insulin in post-prandial glucose levels, and preventing the production of glucose in the liver (Tran, Zielinski *et al*. 2015). Although initially T2DM may be able to be treated with lifestyle choices and oral medication, T2DM gets progressively worse and thus insulin therapy is often introduced. Patients and physicians can be reluctant to start insulin due to the fact that it must be injected, it can induce hypoglycaemia if not correctly administered, and can induce weight gain (Swinnen, Hoekstra *et al*. 2009).

A final method of inducing weight loss and improving T2DM is bariatric surgery. This can involve one of several procedures that either reduces the size of the stomach (gastric band or sleeve gastrectomy) or bypasses a large portion of the stomach

(gastric bypass). In a study by Schauer *et al.*, a group of T2DM patients that underwent surgery had 22-24% weight reduction, compared to ~4% in those who underwent intensive medical therapy (Schauer, Bhatt *et al*. 2014). After a three year follow-up, the surgical group had significantly more rapid, larger and more sustained reductions in $HbA1_c$ values and fasting plasma glucose than the medical-therapy group (Schauer, Bhatt *et al*. 2014). Similar results were found in another study, albeit one with a small number of subjects: 50% of the 38 participants who underwent bariatric surgery sustained a T2DM remission at five years, compared with none of the 15 participants who underwent medical therapy (Mingrone, Panunzi *et al*. 2015). Whilst these results seem positive and show that bariatric surgery may represent a useful way to induce T2DM remission, further research is needed to determine the long term benefits of using bariatric surgery as treatment for T2DM. It is also important to balance the positive effects with an understanding of the cost, availability and risks of surgery, as well as the fact that diabetes remission is not guaranteed.

1.1.7 Mechanisms Contributing to Metabolic Diseases

There are many mechanisms that can contribute to the risk of developing metabolic diseases such as T2DM. Oxidative stress has been implicated as a major contributory factor to the pathophysiology of a number of diseases and conditions including cancer, sepsis and metabolic diseases (Stepien, Heaton *et al*. 2017). It occurs when cells can no longer cope with the number of Reactive Oxygen Species (ROS) that are produced. Oxidation of molecules is essential for life, and during metabolism in eukaryotes, oxidation results in the formation of ROS. Cells naturally produce antioxidants to counterbalance this ROS production, and to protect the cell from ROS damage. However, if ROS production increases to a point where antioxidants can no longer protect against them, the highly reactive ROS molecules can cause damage and stress within the cell. This process can lead to the development of insulin resistance, dyslipidemia, β-cell dysfunction, impaired glucose tolerance and ultimately T2DM (Tangvarasittichai 2015).

Mitochondrial dysfunction is another mechanism that can increase the risk of developing T2DM. It arises either from an inadequate number of mitochondria, an inability to provide necessary substrates to mitochondria, or a dysfunction in their electron transport and adenosine triphosphate (ATP)-synthesis machinery (Nicolson 2014). In these situations, the oxidation of fuels used to create energy is reduced and, as such, lipid accumulation occurs which can contribute to the inhibition of insulin signalling. Additionally, decreases in substrate oxidation can lead to electron leakage through the electron transport chain (ETC) and the subsequent formation of superoxide, a form of ROS. This can lead to mitophagy (removal of damaged

mitochondria and prevention of cell death) or, under high stress levels, apoptosis (Montgomery and Turner 2015). Through these mechanisms, mitochondrial dysfunction can contribute to the development of metabolic diseases such as T2DM.

Studies have indicated that adipose tissue hypoxia can also contribute to insulin resistance (Ye 2011) (Regazzetti, Peraldi *et al*. 2009). Hypoxia can occur in the adipose tissue of obese individuals as it expands. Despite the substantial increase in adipose tissue mass, the proportion of cardiac output and the extent of the blood flow to the tissue are not increased, resulting in adipocyte clusters that are distant from the vasculature (Trayhurn 2013). This can initiate the inflammatory process and can also contribute to insulin resistance in these cells.

1.1.8 Endoplasmic Reticulum Stress

One cellular mechanism that forms a link between obesity and T2DM is endoplasmic reticulum stress. The endoplasmic reticulum (ER) is a dynamic organelle found within most eukaryotic cells, which has essential functions responsible for cellular homeostasis, development, and stress responsiveness. These functions include (i) synthesis, folding, modification, and transport of proteins; (ii) synthesis and distribution of phospholipids and steroids; (iii) storage of calcium ions within its lumen and their regulated release into the cytoplasm (Bravo, Parra *et al*. 2013). Perturbations affecting any of these processes can lead to ER stress, causing an aggregation of unfolded and misfolded proteins in the lumen of the ER. ER stress can be induced in a number of situations including nutrient and energy fluctuations, viral infections, hypoxia, the presence of toxins and increased demand on the synthetic machinery (Hotamisligil 2006). When the ER becomes stressed, it initiates a complex response system known as the unfolded protein response (UPR) in an attempt to restore the functional integrity of the organelle.

The mammalian UPR consists of three main branches, each involving a different transmembrane protein that senses the stress: protein kinase RNA-like endoplasmic reticulum kinase (PERK), inositol-requiring enzyme-1 alpha (IRE1α), and activating transcription factor 6 (ATF6). In unstressed conditions, these three transmembrane proteins are bound by the chaperone binding immunoglobulin protein (BiP) via their luminal domain, rendering them inactive. Accumulation of unfolded and misfolded proteins in the ER results in the movement of BiP away from these transmembrane sensor proteins to assist with the folding of the aggregated proteins. Dissociation of

BiP leads to the dimerisation and trans-autophosphorylation of IRE1α and PERK, as well as the translocation of ATF6 to the Golgi apparatus. This activates the three proteins and initiates complex signalling cascades that are transduced to the cytoplasm via the cytoplasmic portion of each protein (Bravo, Parra *et al*. 2013, Dufey, Sepúlveda *et al*. 2014) (Figure 1.1.8.1).

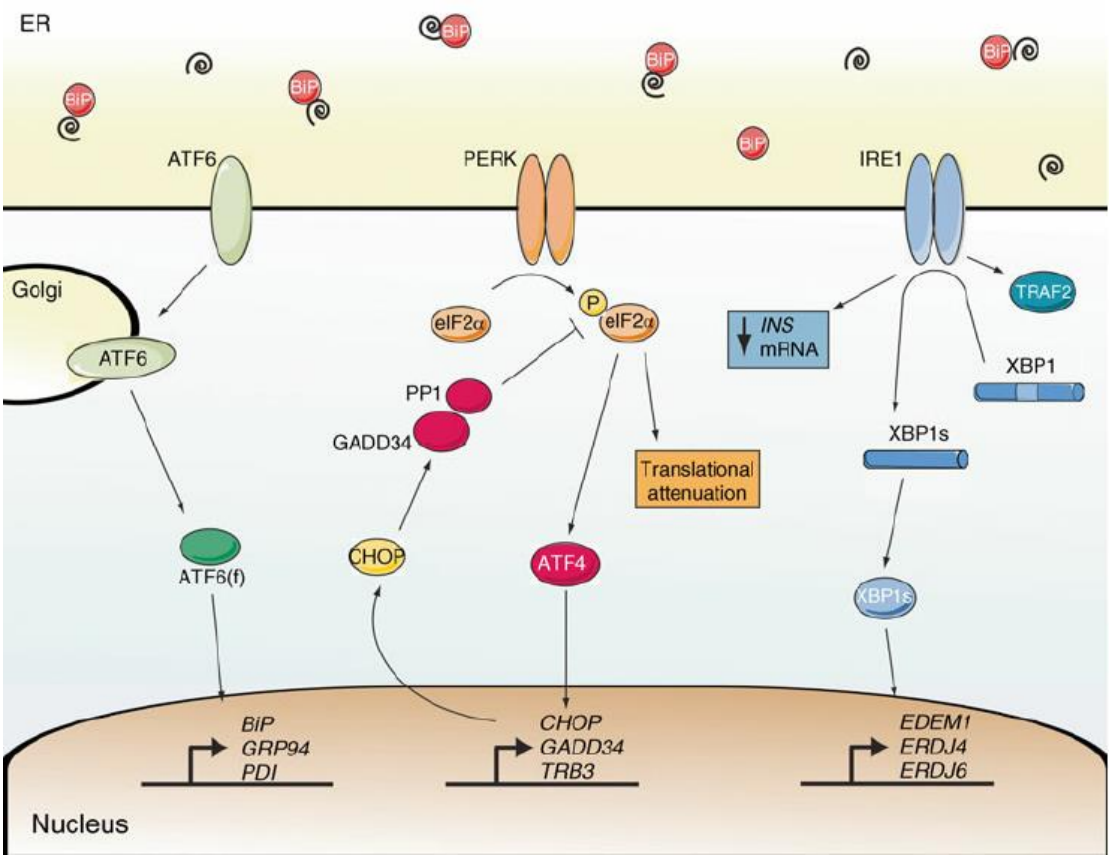

Figure 1.1.8.1 The Unfolded Protein Response: The unfolded protein response (UPR) is initiated by an accumulation of unfolded or misfolded proteins in the endoplasmic reticulum (ER). Under homeostatic conditions, the chaperone binding immunoglobulin protein (BiP) is bound to the transmembrane sensor proteins activating transcription factor 6 (ATF6), protein kinase RNA-like endoplasmic reticulum kinase (PERK) and inositol-requiring enzyme-1 alpha (IRE1α). Upon accumulation of unfolded proteins, BiP dissociates from the sensor proteins in order to assist with the folding of nascent proteins. This activates ATF6, PERK and IRE1, initiating three protein cascades that result in general translation attenuation and upregulation of specific proteins involved in protein folding and protein degradation in an attempt to reduce the ER workload. *Figure from (Eizirik, Miani et al. 2013).*

Under ER stress conditions, one of the three signalling cascades begins with the dimerisation of IRE1 and the subsequent phosphorylation of its alpha subunit, forming phospho-IRE1α (P-IRE1α). This activates the endoribonuclease activity of IRE1α which catalyses the splicing of a 26 base-pair intron from the ubiquitously expressed mRNA of unspliced X-box binding protein-1 (u-XBP1). This results in a frameshift and the subsequent translation of a 40kDa spliced isoform (sp-XBP1) rather than the 33kDa unspliced isoform (u-XBP1). The spliced, active isoform regulates genes involved in ER protein synthesis, folding, glycosylation, endoplasmic reticulum-associated protein degradation (ERAD), redox metabolism, autophagy, lipid biogenesis and vesicular trafficking (Bravo, Parra *et al*. 2013). The proteins that are then translated help to alleviate the stress experienced by the ER and return the cell to homeostasis (Figure 1.1.8.2).

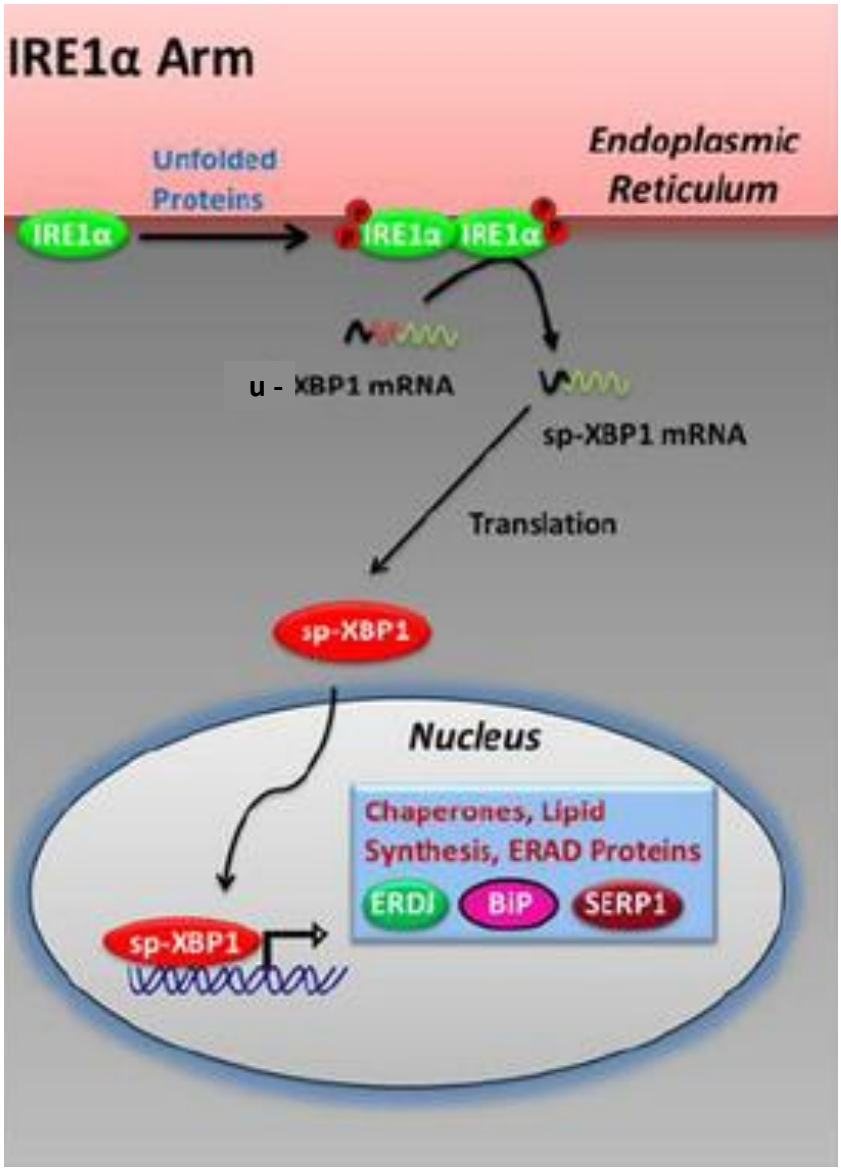

Figure 1.1.8.2 IRE1 Arm of the Unfolded Protein Response: Under conditions of endoplasmic reticulum stress, binding immunoglobulin protein (BiP) dissociates from inositol-requiring enzyme 1 (IRE1), resulting in dimerisation and the phosphorylation of the alpha subunit of IRE1. This active, phosphorylated form of IRE1 splices the mRNA of unspliced X-box binding protein 1 (u-XBP1), producing spliced-XBP1 (sp-XBP1), with the resultant protein upregulating the translation of other proteins which assist in reducing the stress, such as endoplasmic reticulum oxidoreductin 1 (ERO1), BiP, and stress-associated endoplasmic reticulum protein 1 (SERP1). *Figure adapted from (Andruska, Zheng et al. 2015).*

Dimerisation and phosphorylation of another of the transmembrane sensor proteins, PERK, activates its cytoplasmic kinase domain. This domain catalyses the phosphorylation of the alpha subunit of eukaryotic translation initiation factor-2 (eIF2α), increasing the affinity of eIF2α for eIF2β. Under normal conditions, eIF2β

provides the vital role of guanosine diphosphate (GDP)/guanosine triphosphate (GTP) exchange during cap-dependent protein translation. Phosphorylated eIF2α (P-eIF2α) sequesters eIF2β, thereby inhibiting GDP/GTP exchange and thus cap-dependent protein translation (Lewerenz and Maher 2009). Through this process, general protein translation is reduced, preventing more nascent proteins from entering the ER and contributing to the stress. Some mRNAs contain an upstream open reading frame (ORF) in their 5'-untranslated region which, under normal conditions, prevents translation; however, when eIF2α is phosphorylated, the ORF is bypassed and translation occurs (Barbosa, Peixeiro *et al*. 2013, Bravo, Parra *et al*. 2013, Dufey, Sepúlveda *et al*. 2014). One such protein that is preferentially translated when eIF2α is phosphorylated is activating transcription factor 4 (ATF4), a transcription factor that upregulates a cluster of UPR target genes involved in amino acid metabolism, antioxidant response, folding, and the regulation of apoptosis (Dufey, Sepúlveda *et al*. 2014). Two genes upregulated by ATF4 are C/EBP homologous protein (CHOP), and growth arrest and DNA damage-inducible 34 (GADD34). GADD34 contributes to a negative feedback loop that dephosphorylates P-eIF2α under prolonged ER stress, whilst CHOP regulates the transcription of proteins that trigger apoptosis. These proteins, which are only translated following sustained ER stress, represent a 'switch' in the aim of the UPR from returning the cell to homeostasis to promoting cell death in order to protect the organism (Dufey, Sepúlveda *et al*. 2014, Ariyasu, Yoshida *et al*. 2017) (Figure 1.1.8.3).

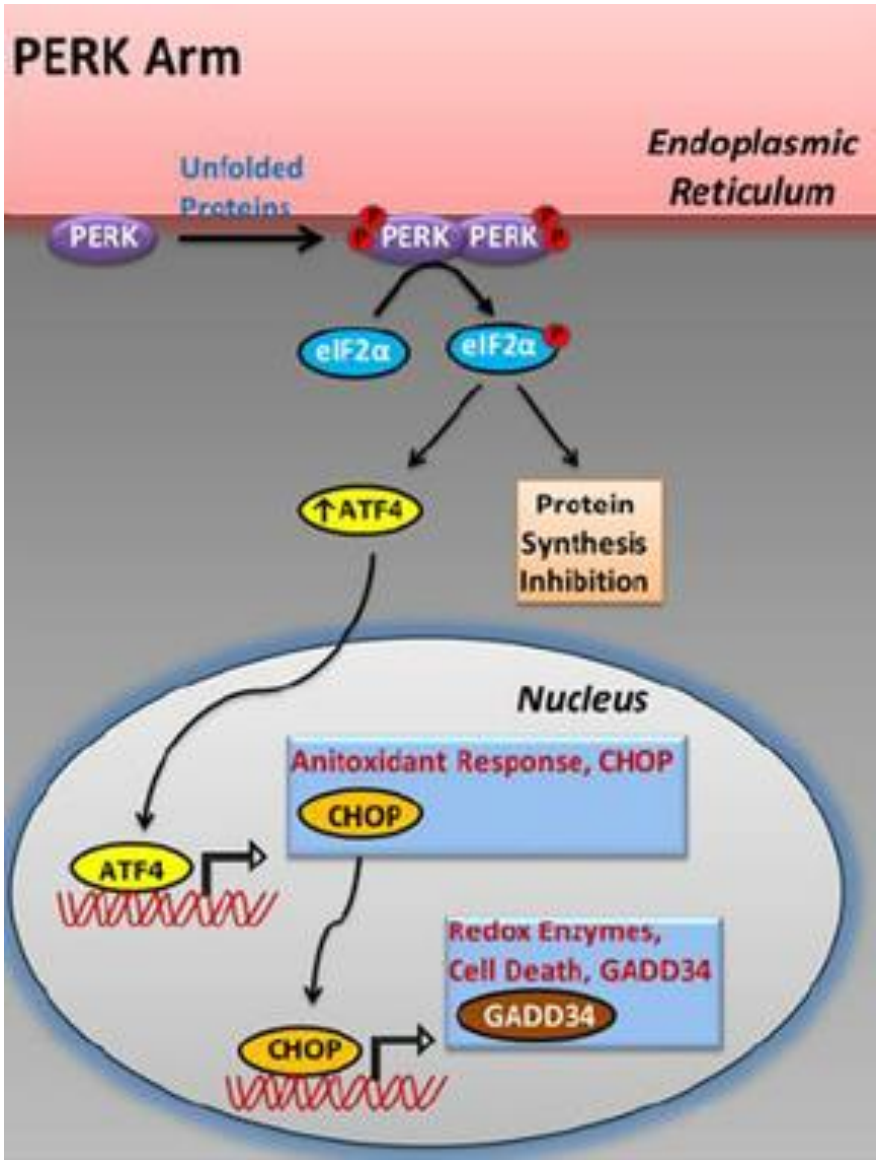

Figure 1.1.8.3 PERK Arm of the Unfolded Protein Response: Under conditions of endoplasmic reticulum stress, protein kinase RNA-like endoplasmic reticulum kinase (PERK) is activated, causing it to dimerise and autophosphorylate. Phospho-PERK then phosphorylates the alpha subunit of eukaryotic initiation factor 2 (eIF2α) which upregulates activating transcription factor 4 (ATF4). ATF4 in turn upregulates proteins such as C/EBP homologous protein (CHOP) and growth arrest and DNA damage-inducible 34 (GADD34) which, after prolonged ER stress, initiate apoptotic processes in order to protect the organism. *Figure adapted from (Andruska, Zheng et al. 2015).*

ATF6 activation differs from that of IRE1α and PERK in that, under ER stress conditions, it is transported in vesicles to the Golgi apparatus where it is cleaved by proteases. The N-terminal fragment, p50ATF6, then translocates to the nucleus

where it promotes the transcription of chaperones such as BiP, transcription factors CHOP and XBP1, as well as other UPR genes (Bravo, Parra *et al*. 2013, Ariyasu, Yoshida *et al*. 2017) (Figure 1.1.8.4).

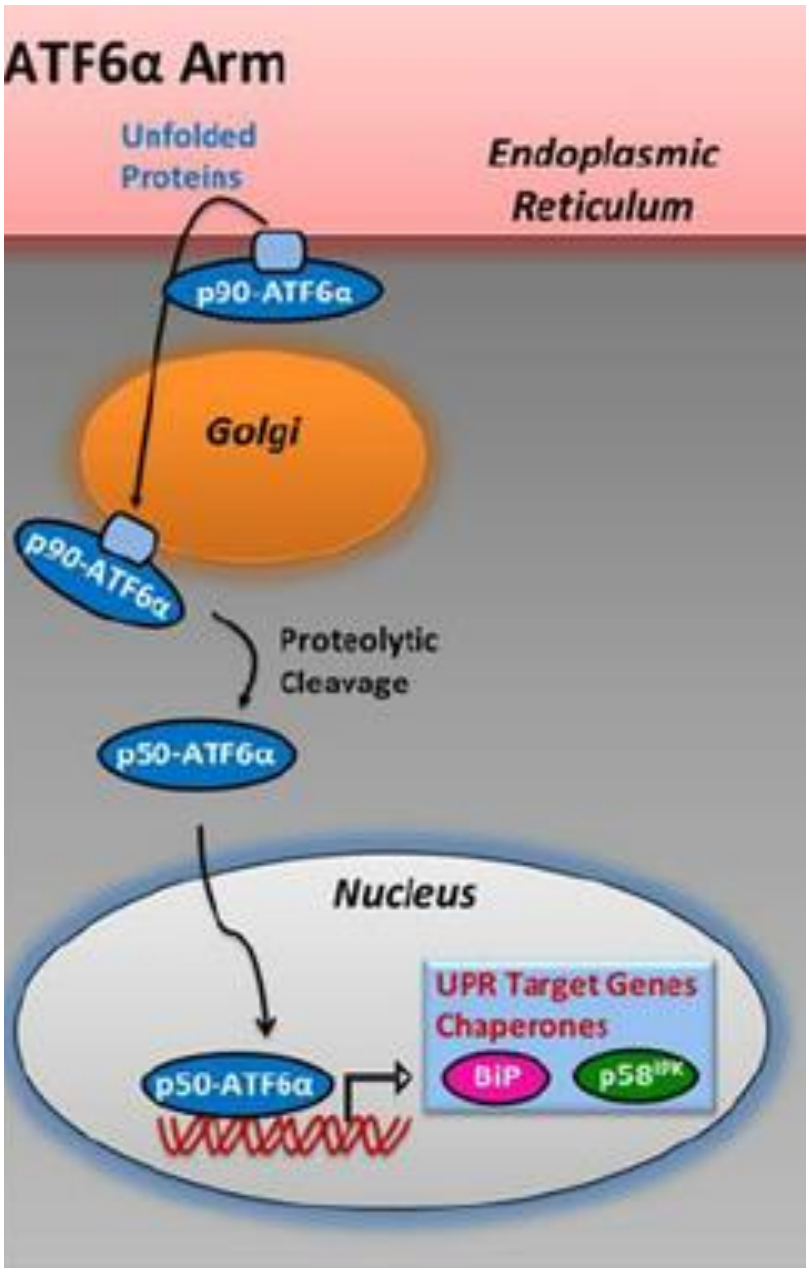

Figure 1.1.8.4 ATF6 Arm of the Unfolded Protein Response: During endoplasmic reticulum stress, the alpha subunit of activating transcription factor 6 (p90-ATF6α) is translocated to the Golgi, where it is cleaved by proteases. The N-terminal fragment, p50-ATF6α, then enters the nucleus and upregulates chaperones and co-chaperones such as binding immunoglobulin protein (BiP) and protein kinase inhibitor p58 (p58IPK) in order to reduce the stress experienced by the ER. *Figure adapted from (Andruska, Zheng et al. 2015).*

1.1.9 Inflammation and Insulin Resistance

There is a significant presence of ER stress in obese patients (Boden, Duan *et al*. 2008, Kawasaki, Asada *et al*. 2012), and whilst the definitive cause of this is unknown there are several possible ways in which ER stress could be caused by obesity. Firstly, it could be due to the increased demand for protein production required to process excess nutrients and support the expansion of adipose tissue. It is also possible that the nutrients themselves may serve as direct signals that induce ER stress, for example free fatty acid (FFA) levels are increased in the serum of obese patients and it has been shown that FFAs can lead to insulin resistance through the JNK (c-Jun N terminal kinase) pathway. It could be that ER stress is the means through which FFAs activate JNK (Kawasaki, Asada *et al*. 2012).

Many of the mechanisms that contribute to insulin resistance and other metabolic disorders are associated with ER stress. For instance, the reduced vasculature that occurs in obese adipose tissue leads to hypoxia and glucose deprivation, which are both inducers of ER stress (Gregor and Hotamisligil 2007, Ye 2011, de la Cadena, Hernández-Fonseca *et al*. 2014). Furthermore, prolonged ER stress can generate oxidative stress and induce mitochondrial dysfunction via Ca^{2+} signalling. Similarly mitochondrial dysfunction can induce ER stress through disturbances in Ca^{2+} homeostasis (Park 2014).

Once ER stress is induced, each arm of the UPR produces proteins that contribute either to homeostasis of the cell by reducing ER stress, or to apoptosis if ER stress cannot be relieved. However, during this process pro-inflammatory proteins are also upregulated. If activated acutely, ER stress and inflammation safeguard the cellular

viability and functions. When chronically induced however, they can contribute to many diseases including T2DM, neurodegenerative diseases, atherosclerosis, arthritis, respiratory diseases, irritable bowel syndrome, cardiovascular diseases, and cancer (Chaudhari, Talwar *et al*. 2014). For example, the P-IRE1α arm of the UPR induces the activation of several inflammatory markers including NF-κB (nuclear factor kappa-light-chain-enhancer of activated B cells) and JNK (Urano, Wang *et al*. 2000, Ozcan, Cao *et al*. 2004, Wang and Kaufman 2014, Cao, Luo *et al*. 2016). NF-κB is a master controller of inflammation which enters the nucleus and upregulates further inflammatory cytokines, whilst activated JNK triggers the inhibitory phosphorylation of serine residues on the insulin receptor substrate 1 (IRS-1) (Lawrence 2009, Cao, Luo *et al*. 2016). IRS-1 is essential in transmitting signals from insulin receptors to intracellular pathways that respond to the insulin signal. Tyrosine phosphorylation of IRS-1 by the insulin receptor is necessary in this process as it introduces multiple binding sites for proteins that transmit the signal further downstream. When JNK is activated by the P-IRE1α arm of the UPR, however, it leads to the inhibitory phosphorylation of a serine molecule on IRS-1 which prevents the necessary tyrosine phosphorylation and contributes to reduced insulin sensitivity (Aguirre, Uchida *et al*. 2000, Sun, Wang *et al*. 2015). This demonstrates one of the ways in which obesity can lead to T2DM, via ER stress.

1.1.10 ER Stress and its Impact on Oxidative Stress

Prolonged activation of the ER stress pathway may generate oxidative stress alongside inflammation, causing a toxic accumulation of reactive oxygen species (ROS) within the cell. This is due to the increase in production of chaperones, which aid the folding of nascent proteins by forming disulphide bonds in the ER lumen. These chaperones use molecular oxygen as the final electron recipient in this process, generating reduced molecular oxygen that subsequently accumulates in the ER. Short term activation of the UPR buffers this effect through upregulation of Nrf2 (nuclear factor erythroid 2-related 2) via the PERK pathway, which neutralises the toxic species (Gregor and Hotamisligil 2007). Prolonged activation, however leads to increased ROS levels that induce further inflammatory responses and ER stress (Ozgur, Turkan *et al*. 2014).

The activities of resident ER folding enzymes are highly dependent on redox homeostasis, and as such the ER redox state must be carefully maintained to allow disulphide formation in nascent proteins whilst maintaining sufficient reducing power to break incorrectly formed disulphides (Wilkinson and Gilbert 2004). The redox state in the ER is therefore tightly controlled by several redox mechanisms, such as the glutathione disulphide/glutathione (GSSG/GSH) cycle, and protein disulphide isomerase (PDI) reactions (Chong, Shastri *et al*. 2017). Glutathione exists in two states – reduced (GSH), and oxidised (GSSG). While reduced, GSH is able to donate a reducing equivalent ($H^+ + e^-$) to other molecules, such as ROS, to neutralise them. During this process, glutathione becomes reactive itself and binds with another reactive glutathione molecule to form glutathione disulphide (GSSG).

Through this process, GSH helps to maintain the ER thiol redox environment (Chakravarthi, Jessop *et al*. 2006, Dixon, Heath *et al*. 2008).

Protein disulphide isomerase (PDI) is one of the most abundant proteins in the ER. It is an essential folding catalyst and chaperone that assists in the critical role of native disulphide bond formation (oxidation), breakage (reduction) and rearrangement (isomerisation) in proteins (Wilkinson and Gilbert 2004, Winter, McCormack *et al*. 2007). The oxidase activity of PDI allows it to form disulphide bonds in protein substrates. However, disulphide formation that occurs early during the folding of nascent proteins is often prone to error – either between the wrong cysteine groups, or between the right cysteine groups, but in an incorrect configuration due to an incorrect temporal order (Wilkinson and Gilbert 2004). This impedes further folding and can result in a misfolded or unfolded protein. In order to correct this, the incorrect disulphide bond must be broken and reformed in the correct manner. PDI is able to continually modify disulphide bonds as long as it is oxidised after each reaction. Oxidation of PDI involves endoplasmic reticulum oxireductin 1 (ERO1) and possibly glutathione, which mediate the removal of electrons from PDI (Chakravarthi, Jessop *et al*. 2006, Dandekar, Mendez *et al*. 2015).

When increased levels of ROS occur, the careful balance of redox homeostasis in the ER can be disrupted. This prevents ER-resident proteins such as PDI and glutathione from functioning correctly, and thus the re-folding or degrading of unfolded and misfolded proteins is not carried out and ER stress can worsen (Ozgur, Turkan *et al*. 2014).

1.1.11 ER Stress and its Impact on Mitochondrial Dysfunction

An additional consequence of increased ROS levels produced during ER stress is the release of calcium ions from the ER, the main intracellular reservoir for calcium, which are then taken up by the mitochondria. Most eukaryotic cells rely on mitochondrial oxidative phosphorylation to supply the energy source ATP (adenosine triphosphate); however, mitochondria are also important in determining continued cell survival and cell death. The ER forms physical contacts with mitochondria known as mitochondria-associated membranes, or MAMs, which have been associated with the delicate balance between supporting the survival of the cell and initiating the cell death pathway. Crosstalk between the two organelles is important for the monitoring of calcium homeostasis, as well as regulating lipid metabolism, autophagy and mitophagy (Marchi, Patergnani *et al*. 2014, Rieusset 2018). During the early stages of ER stress, the number of mitochondria-ER interactions increases, facilitating improved calcium transfer from the ER to the mitochondria. This initial increase in calcium enhances mitochondrial bioenergetics and ATP production that safeguards cellular functions. However, the sudden influx of calcium into mitochondria following prolonged ER stress, along with ROS accumulation and ATP depletion, instead promotes mitochondrial collapse and triggers apoptotic cell death (Figure 1.1.11). This occurs through upregulation of pro-apoptotic proteins and opening of the mitochondrial permeability transition pore (MPTP), which depolarises the inner membrane leading to mitochondrial swelling, release of cytochrome *c*, cell damage and apoptosis (Sivitz and Yorek 2010, Malhotra and Kaufman 2011, Bravo, Gutierrez *et al*. 2012, Chaudhari, Talwar *et al*. 2014). This pathway demonstrates one of the ways in which chronic ER stress can lead to cell death.

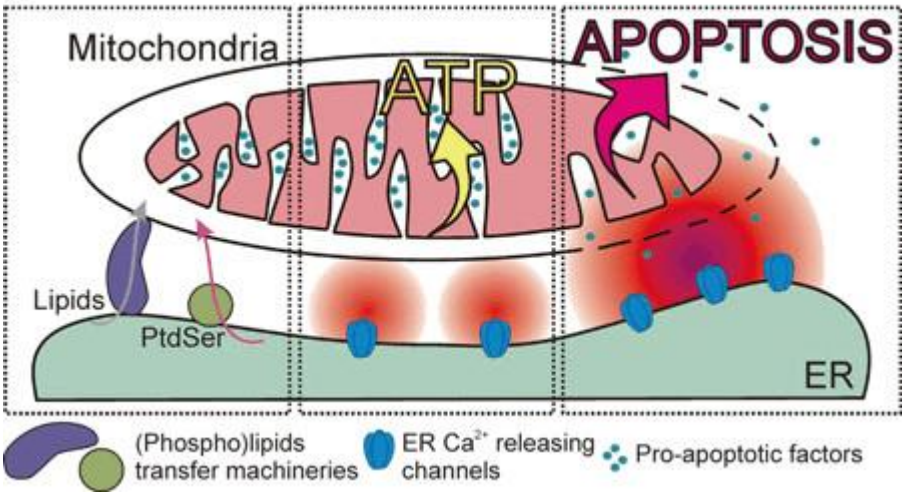

Figure 1.1.11 Ca^{2+} signalling between Endoplasmic Reticula and Mitochondria: Ca^{2+} transfer between endoplasmic reticula (ER) and mitochondria is important to monitor calcium homeostasis, and to regulate lipid metabolism, autophagy and mitophagy. Initial Ca^{2+} transfer during early ER stress enhances mitochondrial bioenergetics and ATP production which safeguards cellular functions, whilst increased Ca^{2+} transfer during prolonged ER stress promotes apoptosis. *Figure from (Filadi, Zampese et al. 2012).*

1.1.12 Mitochondrial Dysfunction

Dysfunctional mitochondria may have a direct link to insulin resistance and the development of T2DM (Lowell and Shulman 2005). Healthy mitochondrial function depends on the number of mitochondria within the cell, as well as their morphology and metabolism. For mitochondrial function to be efficient, mitochondria must constantly move throughout the cell and localise to intracellular sites where ATP production is most essential. As they move, mitochondria undergo highly co-ordinated processes of fission, whereby the organelle divides into two or more separate structures, and fusion, where two separate organelles join together to form one (Figure 1.1.12) (Scott and Youle 2010). This continuous process both mixes the mitochondrial genome whilst distributing the mitochondria into an efficient network, and maintains an optimal number of healthy mitochondria. This important balance of fission and fusion relies on proteins such as mitofusin (MFN), involved in docking the mitochondria, and the presenillin-associated rhomboid-like (PARL) protein which maintains morphological integrity. There is evidence showing that MFN is reduced in obese humans and rodents (Bach, Pich *et al*. 2003), and that insulin resistance can arise when polymorphisms of PARL occur (Walder, Kerr-Bayles *et al*. 2005, Sivitz and Yorek 2010).

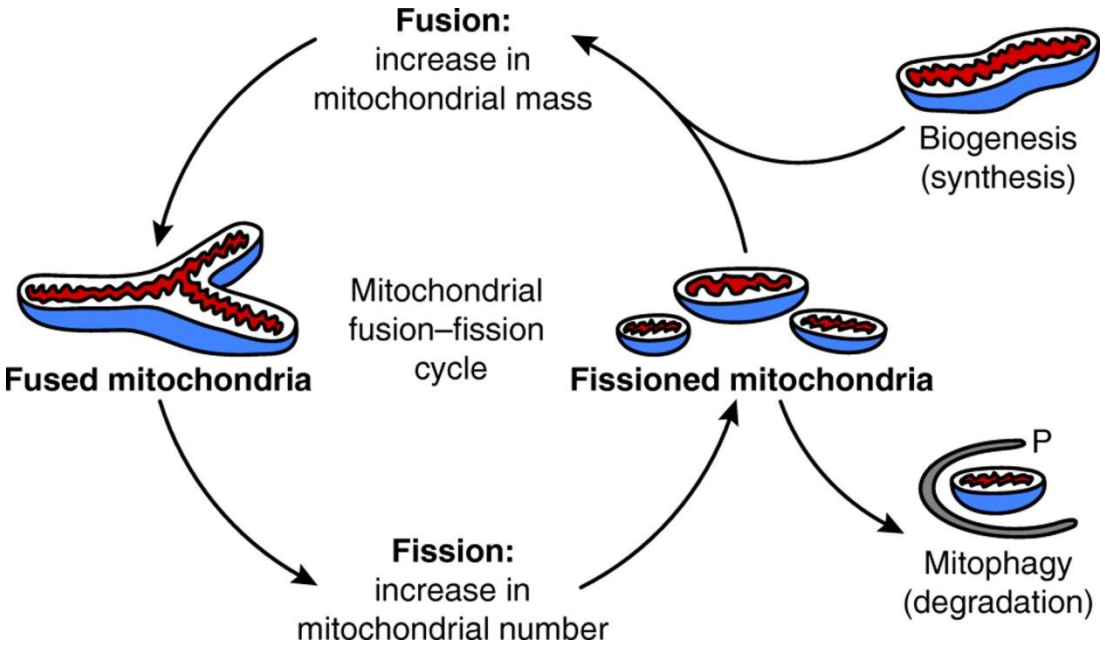

Figure 1.1.12 Mitochondrial Dynamics: Mitochondria undergo constant fission and fusion events within the cell. This allows mitochondrial DNA to mix, and an optimal number of healthy mitochondria to be maintained. *Figure from (Seo, Joseph et al. 2010)*.

Further to mitochondrial dynamics being involved in the development of insulin resistance, perturbed mitochondrial biogenesis can also contribute to the problem. A reduction in mitochondrial biogenesis can lead to a decrease in substrate oxidation for molecules such as fatty acids, which leads to an accumulation of lipids. Through this process, diacylglycerols (DAG) and ceramides (CER), metabolically active lipid mediators, accumulate and can inhibit insulin signalling. DAG activates protein kinase C which inhibits the insulin receptor (Li, Soos *et al*. 2004), whilst CER inhibits protein kinase B which is required for the insulin-induced translocation of glucose transporter 4 (GLUT4) to the plasma membrane (Summers, Garza *et al*. 1998, Montgomery and Turner 2015). Decreases in substrate oxidation also affect electron flow through the electron transport chain (ETC), which causes electron leakage and formation of ROS, independent from the ROS linked to ER stress discussed in section 1.1.10. ROS can damage mitochondria and lead to mitophagy or apoptosis,

decreasing mitochondrial number and further reducing substrate oxidation, aggravating the existing lipid accumulation (Montgomery and Turner 2015).

In terms of reduced mitochondrial function in white adipose tissue in obesity and T2DM, mitochondrial number and functions such as respiration and fatty acid oxidation are all decreased in the adipocytes of *db/db* mice, which are used as a model of obesity and diabetes due to their deficient leptin receptor activity (Choo, Kim *et al*. 2006). It is possible that mitochondrial dysfunction in adipose tissue may result in a lack of suppression of lipolysis. Increased levels of free fatty acids (FFA) that are formed through lipolysis have been shown to inhibit insulin-stimulated glucose uptake into muscle and liver (Boden 1999, Krebs and Roden 2005), and as such the FFA release due to mitochondrial dysfunction in adipocytes could contribute to the insulin resistance seen in T2DM. As well as this, it has been found that both genetic and diet-induced obesity result in decreased mitochondrial density and oxidative phosphorylation activity in adipose tissue (Richardson, Kashyap *et al*. 2005, Sparks, Xie *et al*. 2005). This could contribute to adipose tissue dysfunction and exacerbation of insulin resistance.

1.1.13 Factors that may Stimulate or Mitigate ER Stress

As discussed, obesity is one condition that induces ER stress, which can then contribute to reduced insulin sensitivity. There are several perturbations associated with obesity that may initiate ER stress in adipose tissue, for instance; overnutrition, endotoxemia, hyperglycaemia, elevated circulating free fatty acids, and glucose deprivation (Pagliassotti, Moran *et al*. 2014). Overnutrition is one of the main factors contributing to obesity, and this places an increased demand on the endoplasmic reticulum as it must synthesise proteins to aid in the processing and storage of these nutrients. Some nutrients may also potentially act as ER-stress-inducing signals themselves (Gregor and Hotamisligil 2007). Lipopolysaccharide (LPS), also known in the literature as endotoxin, is a bacterial fragment that forms the outer membrane of gram-negative bacteria and is naturally found in the gut. It has been shown to increase the expression of ER stress markers in human primary adipocytes (Alhusaini, McGee *et al*. 2010). The same study also demonstrated that high glucose and saturated fatty acids both increase levels of ER stress markers. Similarly, Jiao *et al.* showed that ER stress was induced in 3T3-L1 mouse adipocytes following exposure to a mixture of free fatty acids (Jiao, Ma *et al*. 2011). The exact mechanisms for these inducers of ER stress are currently unknown, and more work is required to determine if these results represent *in vivo* situations. As discussed previously, due to the decreased vasculature of adipose tissue in obese patients, areas of such tissue can become hypoxic. This hypoxia can induce insulin resistance in these cells which thus leads to glucose deprivation. Additionally, N-linked glycosylation, an important process in the production and correct folding of some proteins, requires glucose for the process to be carried out. Glucose deprivation can therefore lead to ER stress, as

without correct N-linked glycosylation, misfolded and unfolded proteins will accumulate and trigger the UPR (Xu, Bailly-Maitre *et al*. 2005, Gregor and Hotamisligil 2007). Tunicamycin, a chemical formed from a mixture of antibiotics, also blocks N-linked glycosylation and is commonly used as an artificial inducer of ER stress in experiments. Other chemicals that are often used to artificially induce ER stress include thapsigargin, Brefedin A, dithiothreitol (DTT), and MG132, which all act in different ways to induce this stress (Oslowski and Urano 2011).

Thapsigargin inhibits sarcoplasmic/endoplasmic reticulum Ca^{2+}/ATPase (SERCA), and thus reduces the levels of calcium in the ER. This leads to many chaperones that are calcium-dependent, such as calnexin, losing their chaperone activity causing a build-up of unfolded proteins. Brefeldin A prevents the transport of proteins from the ER to the Golgi apparatus, and induces the retrograde transport of proteins from the Golgi back to the ER, again leading to the accumulation of proteins in the ER. DTT is a strong reducing agent and prevents the formation of disulphide bonds. This induces ER stress very quickly; however, it also blocks disulphide-bond formation of nascent proteins in the cytosol and therefore is not only specific to inducing ER stress. MG132 however, blocks the ERAD (ER-associated protein degradation) pathway and thus prevents the degradation of misfolded proteins, allowing them to build up in the ER lumen (Oslowski and Urano 2011).

As well as these factors that stimulate ER stress, there are also factors that mitigate it. Unsurprisingly, weight loss in obese patients reduces ER stress. This is documented in several studies with patients who underwent bariatric surgery, in the adipose tissue of obese and lean individuals, and in the adipose tissue of people with a range

of BMIs (Boden, Duan *et al*. 2008, Sharma, Das *et al*. 2008, Gregor, Yang *et al*. 2009, Boden and Merali 2011). Antioxidants have also been found to prevent and reduce ER stress in liver cells (Malhotra, Miao *et al*. 2008), and to partially protect against ER stress in adipocytes (Kajimoto, Minami *et al*. 2014). Additionally, improving the lipid profile has been shown to protect against ER stress. Reports have shown that high density lipoprotein (HDL) inhibits the ER stress response induced by oxidised low density lipoprotein (ox-LDL) in human endothelial cells, macrophages, and more recently, 3T3-L1 adipocytes (Muller, Salvayre *et al*. 2011, Niculescu, Sanda *et al*. 2013, Song, Wu *et al*. 2016). There is also evidence that anti-inflammatory mediators, such as ethyl pyruvate and bullatine A, can protect against ER stress (Ren, Zhou *et al*. 2014, Wang, Liu *et al*. 2014).

Whilst losing weight is most likely to reduce ER stress and the development of T2DM, many obese people struggle to achieve and maintain a healthy BMI. It may therefore be beneficial to investigate other ways of reducing ER stress and the risk of T2DM. This would allow such people to improve their metabolic health whilst they are trying to lose weight, and maintain this healthier status even if they do not achieve and maintain a healthy BMI. One possible way of doing this is to research those dietary factors that may prevent or reduce the intensity of ER stress, thus reducing the risk of obese individuals developing T2DM.

1.1.14 The Impact of Broccoli on Health

Studies have shown that diets rich in cruciferous vegetables, such as broccoli, reduce the risk of myocardial infarction and cardiovascular related mortality, and reduce the incidence or progression of various cancers, including lung (Lam, Ruczinski *et al*. 2010), bowel (Seow, Yuan *et al*. 2002), kidney (Hsu, Chow *et al*. 2007), and prostate (Kirsh, Peters *et al*. 2007, Bosetti, Filomeno *et al*. 2012) (Traka, Saha *et al*. 2013). Broccoli has naturally high levels of glucoraphanin which can lead to the upregulation of antioxidants once ingested, and it is this that has been attributed to these health benefits. There is now a 'Super Broccoli', known as Beneforté that has been specifically bred to contain 2-3 times more glucoraphanin than other broccoli varieties and is now available at 10 popular supermarkets in the UK (Quadram Institute Bioscience 2013). Cruciferous vegetables have also been shown to lower inflammation *in vivo* in both animal and human studies (Youn, Kim *et al*. 2010, Hwang and Lim 2014, Jiang, Wu *et al*. 2014), as well as improving the lipid profile of humans (Bahadoran, Mirmiran *et al*. 2012, Jeon, Kim *et al*. 2013, Armah, Derdemezis *et al*. 2015). Broccoli therefore has many of the qualities described above that have been shown to reduce ER stress, and has also been shown to have health benefits demonstrated in numerous other diseases. Hence, it is possible that broccoli may protect against ER stress, and therefore reduce the risk of obese patients developing T2DM.

Cruciferous vegetables are characterised by their high content of glucosinolates, which are converted to isothiocyanates by the enzyme myrosinase. Myrosinase is physically separated from the glucosinolates within the plant cells, but is released

when the cells are damaged, for instance by microbial attack, insect predation, and mechanical food processing such as chewing or food preparation (Herr and Büchler 2010). The primary glucosinolate in broccoli is glucoraphanin, which upon interaction with myrosinase is converted to the isothiocyanate sulforaphane, which has a key role in the anti-carcinogenic effects of broccoli. There are several diverse mechanisms by which sulforaphane acts in an anti-carcinogenic manner, including eliminating ROS and enhancing antioxidative cellular activity, inducing cell cycle arrest and apoptosis in cancer cells, reducing inflammatory mediators, inhibiting angiogenesis-activating transcription factors, and eliminating tumorigenic pancreatic cancer stem cells (Juge, Mithen *et al*. 2007). The mechanisms by which sulforaphane acts depend upon the stage of carcinogenesis, and it is likely that multiple mechanisms interact to reduce carcinogenic risk by modulating cell growth and cell death signals to suppress cancer progression (Juge, Mithen *et al*. 2007, Clarke, Dashwood *et al*. 2008). The mechanism by which broccoli reduces inflammation has not been as thoroughly studied as its anti-cancer properties, however it is thought that the sulforaphane produced from broccoli inactivates NF-κB, a key modulator in inflammatory pathways, and can also inhibit the production of cytokines which are upregulated during inflammation (Mirmiran, Bahadoran *et al*. 2012).

A study by Zhang *et al.* has also shown that sulforaphane can induce adipocyte browning, as well as promote glucose and lipid utilisation (Zhang, Chen *et al*. 2016). This is important, as adipocyte browning, the process of brown adipocytes appearing in WAT, has the potential to protect against diet-induced obesity (Cui and Chen 2016). Additionally, this study reported that sulforaphane upregulated glucose uptake, lipolysis and fatty acid oxidation, while suppressing the synthesis of

triglycerides. These findings suggest that the browning of adipocytes, induced by sulforaphane, in turn promotes glucose and lipid utilisation in adipocytes and therefore has the potential to improve metabolic load on the body (Zhang, Chen *et al*. 2016). This research, along with previous studies on the effect of broccoli on cancer, inflammation, and lipid profiles, suggests that broccoli may have the potential to reduce the risk of T2DM through mechanisms that reduce processes such as ER stress.

1.2 Modelling the ER Stress Pathway to Understand its Dynamics

1.2.1 The Importance of Studying Time Series Data

The pathways involved in the UPR, and the protein interactions that occur in order to create the biological response to ER stress have been well studied, leading to a comprehensive map of genomic and proteomic reactions to describe the process. However, our understanding of the UPR and how it changes in response to different treatments is limited by the lack of knowledge about the time frame over which these interactions occur, and how the response varies over time. For instance, following treatment, should one expect a response in minutes, hours or days? Similarly, a certain treatment may be effective because it delays or speeds up a certain pathway response. Investigating time series data is therefore important in order to gain a full understanding of the ER stress response and how it changes following various interventions.

Time series data have been important in studying the responses of many biological systems. For instance, time series data have been used to provide more information on the mechanisms of respiratory oscillations of yeast (Murray, Beckmann *et al*. 2007), and their adaptation to temperature stress (Strassburg, Walther *et al*. 2010). Similarly, time series data have been used to elucidate the adaptation mechanisms of plants to various stresses (Kaplan, Kopka *et al*. 2004, Kim, Bamba *et al*. 2007, Urano, Maruyama *et al*. 2009, Espinoza, Degenkolbe *et al*. 2010) . Time series data have also been used to study human metabolism and responses, such as metabolic profile responses of stored red blood cells to hypoxia (Kinoshita, Tsukada *et al*. 2007),

and to create a model to distinguish and connect early and later drug responsive gene targets (Zhang, Mourad *et al*. 2012, Sriyudthsak, Shiraishi *et al*. 2016).

Time series data are also useful for parameterising and validating simulated behaviours predicted by mathematical models, which are often used to aid the study of biological responses. Mathematical modelling involves describing a system using mathematical concepts, which allows the user to study the effects of different components of the system, as well as make predictions about its behaviour under different conditions. These predictions must then be validated by real-life time series data in order to refine the model and confirm its accuracy (Quinn and Kohl 2013).

1.2.2 Mathematical Modelling in Biology

Biological systems invariably contain large numbers of molecules which all have multiple possible interactions that result in an exact response. For instance, the simple yeast system, *Saccharomyces cerevisiae,* contains 1418 metabolites, which participate in 2110 reactions (Heavner, Smallbone *et al*. 2012). This results in a complex network that cannot be explained and understood easily in simple terms. Mathematical modelling and computer simulations of such systems allow them to be visualised and studied in a way that elucidates their dynamics, regulation and responses.

Several mathematical models that describe different biological events have been developed and are now well-used in biology. Examples of these are the Michaelis-Menten model (Figure 1.2.2) that describes the dynamics of enzyme catalysed reactions, the Hodgkin-Huxley model of action potentials in neurons, the Lotka-Volterra model characterising the interaction of species, and epidemiological models of epidemics (Torres and Santos 2015). There are also many pharmacokinetic/pharmacodynamic (PK/PD) models which are used to categorise the pharmacological effects of different compounds, simulate different dosing schedules and understand underlying mechanisms of drug response (Kamath, Yip *et al*. 2014, Tuntland, Ethell *et al*. 2014, Wind, Schnell *et al*. 2017).

Although there exist many useful mathematical models in biology and biomedicine, the creation and parameterisation of models that describe complex biological systems can be incredibly challenging. This is due to the fact that such systems are multiscale, usually composed of many interactions that affect outcomes at different

levels, *e.g.* molecular, cellular, in tissue, whole animals and ecological (Torres and Santos 2015). As well as this, biochemical reactions often obey nonlinear reaction kinetics, in that an increase in initial concentration of material does not necessarily result in a proportional increase in the end product. Finally, many of the occurrences within a cell or organism are random, or stochastic, and can lead to unexpected behaviour of the entire system (Fischer 2008). However, due to the advancement in technology for developing models over recent decades as well as for gathering large quantities of biological data (big data), using mathematical models to describe biological systems is becoming ever more commonplace despite the challenges that it involves.

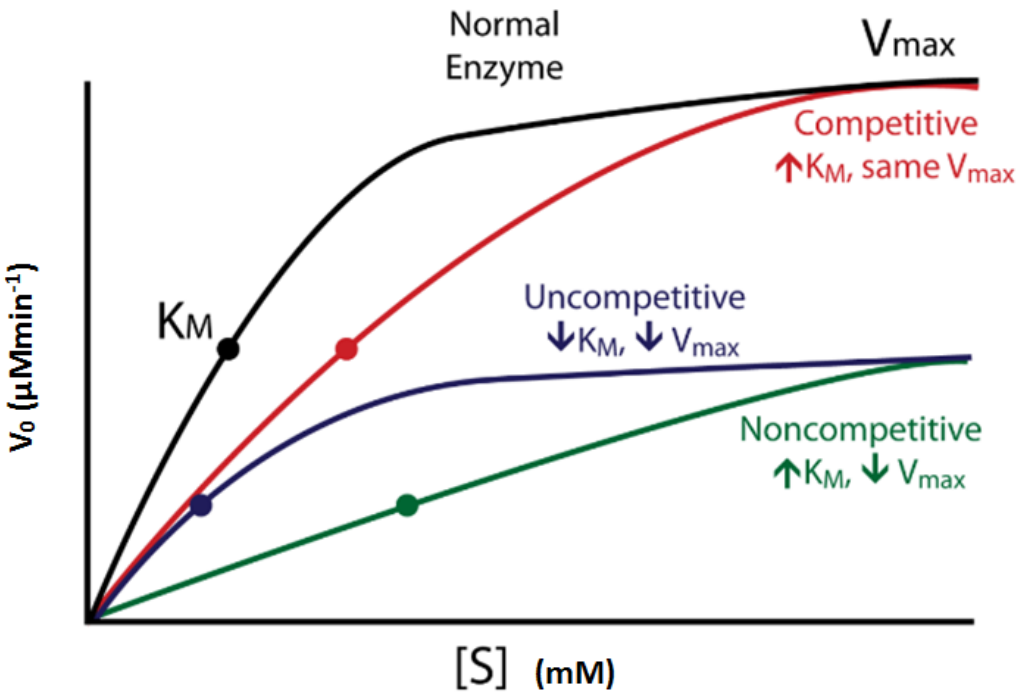

Figure 1.2.2 Michaelis-Menten Model: The Michaelis-Menten saturation curve for an enzyme reaction showing the relation between the substrate concentration ([S]) and reaction rate (V_o) for enzymes undergoing different types of inhibition. K_M = Michaelis constant, V_{max} = maximum reaction rate. *Figure adapted from (Team 2017).*

Models that successfully describe a biological system by taking into consideration the factors outlined above allow researchers to better understand the process that is occurring, as well as how the system is likely to respond to external or internal signals and perturbations (Quinn and Kohl 2013). Suitable models of biological systems allow computer simulations to be run that predict such responses. These dry experiments are much cheaper and less time-consuming than the equivalent wet lab experiments once a robust and valid model has been created, and as such can be used to support experiment design by determining optimal conditions to use in future wet experiments (Fischer 2008).

1.2.3 Factors to Consider when Designing a Mathematical Model

Building a mathematical model of a biological system requires a constant improvement of understanding, both in terms of biological insights and how the model can be adapted to incorporate these new insights (Figure 1.2.3). Before creating a model of a biological system, one must therefore consider several aspects of the process so that the model is able to describe the system effectively without it becoming so complex that it is unmanageable. This is a hard balance to achieve in biology due to the complexity of most processes, and one must define those interactions that are essential to the system versus those which can be omitted in order for the model to remain feasible, and more easily analysed and managed. Understanding more about what type of model will best describe the biological system under question is important in order to achieve the most relevant results. There are several areas to consider in terms of defining the model, for instance; whether the model is linear/non-linear, static/dynamic, or deterministic/probabilistic.

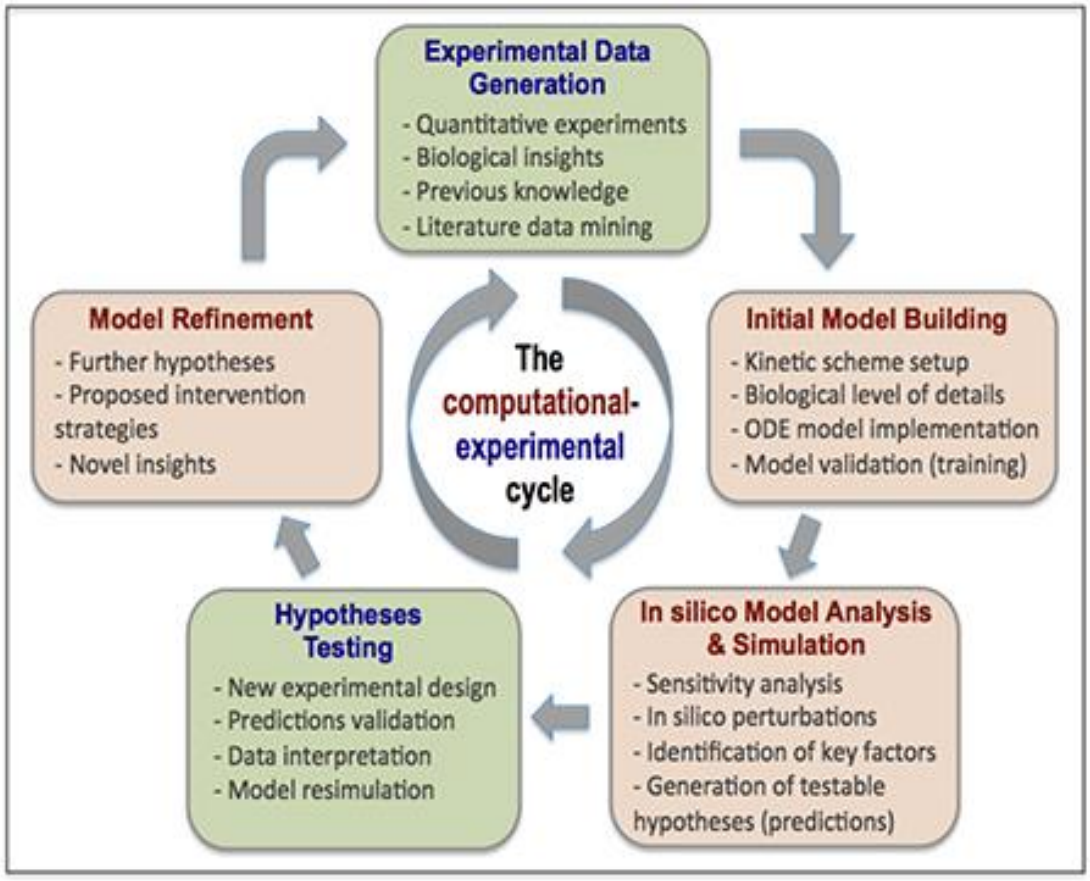

Figure 1.2.3 The Computational-Experimental Cycle: Building a mathematical model of a biological system requires a constant cycle where experimental data are continuously gathered in order to first build the model, parameterise it, validate it, and then incrementally improve it. *Figure from (Nguyen 2015).*

The linearity of a model is determined by whether an increase in the initial level of product results in a proportional increase in the end product. If this is true for every interaction within the system, then the model of that system is said to be linear. This is very rare in biological pathways as most molecules (*e.g.* proteins) have an effect on numerous others. This non-linearity tends to result in biological models being harder to study (McIntosh and McIntosh 1980).

Whether a model is static or dynamic depends on whether the model accounts for changes in the system over time. A static model describes a system that is in

equilibrium, as opposed to one where the model equations will need to account for adaptations within the system over time, which is known as a dynamic model. Dynamic models often consist of differential equations which describe the rates of change of physical quantities (*e.g.* molecules) over time, as well as a vector of state variables sufficient in dimension to summarise the properties of interest and for predicting how these properties will change over time (Ellner and Guckenheimer 2006). Validated dynamic models are used widely in biological modelling as they have a basis for predicting the long-term consequences of the processes currently operating in the system (Ellner and Guckenheimer 2006). The inclusion of kinetic rate equations and model parameters for dynamic models is required in order to provide detailed quantitative description, quantitative prediction and relevant dynamic behaviours. However, these requirements make dynamic models much more complicated to create and they are therefore generally limited to small-scale systems (Sriyudthsak, Shiraishi *et al*. 2016).

A deterministic model has variable states that are entirely determined by the structure and parameters of the model, and as such will repeatedly perform in the same way for a given set of initial conditions. A probabilistic model, or stochastic model, however, incorporates randomness or uncertainty specified in a precise mathematical way to characterise the performance of a system (Sriyudthsak, Shiraishi *et al*. 2016). It contains some variable states that are not described by unique values, but are calculated through probabilistic statistics, resulting in each run of a given model producing different results, whilst the statistical properties of the results of many runs are pre-determined by the mathematical formulation of the model (Wilkinson 2009). This allows predictions, information extraction, and

stochastic structure description to be carried out. Biochemical kinetics at the single-cell level are intrinsically stochastic (McAdams and Arkin 1999), and it is now generally accepted that stochastic modelling of biosystems is required in order to properly capture the multiple sources of heterogeneity in a realistic way (Wilkinson 2009). However, modelling biological systems in this way is more computationally demanding than deterministic modelling, and it is also harder to fit experimental data to such models, presenting more challenges for creating suitable, realistic models of biological systems (Sriyudthsak, Shiraishi *et al*. 2016).

Once key characteristics have been decided upon in order to create the most appropriate model for the system under study, the molecular species that are to be included in the model should be determined. Only those species that are essential to the process should be included and any that create unnecessary complexity in the model should be excluded. This process of choosing when to be biochemically accurate and when to approximate can be one of the most challenging steps in creating a mathematical model of a biological system (Le Novère 2015). Once the components of the model have been identified, information about the interactions between them should be obtained. This can be done either through experimental research or through conducting a reliable literature search, which allows a pathway to be created that describes the system appropriately and provides an outline for the model (Le Novère 2015).

1.2.4 Designing Dynamic Models using Time Series Data

Dynamic models involve physical constituents, known as variables (*e.g.* proteins) as well as parameters which provide more information about the variables and the interactions between them (*e.g.* kinetics and equilibrium constants) (Le Novère 2015). Ordinary differential equations (ODEs) are usually used to define the model equations, which are formed based on the known kinetics, such as simple mass action, Michaelis-Menten, or Hill type kinetics (Soliman and Heiner 2010). Parameters are then required to populate the ODEs, regardless of the format the ODEs take. These may be estimated from experimental data – however, since such experimental data often include biological variation and analytical errors, parameter estimation from biological data can be a challenging and time-consuming process.

There are essentially two methods to estimate parameter values – bottom-up, which involves determining enzymatic kinetic rates through *in vitro* enzymatic assays; and top-down, which indirectly estimates parameters from time series data (Sriyudthsak, Shiraishi *et al*. 2016). The bottom-up method involves each parameter being individually determined through experiments, and then integrated into a final model. However, this approach can be expensive and timely when obtaining parameter values for every reaction individually. The top-down approach allows estimation of multiple parameters from limited data sets by minimising the difference between experimental time-series data and model predictions. This approach is quicker and cheaper, however it relies on the accuracy of the datasets (Schadt 2013). Generally, the more parameters involved in a model, the more complex and less accurate parameter estimation becomes. However, a reasonable number of model equations

and parameters are required in order to accurately reproduce the biological observations and predict different scenarios, thus a compromise between model complexity and accuracy is a common challenge (Sriyudthsak, Shiraishi *et al*. 2016).

Constraints are also required in order to give context to what the model represents, and under what conditions the model is realistic. From this information, a series of equations can be formed that describe the system within the constraints applied – it is these equations along with the parameters and constraints that form the model. Following construction of the model, a comprehensive evaluation should be carried out to determine how well it represents the real life data, as well as analysis of any discrepancies that are highlighted throughout this process. Examples of analysis that can be undertaken include; steady state analysis, which analyses the behaviour of a system in an equilibrium state (Antunes, Gonzalez *et al*. 2015); linearisation, which allows the assessment of local stability of the equilibria of a nonlinear system (Hinrichsen and Pritchard 2005); and asymptotic analysis, which describes the system's limiting behaviour by finding conditions that the system approaches, but will never actually reach (Dalwadi, Garavaglia *et al*. 2018).

1.2.5 Modelling the Unfolded Protein Response

There have been several attempts at creating a useful model of the UPR ranging from small models that are missing biological detail, to larger models that require many parameters that may not be as accurate and use arbitrary parameter estimation (Rutkowski, Arnold *et al*. 2006, Trusina, Papa *et al*. 2008, Erguler, Pieri *et al*. 2013). Trusina and collaborators modelled a simplified yeast version of the UPR in 2008, for which the schematic and system equations are shown in Figure 1.2.5 (Trusina, Papa *et al*. 2008). The focus of this work was to propose explanations as to why the translation attenuation (TA) mechanism varies in importance between cells, and is non-existent in lower eukaryotes such as yeast. Models of the UPR were constructed both with and without the TA mechanism, and it was discovered that the number of unfolded proteins during a response was reduced in the system that contained the TA mechanism, as was the accumulation of chaperones between two consecutive pulses of stress. This research is a prime example of how systems biology can provide more insight into the processes occurring in biological pathways; however, it is unclear what experimental data, if any, were used to parameterise and test the fit of the model to reality. This is a common problem also seen in subsequent models of the UPR, where there is a lack of suitable experimental data that can be used to characterise and validate the model effectively. As such, these models are qualitative in nature rather than quantitative.

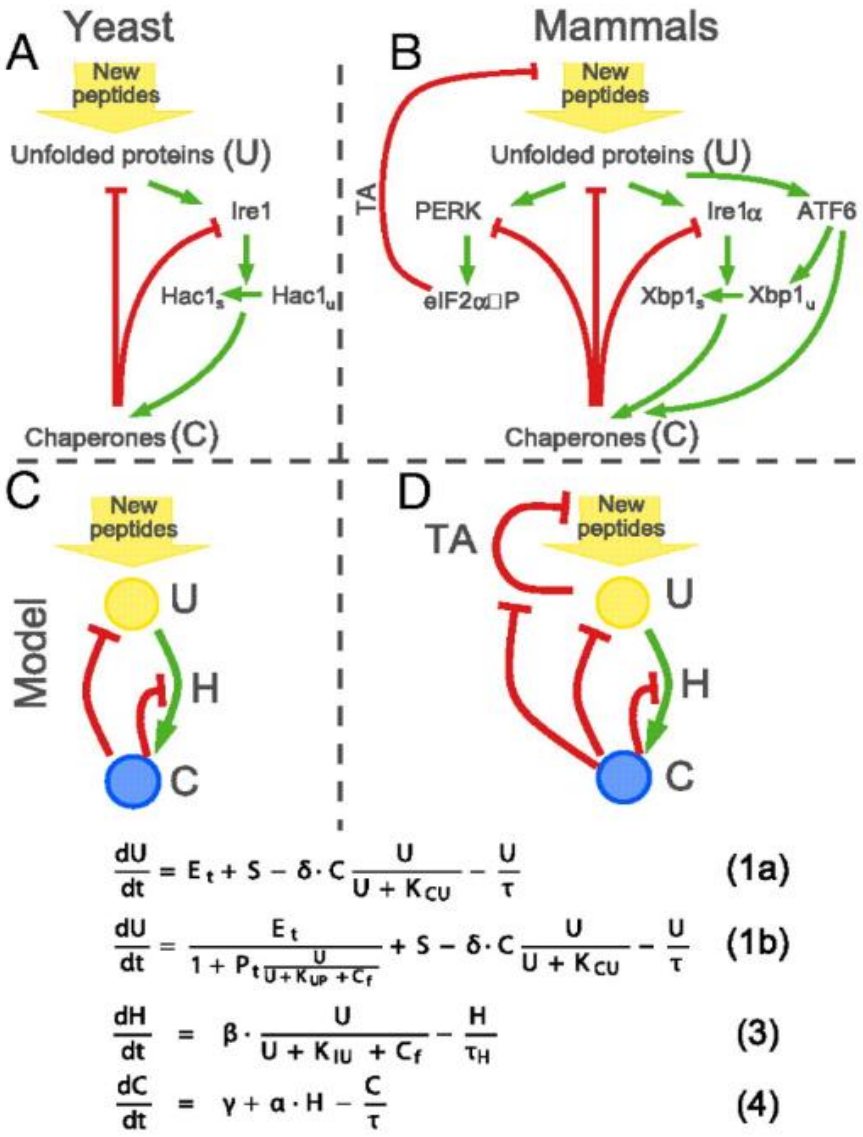

$$\frac{dU}{dt} = E_t + S - \delta \cdot C\frac{U}{U + K_{CU}} - \frac{U}{\tau} \quad (1a)$$

$$\frac{dU}{dt} = \frac{E_t}{1 + P_t\frac{U}{U+K_{UP}+C_f}} + S - \delta \cdot C\frac{U}{U + K_{CU}} - \frac{U}{\tau} \quad (1b)$$

$$\frac{dH}{dt} = \beta \cdot \frac{U}{U + K_{IU} + C_f} - \frac{H}{\tau_H} \quad (3)$$

$$\frac{dC}{dt} = \gamma + \alpha \cdot H - \frac{C}{\tau} \quad (4)$$

Figure 1.2.5 Example Model from Trusina *et al.* 2008: Unfolded protein response (UPR) network in **(A)** yeast and **(B)** mammalian cells. A simplified version of the UPR **(C)** without or **(D)** with the translation attenuation mechanism, and corresponding mathematical models, developed by Trusina *et al.*, where U represents unfolded proteins, H represents the upregulation of histone acetyltransferase 1 (Hac1) or its mammalian homologue, X-box binding protein (Xbp1), and C represents the upregulation of chaperones (Trusina, Papa *et al. 2008)*.

Another model of the UPR presented by Rutkowski *et al.* investigated the differences in the expression patterns of UPR proteins that contribute to cell survival or cell death (Rutkowski, Arnold *et al*. 2006). This model provided useful insight into how the

outcome of the UPR switches from survival to apoptosis, revealing that proteins involved in the apoptotic pathway appear to be relatively unstable compared to those in the survival pathway. This results in their rapid degradation following their initial upregulation after stress, and thus an intense episode of ER stress was required for the apoptotic pathway to succeed. As proteins involved in the survival pathway remain upregulated for longer periods of time, this provided an explanation as to why cells survive mild episodes of ER stress despite the initial upregulation of both survival and apoptotic proteins. Whilst this model has provided useful information on a possible mechanism for the switch between cell survival and cell death following ER stress, it only considered three proteins and their corresponding mRNAs and does not take into account other proteins that transfer the stress signals between them. In addition, each ODE only consists of a linear synthesis term and a linear degradation term, whilst in reality there is much more complexity to the up- and down-regulation of these proteins, including negative feedback loops, and the production of these proteins in other pathways. Despite this, the modelling predictions were measured against outcomes from experimental data and appeared to match these findings, suggesting that there is some accuracy to the model.

Erguler *et al.* (Erguler, Pieri *et al*. 2013) also investigated the mechanism by which the UPR outcome switches between survival and death. The nonlinear model presented in this research was much more detailed than that created by Rutkowski *et al.*, with 27 species interconnected by 62 biochemical reactions in four different compartments. This resulted in an incredibly large number of parameters (82) required to describe the model. Due to this large number of parameters, the authors noted that it was not possible to carry out parameter estimation using experimental

data. In addition to this, due to the lack of sufficiently time-resolved studies on mammalian systems, arbitrary units of time and concentration were allocated to the model states and parameters. As such, results from this model can, at best, only be considered qualitative, as the model requires parameterisation using experimental data before quantitative values can be generated. Using this model, the authors demonstrated that the UPR may adopt low, intermediate and high activity states depending on the level of stress, and that the intermediate state may exhibit oscillations in translation attenuation and apoptotic signals. Whilst these results demonstrated an interesting concept as to how cells adapt to different levels of stress, the lack of experimental validation must be addressed before they can be trusted and used to further explore the stress response. Additionally, due to the high dimension complexity and the large number of parameters involved in the model, it is likely that it will need to be reduced in order or structure before robust parameter estimation can be carried out with experimental data, a necessary process before it can become a useful tool in potentially predicting experimental results.

Despite these models providing more information on parts of the UPR, there is yet to be designed a useful model of the entire UPR that can be used to aid further experiments. This is most likely due to the complexity of the response, and the lack of experimental time series data that have been collected and utilised to validate such models. As such any smaller models, although useful for their original purpose, may lack biological accuracy, and higher dimensional models have not been suitably parameterised using experimental data.

This thesis explores the potential of designing a model of the UPR that focuses on one of its three biological pathways. In doing so, it reduces the complexity of the model whilst retaining biological accuracy of that pathway. The number of parameters required is therefore moderated and they are more likely to retain accuracy. Similarly, although the biological interactions included in the model will be reduced, those that are excluded will mostly be from pathways that have little crossover with the one modelled and the biological integrity will therefore be retained. This highlights an interesting compromise between complexity and accuracy of the model that minimises the negative impact of both sides of the compromise.

The final intention is to continue to develop separate models for each arm of the UPR in order to study them individually before combining the models in order to create a full model of the entire UPR. Both the individual models and the larger combined model should provide more detailed information about how the UPR responds over time, and to different input perturbations. This information can then be utilised when designing future experiments.

1.3 Research Hypothesis, Aims and Objectives

1.3.1 Research Hypothesis

The hypothesis for this research is as such: Broccoli, in the form of freeze dried broccoli powder, protects adipocytes against ER stress induced by tunicamycin. Time series data from this research will aid in the construction of a mathematical model characterising the unfolded protein response.

1.3.2 Research Aims

5. To create a mathematical model of a pathway in the unfolded protein response using experimental time series data.
6. To study ER stress in more detail by analysing how the expression of key ER stress proteins varies over time following treatment with tunicamycin.
7. To investigate the potential protective effects of broccoli against ER stress in adipocytes.
8. To examine the effects of broccoli on other mechanisms that also contribute to metabolic disease, such as ROS and mitochondrial dysfunction.

1.3.3 Research Objectives

1. The unfolded protein response is a complex system that may benefit from the development of a mathematical model to characterise it in order to understand how the interactions comprising the response change over time and in response to different input perturbations. In order to represent the response as accurately as possible with the available information in the

literature, the model that is developed will be dynamic, non-linear and built on basic mechanistic mass balance principles. Using mass action kinetics, a series of coupled ordinary differential equations will be created to describe the system dynamics and response. Experimental time series data of ER stress induced by tunicamycin will be collected at 17 time points over 72 hours, and these data will be used to parameterise and validate the model.

2. There are currently very little time series data on proteins involved in ER stress, and as such it is not clear at what time point/s data should be collected to study the effects of various treatments. Data collected in the time series experiments will not only be useful for model parameterisation as described above, but will also be analysed biologically to elucidate protein expression patterns. This will be extremely useful for biological understanding and future experiments to determine at which time points data should be collected in order to obtain the most useful results.

3. Broccoli has been shown to have many beneficial properties, such as improving lipid profiles, lowering inflammation and upregulating antioxidants in humans. It has thus been shown to reduce the risk of many cancers and inflammatory diseases. It is possible that, due to these properties, broccoli is able to protect against or reduce ER stress in adipocytes, which represents one of the major links between obesity and T2DM. As such, broccoli may be able to reduce the risk of obese patients developing T2DM. In order to investigate this, human adipocytes will be cultured and treated with a

broccoli extract, tunicamycin or a combination of the two. Protein and RNA samples will be collected and studied through Western Blotting, qRT-PCR and transcriptomic techniques in order to study the ER stress pathway and the effects of the treatments.

4. ER stress is often linked to ROS and mitochondrial dysfunction which can both contribute further to metabolic diseases. It is therefore possible that broccoli may have a direct or indirect effect on these mechanisms. This will be investigated by treating cultured human adipocytes with a broccoli extract, tunicamycin, or a combination of the two, as above. Various techniques such as mitochondrial stress tests and colorimetric ROS assays will be undertaken in order to investigate any effects the different treatments have and to determine whether broccoli may reduce the risk of metabolic diseases via different mechanisms.

Chapter 2:

Materials and Methods

2.1 Tissue Culture

2.1.1 Human Preadipocyte Chub-S7 Cell Line

The Chub-S7 cell line is a human subcutaneous white pre-adipocyte cell line which has been immortalised by the coexpression of human telomerase reverse transcriptase (hTERT) and papillomavirus E7 oncoprotein (HPV-E7) genes (Darimont, Zbinden *et al*. 2003). The cell line has been validated as a good model of human adipocyte biology as the cells retain the ability to undergo adipogenesis, and have been used to study the regulation of lipogenesis (Qiao, Maclean *et al*. 2005, Gathercole, Bujalska *et al*. 2007, Gathercole, Morgan *et al*. 2011).

2.1.2 Cell Culture Media Composition

Growth, differentiation and nutrition media were used in order to grow and differentiate the Chub-S7 cells during cell culture.

Growth media:

- DMEM/Ham's F-12 phenol-free medium 500ml (Invitrogen #11039047)
- Pencillin/streptomycin/L-glutamine 100x, 5ml (1%) (Invitrogen #10378-016)
- Fetal bovine serum 50ml (10%) (Biosera # S1810)

Differentiation media:

- DMEM/Ham's F-12 phenol-free medium 500ml (Invitrogen #11039047)
- Fetal bovine serum, 15ml (3%) (Biosera #S1810)
- Preadipocyte differentiation supplement pack x1 (Promocell #C-39436)
- PromoCell supplements (listed with final concentrations):

- Insulin, recombinant human 0.5µg/ml
- Dexamethasone 400ng/ml
- D-biotin 8µg/ml
- Isobutylmethylxanthine (IBMX) 44µg/ml
- L-thyroxine 9ng/ml
- Ciglitazone 3µg/ml

Nutrition media:

- DMEM/Ham's F-12 phenol-free medium 500ml (Invitrogen #11039047)
- Adipocyte nutrition supplement pack x1 (Promocell #C39439)
- PromoCell supplements (listed with final concentrations):
  - Insulin, recombinant human 0.5µg/ml
  - Dexamethasone 400ng/ml
  - D-biotin 8µg/ml
  - Fetal calf serum 3%

2.1.3 Growth and Differentiation of Preadipocytes

Chub-S7 cells were grown in T75 flasks until they reached 80% confluency, at which point they were seeded on to treated polystyrene 6-well or 12-well plates (Corning) that had been coated with gelatin, at a density of 25,000 cells per cm^2. In order to transfer cells from the T75 flask to the culture plates, media was aspirated and the cells washed three times with warm phosphate buffered saline (PBS) (37^oC). 5ml of 0.05% trypsin-ethylenediaminetetraacetic acid (trypsin-EDTA) was then added to the cells and left to incubate for 3 minutes before cells were dislodged by gentle tapping.

15ml of growth media was subsequently added to the trypsin-EDTA in order to neutralise it, and the solution was centrifuged at 1000rpm for 5 minutes to form a pellet. The supernatant was removed, and cells were resuspended in 5ml growth media before being counted with a haemocytometer and seeded on to plates. The seeding process required the addition of enough growth media to allow the desired number of cells to be added to each well in a volume of 1ml growth media. A further 1ml of growth media was then added once the cells had adhered to the bottom of the plate. During the cell culture period, growth media was changed every 48-72 hours until cells were confluent, at which point they were incubated in growth media for a further two days. Differentiation media was then used to initiate differentiation (day 0). From day 0 to day 6 of adipogenesis, differentiation media was changed every 48 hours; on day 6 media was changed to nutrition media and refreshed every 48 hours until day 14.

2.1.4 Treatments

Following growth and differentiation of Chub-S7 cells, basal media was applied to cells for 24 hours prior to treatments in order to remove the effects of growth factors and other components in the nutrition media, and to allow the cells to equilibrate to the basal media before treatments were added. Each treatment, including the vehicle control, was placed in fresh basal media on the day of treatment. The concentration of tunicamycin (Tun) (Sigma #7765), 750ng/ml, was chosen according to previous studies investigating ER stress that used between 0.5µg/ml and 2.0µg/ml (Ozcan, Cao *et al*. 2004, Alhusaini, McGee *et al*. 2010, Mondal, Das *et al*. 2012), and

was diluted in dimethyl sulfoxide (DMSO). Broccoli extract was prepared by adding 10ml of 100% ethanol to 1g of freeze dried broccoli powder (*hybrid Brassica oleracea* var. *italic*) and sonicating for 5 mins (10s on, 20s off x 10) on ice. This solution was then filtered using a 0.22µm steriflip filter (Millipore, SE1M179M6), and placed in a speed vacuum concentrator until there was no liquid left, at which point the remaining solid was resuspended in ethanol to create the desired concentration. The same volume of vehicle was applied to each well, including control wells, and all treatment media was filtered through a 0.22µm filter before being applied. All treatment was refreshed every 24 hours.

2.1.5 Collection of Protein and RNA

Protein samples were collected from culture cells using a lysis buffer consisting of 5ml 1x radioimmunoprecipitation assay buffer (RIPA) (Millipore UK), 100µl of dissolved protease and phosphatase inhibitors (2 Roche Complete Mini protease inhibitor cocktail tablets and 8mg sodium fluoride (NaF, Fisher Scientific) and 20mg sodium vanadate (Na3VO4, Acros Organics) in 2ml 1 x RIPA). 250µl of protein lysis buffer was added to each well at 4^{o}C and cells were subsequently scraped with a sterile scraper for 30 seconds. The contents of the well was then agitated with a pipette to promote cell lysis before being collected and stored at -80^{o}C. This process was also used to collect RNA samples from cultured cells, using 350µl Buffer RLY (Bioline) and 3.5µl β-mercaptoethanol (β-ME) (Sigma) per well instead of protein lysis buffer. Either three or six protein and RNA samples were collected for each time point.

2.2 Analysis of Samples

2.2.1 Protein Analysis

Protein concentrations were determined using the Bradford assay, whereby 2µl of protein sample was added to 1ml of 1:4 Bradford stock reagent (Biorad, #5000006) and colorimetrically compared to known concentrations of bovine serum albumin (BSA) also added to 1ml of Bradford reagent. Western blot analysis was performed using a previously described method (Alhusaini, McGee *et al*. 2010). In brief, 20µg of protein sample was loaded onto a 10% denaturing polyacrylamide gel (GeneFlow, UK), separated by electrophoresis and transferred at 4^{o}C, 25V overnight to membrane filter Immobilon-P transfer membranes with 0.45µm pore size (Fisher). Ponceau stain (Sigma-Aldrich, P7170) was then applied and membranes cut into strips containing different target proteins, before being washed in PBS and blocked in 0.2% I-Block PBS-tween (PBS-T) for 24 hours. Membranes were incubated in a primary antibody diluted in 0.2% I-Block PBS-T (p-eIF2α 1:500, total eIF2α 1:500, BiP 1:500, β-actin 1:1000, Cell Signalling) at 4^{o}C overnight; β-actin was used to confirm equal protein loading. Membranes were washed six times for five minutes in PBS-T and incubated in anti-rabbit IgG (whole molecule), horseradish peroxidase antibody produced in goat, IgG fraction of antiserum, buffered aqueous solution (Sigma #A9169). The chemiluminescent detection system, enhanced chemiluminescence/enhanced chemiluminescence+ (ECL/ECL+) (GE Healthcare, UK), was used to visualise protein bands, and densitometry was conducted using ImageJ software.

2.2.2 RNA Processing and Quantitative Real-Time Polymerase Chain Reaction

RNA was extracted from cell culture samples using Isolate II RNA Mini Kit (Bioline, #BIO-52073) according to manufacturer's instructions. RNA was eluted in 10µl RNase-free water and 1µl of each sample was used to quantify in duplicate using a spectrophotometer (Nanodrop ND-100, Labtech) at an absorbance of 260nm. 200ng of RNA from each sample was used to perform cDNA synthesis with a Bioline mRNA reverse transcription kit (#BIO-65026) according to manufacturer's instructions. Quantitative real-time polymerase chain reaction (qRT-PCR) was used to measure gene expression, using ABI 7500 standard sequence detection system (Applied Biosystems, UK). 25µl sample volume was assayed, containing the cDNA sample, Taqman Universal PCR mastermix (#4304437 Applied Biosystems, UK), and a specific commercially available Taqman gene expression assay (ThermoFisher Scientific, UK, CHOP (DDIT3): Hs00358796_g1; ATF4: Hs00909568_g1; ATF6: HS00232586_M1). All reactions were assayed in triplicate and multiplexed with a housekeeping gene, 18S, a pre-optimised control probe (Applied Biosystems, UK). qRT-PCR was carried out as per the manufacturer's instructions: 50^{o}C for two minutes, 95^{o}C for 10 minutes, followed by 40 cycles of 95^{o}C for 15 seconds, and then 60^{o}C for 1 minute. Data analysis was carried out using the following formula:

$$mRNA\ expression = 2^{-\Delta Ct}, \text{ where } \Delta Ct = \text{target gene Ct} - 18S\ Ct$$

2.2.3 Oil Red-O Staining

Following the growth and differentiation of Chub-S7 cells as described above, Oil Red-O (ORO) stock solution was prepared by dissolving 0.5g of ORO powder in 200ml isopropanol in a 56^{o}C water bath for 1hr. Working ORO solution was then prepared by diluting stock ORO with distilled water to make a 60% solution, which was then stirred well and left to stand for 10 minutes before being filtered through Whatman No 42 filter paper. Media was removed from each well and cells were washed twice with PBS before being fixed with 4% formalin for 15 minutes at room temperature. Excess formalin was removed and cells were washed twice with PBS for 5 minutes at room temperature, before being rinsed with 60% isopropanol. 500µl of working ORO was added to each well and incubated at room temperature for 30 minutes, before being removed and cells washed with PBS. Cells were then viewed under a light microscope to assess lipid accumulation, and digital photographs were taken.

2.2.4 Seahorse Cell Mitochondria Stress Test

Oxygen consumption rate (OCR) and extracellular acidification rate (ECAR) were measured using a Seahorse XF24 Extracellular Flux Analyser (Seahorse Bioscience, Agilent Technologies). Chub-S7 cells were grown in T75 flasks and seeded onto gelatin-coated 24-well plates (Seahorse Bioscience, 100850-001) at an optimised density of 10,000 cells per well. Cells were grown, differentiated and treated using the standard protocols described in sections 2.1.3 and 2.1.4 above; each experimental group had five replicates. The assay was performed in sterile, unbuffered assay media prepared with seahorse base media (Seahorse Bioscience,

102365-100) at 37°C, pH 7.4. This media also contained 1mM sodium pyruvate (Sigma, S8636), 2mM glutamine glutamax (Seahorse, included with plates) and 17.5mM glucose (Sigma, G8769).

Following a 30 minute calibration step and a 30 minute equilibration step, the assay protocol consisted of the following steps repeated for three cycles: mix (3 minutes), wait (2 minutes), measure (3 minutes). These cycles were initiated before and after each injection of Oligomycin (Sigma, O4876), Carbonyl cyanide-p-trifluoromethoxyphenylhydrazone (FCCP) (Sigma, C2920) and combined Rotenone (Sigma, R8875) and Antimycin A (Sigma, A8674). The injection of optimised reagents or vehicle control was done from a 10-fold concentrated stock solution to give final concentrations as described: 2 µM Oligomycin, 2 µM FCCP, 0.5 µM Rotenone/Antimycin A.

2.2.5 Endogenous Antioxidant Activity Assays

Endogenous antioxidants superoxide dismutase (SOD) and catalase were measured using OxiSelect*TM* Superoxide Dismutase Activity Assay (STA-340) and OxiSelect*TM* Catalase Activity Assay (STA-341) kits (Cell Biolabs). Chub-S7 cells were grown, differentiated and treated as described in sections 2.1.3 and 2.1.4 above, after which cells were washed three times with ice-cold PBS and harvested with a cell scraper in 1ml ice-cold PBS. Samples were sonicated on ice and vortexed to encourage homogenisation, before being centrifuged and stored at -80°C until assayed. All assays were carried out in accordance with manufacturer's instructions within one month of sample collection, using a PheraStar FS microplate reader (BMG Labtech)

to measure absorbance. Data analysis was carried out as per manufacturer's instructions.

2.2.6 Quantification of Total Reactive Oxygen and Nitrogen Species

Total reactive oxygen and nitrogen species (ROS/RNS) were measured using OxiSelect^{TM} *in vitro* ROS/RNS assay kit (STA-347, Cell Biolabs). Chub-S7 cells were grown, differentiated and treated as described in sections 2.1.3 and 2.1.4 above, after which cells were washed three times with ice-cold PBS and harvested with a cell scraper in 1ml ice-cold PBS. Samples were sonicated on ice and vortexed to encourage homogenisation, before being centrifuged and stored at -80^{o}C until assayed. The assay was carried out according to manufacturer's instructions, and fluorescence was measured after 30 minutes using a PheraStar FS microplate reader (BMG Labtech) with a 485/538nm filter and 530nm cutoff. Data analysis was carried out as per manufacturer's instructions.

2.2.7 Transcriptomics

Chub-S7 cells were grown, differentiated and treated as described in sections 2.1.3 and 2.1.4 above. Following protein analysis, RNA samples from the time point where cells exhibited the most protection against tunicamycin-induced ER stress by broccoli extract, 36 hours, were sequenced. RNA quality was assessed using a bioanalyser (Agilent 2100) before the mRNA samples were converted into libraries of template molecules using TruSeq RNA V2 (Illumina) as per manufacturer's instructions (Illumina 2014). These libraries were then sequenced on a MiSeq platform, Illumina,

using a 75bp paired-end run, as per manufacturer's instructions (Illumina 2015). The resulting data were quality checked using FastQC software (Andrews 2010), and adapters sequences as well as low quality regions in reads were trimmed using Trimmomatic software (Bolger, Lohse et al. 2014). Post trimming, BBNorm software (BBMap 2018) was employed to normalise coverage by down-sampling reads to obtain a flat coverage and also accelerate transcriptome assembly of all samples. Using these normalised reads, the transcriptomics assembly was prepared using Ray software (Boisvert, Raymond et al. 2012). Transcript quantification of individual samples was done with the above prepared transcriptome assembly using Salmon software (Patro, Duggal et al. 2013). Salmon uses a quasi-mapping based approach which has two steps – indexing and quantification. The indexing step is independent of the reads, and was therefore only required to be run once for a particular set of reference transcripts, whilst the quantification step is sample specific and was therefore run for each sample set.

Post quantification, DESeq2 (Love, Huber et al. 2014) was used to perform comparisons between various sample conditions and the results were filtered using log2FC of greater than 0.5 and P-adj value of less than 0.1, where P-adj is the adjusted p-value following correction for multiple testing. Finally, the transcripts that were differentially expressed were searched against Uniprot protein human sequences set using RAPSearch2 (Zhao, Tang et al. 2012). The annotations linked to the resulting protein IDs were fetched using ID mapping files present in the Uniprot website (UniProt 2018). Accordingly, the GO annotation and pathway information was obtained.

2.2.8 Statistical Analysis

Statistical analyses were undertaken using Microsoft Excel 2010. Data are reported as mean ± standard error of the mean (SE), unless otherwise specified. Comparisons between samples were performed via two-tailed t-tests. $p < 0.05$ was considered statistically significant, and significance levels are indicated as follows: *$p < 0.05$, **$p < 0.01$, ***$p < 0.001$, and where more than one comparison was made: #$p < 0.05$, ##$p < 0.01$, ###$p < 0.001$; +$p < 0.05$, ++$p < 0.01$, +++$p < 0.001$; ^$p < 0.05$, ^^$p < 0.01$, ^^^$p < 0.001$.

CHAPTER 3:

Modelling the Unfolded Protein Response

3.1 Introduction

3.1.1 Obesity and Type 2 Diabetes Mellitus

Obesity is a global epidemic, with the World Health Organisation reporting that the number of cases worldwide has almost tripled since 1975 (World Health Organisation 2017). This is important as there are a range of serious health conditions that are associated with obesity, including type 2 diabetes mellitus (T2DM), heart disease, and some types of cancer (De Pergola and Silvestris 2013, Cefalu, Bray *et al*. 2015, Ndumele, Matsushita *et al*. 2016). Despite the number of diseases that are linked with obesity, it is T2DM that has a particularly strong interdependent relationship with the condition, and it has been shown that obesity accounts for 80-85% of the risk of developing T2DM (diabetes.co.uk 2017). It is not fully understood how the development of insulin resistance is caused by obesity, but it is likely due to a combination of responses activated during the condition. Inflammation, mitochondrial dysfunction, reactive oxygen species (ROS) and hypoxia have all been shown to occur during obesity and in turn can reduce the effectiveness of insulin signalling (Hummasti and Hotamisligil 2010, Kawasaki, Asada *et al*. 2012, Tripathi and Pandey 2012). Another response that occurs during obesity is endoplasmic reticulum stress, which can be induced by each of the conditions listed above, and can lead to reduced insulin sensitivity and T2DM.

3.1.2 Endoplasmic Reticulum Stress

The endoplasmic reticulum (ER) is a cellular organelle which is responsible for the correct folding and trafficking of proteins, the synthesis of lipids, and the maintenance of calcium homeostasis. Nascent proteins enter the ER lumen as they are being synthesised, and chaperones within the ER assist in their correct folding before they are distributed to their final destination. However, if the rate of nascent proteins entering the ER exceeds the rate that can be correctly folded with the available chaperones, the ER becomes stressed and filled with unfolded and misfolded proteins that cannot be trafficked to their destination. In these conditions, the unfolded protein response (UPR) is activated in an attempt to relieve the stress, or to initiate apoptosis in order to protect the organism if the stress cannot be relieved.

There are three main pathways in the UPR, each controlled by different transmembrane sensor proteins: activating transcription factor 6 (ATF6), protein kinase RNA-like endoplasmic reticulum kinase (PERK) and inositol-requiring enzyme-1 alpha (IRE1α) (Figure 3.1.2) (Carrara, Prischi *et al*. 2013). Under normal conditions, these sensor proteins are bound to the ER-resident chaperone binding immunoglobulin protein (BiP); however when ER stress ensues, BiP is separated from the sensors in order to assist with folding the excess number of unfolded proteins. This separation from BiP activates the sensor proteins, either through dimerisation and transphosphorylation (as with PERK and IRE1α), or translocation to the Golgi where cleavage occurs (as with ATF6) (Gardner, Pincus *et al*. 2013). Once these sensor proteins are activated, they initiate cascades which result in the inhibition of general

translation, upregulation of chaperones and activation of the endoplasmic-reticulum-associated protein degradation (ERAD) process (Hetz, Chevet *et al*. 2015). Consequently, fewer nascent proteins enter the ER, more chaperones are available to help fold the existing unfolded proteins, and any misfolded proteins are degraded through the ERAD process. However if the stress continues despite these measures, the UPR switches to upregulate proteins involved in apoptosis in an attempt to save the organism from the stressed cell (Dufey, Sepúlveda *et al*. 2014).

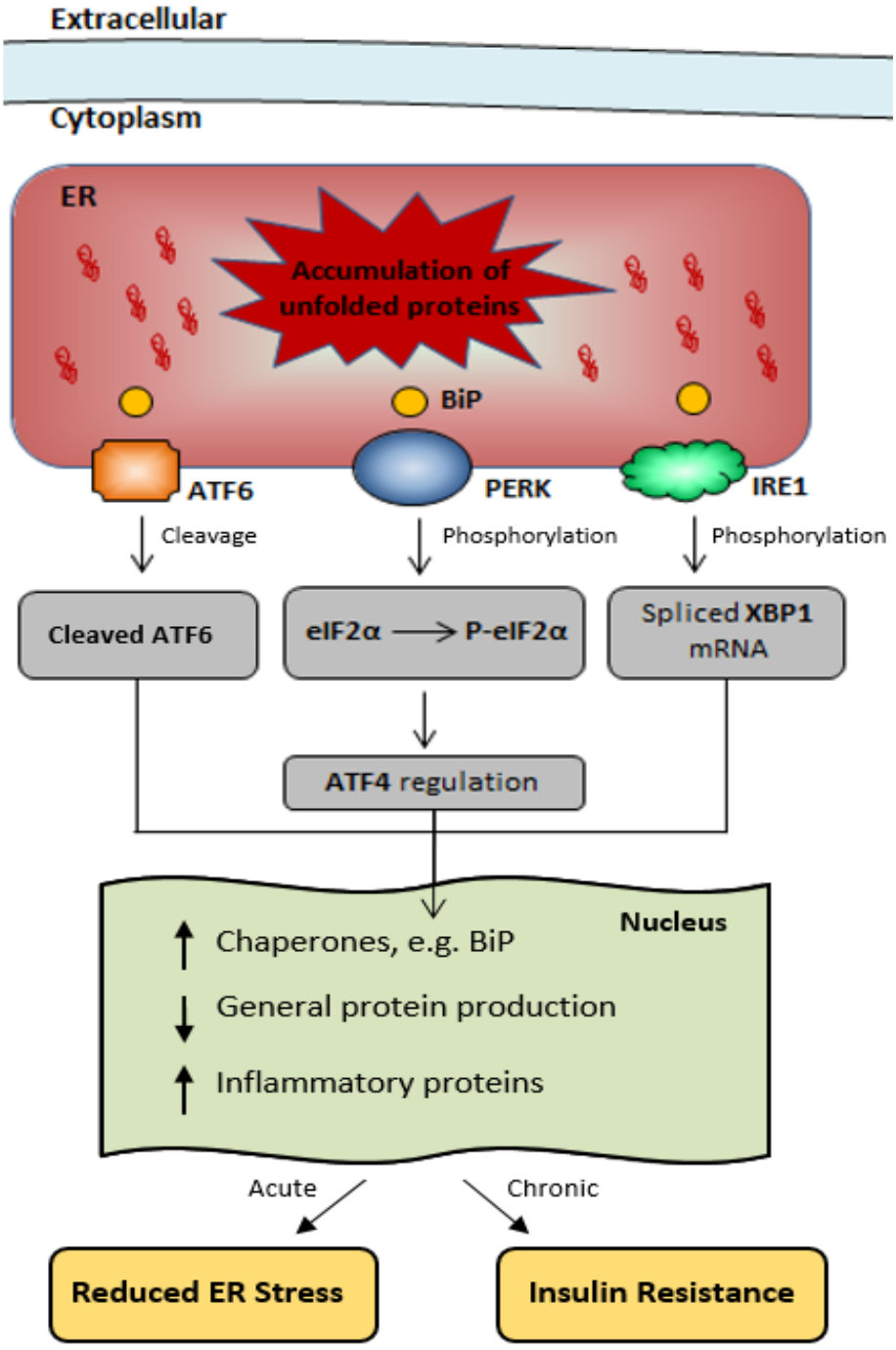

Figure 3.1.2 Unfolded Protein Response: Stress within the endoplasmic reticulum (ER) causes the unfolded protein response (UPR) to be initiated. This involves the dissociation of BiP (binding immunoglobulin protein) from ATF6 (activating transcription factor 6), PERK (protein kinase RNA-like endoplasmic reticulum kinase) and IRE1 (inositol requiring enzyme 1), initiating three protein cascades which result in the phosphorylation of eIF2α (eukaryotic initiation factor 2α), activation of ATF4 (activating transcription factor 4), and the splicing of XBP1 (X-box binding protein 1). These cascades cause the upregulation of chaperones and ERAD (endoplasmic-reticulum-associated degradation) proteins, and the downregulation of general protein translation. Acute UPR activation can reduce ER stress, however chronic activation can induce insulin resistance. *Figure adapted from (Chakrabarti, Aboulmouna et al. 2016).*

Despite the UPR being a mechanism designed to reduce ER stress, many of the downstream pathways cause upregulation of pro-inflammatory mediators, such as NFκB and JNK (Zhang and Kaufman 2008). Activation of these proteins can lead to the inhibitory phosphorylation of insulin receptor substrate 1 (IRS-1), a key component of the insulin signalling pathway, and can consequently induce insulin resistance (Flamment, Hajduch *et al*. 2012). During obesity, cellular responses occur that induce ER stress over a prolonged period of time due to constant stimulation by nutrient intake and high fat diets. Consequently, the increased level of ER stress is maintained, creating a state of chronic inflammation which contributes to long-term insulin resistance through the inhibitory phosphorylation of IRS-1, which can eventually lead to T2DM (Hotamisligil 2008, Schonthal 2012).

As chronic ER stress is one of the components that links obesity to T2DM (Hotamisligil 2008), it may be possible to reduce the risk of subjects developing T2DM by mitigating the ER stress that they experience. In order to do this, it is important to first develop the understanding of the pathways within the UPR. It is not sufficient to examine individual molecules within such a complex biological pathway; interactions between the molecules must also be assessed to allow investigation of regulatory processes and how disruption of the pathway may affect the outcome (Klipp and Liebermeister 2006). Mathematical modelling is a crucial tool in this respect as it not only allows the individual molecular interactions to be studied, but also has the potential to show how these interactions contribute to the system as a whole (Fischer 2008).

3.1.3 Mathematical Modelling of the Unfolded Protein Response

Mathematical modelling has become increasingly recognised in biological sciences as a useful tool to aid the understanding of spatio-temporal pattern formations in biological systems (Motta and Pappalardo 2013). Models are being utilised in many different research areas, and even within the study of diabetes there is an array of models that vary in focus from molecular and cellular biology through clinical science to health service research. A summary of the mathematical models that have been created to aid the understanding of diabetes can be found in a review by Ajmera *et al.* (Ajmera, Swat *et al*. 2013). This review details how, despite the large number of models aiding the research into diabetes, there is still a large disproportion between the data collected from experimental approaches and their representation in mathematical models. This is accurate for research into the UPR, as there has been much study into it experimentally, yet there are comparatively very few attempts at mathematically modelling the response. There have, however, been some previous attempts at using mathematical models to study the UPR.

Trusina and collaborators created a simplified model of the yeast UPR in order to investigate why the translation attenuation (TA) mechanism is more important in some cell types than others (Trusina, Papa *et al*. 2008). Rutkowski *et al.* used a linear model of the UPR to examine how protein expression patterns vary between those that contribute to cell survival compared to those that contribute to cell death (Rutkowski, Arnold *et al*. 2006). Finally, Erguler *et al.* created a large model that investigated how the UPR switches between favouring cell survival and apoptosis (Erguler, Pieri *et al*. 2013). These models vary greatly with regards to complexity and

biological detail, demonstrating the challenge of modelling such a complex biological pathway. It is unclear what experimental data, if any, Trusina *et al.* used for parameterisation, and whilst Rutkowski *et al.* created a small model that was therefore able to be parameterised and semi-validated with experimental data, it lacked biological detail. Conversely, Erguler *et al.* created a biologically accurate, detailed model of the UPR that was unable to be validated due to its complexity. This demonstrates the importance of considering the complexity of the model as well as gathering experimental data that will allow effective parameterisation and validation.

The aim of the study in this chapter was therefore to investigate the complexity of UPR model that would best provide a balance between biological detail and accuracy of parameter estimation using experimental data. For this, literature searches and experimental studies were undertaken to:

1. Identify the appropriate level of complexity for a mathematical model of the UPR.
2. Collect experimental data of proteins involved in the UPR that can be used to aid model development.
3. Develop a mathematical model of the UPR based on information from the literature search and experimental data.

3.2 Methods

3.2.1 Cell Culture

In order to gather experimental data that could aid in the development and validation of a mathematical model of the UPR, adipogenesis was induced in Chub-S7 preadipocytes for 14 days. Oil Red-O staining was carried out at the beginning and end of the differentiation process to ensure that the pre-adipocyte cells had differentiated into mature adipocytes, by identification of red stained lipid droplets. Cells were then exposed to 750ng/ml tunicamycin for 24, 48 or 72 hours, with fresh tunicamycin exposure every 24 hours. Control cells were grown in the same manner and treated with the same concentration of DMSO, the vehicle for tunicamycin. Following this, cells were harvested, protein extraction was carried out and the expression of UPR proteins was assessed via Western blot analysis.

3.2.2 Initial Modelling of the UPR

A literature search was carried out in order to determine the best methods to evaluate the proteins studied during this experiment through a modelling approach. A mass action kinetics approach was implemented to create ordinary differential equations (ODEs) and these ODEs were then entered into Berkeley Madonna – a software package that solves differential equations numerically using the Runge-Kutta 4^{th} order algorithm and enables the output to be mapped against and fitted to experimental data. Parameters were then manually adjusted using the programme's slider function with the aim of reducing the difference between the model output

and the dataset. The complexity of the model was considered throughout this process with the aim of ensuring accuracy, whilst maintaining manageability.

3.3 Results

3.3.1 Oil Red-O Staining Confirmed Pre-Adipocyte Differentiation

Oil Red-O staining of cells before (day 0) and after (day 14) the differentiation process highlighted a substantial accumulation of lipid droplets, confirming that the cells had differentiated into mature adipocytes over the time-frame (Figure 3.3.1.1).

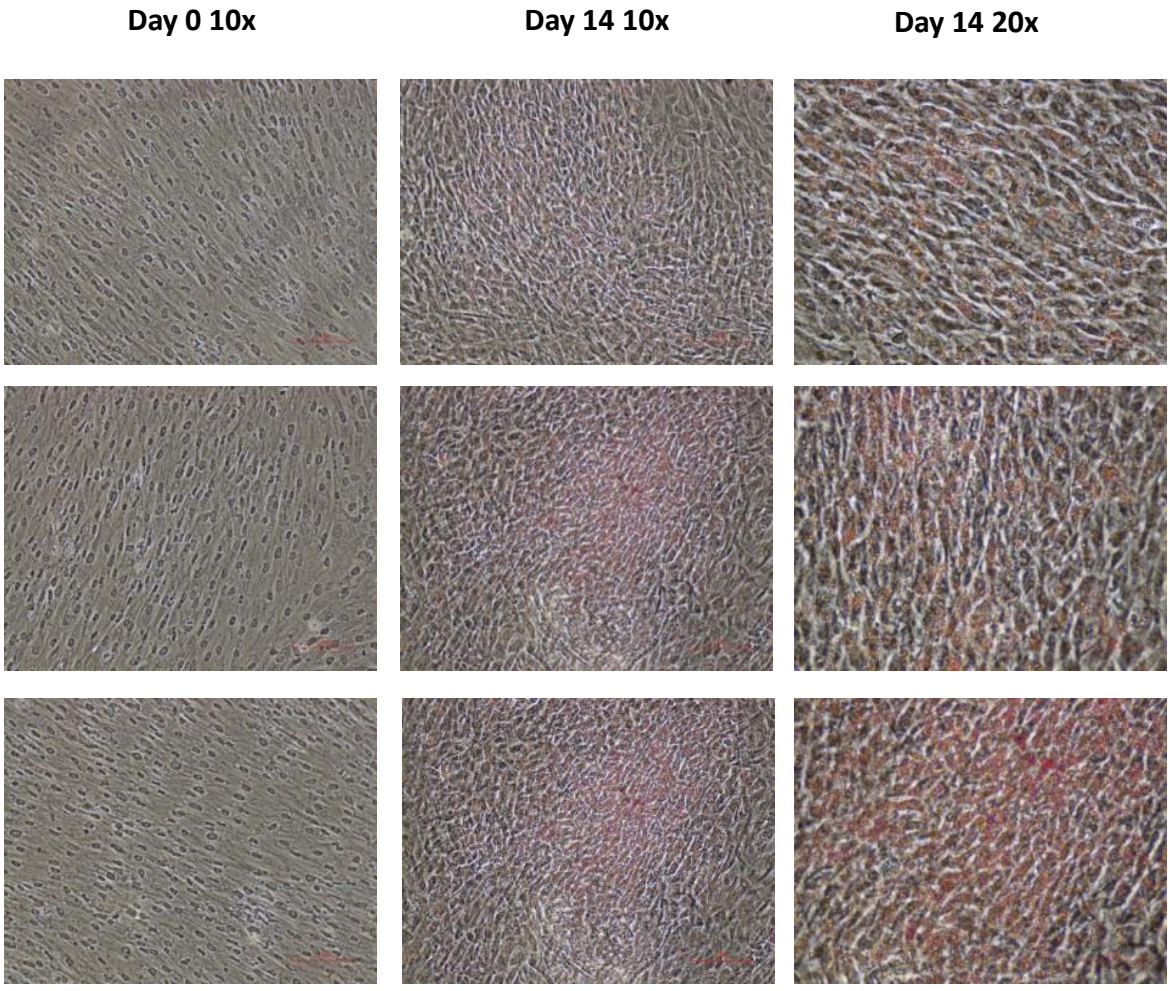

Figure 3.3.1.1 Adipocyte Staining: Oil Red-O staining of Chub-S7 cells at Day 0 and Day 14 of differentiation show a build-up of stained lipid droplets at the end of the differentiation process, indicating cells have developed into mature adipocytes.

3.3.2 Protein Expression of UPR Markers Following Treatment with Tunicamycin

Western blot analysis of samples exposed to tunicamycin over 24, 48 or 72 hours revealed that all ER stress proteins measured experienced changes in expression over time. BiP increased steadily over time, whilst P-PERK and PERK both experienced changes in expression that could indicate that oscillation is occurring (Figures 3.3.2.1 and 3.3.2.2). The ratio of P-PERK to PERK was also studied in order to determine how phosphorylation rate varied independently of the availability of PERK molecules. Studying this ratio also indicated a possible oscillation was occurring, with an inverse pattern to that of P-PERK and PERK (Figure 3.3.2.2). Arbitrary units were used as Western blotting is a semi-quantitative technique that allows comparison between samples but does not provide a quantitative concentration.

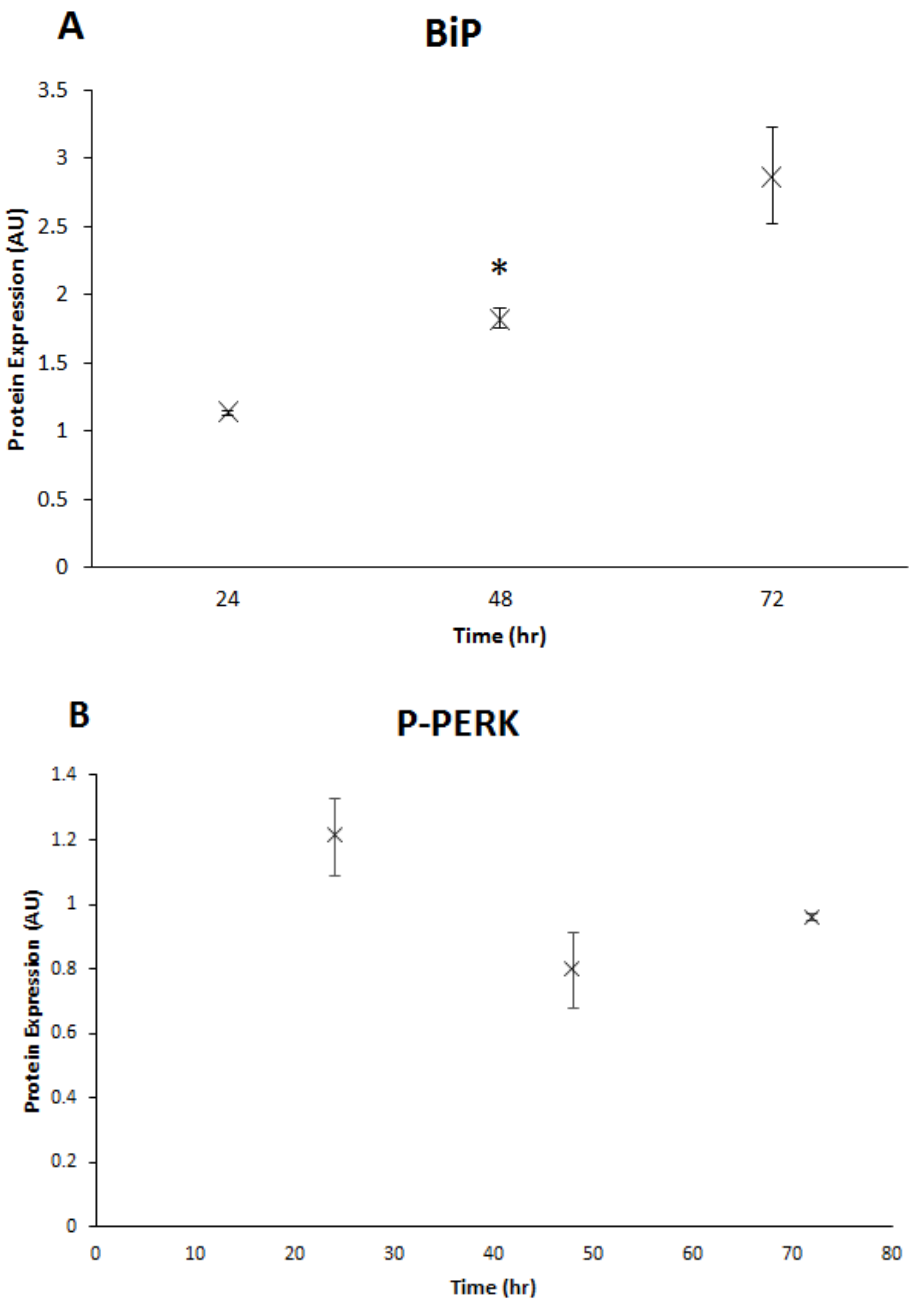

Figure 3.3.2.1 Expression of BiP and P-PERK Proteins following Tunicamycin Treatment: Expression of endoplasmic reticulum (ER) stress proteins **(A)** binding immunoglobulin protein (BiP) and **(B)** phosphorylated protein kinase RNA-like endoplasmic reticulum kinase (phospho-PERK) following treatment with 750ng/ml tunicamycin over 72 hours. BiP expression increased uniformly over time, whilst P-PERK underwent a flux that may indicate oscillation of expression. Statistical analysis was performed for 48 and 72 hour time points vs. 24 hour time point, p-value: * $p < 0.05$.

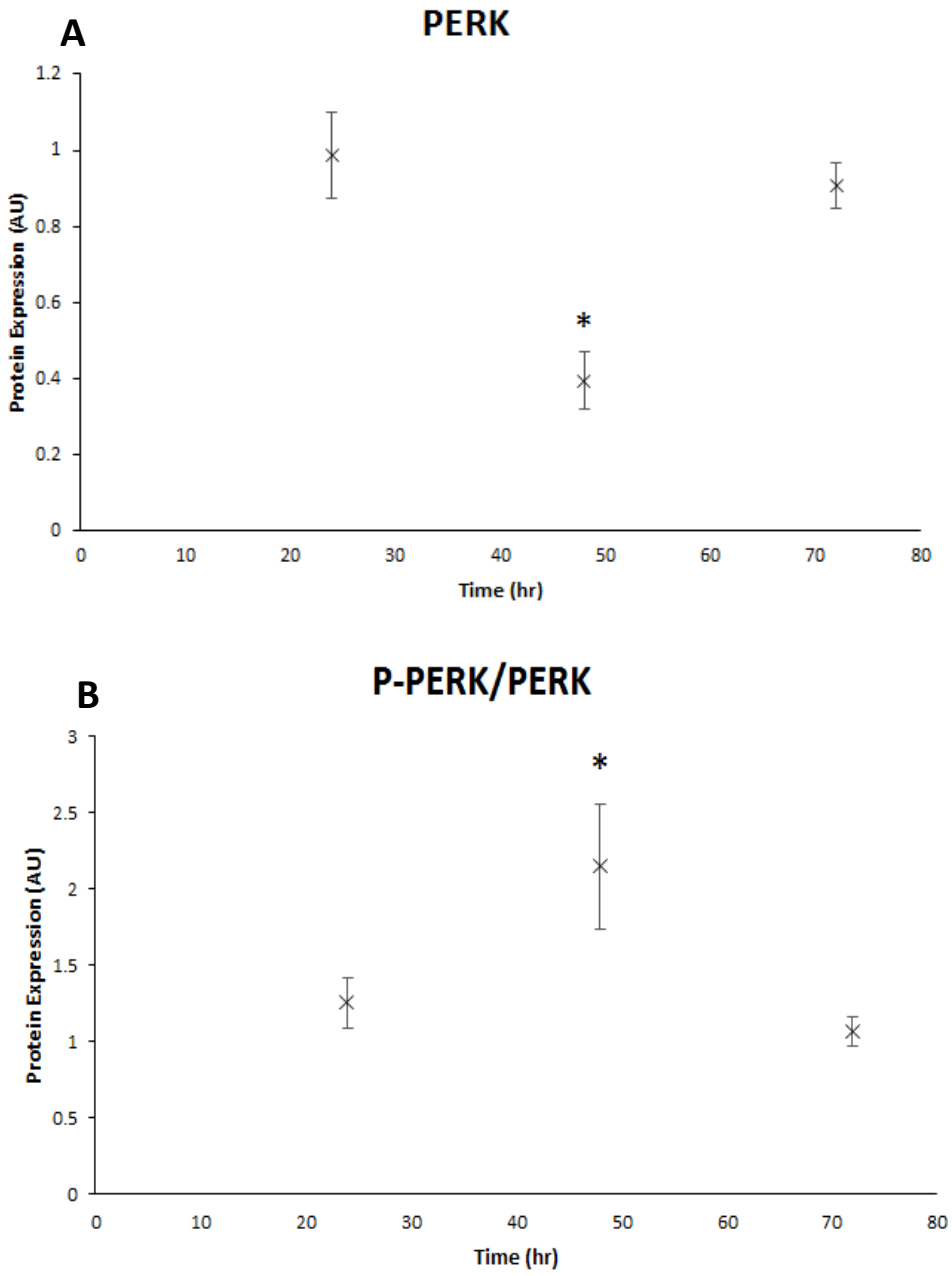

Figure 3.3.2.2 Expression of PERK and Relative P-PERK following Tunicamycin Treatment: Expression of endoplasmic reticulum (ER) stress proteins **(A)** protein kinase RNA-like endoplasmic reticulum kinase (PERK) and **(B)** phospho-PERK (P-PERK) relative to PERK following treatment with 750ng/ml tunicamycin over 72 hours. PERK experienced changes in expression that could indicate oscillation, whilst P-PERK/PERK ratio underwent an increase followed by a decrease, revealing that phosphorylation rate had an inverse pattern to the protein expressions of PERK and P-PERK. Statistical analysis was performed for 48 and 72 hour time points vs. 24 hour time point, p-value: * $p < 0.05$.

3.3.3 Model Creation

A literature search revealed that the UPR involves hundreds of protein and mRNA molecules interconnected by over one thousand interactions (Chakrabarti, Aboulmouna *et al*. 2016). Modelling the entire system would therefore result in an unmanageable number of parameters that would not be reliably estimated; hence it was decided that only one pathway of the three involved in the UPR should be modelled. Studying the UPR process revealed the PERK pathway (Figure 3.3.3) as the most appropriate pathway to choose based on previous models and prior knowledge in the literature. The PERK pathway is important in both the survival and apoptotic processes, and is the sole contributor to the translation attenuation that occurs during the UPR. Additionally, the reactions responsible for the initiation of translation attenuation occur early in the pathway and only involve protein modification rather than gene translation. This immediately simplified the modelling process for the translation attenuation system as only protein data was required. Terms for the translation of genes into proteins would not be needed, and as such gene data would not be necessary to verify this. In summary, the initial section of the PERK pathway was identified as a useful portion of the UPR to model as it has a distinct function that involves few molecules, all of which are proteins. It may therefore provide useful information without the need to include a large number of species that would reduce the reliability of parameterisation. One must take care to avoid overparameterisation when creating a model in order to allow effective prediction of future data points. Overparameterisation increases the complexity of a model to an extent where it fits all or most of the available data, which can lead to poor predictive power when extrapolating to predict new data points. It can also require more computer power,

slowing the process of running the model, and can reduce parameter identifiability – reducing the chance of determining individual parameters. The complexity of a model can also vary depending on what species measurements are possible to collect, as well as what data are available. Model reduction may be necessary in order to assess the appropriate level of complexity. This involves creating models with varying complexity and comparing the resulting outputs using some appropriate measure (e.g. Akaike information criterion (AIC), Bayesian information criterion (BIC). There are also certain limitations associated with the creation of a mathematical model of this biological pathway. For instance, the ability to sufficiently parameterise the model relies upon a comprehensive knowledge of the pathway itself, and whilst the pathway has been studied extensively, there are still some aspects that are unknown which would aid in the parameterisation. Considering the computational power is also important when studying such as complex pathway, as well as the amount of data collected to support it. The dataset collected in this investigation was not large enough to support a large scale model of the entire pathway, and as such a sub-model describing a distinct part of the system was designed instead, allowing it to be adequately characterised and robustly parameterised with regards to the data available. The biochemical reactions involved in the model are shown in Figure 3.3.3. This simple model was created with the intention of expanding it to involve further downstream interactions.

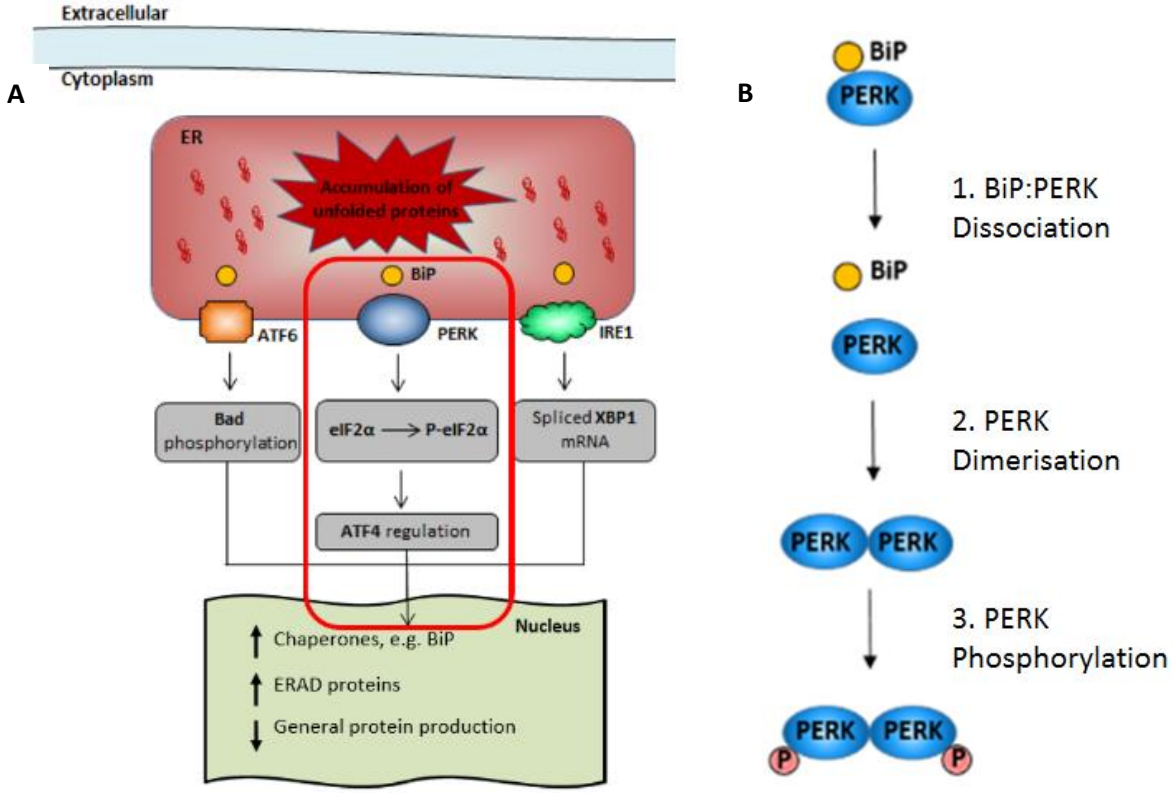

Figure 3.3.3 The PERK Pathway: **(A)** The unfolded protein response initiates a series of cascades involving activating transcription factor 6 (ATF6), protein kinase R-like endoplasmic reticulum kinase (PERK) and inositol requiring enzyme 1 (IRE1), when the endoplasmic reticulum (ER) can no longer cope with the demand of unfolded proteins. ATF6 initiates Bcl-2-associated death promoter (Bad) phosphorylation, whilst inositol requiring enzyme 1 (IRE1) splices x-box protein 1 (XBP1). The PERK pathway (highlighted) specifically activates the translation attenuation system through phosphorylation of the alpha subunit of eukaryotic initiation factor 2 (eIF2α) and upregulation of activating transcription factor 4 (ATF4), which decreases general protein production. ATF6 and IRE1 pathways upregulate endoplasmic-reticulum-associated protein degradation (ERAD) proteins, as well as chaperones such as binding immunoglobulin protein (BiP). *Figure adapted from (Chakrabarti, Aboulmouna et al. 2016)* **(B)** The initial part of the PERK pathway cascade involves three steps: 1. Dissociation of BiP from PERK, 2. PERK dimerisation, and 3. PERK phosphorylation.

The three reactions used for the model included the dissociation of BiP:PERK proteins, followed by PERK dimerisation and phosphorylation (Figure 3.3.3B). This model involved five species: BiP:PERK, BiP, PERK, PERK:PERK and Phospho-PERK, and six parameters. In each of these reactions, the rate is directly proportional to the

product of the concentrations of the reactants, and a mass action kinetics approach was therefore used to create ODEs to describe the pathway. The nonlinear ODEs derived from the chemical reactions are described below:

1. $\frac{d}{dt}(BiP) = kd1(BiP{:}PERK) - ka1(BiP)(PERK)$
2. $\frac{d}{dt}(BiP{:}PERK) = ka1(BiP)(PERK) - kd1(BiP{:}PERK)$
3. $\frac{d}{dt}(PERK) = kd1(BiP{:}PERK) - ka1(BiP)(PERK) + kd2(PERK{:}PERK) - ka2(PERK)(PERK)$
4. $\frac{d}{dt}(PERK{:}PERK) = ka2(PERK)(PERK) - kd2(PERK{:}PERK) + k4(PPERK) - k3(PERK{:}PERK)$
5. $\frac{d}{dt}(PPERK) = k3(PERK{:}PERK) - k4(PPERK).$

These nonlinear ODEs were entered into the Berkeley Madonna programme, and parameters were estimated to permit synthetic simulations. Constraints were placed on the model for simulation and parameter fitting purposes, namely that all species are non-negative (based on the fact that it is not possible to have a negative amount of protein), and model parameters/rate constants, once assigned, are also non-negative.

3.3.4 Parameter Estimation Using Experimental Data

In order to test the goodness-of-fit and better parameterise the model, the experimental data for BiP, PERK and phospho-PERK protein expression (Figure 3.3.2) were entered into the programme and compared with the model output. Using the slider function in Berkeley Madonna, the parameters were adjusted to minimise the differences between the model-generated and experimental data to perform a basic sensitivity analysis. This slider function prompts the model to re-run instantly with each movement of a slider, displaying the new solution immediately and allowing fine-tuning of the model output. The output from this initial model was biologically qualitatively realistic, as determined using biological insight to study the geometric shape of the output and match the long term data to known biological behaviours of the system (Figure 3.3.4).

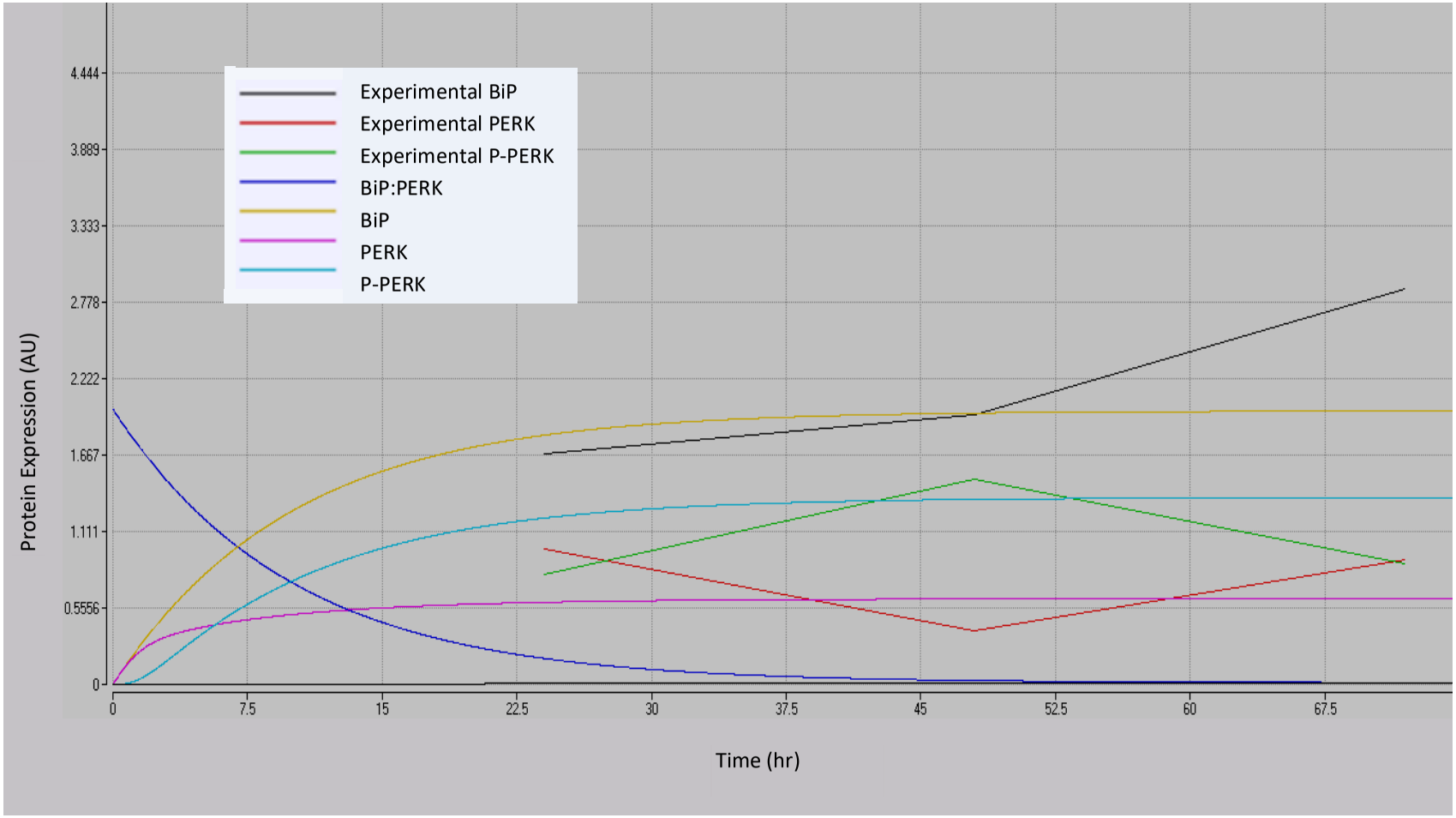

Figure 3.3.4 PERK Pathway Model Output against Experimental Data: Experimental data for the initial part of the protein kinase R-like endoplasmic reticulum kinase (PERK) pathway of the unfolded protein response (UPR) was collected by treating Chub-S7 adipocytes with 750ng/ml tunicamycin for 24, 48 or 72 hours and analysing the protein expression of binding immunoglobulin protein (BiP), PERK and Phospho-PERK (P-PERK). A mathematical model of this pathway was created using six nonlinear ordinary differential equations. These included terms for the BiP:PERK complex (blue), unbound BiP (yellow), PERK (pink) and P-PERK (blue). Parameters were adjusted to create an output that most represented the available experimental data. The model output was biologically qualitatively accurate and indicated that most changes in protein expression occurred within the first 12 hours of treatment. Lines between experimental data points represent linkages between discrete mean values for data collected and are not true trajectories over time.

As the experimental data used to parameterise the model were only over three time points (24hr, 48hr and 72hr), this was intended to give a better initial indicator of what order of magnitude the parameters might take, with the knowledge that more regular time points would be needed to reliably parameterise the model. A summary of the model data is displayed in Table 3.3.5, showing the initial conditions and values for species, as well as parameter values obtained from the model. There is limited data published on concentrations of proteins present in unstressed conditions, so for this model biological insight was used and the BiP:PERK complex was the only species with an initial condition more than zero, as this complex is known to be present in unstressed conditions, and dissociate in conditions of stress (Grootjans, Kaser *et al*. 2016). The value for the initial condition of the BiP:PERK complex was also considered as an unknown parameter as this cannot be readily measured or assigned. This initial condition parameter was then adjusted along with parameter values to best fit the experimental data.

A

Species	Initial Condition (A.U.)	Known Values (A.U.)		
		24hr	48hr	72hr
BiP	0	1.67	1.96	2.87
BiP:PERK	2	-	-	-
PERK	0	0.99	0.39	0.91
PERK:PERK	0	-	-	-
Phospho-PERK	0	0.80	1.49	0.88

B

Parameter	Description	Parameter Value	Parameter Unit
kd1	Dissociation of BiP and PERK	0.1	Arbitrary
ka1	Association of BiP and PERK	0.001	Arbitrary
ka2	Association of PERK molecules to form dimer	1.4	Arbitrary
kd2	Dissociation of PERK dimer	0.4	Arbitrary
k3	Phosphorylation of PERK dimer	0.001	Arbitrary
k4	De-phosphorylation of P-PERK dimer	0.2	Arbitrary

Table 3.3.5 Species and Parameter Details of Initial PERK Model: A mathematical model of part of the protein kinase R-like endoplasmic reticulum kinase (PERK) pathway of the unfolded protein response (UPR) was created using nonlinear ordinary differential equations and was compared with experimental data. These tables describe **(A)** initial conditions and known values for the species in the model and **(B)** parameter values for the model. Arbitrary units were used as the protein measurement technique is semi-quantitative and gives non-dimensional results.

3.4 Discussion

This study was designed to produce a mathematical model of the UPR, with a complexity that would allow an appropriate compromise between biological detail and parameter estimation. The experimental data collected during this study provided an insight into the effect of tunicamycin on Chub-S7 cells, revealing that whilst BiP expression increased uniformly over time, PERK and P-PERK appeared to have a more cyclic expression profile. Developing a mathematical model of the initial part of the PERK pathway highlighted that focussing on one particular arm of the UPR may allow the creation of more manageable models, whilst retaining biological accuracy. This model also indicated that much of the change in protein expression might occur within the first 12 hours of treatment, providing useful information regarding future experimental procedures.

Experimental data collected during this research supported the numerous studies showing that tunicamycin alters the expression of UPR proteins (Oslowski and Urano 2011, Hou, Gutschmidt *et al*. 2014, Wang, Wang *et al*. 2015), however this had not been identified in differentiated Chub-S7 cells before. This data also highlighted how different proteins respond to tunicamycin treatment in different ways. The expression of BiP, a chaperone which binds to each of the sensor proteins within the UPR and acts as a switch to control the UPR response, increased steadily, whilst PERK and P-PERK expression appeared to vary, with a possible cyclic expression profile. This is the first experimental evidence that supports the outcome of the model created by Erguler *et al.* which suggested that many of the system components dramatically oscillate between low and high activity states (Erguler, Pieri *et al*. 2013).

This cyclic expression was also observed with the P-PERK/PERK ratio, which exhibits the inverse expression profile to both PERK and P-PERK. This ratio provides information on the rate of phosphorylation of PERK, and these results highlight the importance of studying the ratio in order to better understand the activation of the UPR. The ratio is important as the rate of phosphorylation is a better indicator of the level of ER stress occurring compared to the raw expression of either PERK or P-PERK, as it represents the protein's capacity for signal transduction (PERK) vs. its activation (P-PERK) (Bass, Wilkinson *et al*. 2017). These results demonstrate that the ratio can greatly differ from the raw expression values, and as such it is important to study both types of data.

The biologically qualitatively realistic output from the mathematical model, which consisted of six nonlinear ODEs, highlighted that modelling each particular arm of the UPR separately may allow more accurate parameter estimation without compromising biological detail. This identified a novel solution to the problems experienced by Rutkowski and Erguler regarding the difficulty of parameter estimation when model complexity is increased to prioritise accurate biological detail. Attempts to compare parameter values from this model with those developed by Rutkowski and Erguler highlighted the large variety in model development, as only two similar parameters were included in this model and Erguler's, whilst Rutkowski's model only included parameters for the translation, transcription and degradation of protein and mRNA rather than the interactions between them.

Results from this study have also demonstrated the importance of combining experimental data with mathematical models. Studying the experimental data alone

provided novel data indicating that tunicamycin alters the expression of different UPR proteins in different ways. Using these data to parameterise and validate the mathematical model provided information regarding time points where most changes are likely to occur, which can be used to more appropriately plan future experiments. The success of this initial model indicated that collecting more granular time series data, along with developing ODEs that better represent the data collected, may be worthwhile to more accurately estimate the activity of proteins not directly measured through experimental procedures. This would also allow further analysis into the cyclic expression of proteins in the translation attenuation system.

Whilst the data collected during this study provided a broad overview of the expression profiles of the proteins studied, it also highlighted the importance of obtaining data on acute expression to determine the immediate impact of tunicamycin on protein expression. As such, this study has provided important information not only with regards to the data collected and the model developed, but also with regards to which time points to study in the future and how often to collect data in order to support an improved mathematical model of the UPR.

3.5 Conclusions

This study has demonstrated that tunicamycin induces ER stress in Chub-S7 cells, resulting in varying responses in UPR protein expression profiles. It has also provided the first experimental evidence in support of Erguler's theory that proteins involved in the translation attenuation system experience an oscillating expression profile. The mathematical model developed was qualitatively biologically accurate, and identified a novel solution to the common problem of modelling biological systems by modelling individual functions of a system rather than the system itself. This chapter has contributed to the first aim of this thesis, to create a mathematical model of a pathway in the unfolded protein response using experimental data.

CHAPTER 4:

Studying the Unfolded Protein Response over Time

4.1 Introduction

4.1.1 Biological Data in the Parameterisation Process

In recent years, the use of *in silico* modelling to study biological systems has become more widespread, allowing users to analyse complex high-dimensional systems more easily. These biological models are important as they allow users to view simulations of the system under various conditions, as well as make informed decisions based on predictions that the model makes. In order for these models to make accurate simulations and predictions, they must be validated using as large a data set as possible, as well as expert knowledge (Hussain, Langmead *et al*. 2015). One of the challenges encountered when creating a biological model is finding values for parameters that allow the model to replicate biological data accurately. Once these parameters have been determined, however, the model can be used to simulate the activity of the biological system under a variety of conditions. Such models of biological systems are relevant to communicate concepts, test hypotheses, enhance the understanding of the dynamic characteristics of the system, and as such help to drive forward biological research objectives (O'Hara, Livigni *et al*. 2016).

In order to parameterise a model, experimental data must be collected with the understanding that they are likely to contain some degree of error or inaccuracy. There are many inaccuracies involved with collecting biological data in a living system and it is in the researcher's interest to reduce these as much as possible. In order to decrease the impact of any inaccuracies, a surplus of data can be collected to compensate for any uncertainty in measurements (Ledder 2013). Collecting multiple biological samples for the same data point allows any inconsistencies to be identified

and a suitable procedure, such as removal of an inconsistent point or artefact, to be carried out. Considering each averaged time point in conjunction with the rest of the time series data also allows the identification of potential inaccurate results, or outliers, and as such a time series with frequent time points which each have multiple sample replicates limits the level of inaccuracy within the data (Wooley and Lin 2005).

4.1.2 Time Series Data

Time series data, a collection of data points over a specific period of time that represents the state variables over that time-frame, are often used for the parameterisation of models (Guo, Abdelraouf *et al*. 2011, Mochan, Swigon *et al*. 2014, Cantone, Santos *et al*. 2017). The more frequent the time points, the more reliable and useful the data are in the parameterisation process, and the finer granularity the data will have. The previous chapter discussed an initial model for the unfolded protein response (UPR), however in order to create a more robustly parameterised, fine-tuned and detailed model, a larger time series dataset was required. Collecting time series data is not only useful for model parameterisation and validation, but can also provide detailed information about the biological system directly. Currently in the literature, there is a lack of time series data for the UPR, with most researchers looking at just one time point whilst comparing a treatment with a control. Studies that have collected samples at multiple time points have usually studied a limited number of time points over a matter of hours. For instance, one of the more comprehensive time series investigations into the UPR, carried out by Mintz *et al*. in 2008, studied a restricted number of time points, four, over a short

time frame of 24 hours (Mintz, Vanderver *et al*. 2008). The lack of sufficient time series data available has limited our understanding of how the UPR varies over a longer time-frame – information which may shed light on how certain interactions impact on the total response, and at what point the UPR undergoes the most flux or enters a steady state.

The aim of the research in this chapter was to collect a more granulated, comprehensive time series dataset of the UPR over a longer time-frame than has previously been studied. The ambition was to understand how the adipocyte UPR responds to tunicamycin over time, as well as to develop and extend the mathematical model described in the previous chapter.

4.2 Methods

4.2.1 Cell Culture

Adipogenesis was induced in Chub-S7 preadipocytes for 14 days. Lipid accumulation was confirmed as explained in Chapter 3. Cells were exposed to 750ng/ml tunicamycin for the following lengths of time: 0hr, 30 mins, 1hr, 2hr, 4hr, 6hr, 12hr, 18hr, 24hr, 30hr, 36hr, 46hr, 48hr, 54hr, 60hr, 66hr, or 72hr, with fresh Tunicamycin exposure every 24 hours. Control cells were grown in the same manner and treated with the equivalent concentration of DMSO vehicle (Figure 4.2.1). Following treatment, cells were harvested and protein extraction was carried out to allow analysis by Western blot. Six samples at each time point were collected, processed and analysed in order to increase the reliability of the results.

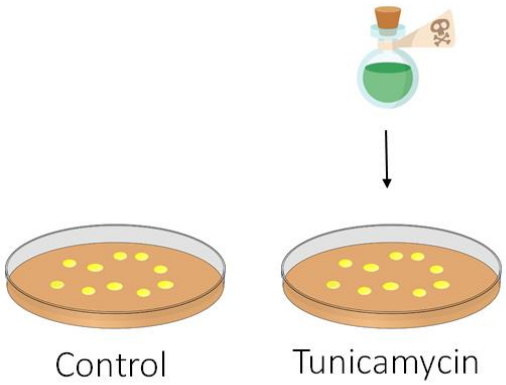

Figure 4.2.1 Treatment of Adipocytes with Tunicamycin: Chub-S7 adipocytes were grown and differentiated before being treated with tunicamycin (750ng/ml). Control cells were grown in the same manner and treated with the equivalent concentration of DMSO. Protein samples were collected at 17 time points over 72 hours (0hr, 30 mins, 1hr, 2hr, 4hr, 6hr, 12hr, 18hr, 24hr, 30hr, 36hr, 46hr, 48hr, 54hr, 60hr, 66hr, or 72hr).

4.2.2 Model Development and Parameterisation

Following protein extraction and analysis, biological data from the 17 time points were imported into Berkeley Madonna and compared against the previous model simulation. The ODEs were re-assessed for biological accuracy using information from the previous chapter regarding appropriate model complexity, and the slider function was used within Berkeley Madonna to give an initial estimate for the unknown parameter values. The *Curve Fit* function was then utilised to computationally identify parameter values that resulted in the closest match between the model simulation and biological data. The residual sum of squares was calculated for the species in each model and was used as a measure in order to assess whether changes to model parameters resulted in a closer fit to experimental data.

4.3 Results

4.3.1 ER Stress Proteins Respond in Different ways to Tunicamycin Treatment over Time

As anticipated, the expression of all UPR proteins analysed was altered following treatment with tunicamycin, a known inducer of ER stress. The expression of BiP, a chaperone that dissociates from each sensor protein to assist with protein folding during stress, increased steadily over time, reaching a peak of 9.5-fold its original expression level over the 72 hours (Figure 4.3.2.1).

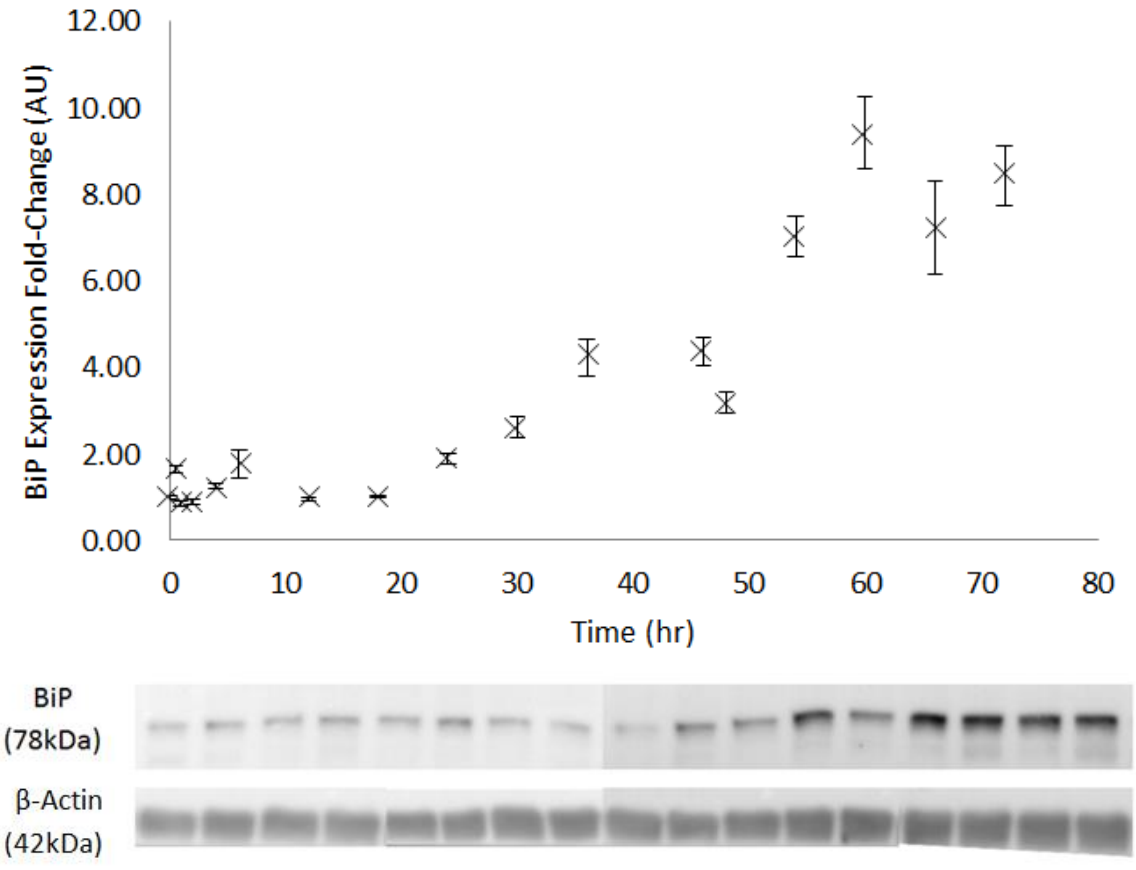

Figure 4.3.1.1 BiP Expression following Tunicamycin Treatment: Following treatment of Chub-S7 adipocytes with 750ng/ml tunicamycin, binding immunoglobulin protein (BiP) expression increased steadily over 72 hours, peaking at 9.5-fold its original expression level. This is demonstrated in both the graph and via the Western blot images of BiP and the housekeeping control protein, β-Actin.

P-eIF2α is involved in the translation attenuation system through inhibiting guanosine diphosphate (GDP)/guanosine triphosphate (GTP) exchange. These results indicated that P-eIF2α underwent an initial peak in expression before experiencing a slight oscillation (Figure 4.3.1.2).

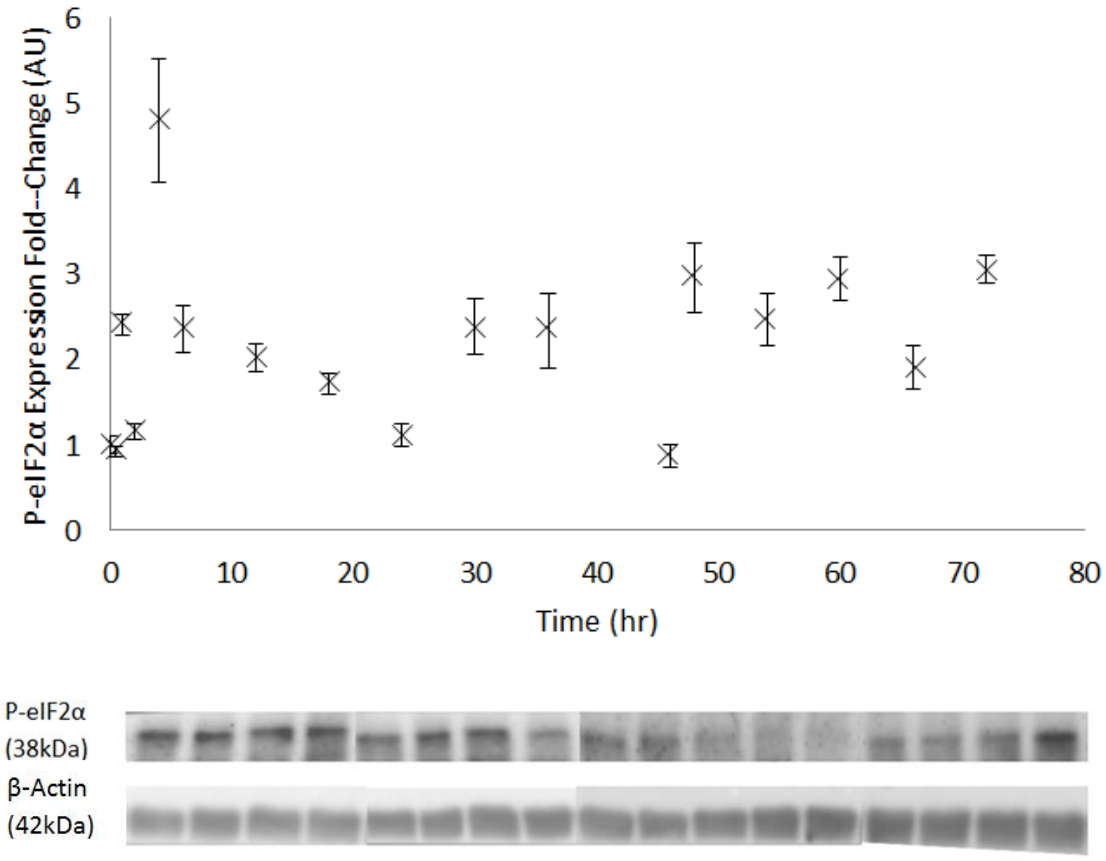

Figure 4.3.1.2 P-eIF2α Expression following Tunicamycin Treatment: The expression of phosphorylated eukaryotic initiation factor 2 alpha (P-eIF2α) was measured in Chub-S7 adipocytes following treatment with 750ng/ml tunicamycin over time. As illustrated in the graph and Western blot images, P-eIF2α expression underwent an initial peak before experiencing a slight oscillation.

Expression of eIF2α, the inactive form of P-eIF2α which is activated through phosphorylation by P-PERK, varied the most out of the three proteins studied and exhibited a more prominent oscillation. There was a large 70% reduction in expression within the first 30 minutes, after which oscillation occurred with amplitude increasing over time (Figure 4.3.1.3).

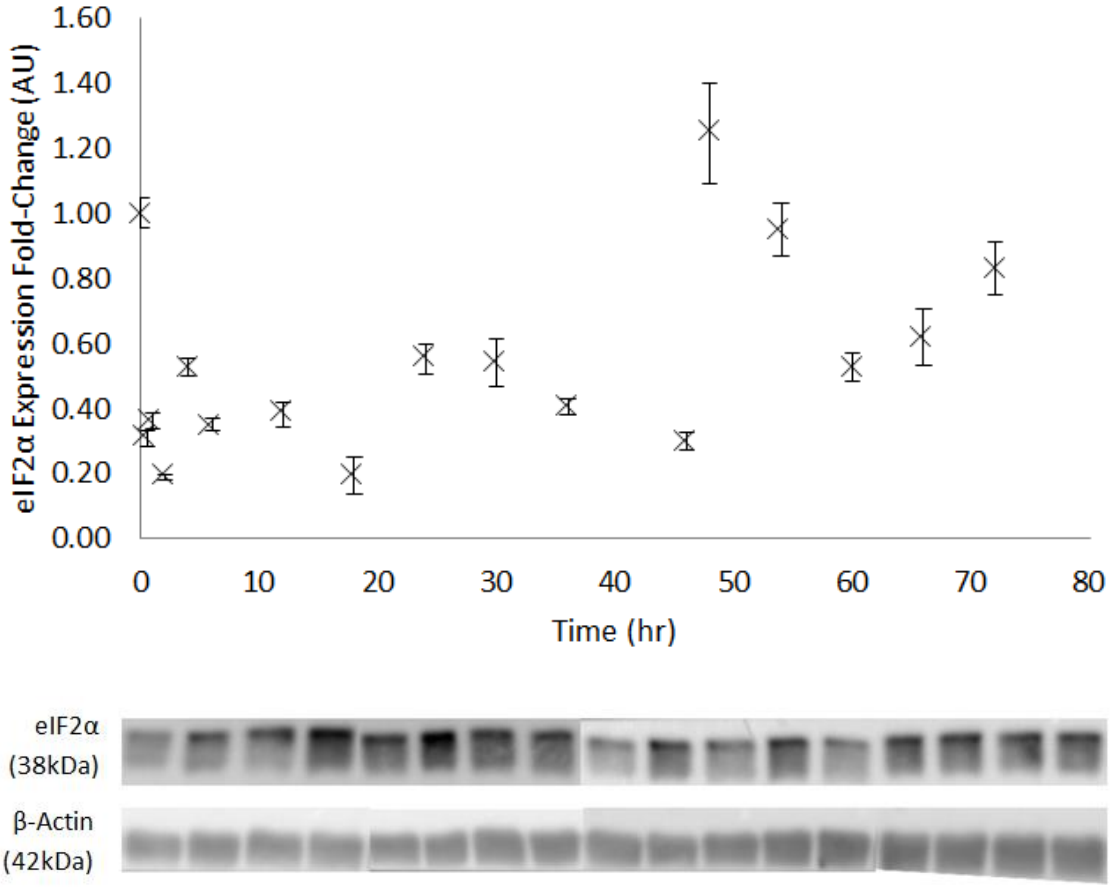

Figure 4.3.1.3 eIF2α Expression following Tunicamycin Treatment: Eukaryotic initiation factor 2 alpha (eIF2α) protein expression was analysed in Chub-S7 adipocytes following treatment with 750ng/ml tunicamycin over time. Western blot analysis revealed an oscillation of eIF2α protein expression. This is demonstrated in both the graph and Western blot images, along with the β-Actin control.

The perceived oscillatory effect of P-eIF2α and eIF2α is confirmed when taking into account the ratio of the two proteins. This is an important process to understand if

the change in P-eIF2α is due to an altered rate of phosphorylation, or because there is a variation in the concentration of eIF2α available to be phosphorylated. These results illustrated a clear oscillation whereby the relative expression of P-eIF2α rises rapidly within the first 6 hours before falling and continuing to oscillate between 3-fold and 9-fold of the resting state (Figure 4.3.1.4).

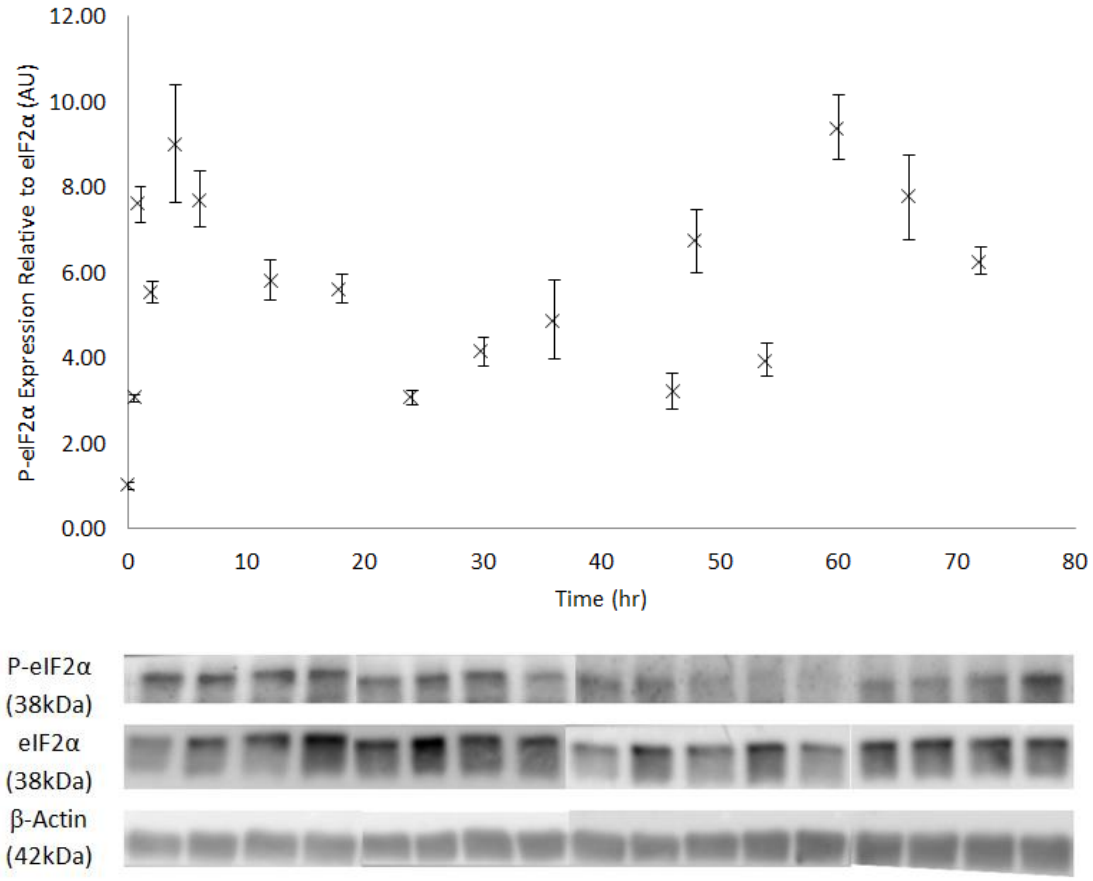

Figure 4.3.1.4 P-eIF2α Expression Relative to eIF2α following Tunicamycin Treatment: Expression of phosphorylated eukaryotic initiation factor 2 alpha (P-eIF2α) relative to its un-phosphorylated counterpart, eIF2α, was analysed in response to treatment with 750ng/ml tunicamycin in Chub-S7 adipocytes. Analysis revealed a clear oscillation of phosphorylation rate that altered between 3-fold and 9-fold of the resting state value. Western blot images are provided alongside the β-Actin control.

4.3.2 Comprehensive Time Series Data Allowed More Accurate Model Simulation

Expanding on knowledge gained from creating the mathematical model in the previous chapter, the process of extending the model to incorporate these new biological results was assisted by creating a biological schematic of the system being modelled (Figure 4.3.2.1). The previous model provided information on the ideal complexity for this model, ensuring only relevant interactions that could be reliably parameterised, or are essential to the biological integrity, were represented.

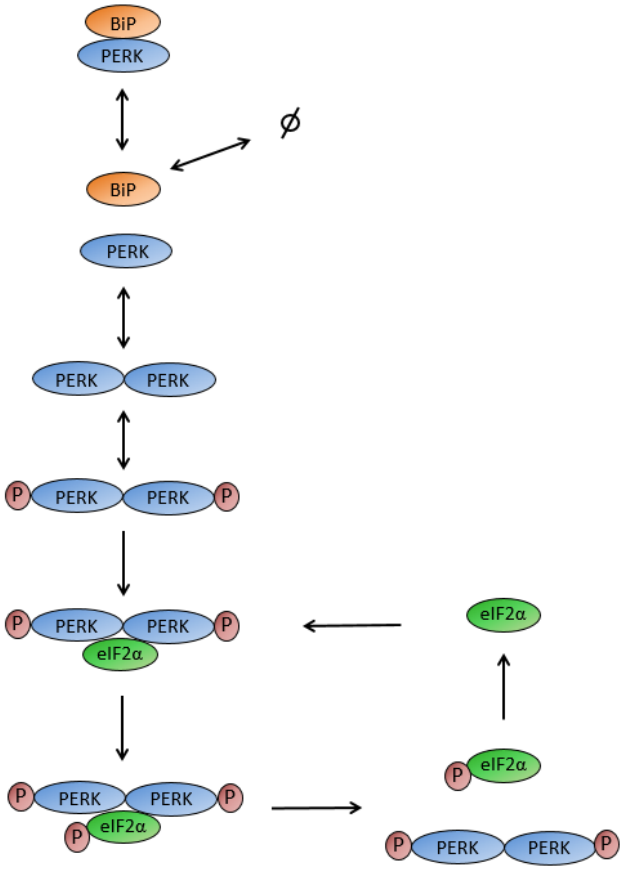

Figure 4.3.2.1 Model Schematic for PERK Pathway: A schematic of the protein kinase RNA-like endoplasmic reticulum kinase (PERK) pathway within the unfolded protein response (UPR) was developed, including only those proteins essential to the initiation of translation attenuation. This reduced complexity enabled kinetic equations to be created in order to develop a mathematical model of the pathway. Proteins involved include binding immunoglobulin protein (BiP), PERK and eukaryotic initiation factor 2 alpha (eIF2α). P indicates a phosphate group added during phosphorylation. Ø denotes BiP leaving the system as it enters other pathways not considered here.

Using the schematic in Figure 4.3.2.1, a set of kinetic equations was developed to aid in the translation of the schematic into the corresponding ODEs. The kinetic equations include the parameters involved in each reaction, and are displayed in equations 1-6 below, where:

BiP = binding immunoglobulin protein,

PERK = protein kinase RNA-like endoplasmic reticulum kinase,

PPERK = phosphorylated PERK,

eIF2α = eukaryotic initiation factor 2 alpha,

PeIF2α = phosphorylated eIF2α,

BiPX = BiP bound to proteins other than PERK (such as other UPR sensors or unfolded proteins),

PERK:PERK = PERK dimer,

PPERK:PPERK = phosphorylated PERK dimer,

PPERK:PPERK:eIF2α = PPERK dimer in complex with eIF2α,

PPERK:PPERK:PeIF2α = PPERK dimer in complex with PeIF2α:

1. $BiP{:}PERK \underset{ka1}{\overset{kd1}{\rightleftharpoons}} BiP + PERK$

2. $BiP \underset{k15}{\overset{k11}{\rightleftharpoons}} BiPX$

3. $PERK + PERK \underset{kd2}{\overset{ka2}{\rightleftharpoons}} PERK{:}PERK$

4. $PERK{:}PERK \underset{k4}{\overset{k3}{\rightleftharpoons}} P\text{-}PERK{:}P\text{-}PERK$

5. $P\text{-}PERK{:}P\text{-}PERK + eIF2\alpha \underset{kd5}{\overset{ka5}{\rightleftharpoons}} P\text{-}PERK{:}P\text{-}PERK{:}eIF2\alpha \xrightarrow{k6} P\text{-}PERK{:}P\text{-}PERK{:}P\text{-}eIF2\alpha \xrightarrow{k7} P\text{-}PERK{:}P\text{-}PERK + P\text{-}eIF2\alpha$

6. $P\text{-}eIF2a \xrightarrow{k8} eIF2\alpha$

The ODEs created from the schematic and kinetic equations formed the base of the new model, and are described in differential equations 7-16, where:

BiP = binding immunoglobulin protein,

PERK = protein kinase RNA-like endoplasmic reticulum kinase,

PPERK = phosphorylated PERK,

eIF2α = eukaryotic initiation factor 2 alpha,

PeIF2α = phosphorylated eIF2α,

BiPX = BiP bound to proteins other than PERK (such as other UPR sensors or unfolded proteins),

BiP:PERK = BiP in complex with PERK,

PERK:PERK = PERK dimer,

PPERK:PPERK = phosphorylated PERK dimer,

PPERK:PPERK:eIF2α = PPERK dimer in complex with eIF2α,

PPERK:PPERK:PeIF2α = PPERK dimer in complex with PeIF2α:

7. $\frac{d}{dt}(BiP{:}PERK) = ka1(BiP)(PERK) - kd1(BiP{:}PERK)$

8. $\frac{d}{dt}(BiP) = kd1(BiP{:}PERK) - ka1(BiP)(PERK) - k11(BiP) + k15(BiPX)$

9. $\frac{d}{dt}(BiPX) = k11(BiP) - k15(BiPX)$

10. $\frac{d}{dt}(PERK) = kd1(BiP{:}PERK) - ka1(BiP)(PERK) + kd2(PERK{:}PERK) - ka2(PERK)(PERK)$

11. $\frac{d}{dt}(PERK{:}PERK) = ka2(PERK)(PERK) - kd2(PERK{:}PERK) + k4(PPERK{:}PPERK) - k3(PERK{:}PERK)$

12. $\frac{d}{dt}(PPERK{:}PPERK) = k3(PERK{:}PERK) - k4(PPERK{:}PPERK) + kd5(PPERK{:}PPERK{:}eIF2\alpha) - ka5(PPERK{:}PPERK)(eIF2\alpha) + k7(PPERK{:}PPERK{:}PeIF2\alpha)$

13. $\frac{d}{dt}(PPERK{:}PPERK{:}eIF2\alpha) = ka5(PPERK{:}PPERK)(eIF2\alpha) - kd5(PPERK{:}PPERK{:}eIF2\alpha) - k6(PPERK{:}PPERK{:}eIF2\alpha)$

14. $\frac{d}{dt}(PPERK{:}PPERK{:}PeIF2\alpha) = k6(PPERK{:}PPERK{:}eIF2\alpha) - k7(PPERK{:}PPERK{:}PeIF2\alpha)$

15. $\frac{d}{dt}(PeIF2\alpha) = k7(PPERK{:}PPERK{:}PeIF2\alpha) - k8(PeIF2\alpha)$

16. $\frac{d}{dt}(eIF2\alpha) = k8(PeIF2\alpha) + kd5(PPERK{:}PPERK{:}eIF2\alpha) - ka5(PPERK{:}PPERK{:}eIF2\alpha)$

In order to compare the model output to experimental data, the following terms were added to express the total amount of each protein measured. These terms were created by summing the different states involving each protein, and are described in equations 17-19, where:

BiP = binding immunoglobulin protein,

PERK = protein kinase RNA-like endoplasmic reticulum kinase,

PPERK = phosphorylated PERK,

eIF2α = eukaryotic initiation factor 2 alpha,

PeIF2α = phosphorylated eIF2α,

BiPX = BiP bound to proteins other than PERK (such as other UPR sensors or unfolded proteins),

PPERK:PPERK = phosphorylated PERK dimer,

PPERK:PPERK:eIF2α = PPERK dimer in complex with eIF2α,

PPERK:PPERK:PeIF2α = PPERK dimer in complex with PeIF2α,

BiPtot = total BiP protein measured via Western blot,

eIF2αtot = total eIF2α measured via Western blot,

PeIF2αtot = total PeIF2α measured via Western blot:

17. $$\frac{d}{dt}(BiPtot) = k12\big(ka1(BiP)(PERK) - kd1(BiP{:}PERK)\big) + k13\big(kd1(BiP{:}PERK) - ka1(BiP)(PERK) - k11(BiP) + k15(BiPX)\big) + k14\big(k11(BiP) - k15(BiPX)\big)$$

18. $$\frac{d}{dt}(eIF2\alpha tot) = k17\big(k8(PeIF2\alpha) + kd5(PPERK{:}PPERK{:}eIF2\alpha) - ka5(PPERK{:}PPERK)(eIF2\alpha)\big) + k18\big(ka5(PPERK{:}PPERK)(eIF2\alpha) - kd5(PPERK{:}PPERK{:}eIF2\alpha) - k6(PPERK{:}PPERK{:}eIF2\alpha)\big)$$

19. $$\frac{d}{dt}(PeIF2\alpha tot) = k19\big(k6(PPERK{:}PPERK{:}eIF2\alpha) - k7(PPERK{:}PPERK{:}PeIF2\alpha)\big) + k20(k7(PPERK{:}PPERK{:}PeIF2\alpha) - k8(PeIF2\alpha))$$

Including terms that express the total amount of each protein measured was necessary as the Western blot method of protein measurement incorporates the entire protein of interest in the result. This is regardless of whether it is bound to another protein in a complex, or if it is in its free form, and thus the ODEs used must reflect this.

An ODE that represents the ratio of P-eIF2α to eIF2α was also added due to the biological significance of this ratio that was observed with the data, allowing more thorough study of the phosphorylation event. This ODE was generated using the quotient rule, which can be used to find the derivative of a function that is the ratio of two differentiable functions. For example, if $f(t) = g(t)/h(t)$, where *g* and *h* are both differentiable and *h* does not equal 0, then the derivative of *f(t), f'(t),* is:

$$f'(t) = \frac{g'(t)h(t) - g(t)h'(t)}{[h(t)]^2}$$

As such, if *f* represents the ratio of P-eIF2α to eIF2α (P-eIF2α:eIF2α), *g* represents the total P-eIF2α measured by Western blot (PeIF2αtot) and *h* represents the total eIF2α measured by Western blot (eIF2αtot), the following equation can be written, where:

PeIF2α:eIF2α = ratio of phosphorylated eukaryotic initiation factor 2 alpha (PeIF2α) and its unphosphorylated counterpart eIF2α,

eIF2α = eukaryotic initiation factor 2 alpha,

PeIF2α = phosphorylated eIF2α,

PPERK:PPERK = phosphorylated PERK dimer,

PPERK:PPERK:eIF2α = PPERK dimer in complex with eIF2α,

PPERK:PPERK:PeIF2α = PPERK dimer in complex with PeIF2α:

20.
$$\frac{d}{dt}(PeIF2\alpha{:}\,eIF2\alpha) = k21((\Big(k17\big(k8(PeIF2\alpha) + kd5(PPERK{:}\,PPERK{:}\,eIF2\alpha) - ka5(PPERK{:}\,PPERK)(eIF2\alpha)\big) + k18\big(ka5(PPERK{:}\,PPERK)(eIF2\alpha) - kd5(PPERK{:}\,PPERK{:}\,eIF2\alpha) - k6(PPERK{:}\,PPERK{:}\,eIF2\alpha)\big)\Big)(PeIF2\alpha tot) - \Big(k19\big(k6(PPERK{:}\,PPERK{:}\,eIF2\alpha) - k7(PPERK{:}\,PPERK{:}\,PeIF2\alpha)\big) + k20\big(k7(PPERK{:}\,PPERK{:}\,PeIF2\alpha) - k8(PeIF2\alpha)\big)\Big)(eIF2\alpha tot))/(eIF2\alpha)^2$$

Once the set of ODEs were entered into Berkeley Madonna, the available slider function was utilised. This allows the user to manually adjust the model output to match the experimental data as best as possible. The residual sum of squares was also calculated, which gave an indicator of the discrepancy between the data and the model. The outputs of this model are documented in Figure 4.3.2.2 and Figure 4.3.2.3, with the residual sum of squares for each species shown in Table 4.3.2.4.

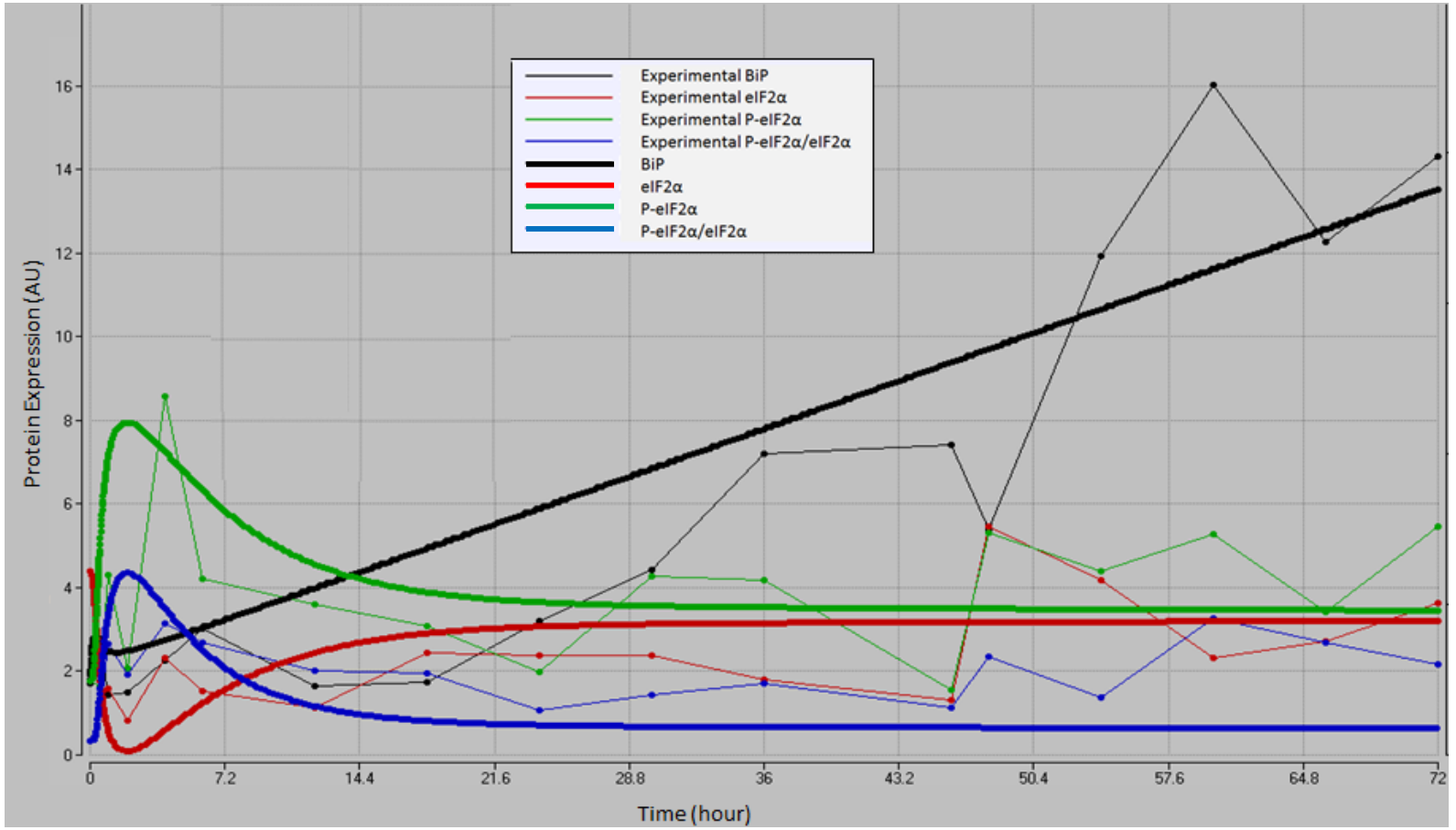

Figure 4.3.2.2 Model Output for PERK Pathway following Manual Parameterisation: A mathematical model of the protein kinase RNA-like endoplasmic reticulum kinase (PERK) pathway of the unfolded protein response was developed and parameterised manually using experimental data, where Chub-S7 adipocytes were treated with 750ng/ml tunicamycin over 72 hours. Proteins measured include binding immunoglobulin protein (BiP): black; eukaryotic initiation factor 2α (eIF2α): red; phospho-eukaryotic initiation factor 2α (P-eIF2α): green; and P-eIF2α/eIF2α ratio: blue. Bold lines represent model output, dotted lines represent experimental data. Lines between experimental data points represent linkages between discrete mean values for data collected and are not true trajectories over time. Initial conditions are as follows (AU) BiP:PERK (10), BiP (1), BiPX (20), PERK (0), PERK:PERK (0), PPERK:PPERK (0), eIF2α (10), PPERK:PPERK:eIF2α (0), PPERK:PPERK:PeIF2α (0), PeIF2α (0), BiPtot (1.70), eIF2αtot (4.38), PeIF2αtot (1.76), PeIF2α/eIF2α (0.35).

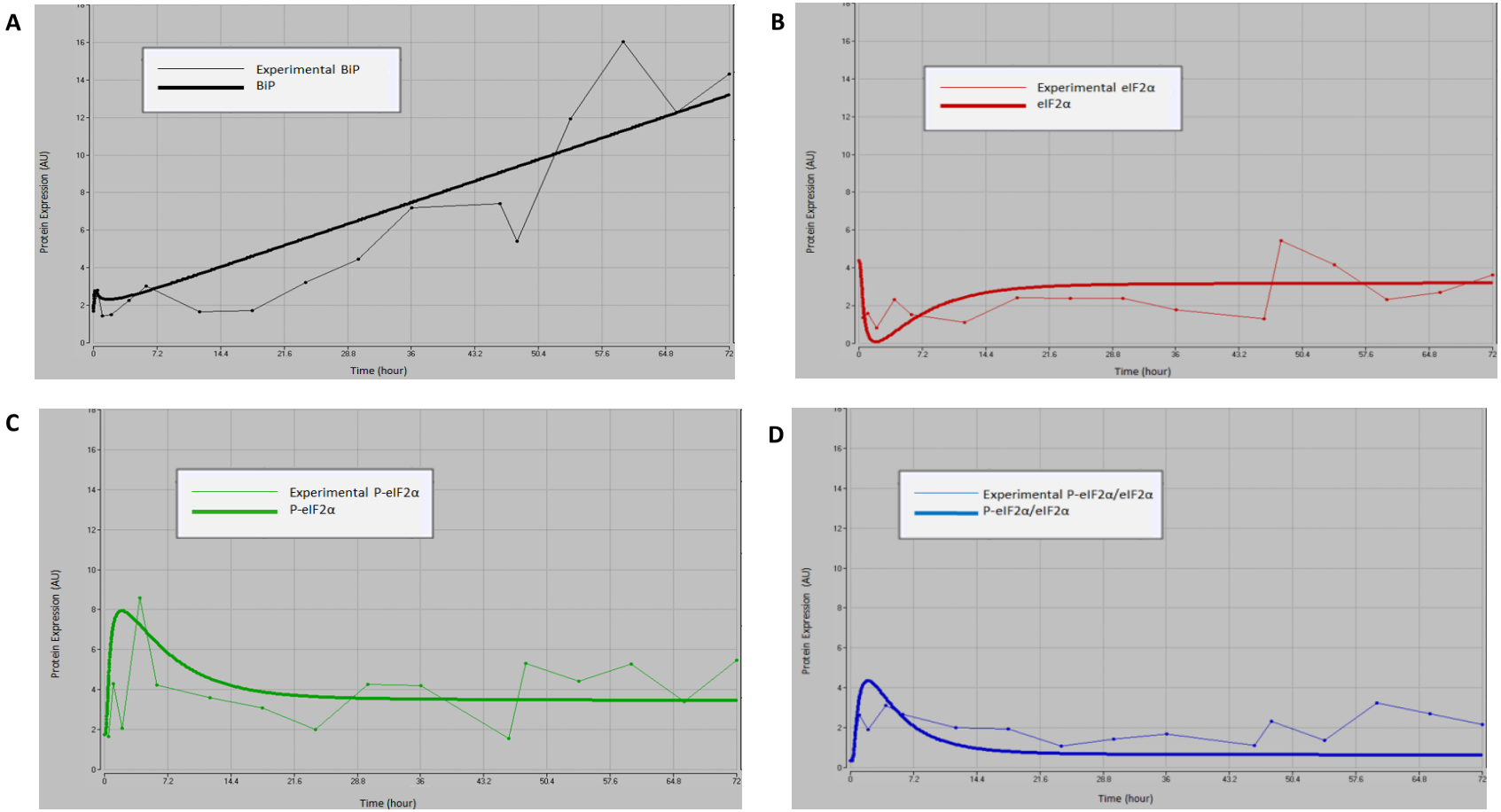

Figure 4.3.2.3 Individual Model Outputs for PERK Pathway following Manual Parameterisation: Proteins involved in the protein kinase RNA-like endoplasmic reticulum kinase (PERK) pathway of the unfolded protein response were mathematically modelled following treatment of Chub-S7 cells with 750ng/ml tunicamycin over 72 hours, using manual parameterisation. Model outputs (bold lines) are shown compared to experimental data (dotted lines) for the following proteins: **(A)** Binding immunoglobulin protein (BiP) **(B)** eukaryotic initiation factor 2α (eIF2α) **(C)** Phospho-eukaryotic initiation factor 2α (P-eIF2α), and **(D)** P-eIF2α relative to eIF2α (P-eIF2α/eIF2α). Lines between experimental data points represent linkages between discrete mean values for data collected and are not true trajectories over time.

Species	Residual Sum of Squares
BiP	76.3
eIF2α	23.6
P-eIF2α	80.8
P-eIF2α/eIF2α	28.0
	208.8

Table 4.3.2.4 Residual Sum of Squares from PERK Model with Manually Adjusted Parameters: Manual parameterisation of the model of the protein kinase RNA-like endoplasmic reticulum kinase (PERK) pathway of the unfolded protein response was carried out to best fit the available experimental data, where Chub-S7 adipocytes were treated with 750ng/ml tunicamycin over 72 hours. The residual sum of squares was calculated for binding immunoglobulin protein (BiP), eukaryotic initiation factor 2 alpha (eIF2α), phosphorylated eIF2α (P-eIF2α) and P-eIF2α relative to eIF2α (P-eIF2α/eIF2α) in order to provide a measure of how well the model fitted the experimental data.

A list of parameters for this model that utilised the slider function in Berkeley Madonna for manual parameterisation are listed in Table 4.3.2.5.

Parameter	Description	Value (AU)
ka1	Association of BiP and PERK	3.04
kd1	Dissociation of BiP and PERK	0.59
k11	Association of BiP and proteins other than PERK	0.002
k15	Dissociation of BiP and proteins other than PERK	0.39
ka2	Association of two PERK molecules to form a dimer	0.47
kd2	Dissociation of PERK dimer	15.8
k3	Phosphorylation of PERK dimer	150
k4	Dephosphorylation of PERK dimer	0.02
ka5	Association of P-PERK dimer with eIF2α	0.63
kd5	Dissociation of P-PERK:P-PERK:eIF2α complex	1.69
k7	Phosphorylation of eIF2α	83.4
k6	Dissociation of P-eIF2α from P-PERK:P-PERK:P-eIF2α complex	54.7
k8	Dephosphorylation of P-eIF2α	8.66
k12	Sum of interactions describing BiP:PERK production	0.01
k13	Sum of interactions describing BiP production	0.10
k14	Sum of interactions describing BiPX production	3.43
k17	Sum of interactions describing eIF2α production	68.3
k18	Sum of interactions describing PPERK:PPERK:eIF2α production	0.01
k19	Sum of interactions describing PPERK:PPERK:PeIF2α production	15.3
k20	Sum of interactions describing PeIF2α	150
k21	Interactions describing PeIF2α divided by interactions describing eIF2α	31.7

Table 4.3.2.5 Parameters used in the Manually Parameterised UPR Model: A mathematical model of the protein kinase RNA-like endoplasmic reticulum kinase (PERK) pathway of the unfolded protein response (UPR) was designed and developed, using experimental data for parameterisation. Experimental data were collected following the treatment of Chub-S7 adipocytes with 750ng/ml tunicamycin over 72 hours. Manual parameterisation using the slider function in Berkeley Madonna software resulted in the parameter values shown.

BiP = binding immunoglobulin protein, PERK = protein kinase RNA-like endoplasmic reticulum kinase, P-PERK = phosphorylated PERK, eIF2α = eukaryotic initiation factor 2 alpha, P-eIF2α = phosphorylated eIF2α, BiPX = BiP bound to proteins other than PERK (such as other UPR sensors or unfolded proteins), BiP:PERK = BiP in complex with PERK, PPERK:PPERK:eIF2α = PPERK dimer in complex with eIF2α, PPERK:PPERK:PeIF2α = PPERK dimer in complex with PeIF2α.

The initial findings using the slider function highlighted the impact that subtle changes in parameter values can have on model output and thus their sensitivity. It was determined that parameters kd1 (which represents the dissociation of the BiP:PERK complex) and ka2 (which represents the association of one PERK protein with another to form a dimer,) were the most sensitive, resulting in large changes in model output with only small changes in parameter values (Figure 4.3.2.7).

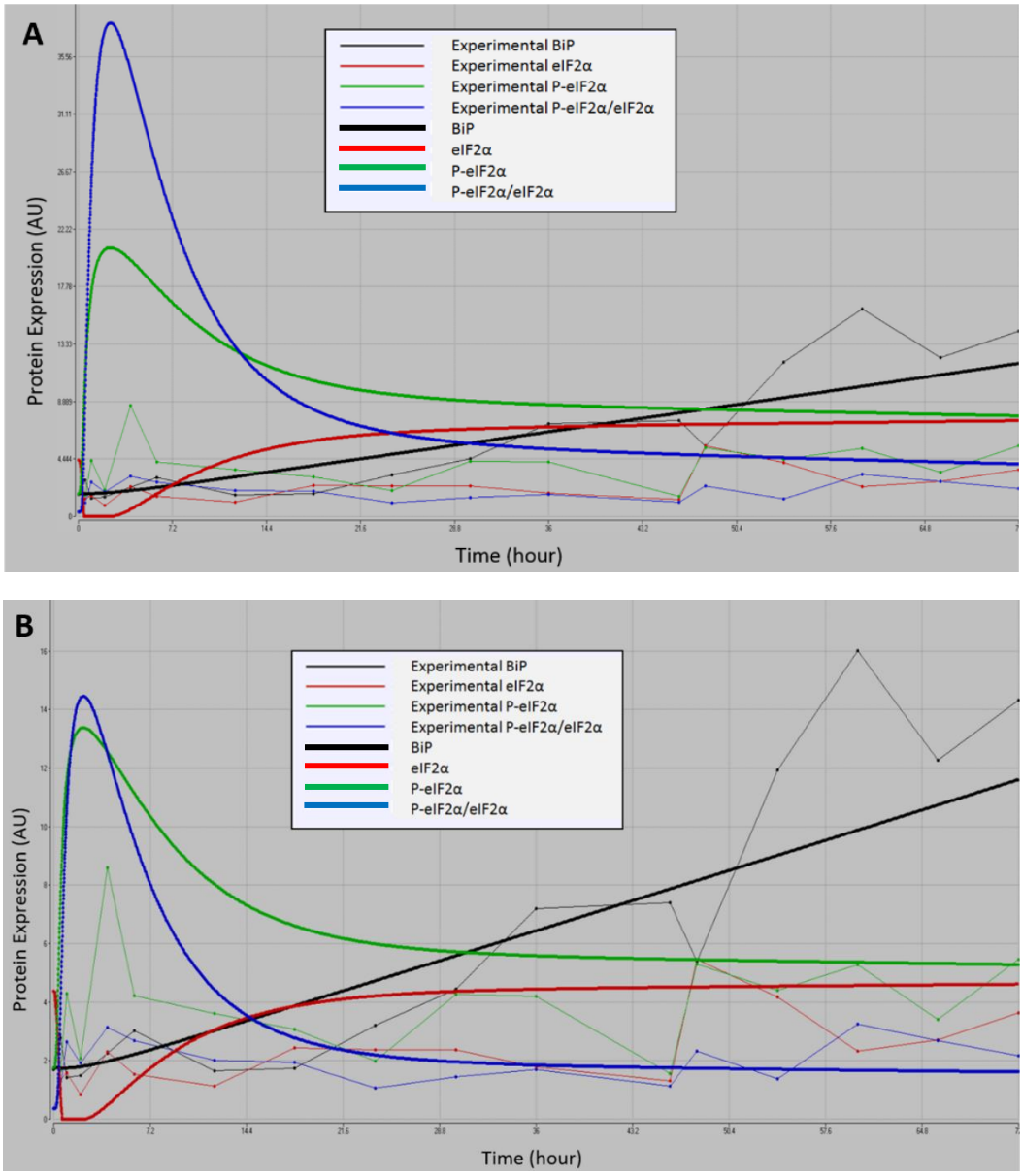

Figure 4.3.2.7 Model output following Sensitivity Analysis: A mathematical model of the protein kinase RNA-like endoplasmic reticulum kinase (PERK) pathway of the unfolded protein response was developed and parameterised using the slider function in Berkeley Madonna. This function was also used to assess parameter sensitivity, where **(A)** kd1, which represents the dissociation of the BiP:PERK complex, and **(B)** ka2, which represents PERK dimerisation, were discovered to be the most sensitive parameters, resulting in the largest changes in model output following a 2-fold change in parameter value. Chub-S7 adipocytes were treated with 750ng/ml tunicamycin over 72 hours and the following protein expressions were measured: binding immunoglobulin protein (BiP): black; eukaryotic initiation factor 2α (eIF2α): red; phospho-eukaryotic initiation factor 2α (P-eIF2α): green; and P-eIF2α/eIF2α ratio: blue. Bold lines represent model output, dotted lines represent experimental data. Lines between experimental data points represent linkages between discrete mean values for data collected and are not true trajectories over time. Initial conditions are as follows (AU) BiP:PERK (10), BiP (1), BiPX (20), PERK (0), PERK:PERK (0), PPERK:PPERK (0), eIF2α (10), PPERK:PPERK:eIF2α (0), PPERK:PPERK:PeIF2α (0), PeIF2α (0), BiPtot (1.70), eIF2αtot (4.38), PeIF2αtot (1.76), PeIF2α/eIF2α (0.35).

Using the slider functions to adjust model output resulted in parameter estimates that could be entered into the *Curve Fit* function. This function computationally identifies parameter values that, if the fitting algorithm converges, are likely to result in a close fit to the experimental data. The parameter estimation from this function resulted in the graphs shown in Figure 4.3.2.8 and Figure 4.3.2.9, and the corresponding residual sum of squares represented in Table 4.3.3.10. Computational parameterisation reduced the overall RSS value by 33% compared to manual parameterisation, indicating that there is less discrepancy between model output and experimental data when the Curve Fit function is utilised.

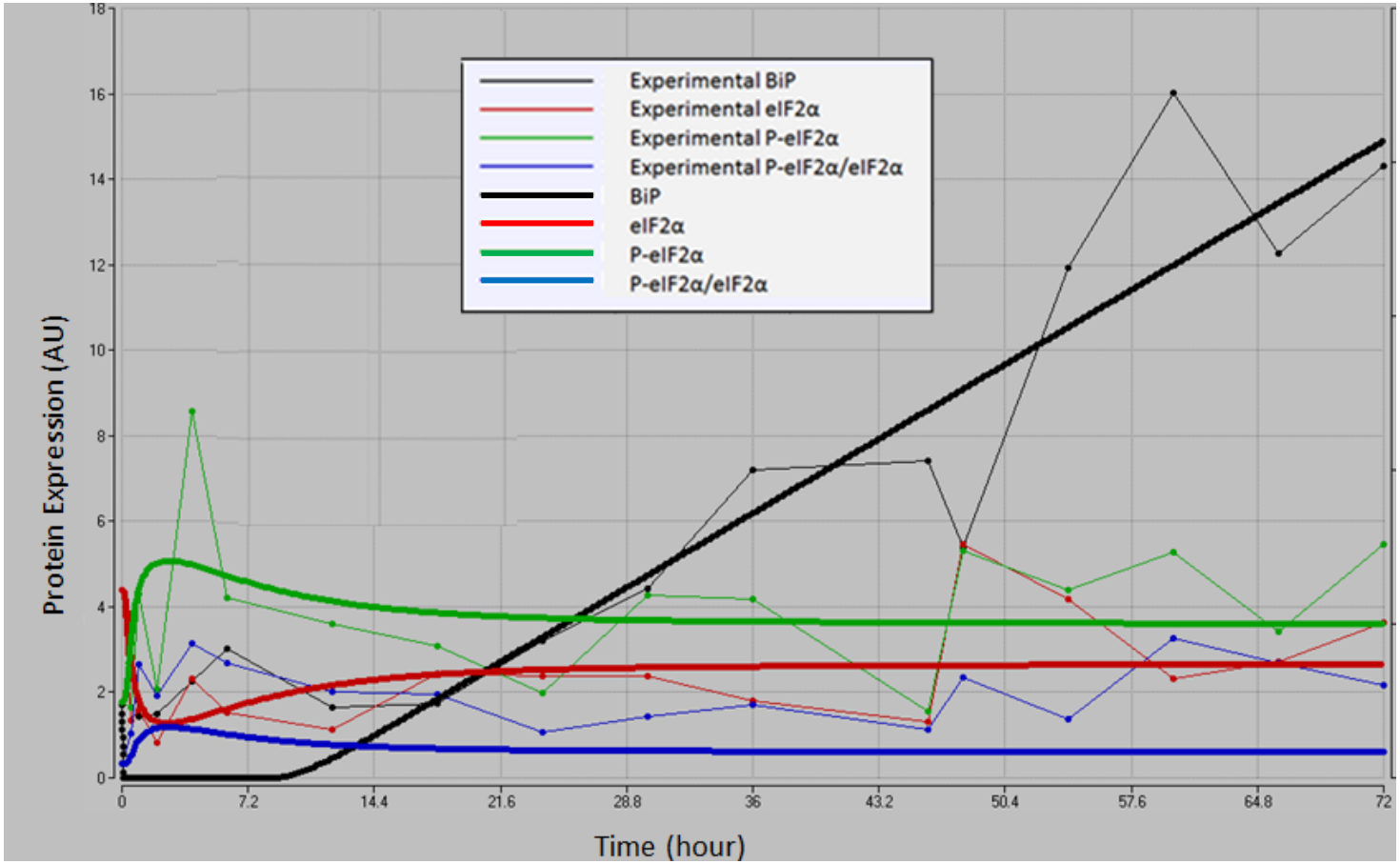

Figure 4.3.2.8 Model Output for PERK Pathway following Computational Parameterisation: A mathematical model of the protein kinase RNA-like endoplasmic reticulum kinase (PERK) pathway of the unfolded protein response was developed and parameterised with the Curve Fit function in Berkeley Madonna software using experimental data. Chub-S7 adipocytes were treated with 750ng/ml tunicamycin over 72 hours and the following protein expressions were measured: binding immunoglobulin protein (BiP): black; eukaryotic initiation factor 2α (eIF2α): red; phospho-eukaryotic initiation factor 2α (P-eIF2α): green; and P-eIF2α/eIF2α ratio: blue. Bold lines represent model output, dotted lines represent experimental data. Lines between experimental data points represent linkages between discrete mean values for data collected and are not true trajectories over time. Initial conditions are as follows (AU) BiP:PERK (10), BiP (1), BiPX (20), PERK (0), PERK:PERK (0), PPERK:PPERK (0), eIF2α (10), PPERK:PPERK:eIF2α (0), PPERK:PPERK:PeIF2α (0), PeIF2α (0), BiPtot (1.70), eIF2αtot (4.38), PeIF2αtot (1.76), PeIF2α/eIF2α (0.35).

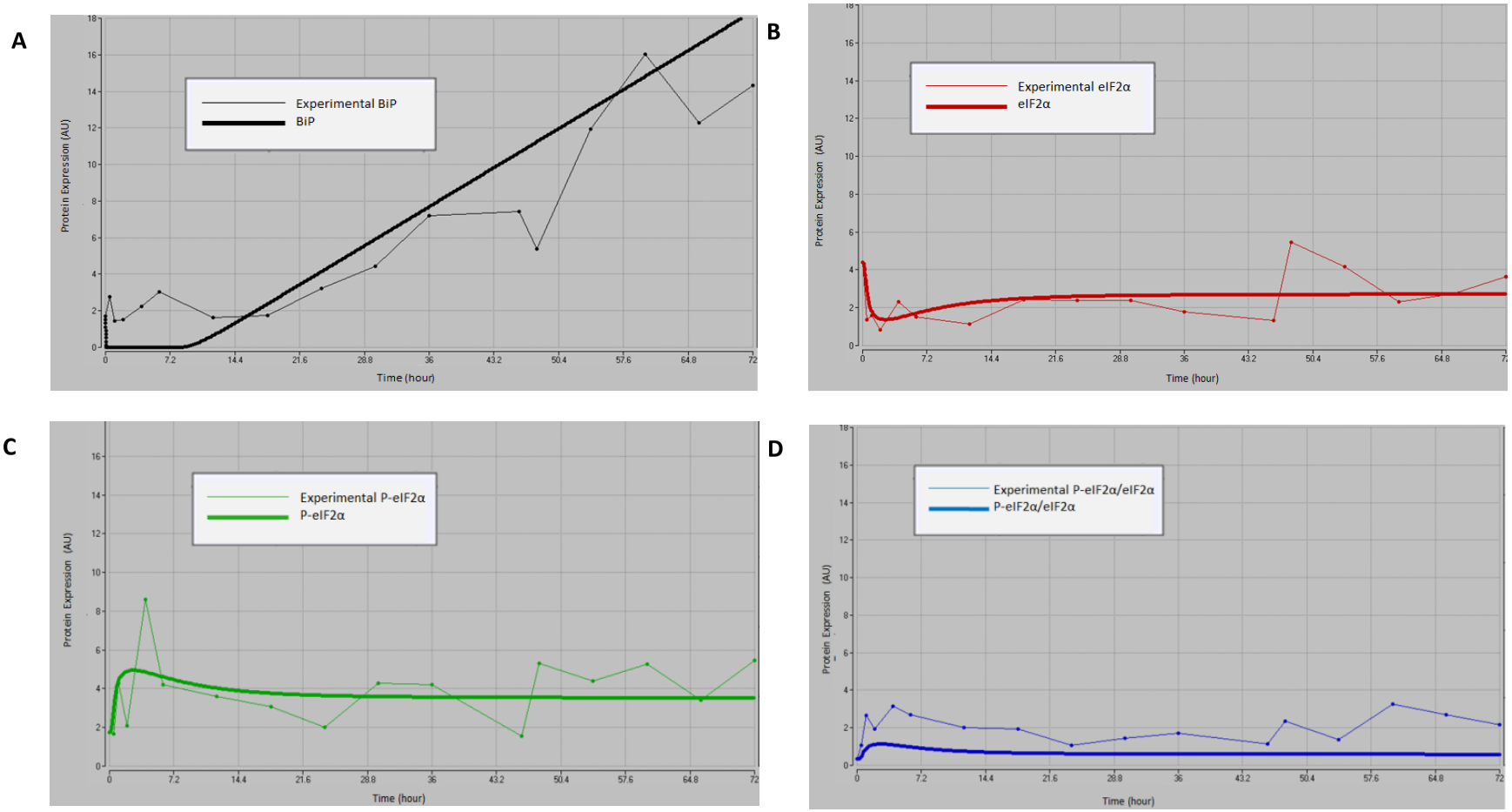

Figure 4.3.2.9 Individual Model Outputs for PERK Pathway following Computational Parameterisation: Proteins involved in the protein kinase RNA-like endoplasmic reticulum kinase (PERK) pathway of the unfolded protein response were mathematically modelled following treatment of Chub-S7 cells with 750ng/ml tunicamycin over 72 hours, using the Curve Fit function in Berkeley Madonna software for parameterisation. Model outputs (bold lines) are shown compared to experimental data (dotted lines) for the following proteins: **(A)** Binding immunoglobulin protein (BiP) **(B)** eukaryotic initiation factor 2α (eIF2α) **(C)** Phospho-eukaryotic initiation factor 2α (P-eIF2α), and **(D)** P-eIF2α relative to eIF2α (P-eIF2α/eIF2α). Lines between experimental data points represent linkages between discrete mean values for data collected and are not true trajectories over time.

Species	Residual Sum of Squares
BiP	63.7
eIF2α	19.5
P-eIF2α	43.9
P-eIF2α/eIF2α	33.9
	160.9

Table 4.3.2.10 Residual Sum of Squares from PERK Model with Computationally Adjusted Parameters: Computational parameterisation of a model of the protein kinase RNA-like endoplasmic reticulum kinase (PERK) pathway of the unfolded protein response was carried out in order to best fit the available experimental data, where Chub-S7 adipocytes were treated with 750ng/ml tunicamycin over 72 hours. The residual sum of squares was calculated for binding immunoglobulin protein (BiP), eukaryotic initiation factor 2 alpha (eIF2α), phosphorylated eIF2α (P-eIF2α) and P-eIF2α relative to eIF2α (P-eIF2α/eIF2α) in order to compare computational parameterisation with manual parameterisation that was previously carried out to determine which provided the best fit to the experimental data.

The final parameter values of the UPR model which resulted in the closest match between model output and experimental data (via the minimum residual sum of squares), are described in Table 4.3.2.11 below.

Parameter	Description	Value (AU)
ka1	Association of BiP and PERK	2.68
kd1	Dissociation of BiP and PERK	0.31
k11	Association of BiP and proteins other than PERK	0.15
k15	Dissociation of BiP and proteins other than PERK	0.4
ka2	Association of two PERK molecules to form a dimer	0.48
kd2	Dissociation of PERK dimer	15.9
k3	Phosphorylation of PERK dimer	159
k4	Dephosphorylation of PERK dimer	0.02
ka5	Association of P-PERK dimer with eIF2α	0.79
kd5	Dissociation of P-PERK:P-PERK:eIF2α complex	1.53
k7	Phosphorylation of eIF2α	94.6
k6	Dissociation of P-eIF2α from P-PERK:P-PERK:P-eIF2α complex	37.3
k8	Dephosphorylation of P-eIF2α	8.23
k12	Sum of interactions describing BiP:PERK production	2.24
k13	Sum of interactions describing BiP production	0.004
k14	Sum of interactions describing BiPX production	3.5
k17	Sum of interactions describing eIF2α production	70.7
k18	Sum of interactions describing PPERK:PPERK:eIF2α production	90.9
k19	Sum of interactions describing PPERK:PPERK:PeIF2α production	16.3
k20	Sum of interactions describing PeIF2α	152
k21	Interactions describing PeIF2α divided by interactions describing eIF2α	23.5

Table 4.3.2.11 Parameters used in PERK Model using Computational Parameterisation: A mathematical model of the protein kinase RNA-like endoplasmic reticulum kinase (PERK) pathway of the unfolded protein response (UPR) was designed and developed, using experimental data for parameterisation. Experimental data were collected following the treatment of Chub-S7 adipocytes with 750ng/ml tunicamycin over 72 hours. Computational parameterisation using the Curve Fit function in Berkeley Madonna software calculated the parameter values shown to give the closest fit between model output and experimental data.

BiP = binding immunoglobulin protein, PERK = protein kinase RNA-like endoplasmic reticulum kinase, P-PERK = phosphorylated PERK, eIF2α = eukaryotic initiation factor 2 alpha, P-eIF2α = phosphorylated eIF2α, BiPX = BiP bound to proteins other than PERK (such as other UPR sensors or unfolded proteins), BiP:PERK = BiP in complex with PERK, PPERK:PPERK:eIF2α = PPERK dimer in complex with eIF2α, PPERK:PPERK:PeIF2α = PPERK dimer in complex with PeIF2α.

4.4 Discussion

This study detailed both acute and chronic expression profiles of UPR proteins, illustrating that the expression of some proteins is immediately affected by tunicamycin treatment, whilst others experience change at a noticeably slower rate. Studying the expression of P-eIF2α and eIF2α supported evidence in the previous chapter that proteins involved in the translation attenuation system experience oscillatory expression. This thesis provides the first experimental data for this cellular response, supporting the model output from Erguler *et al.* who first suggested oscillation of these proteins (Erguler, Pieri *et al*. 2013). A mathematical model was also created that better represented the UPR compared to the initial model presented in Chapter 4. This is attributed to the inclusion of terms for total protein expression as well as using computational parameter estimation which was demonstrated to reduce RSS values compared to simple manual adjustment of parameter values.

Examination of lipid droplets through Oil Red-O staining confirmed that the Chub-S7 preadipocyte cells used in this study had differentiated into mature adipocytes over the 14 day period. This highlights the uniformity of the cell-line that provides the consistency required to use the experimental data for parameterisation of the mathematical model. Comparatively, as primary adipocytes cultured from humans do not have identical genetic composition, they are less uniform, differentiating over different periods of time and as such are less suited for use in mathematical model parameterisation (Kaur and Dufour 2012, Niu and Wang 2015).

Experimental data from this study revealed that the expression of BiP is not dramatically affected by acute treatment of tunicamycin, but has a 9.5-fold increase following chronic treatment. Conversely, P-eIF2α and eIF2α both undergo an immediate increase with acute tunicamycin treatment and experience oscillatory expression with chronic treatment. This difference is most likely due to the fact that BiP translation occurs at the end of protein cascades within the UPR, and phosphorylation of eIF2α is required before further downstream proteins such as activating transcription factor 4 (ATF4) can upregulate BiP (Matassa, Amoroso *et al*. 2013). This may initially seem counter-intuitive, as BiP is an important chaperone that aids in the reduction of ER stress, and therefore cells would benefit from having a quick acute response in its upregulation (Lewy, Grabowski *et al*. 2017). However, as the Western blot procedure only measures the total amount of BiP present in cells, it cannot account for the BiP molecules that have dissociated from sensor proteins such as PERK in order to assist protein folding in the ER. As such, although an increase in BiP production may take longer than other proteins within the UPR, the increase in 'free' BiP that is able to assist protein folding and reduce ER stress is the first process to occur in the UPR pathway, and it is this process that initiates the protein cascades within the UPR (Gong, Wang *et al*. 2017).

The increase in number and granularity of time points allowed a much more reliable analysis of protein expression over time. This resulted in data that clearly demonstrated the oscillation of proteins involved in the translation attenuation system, building on initial evidence from the previous chapter. The additional time series data affirm the predictions made by Erguler *et al.* as discussed in chapter 4 which suggest that the existence of oscillations allows translation to occur for brief

periods during ER stress, enabling routine cellular activity to be carried out during the stress response (Erguler, Pieri *et al*. 2013). Further to this, as experimental data were not used to confirm Erguler's model, these findings provide important information regarding the time scale over which these oscillations occur. These results have further implications for others studying the translation attenuation system of the UPR, as it leaves researchers susceptible to obtaining false positives if only one time point is studied when comparing treated cells to control cells. For instance, if a comparison was made when the protein in question was at a low point in its oscillatory cycle, it may appear that the treatment used did not induce ER stress when in reality the peak expression may simply not have been measured. This suggests that, when studying ER stress, it is more appropriate to examine protein expression over several time points over at least a 24 hour period.

This chapter also highlighted the importance of including terms for ODEs that reflect the biological data collected. The inclusion of terms for total protein expression ensured that the model output more accurately represented useful biological data. This was supported by the increased frequency and reliability of the data collected, as well as through a series of balances and checks which reduced the number of inaccuracies and ensured more biologically accurate model outputs. These outputs were further improved by the use of computationally estimated parameters, which reduced the RSS values by 33% compared to manually adjusted parameters. Sensitivity analysis identified kd1, which represents the dissociation of the BiP:PERK complex, and ka2, which represents the association of two PERK proteins to form a dimer, as the two most sensitive parameters. This can be explained biologically as the dissociation of the BiP:PERK complex is the most important step in the process,

initiating the pathway response, whilst the dimerisation of PERK is the second reaction to occur in the cascade, further demonstrating biological accuracy of the model. This builds upon suggestions from the previous chapter that modelling particular functions of the UPR initially, rather than the system as a whole, may be useful to ensure that parameterisation can occur whilst maintaining accurate biological detail.

4.5 Conclusions

Experiments carried out in this chapter have demonstrated that different UPR proteins respond differently to acute and chronic treatments of ER stress inducers. Additionally, these results have confirmed those in the previous chapter that proteins involved in the translation attenuation system undergo oscillation during ER stress – a theory proposed by Erguler *et al.* that had previously lacked any experimental evidence. This chapter has also highlighted the importance of including ODEs that reflect the biological data collected, including the use of terms for total protein expression, whilst mathematically modelling the response. Novel parameters were estimated using experimental time series data in a form that has not been used before, resulting in a biologically qualitatively accurate mathematical model that has the potential to be used in a predictive capacity, or to test 'what if' input scenarios in the future. As such, these findings suggest that modelling individual functions of the UPR may be more beneficial than modelling the entire system as a whole, satisfying the first and second aims of this thesis as follows:

1. To create a mathematical model of a pathway in the unfolded protein response using experimental time series data.
2. To study ER stress in more detail by analysing how the expression of key ER stress proteins varies over time following treatment with Tunicamycin.

CHAPTER 5:

The Effect of Broccoli on Tunicamycin-Induced ER Stress

5.1 Introduction

It is recognised that obesity can induce chronic ER stress, leading to the misfolding of proteins and dysfunction of cellular processes (Pagliassotti, Kim *et al*. 2016). This occurs through conditions such as overnutrition, endotoxemia, hyperglycaemia, elevated circulating free fatty acids and glucose deprivation (Pagliassotti, Moran *et al*. 2014). Studies have shown that chronic ER stress is one of the mechanisms in obesity that can contribute to insulin resistance and type 2 diabetes (T2DM) either directly, through the inhibitory phosphorylation of insulin receptor substrate 1 (IRS-1), or through other indirect mechanisms (Ozcan, Cao *et al*. 2004, Kawasaki, Asada *et al*. 2012, Lindholm, Korhonen *et al*. 2017).

The UPR, activated during ER stress, can also affect a wide spectrum of physiological functions. Each pathway within the UPR provides a specific function that can be involved in certain developmental and metabolic processes, such as cellular differentiation and neurological activities (Lee, Scapa *et al*. 2008, Mao, Shao *et al*. 2011, Zhu and Lee 2015, Saito and Imaizumi 2017). There is growing evidence suggesting that the individual pathways of the UPR are required for these roles throughout the lifetime of a cell. However, a more intense, chronic upregulation of UPR pathways in response to cellular stress can lead to significant dysfunction, as observed in pathogenesis of diseases (Wu and Kaufman 2006, Matsuzaki, Hiratsuka *et al*. 2015). It may therefore be beneficial to investigate ways to protect cellular systems from significant ER stress and establish ways to reduce the pathogenesis of obesity mediated T2DM.

One potential way to prevent increased ER stress may be through dietary factors that are known to impair mechanisms that initiate the stress. Chronic inflammation, ROS and mitochondrial dysfunction are all such mechanisms that not only induce ER stress but are themselves induced by ER stress and consequently further impair insulin signalling through feedback loops (Cao and Kaufman 2014, Park 2014). As such, it is possible that dietary factors which are known to reduce the intensity of these mechanisms may also reduce the level of ER stress and therefore reduce the risk of insulin resistance and T2DM.

Cruciferous vegetables, such as broccoli, have been studied regarding their potential to impact a number of diseases, and have been shown to reduce the risk of myocardial infarction and cardiovascular related mortality, as well as many types of cancer (Zhang, Shu *et al*. 2011, Bosetti, Filomeno *et al*. 2012, Tang, Meng *et al*. 2017). Studies have also highlighted that such vegetables in powder form can reduce inflammation and improve damaging lipid profiles of humans (Bahadoran, Mirmiran *et al*. 2012, Jiang, Wu *et al*. 2014, Armah, Derdemezis *et al*. 2015). Additionally, broccoli contains high levels of biochemical compounds such as glucoraphanin which, once broken down to sulforaphanes, are known to enhance antioxidant activity and eliminate ROS (Clarke, Dashwood *et al*. 2008, Boddupalli, Mein *et al*. 2012). As such, these qualities suggest that it may be favourable to investigate broccoli extracts as a potential dietary factor to protect against ER stress, and thus reduce T2DM risk.

The aim of this study was therefore to investigate whether a broccoli powder extract could protect against and/or reduce the intensity of ER stress induced by tunicamycin

in order to explore its potential as a dietary supplement that may reduce the risk of subjects developing T2DM.

5.2 Methods

5.2.1 Optimisation of Broccoli Extract Concentration

In order to determine the optimum concentration of broccoli extract (BE) to use, differentiated Chub-S7 preadipocyte cells were exposed to one of the following treatments:

- Vehicle Control (hereafter referred to as Control)
- 750ng/ml Tunicamycin
- 10ng/ml BE
- 1000ng/ml BE
- 100,000ng/ml BE
- 10ng/ml BE + 750ng/ml Tunicamycin
- 1000ng/ml BE + 750ng/ml Tunicamycin
- 100,000ng/ml BE + 750ng/ml Tunicamycin

The concentration of tunicamycin was chosen according to previous studies investigating ER stress that used between 0.5μg/ml and 2.0μg/ml (Ozcan, Cao *et al*. 2004, Alhusaini, McGee *et al*. 2010, Mondal, Das *et al*. 2012). Concentrations of BE were chosen in line with prior evaluations of compounds known to influence ER stress, such as lipopolysaccharide (LPS) (Kusminski, da Silva *et al*. 2007, Alhusaini, McGee *et al*. 2010). Cells were exposed to these treatments for 24hr, 48hr or 72hr to assess acute and chronic impacts. Those cells treated with both BE and tunicamycin were pre-treated with BE for 24hr prior to the addition of tunicamycin, and fresh treatment was provided to all cells every 24hr. Cells were then harvested for RNA, with three samples for each treatment collected per time point (24hr, 48hr or 72hr).

qRT-PCR analysis was carried out in order to study the expression of UPR marker genes.

5.2.2 Time Course Analysis of the Impact of Broccoli Extract

Once the optimum concentration of BE had been determined, a comprehensive time course experiment was designed in order to analyse the impact of BE on ER stress at an increased level of granularity over time. Chub-S7 preadipocyte cells were differentiated into mature adipocytes over 14 days. Cells were treated with 750ng/ml tunicamycin, 10ng/ml BE or a combination of the two; those treated with both tunicamycin and BE were pre-treated with BE for 24hr prior to the addition of tunicamycin. Control cells were grown in the same manner and treated with the equivalent concentrations of the treatment vehicles. Cells were exposed to the treatments for the following lengths of time: 0hr, 30mins, 1hr, 2hr, 4hr, 6hr, 12hr, 18hr, 24hr, 30hr, 36hr, 46hr, 48hr, 54hr, 60hr, 66hr, or 72hr, with fresh treatments provided every 24hr (Figure 5.2.2). Following treatment, cells were harvested and protein extraction was carried out to allow analysis by Western blot. Six samples were collected at each time point for each treatment, which were then processed and analysed.

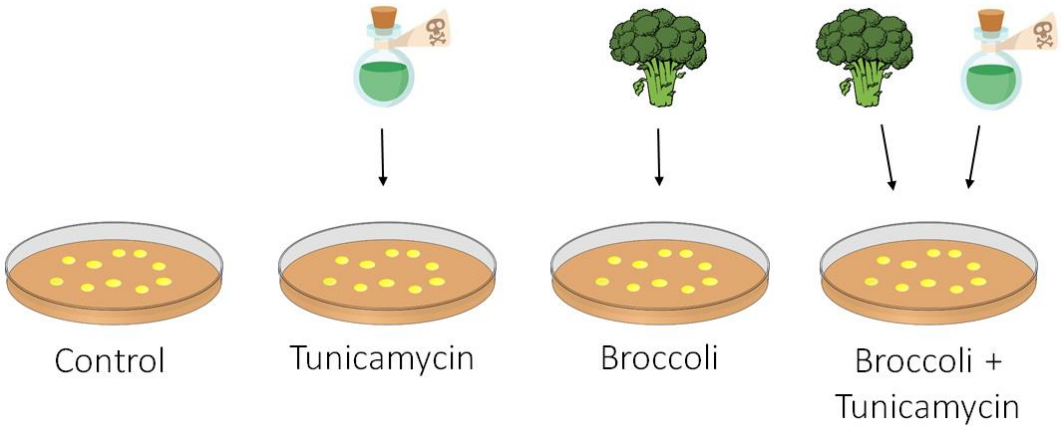

Figure 5.2.2 Treatment of Adipocytes with Tunicamycin and Broccoli Extract: Chub-S7 adipocytes were grown and differentiated before being treated with tunicamycin (750ng/ml), broccoli extract (10ng/ml) or a combination of the two. Control cells were grown in the same manner and treated with the equivalent concentration of treatment vehicles. Protein samples were collected at 17 time points over 72 hours (0hr, 30 mins, 1hr, 2hr, 4hr, 6hr, 12hr, 18hr, 24hr, 30hr, 36hr, 46hr, 48hr, 54hr, 60hr, 66hr, or 72hr).

5.3 Results

5.3.1 Broccoli Extract does not Exacerbate ER Stress

In order to assess whether BE itself had any detrimental effects with regards to physiological ER stress response, differentiated Chub-S7 pre-adipocyte cells were exposed to different concentrations of BE, as well as 750ng/ml tunicamycin to provide a reference for the level of stress occurring. ER stress marker genes ATF4, ATF6 and CHOP cover a range of the UPR pathways and were therefore selected for analysis to assess the level of ER stress occurring. ATF4 is expressed partway through the PERK arm of the UPR, and upregulates both CHOP and GADD34 which are involved in the initiation of apoptosis (Iurlaro and Muñoz-Pinedo 2016, Zong, Feng *et al*. 2017). ATF6 is the initial sensor of the ATF6 arm of the UPR, and also leads to the upregulation of CHOP as well as chaperones such as BiP (Takayanagi, Fukuda *et al*. 2013). RNA analysis of these genes revealed that in most cases there was no significant change in ER stress levels due to BE exposure. In two cases, the 100,000ng/ml BE treatment resulted in significant increases of UPR proteins, increasing the expression of ATF6 and ATF4 at 48hr ($p < 0.01$), and as such this high dose was removed from further investigations; however in all other cases BE concentrations either had no significant effect or, in one case, reduced expression of ER stress proteins by 15% (Figure 5.3.1).

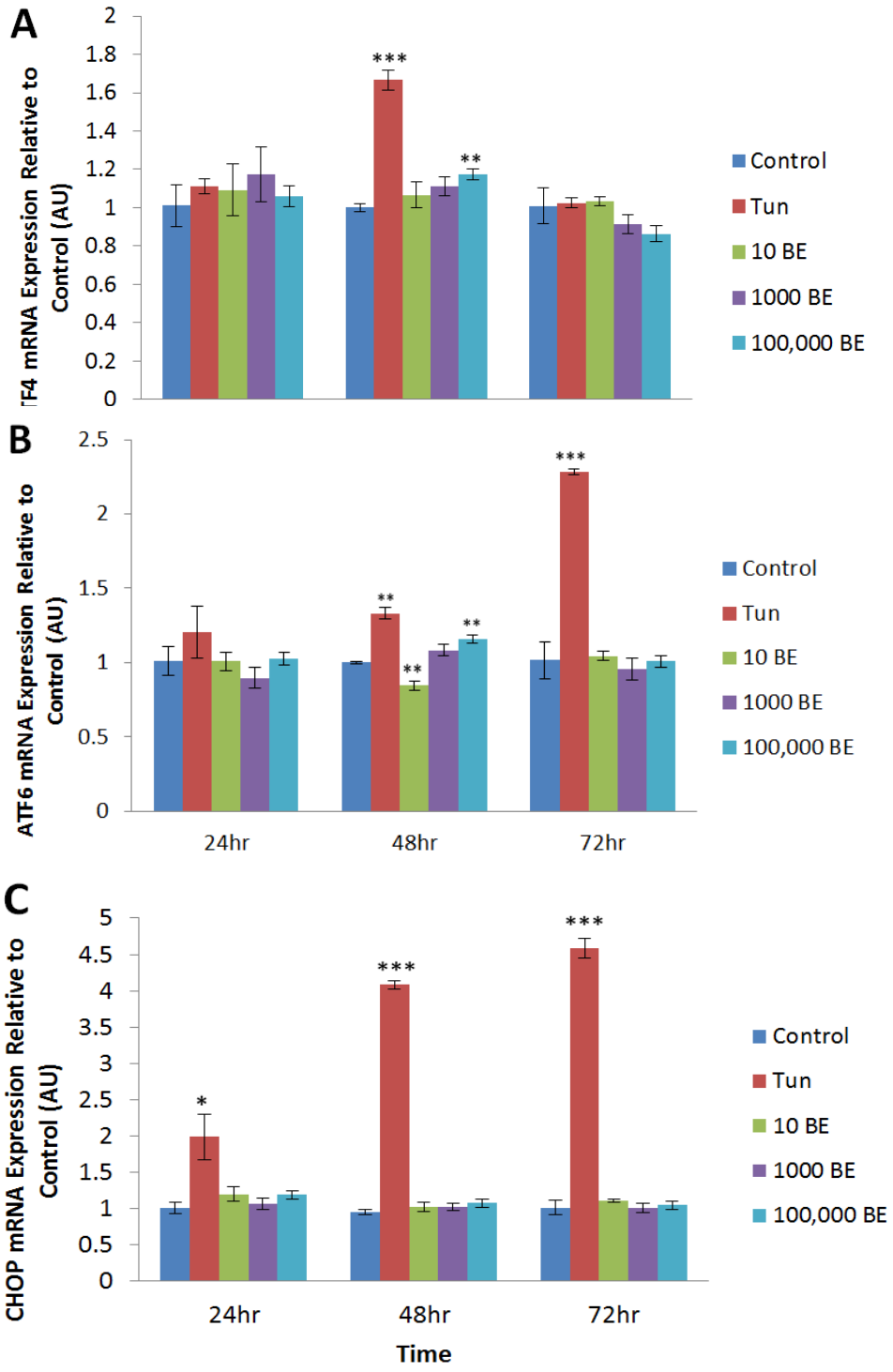

Figure 5.3.1 Effect of Broccoli Extract on Physiological ER Stress mRNA: (**A**) Activating transcription factor 4 (ATF4), (**B**) activating transcription factor 6 (ATF6) and (**C**) CCAAT-enhancer-binding protein homologous protein (CHOP) mRNA were analysed following treatment of Chub-S7 adipocytes with one of three concentrations of broccoli extract (BE; 10ng/ml, 1000ng/ml, 100,000ng/ml) or tunicamycin (Tun; 750ng/ml) to assess whether BE induced endoplasmic reticulum (ER) stress. Statistical analysis was undertaken with control vs. treatment, p-values: * $p < 0.05$, ** $p < 0.01$, *** $p < 0.001$.

5.3.2 Broccoli Extract Reduces Tunicamycin-Induced ER Stress

Expression of ER stress genes ATF4, ATF6 and CHOP was also studied in order to determine the effect of BE on ER stress induced by tunicamycin. Cells were treated with a combination of BE and tunicamycin alongside individual tunicamycin treatment as a reference. Each marker analysed revealed that treatment with BE significantly reduced tunicamycin-induced ER stress at particular time points, with only one time point of ATF6 undergoing a significant increase in stress due to the presence of BE. These results also illustrated that, in many cases, a concentration of 10ng/ml BE was most effective in preventing the increase in expression that occurred with exposure to tunicamycin. As such, this concentration was selected for use in further studies (Figure 5.3.2).

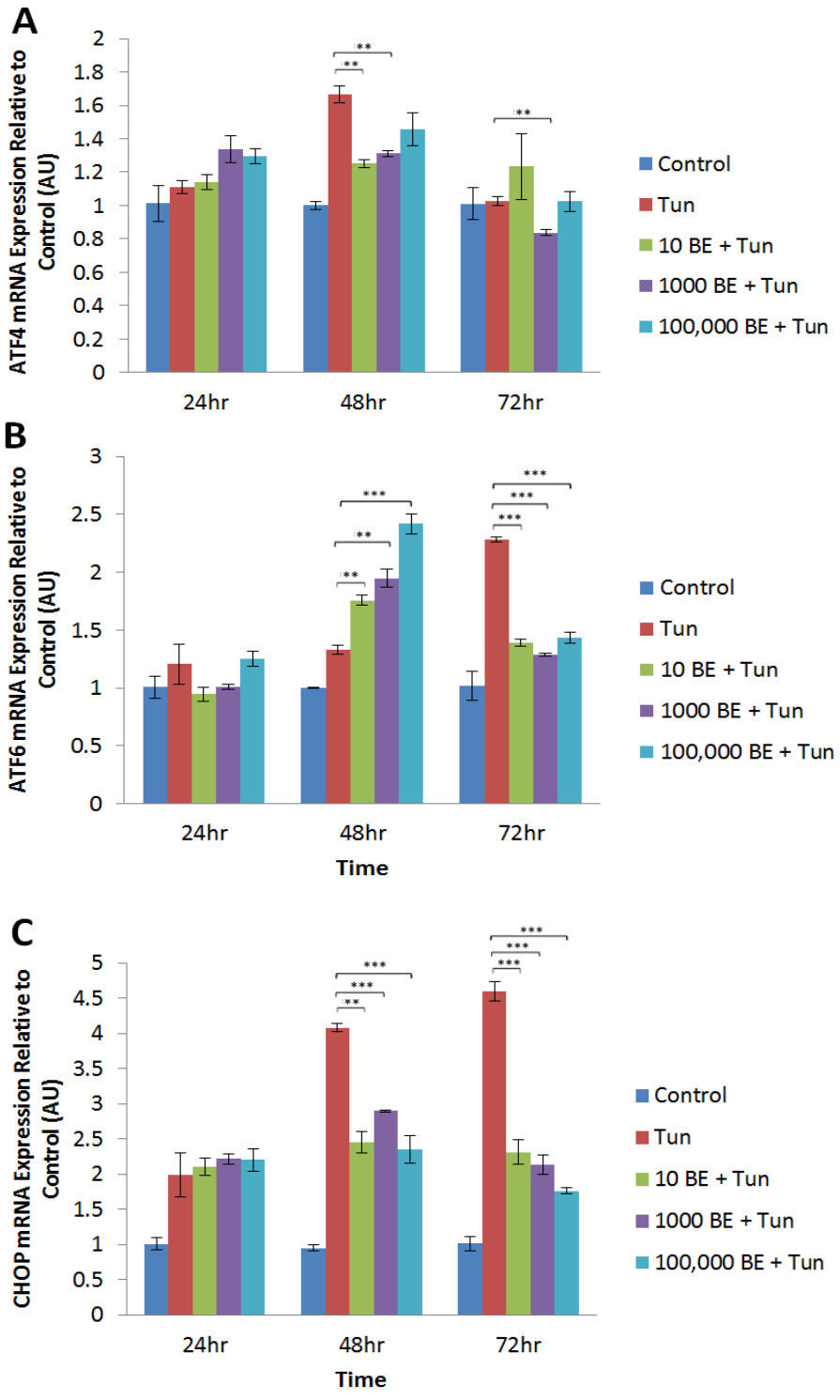

Figure 5.3.2 Effect of Broccoli Extract on Tunicamycin-Induced ER Stress mRNA: mRNA expression of (**A**) activating transcription factor 4 (ATF4), (**B**) activating transcription factor 6 (ATF6), and (**C**) CCAAT-enhancer-binding protein homologous protein (CHOP) was analysed following treatment of Chub-S7 adipocytes with tunicamycin (Tun; 750ng/ml), or a combination of tunicamycin and one of three concentrations of broccoli extract (BE; 10ng/ml, 1000ng/ml, 100,000ng/ml) over time (24hr, 48hr, 72hr). Statistical analysis was carried out with tunicamycin vs. BE+Tun treatments, p-values: * $p < 0.05$, ** $p < 0.01$, *** $p < 0.001$.

5.3.3 Time Series Effect of Broccoli Extract on Unfolded Protein Response

The previous results demonstrated that at certain time points, BE reduced the intensity of the ER stress marker genes studied. In order to explore this effect in more detail, a time series experiment was carried out in which the protective effect of broccoli was examined at 17 time points over 72hr. The protein expression of BiP, P-eIF2α, eIF2α and housekeeping protein β-Actin was examined at each time point, revealing the extent to which BE protects against ER stress.

Assessing the protein expression of BiP added evidence to the earlier finding that BE itself has little to no effect on the expression of UPR markers compared to control cells. A similar profile was formed from both control and BE treated cells, despite there being a significant reduction in expression due to the BE treatment at five time points (2hr, 24hr, 46hr, 48hr and 66hr) ($p < 0.05$) (Figure 5.3.3.1). The addition of BE to the tunicamycin treatment resulted in a delay of the initial peak in expression of BiP from 36hr to 46hr, however at other time points the presence of BE did not demonstrate a particularly strong protective effect against BiP expression, despite significantly reducing its expression at three time points (6hr, 36hr and 48hr) ($p < 0.05$). Furthermore, at 72hr a significant increase in expression occurred when BE was included in the treatment ($p = 0.005$) (Figure 5.3.3.2).

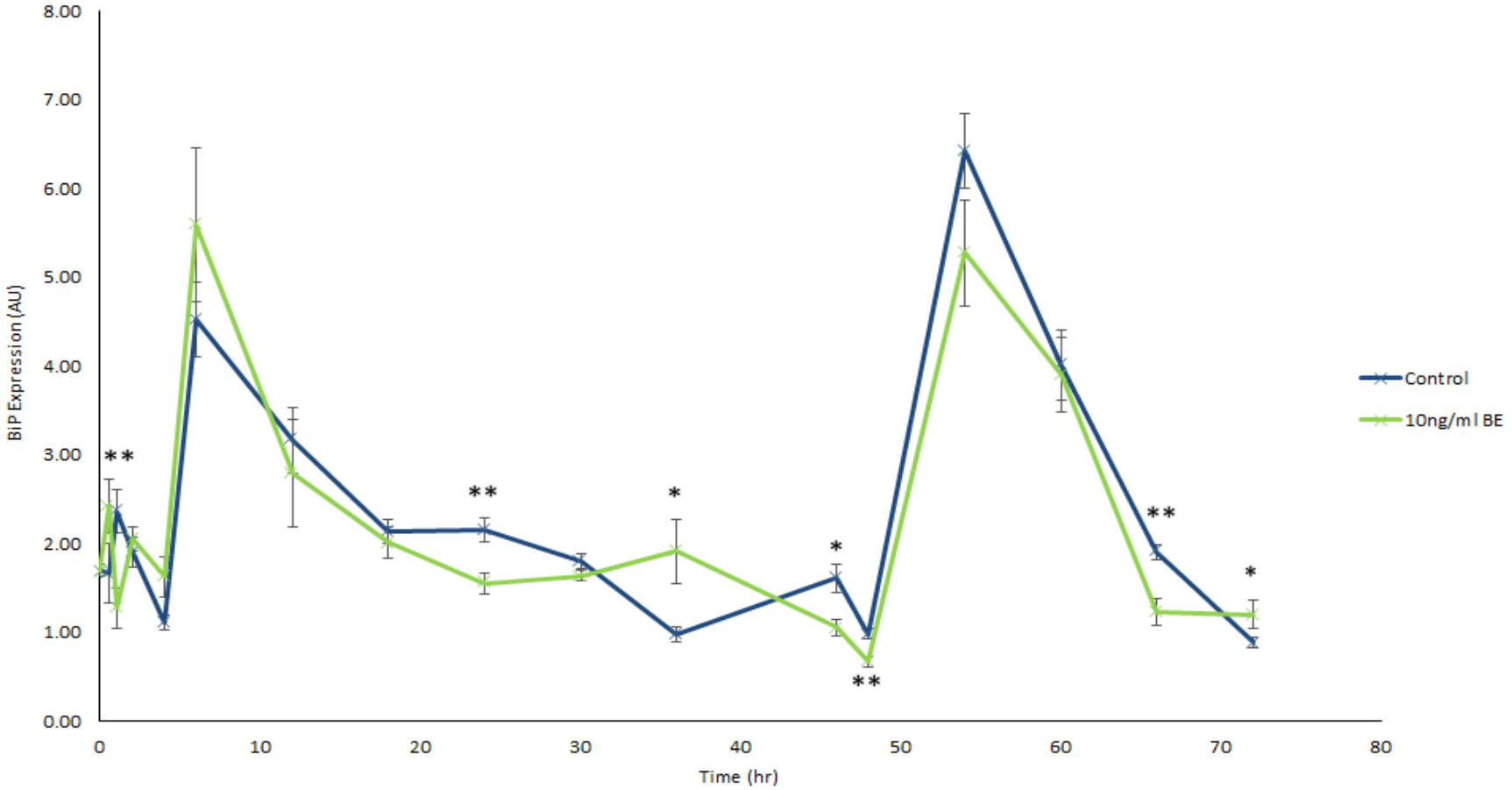

Figure 5.3.3.1 Effect of Broccoli Extract on Physiological Expression of BiP: Protein expression of binding immunoglobulin protein (BiP) following treatment of Chub-S7 adipocytes with broccoli extract (BE; 10ng/ml) compared to untreated control cells (Con), p-values: * $p < 0.05$, ** $p < 0.01$, *** $p < 0.001$. Lines between points represent linkages between discrete mean values for data collected and are not true trajectories over time.

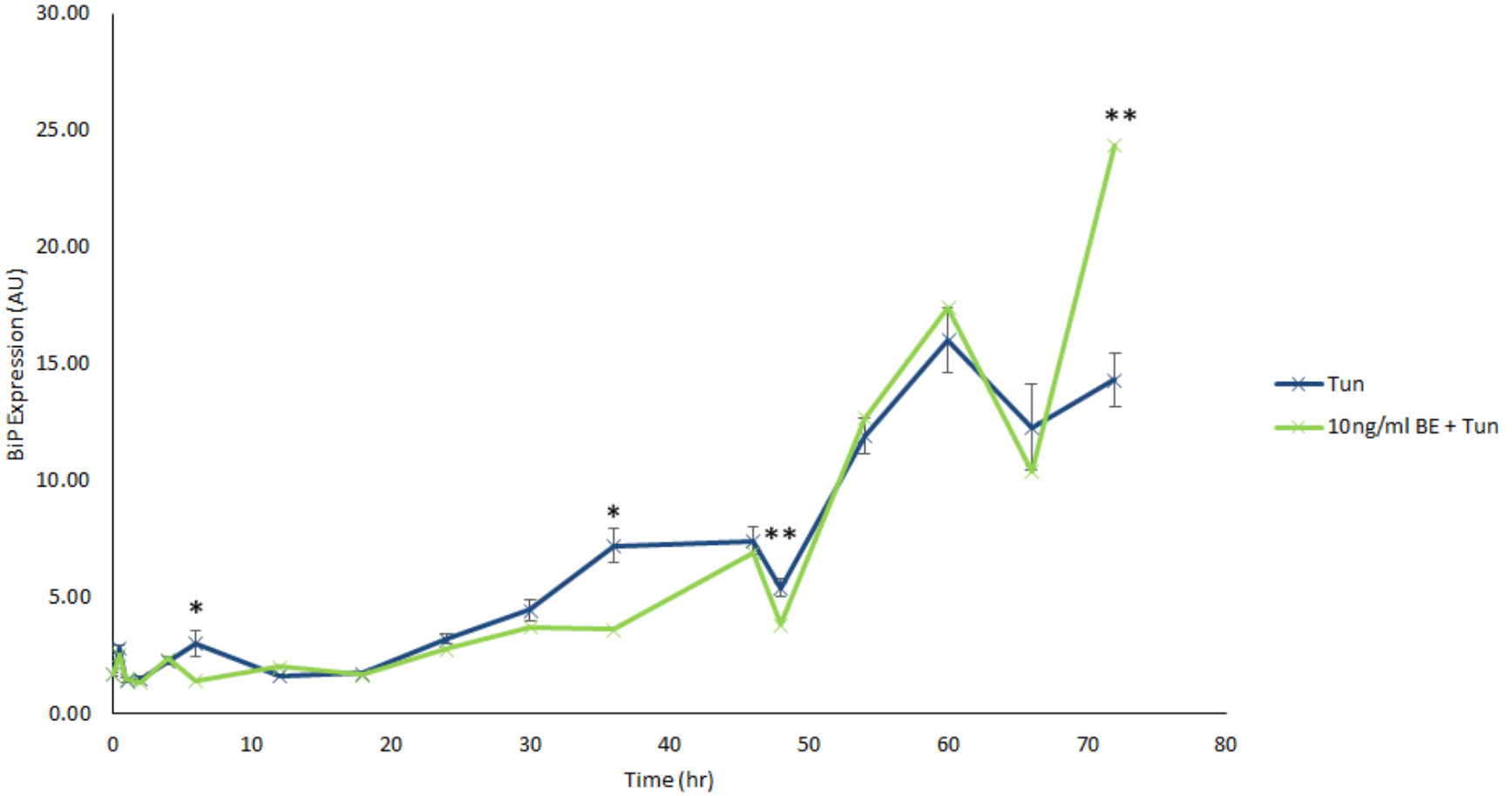

Figure 5.3.3.2 Effect of Broccoli Extract on Tunicamycin-Induced Expression of BiP Protein expression of binding immunoglobulin protein (BiP) following treatment of Chub-S7 adipocytes with tunicamycin (Tun; 750ng/ml) or broccoli extract and tunicamycin combined (BE + Tun; 10ng/ml, 750ng/ml). p-values: * $p < 0.05$, ** $p < 0.01$, *** $p < 0.001$. Lines between points represent linkages between discrete mean values for data collected and are not true trajectories over time.

Studying the expression of P-eIF2α revealed that treatment with BE resulted in a very similar profile compared to control (Figure 5.3.3.3). When investigating whether BE reduces the intensity of the stress response induced by tunicamycin however, it was discovered that the addition of BE to the tunicamycin treatment elicited a protective effect at almost every time point, with a maximum decrease in expression of 51% occurring at 66hr ($p = 0.01$) (Figure 5.3.3.4).

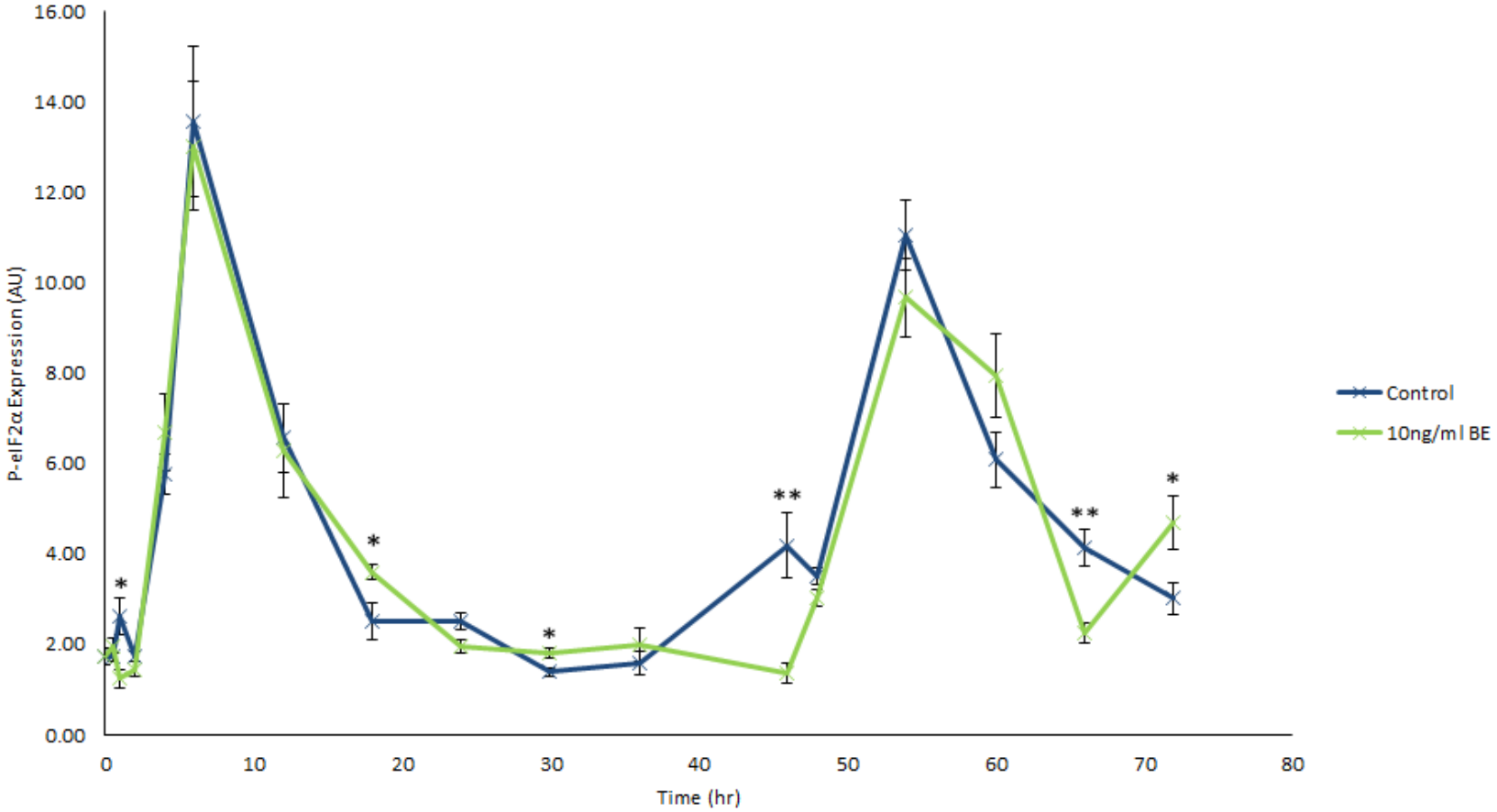

Figure 5.3.3.3 Effect of Broccoli Extract on the Physiological Expression of P-eIF2α: Expression of phosphorylated eukaryotic initiation factor 2 alpha (P-eIF2α) following treatment of Chub-S7 adipocytes with broccoli extract (BE; 10ng/ml) compared to untreated control cells (Con). p-values: * $p < 0.05$, ** $p < 0.01$, *** $p < 0.001$. Lines between points represent linkages between discrete mean values for data collected and are not true trajectories over time.

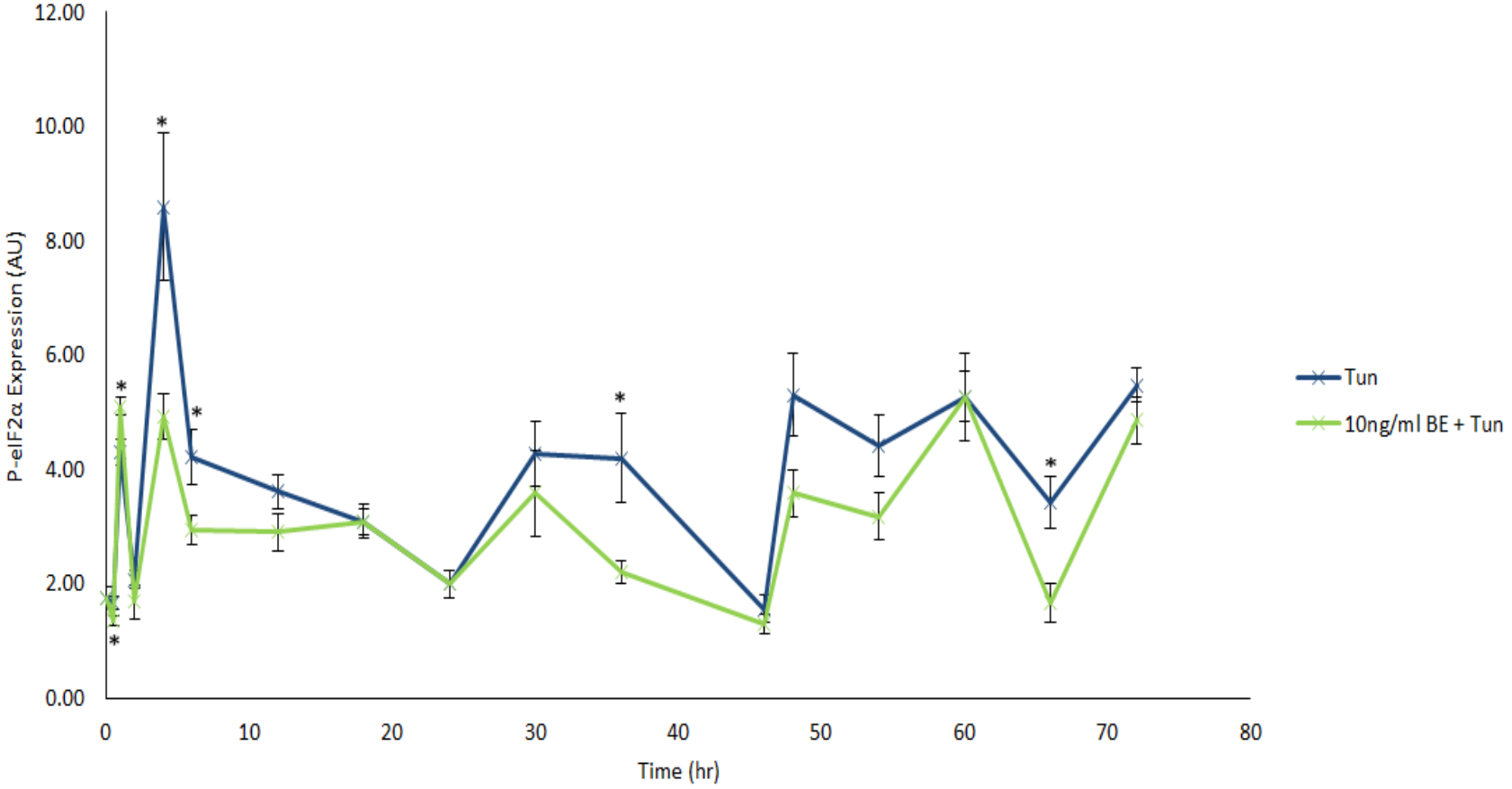

Figure 5.3.3.4 Effect of Broccoli Extract on Tunicamycin-Induced Expression of P-eIF2α: Expression of phosphorylated eukaryotic initiation factor 2 alpha (P-eIF2α) following treatment of Chub-S7 adipocytes with tunicamycin (Tun; 750ng/ml), or a combined broccoli extract and tunicamycin treatment (BE + Tun; 10ng/ml, 750ng/ml). p-values: * $p < 0.05$, ** $p < 0.01$, *** $p < 0.001$. Lines between points represent linkages between discrete mean values for data collected and are not true trajectories over time.

BE had similar effects on eIF2α protein expression to P-eIF2α expression. In cells treated with BE alone, eIF2α was expressed at a similar level compared to the control, with a significantly reduced level of expression at three time points (48hr, 54hr and 66hr), and a reduction of the peak expression at 54hr by 27% ($p = 0.02$) (Figure 5.3.3.5). The presence of BE in the tunicamycin treatment prevented the upregulation of eIF2α that was otherwise observed with tunicamycin treatment. This effect was sustained over time with a maximum 55% decrease in expression occurring at 48hr ($p = 0.002$) (Figure 5.3.3.6).

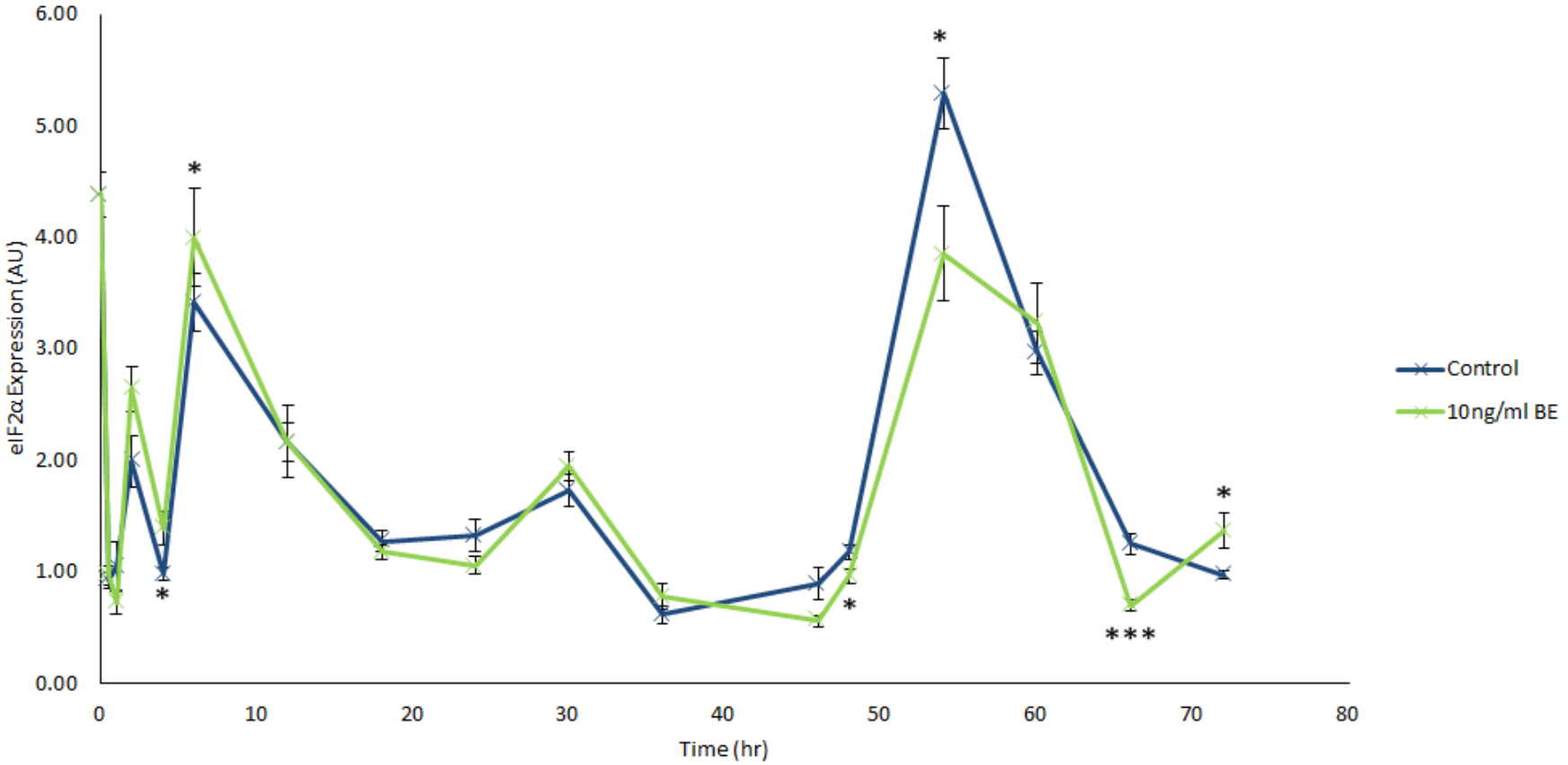

Figure 5.3.3.5 Effect of Broccoli Extract on the Physiological Expression of eIF2α: Eukaryotic initiation factor 2 alpha (eIF2α) protein expression was analysed following treatment of Chub-S7 adipocytes with broccoli extract (BE; 10ng/ml) compared to untreated control cells (Con). p-values: * $p < 0.05$, ** $p < 0.01$, *** $p < 0.001$. Lines between points represent linkages between discrete mean values for data collected and are not true trajectories over time.

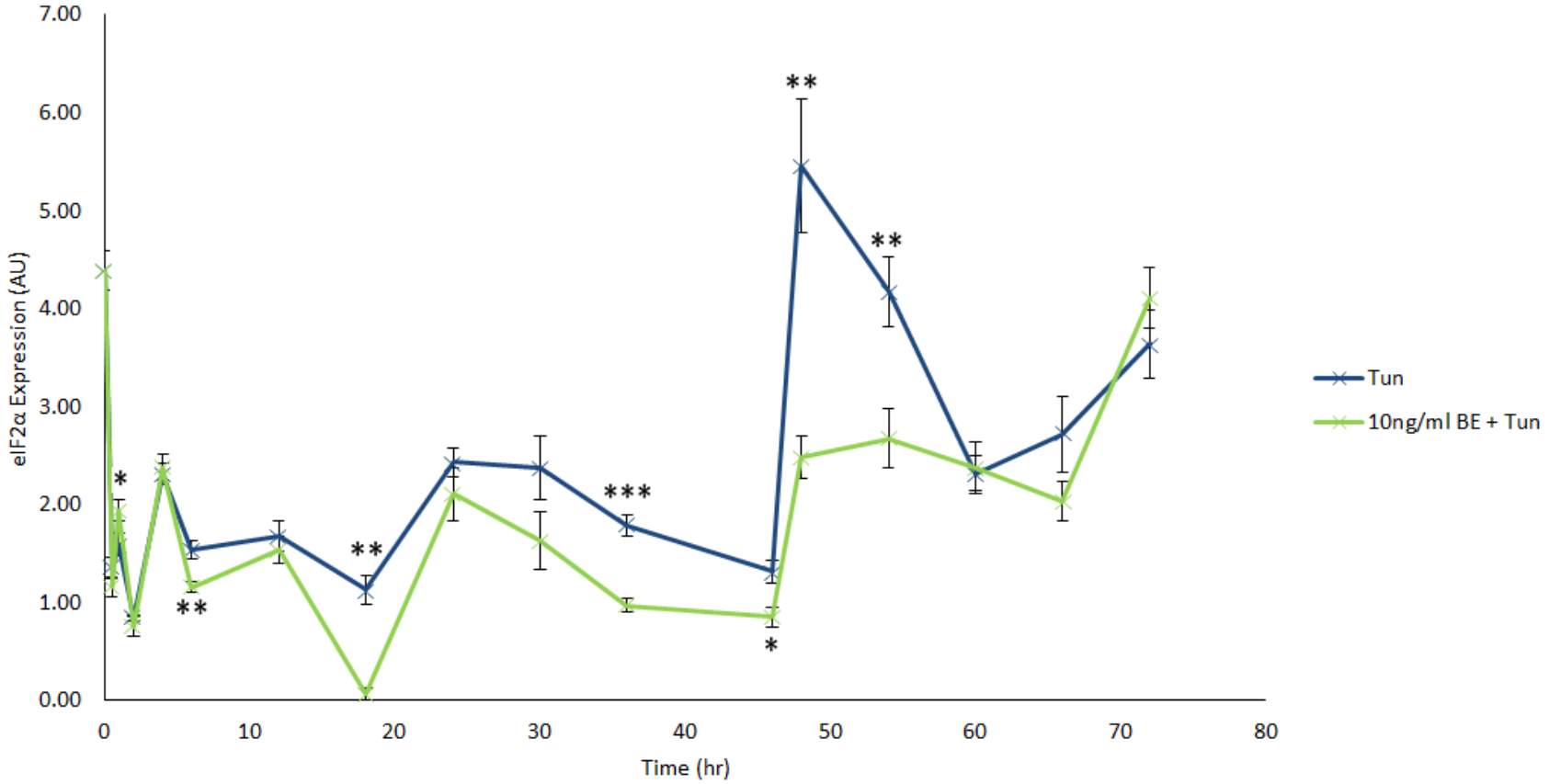

Figure 5.3.3.6 Effect of Broccoli Extract on Tunicamycin-Induced Expression of eIF2α: Eukaryotic initiation factor 2 alpha (eIF2α) protein expression was analysed following treatment of Chub-S7 adipocytes with tunicamycin (Tun; 750ng/ml) or a combination of broccoli extract and tunicamycin (BE+Tun; 10ng/ml, 750ng/ml). p-values: * $p < 0.05$, ** $p < 0.01$, *** $p < 0.001$. Lines between points represent linkages between discrete mean values for data collected and are not true trajectories over time.

The rate of phosphorylation of eIF2α to P-eIF2α was also useful as a measure of ER stress, and as an indicator of the translation attenuation pathway that occurs within the UPR. The relative expressions of the two proteins were used to observe this phosphorylation rate, which revealed that BE reduced the maximum peak rate of phosphorylation naturally occurring in control cells by 37% ($p = 0.01$) (Figure 5.3.3.7).

Broccoli extract in combination with tunicamycin (BE+Tun) significantly reduced the phosphorylation rate relative to tunicamycin on its own at six time points (6hr, 12hr, 18hr, 36hr, 66hr and 72hr) ($p<0.05$). As well as this, the addition of BE altered the oscillation cycle that occurred with the tunicamycin treatment, as described in the previous chapter, delaying the occurrence of the first sustained peak in the phosphorylation rate from 4hr to 18hr. Furthermore, the time periods over which the peaks occurred were reduced when BE was present (Figure 5.3.3.8).

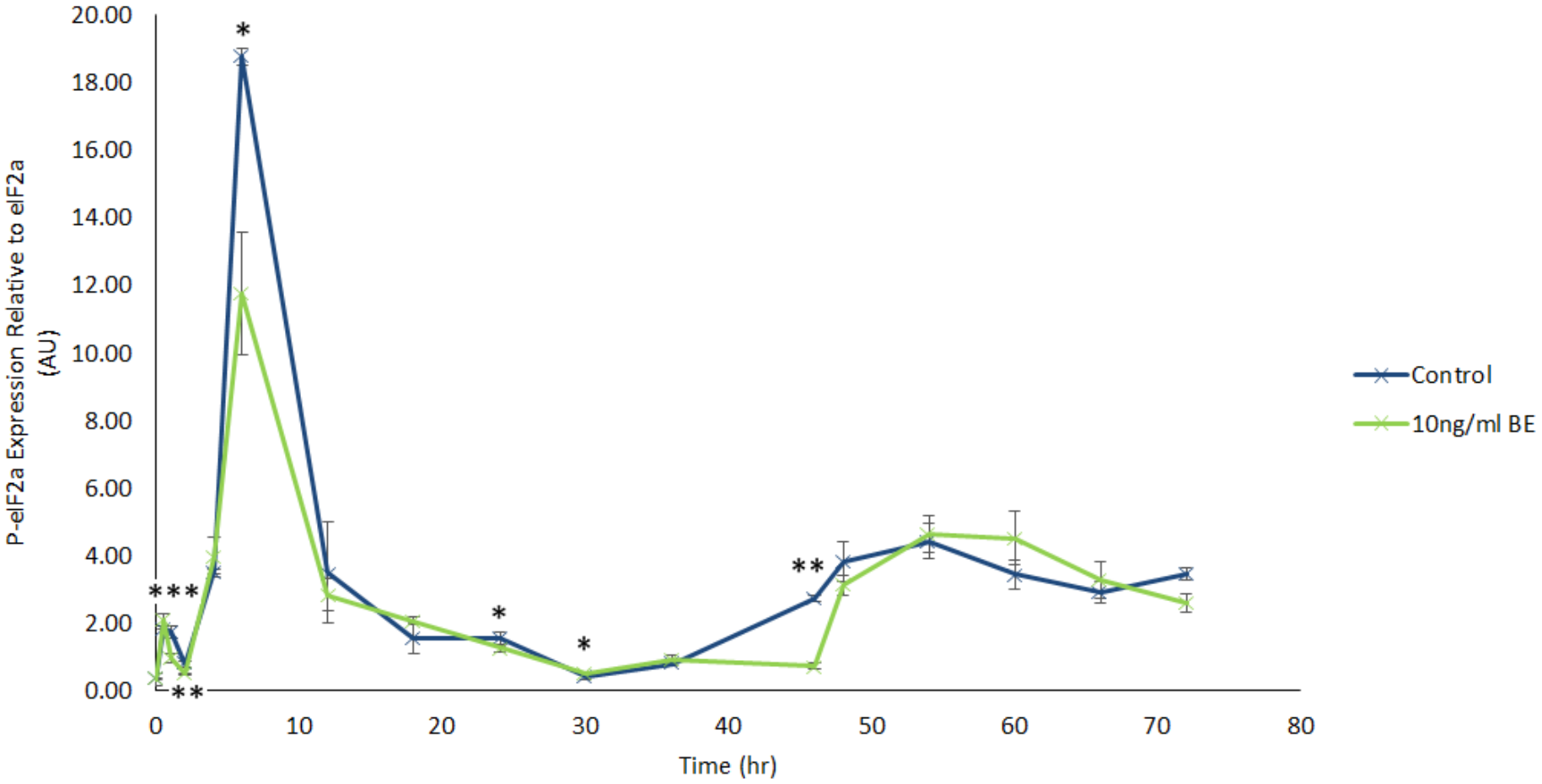

Figure 5.3.3.7 Effect of Broccoli Extract on the Physiological Rate of eIF2α Phosphorylation: Protein expression of phosphorylated eukaryotic initiation factor 2 alpha (P-eIF2α) relative to its un-phosphorylated counterpart (eIF2α) analysed after treatment of Chub-S7 adipocytes with broccoli extract (BE; 10ng/ml) compared to untreated control cells (Con). p-values: * $p < 0.05$, ** $p < 0.01$, *** $p < 0.001$. Lines between points represent linkages between discrete mean values for data collected and are not true trajectories over time.

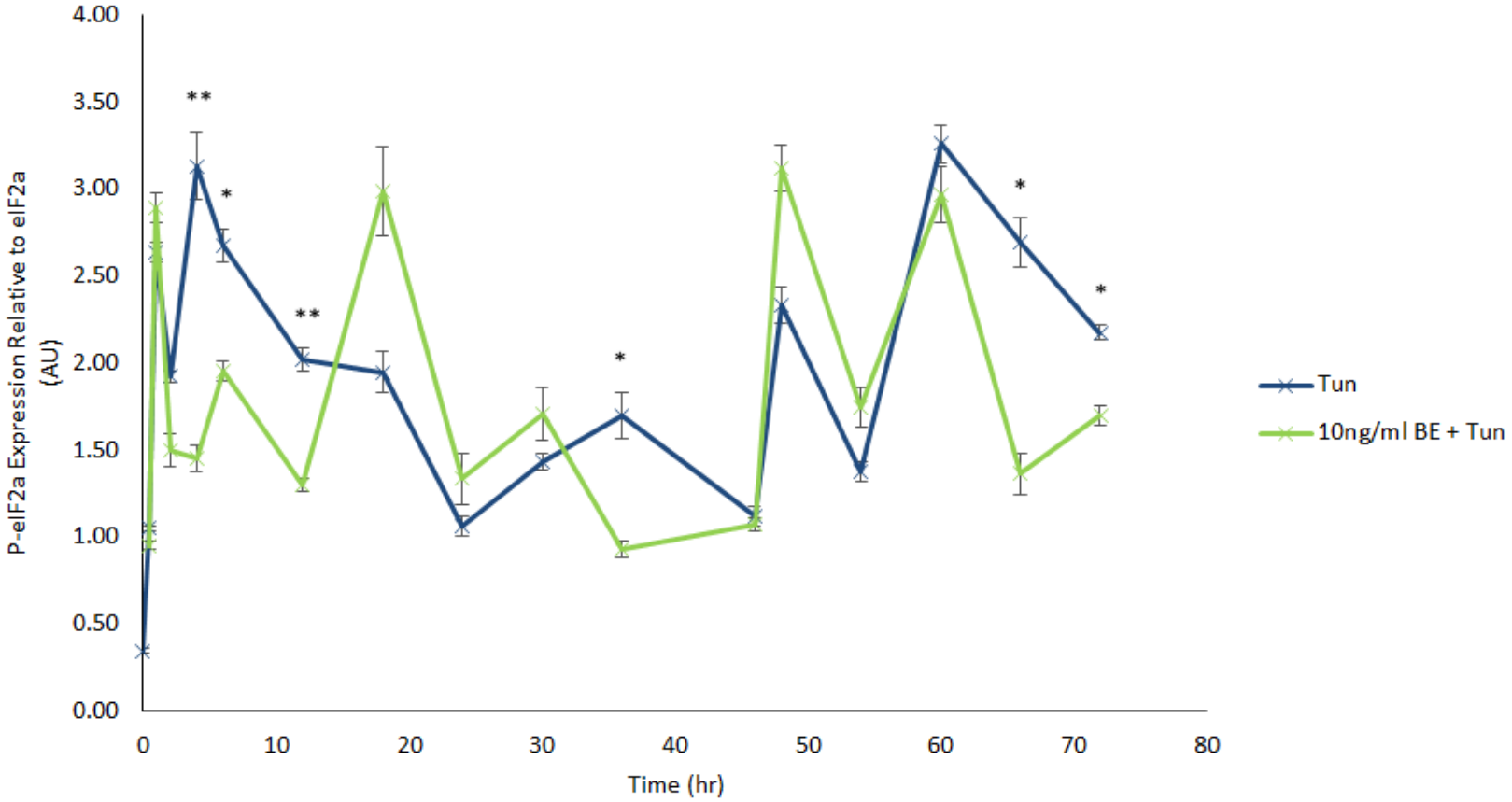

Figure 5.3.3.8 Effect of Broccoli Extract on Tunicamycin-Induced Phosphorylation Rate of eIF2α: Protein expression of phosphorylated eukaryote initiation factor 2 alpha (P-eIF2α) relative to its un-phosphorylated form (eIF2α) analysed after treatment of Chub-S7 adipocytes with tunicamycin (Tun; 750ng/ml) or broccoli extract combined with Tun (BE + Tun; 10ng/ml, 750ng/ml)). p-values: $p < 0.05$, ** $p < 0.01$, *** $p < 0.001$. Lines between points represent linkages between discrete mean values for data collected and are not true trajectories over time.

Representative Western blot images analysed to determine the protein expression of BiP, P-eIF2α, eIF2α and β-Actin following treatment, and used to create figures 5.3.3.1 – 5.3.3.8, are displayed below (Figure 5.3.3.9). This allowed direct comparison of treatments at each time point.

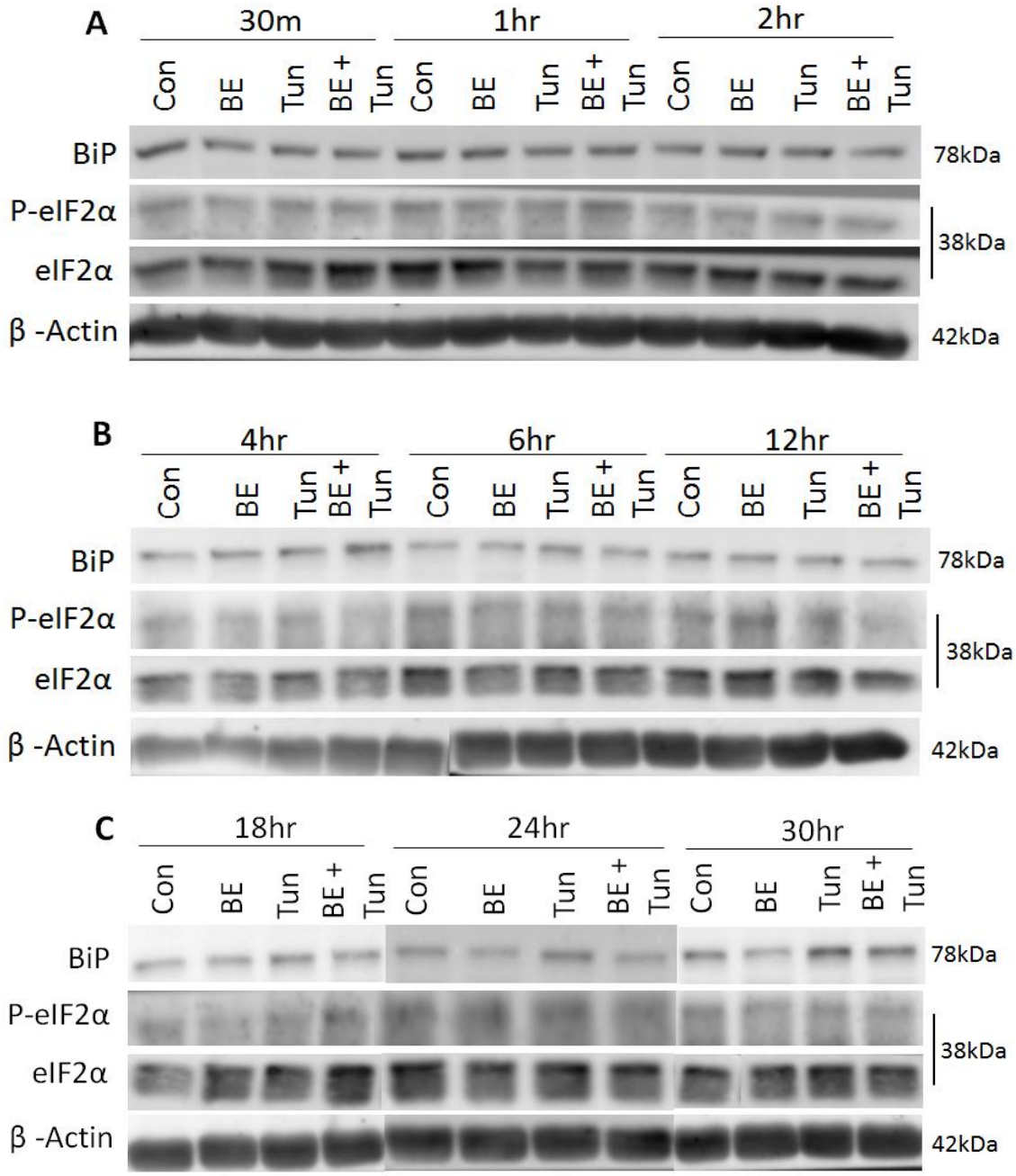

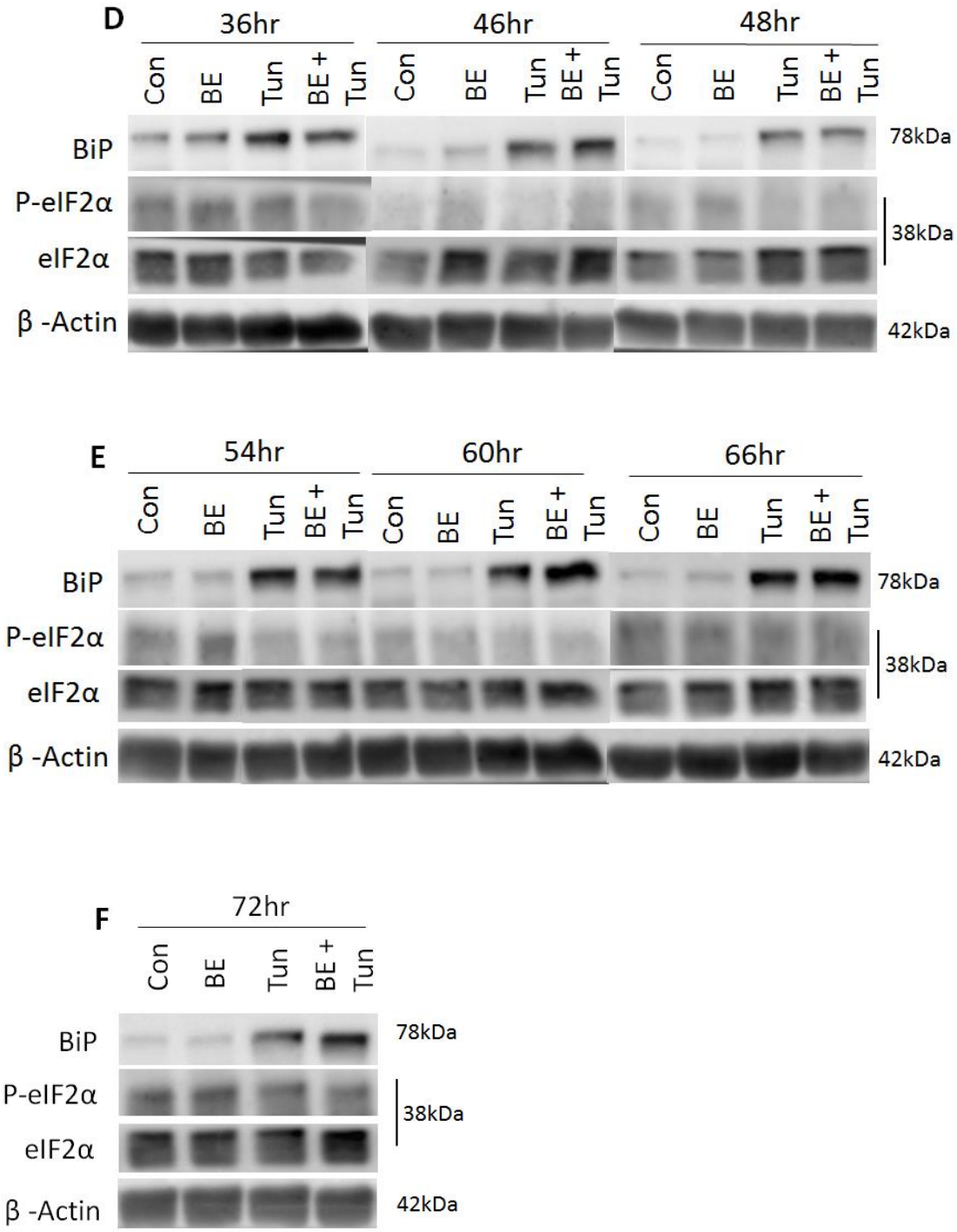

Figure 5.3.3.9 Western Blot Time Series Images: Representative Western blots of binding immunoglobulin protein (BiP), phosphorylated eukaryotic initiation factor alpha (P-eIF2α), eukaryotic initiation factor alpha (eIF2α) and β-Actin expression following treatment with 750ng/ml tunicamycin (Tun), 10ng/ml broccoli extract (BE) or a combination of the two (BE+Tun) compared to control (Con) at (**A**) 30 minutes, 1hr, 2hr (**B**) 4hr, 6hr, 12hr (**C**) 18hr, 24hr, 30hr (**D**) 36hr, 46hr, 48hr (**E**) 54hr, 60hr, 66hr (**F**) 72hr.

Findings from the time series experiment are summarised below as a table of percentage changes in a heat map fashion, with significant changes highlighted (Figure 5.3.3.10). A green cell represents a significantly lower expression of ER stress marker protein in samples containing either BE or BE+Tun, compared to their respective controls (control/tunicamycin), whilst a red cell represents a significantly increased expression due to the presence of BE ($p < 0.05$). As shown, out of the values that were significantly different to control cells, the presence of BE decreased the expression of the marker proteins studied in 67% of cases (Figure 5.3.3.10 A). Similarly, out of the values that were significantly different to tunicamycin treatment, the combined BE and tunicamycin treatment resulted in a decrease in expression in 87% of time points and proteins assessed (Figure 5.3.3.10 B).

A

Sample	% Change			
	BiP	P-eIF2α	eIF2α	P-eIF2α/eIF2α
Con/BE 30m	45.60	14.11	5.02	12.46
Con/BE 1hr	-45.85	-52.57	-31.24	-44.75
Con/BE 2hr	7.83	-16.13	32.29	-37.04
Con/BE 4hr	46.90	15.89	41.06	12.51
Con/BE 6hr	23.44	-3.92	16.96	-37.43
Con/BE 12hr	-11.88	-4.30	0.37	-18.70
Con/BE 18hr	-5.76	42.55	-7.46	31.96
Con/BE 24hr	-27.94	-21.47	-20.33	-17.89
Con/BE 30hr	-8.83	30.08	12.50	31.02
Con/BE 36hr	94.80	25.53	26.87	14.04
Con/BE 46hr	-34.40	-67.28	-37.07	-73.59
Con/BE 48hr	-31.68	-14.00	-18.49	-18.17
Con/BE 54hr	-17.89	-12.47	-27.15	5.10
Con/BE 60hr	-2.61	30.53	8.92	30.83
Con/BE 66hr	-35.82	-45.77	-44.18	12.15
Con/BE 72hr	35.42	55.10	40.66	-24.67

B

Sample	% Change			
	BiP	P-eIF2α	eIF2α	P-eIF2α/eIF2α
Tun/BE+Tun 30m	-8.93	-18.60	-14.31	-9.39
Tun/BE+Tun 1hr	5.31	18.79	21.87	9.61
Tun/BE+Tun 2hr	-10.81	-18.81	-10.83	-21.93
Tun/BE+Tun 4hr	4.93	-42.71	2.80	-53.59
Tun/BE+Tun 6hr	-52.31	-30.50	-24.85	-26.93
Tun/BE+Tun 12hr	21.77	-19.69	-8.14	-35.52
Tun/BE+Tun 18hr	-3.30	0.47	-49.34	53.08
Tun/BE+Tun 24hr	-13.59	14.11	-13.32	25.09
Tun/BE+Tun 30hr	-16.88	-16.17	-31.49	19.20
Tun/BE+Tun 36hr	-49.91	-47.72	-45.91	-45.10
Tun/BE+Tun 46hr	-6.68	-17.49	-35.15	-4.32
Tun/BE+Tun 48hr	-29.42	-32.48	-54.56	33.85
Tun/BE+Tun 54hr	6.35	-28.00	-35.97	27.04
Tun/BE+Tun 60hr	8.85	-0.24	2.45	-8.89
Tun/BE+Tun 66hr	-15.39	-51.05	-25.17	-49.32
Tun/BE+Tun 72hr	70.30	-11.18	12.93	-21.91

Figure 5.3.3.10 Summary of Broccoli Extract Effect on ER Stress (A) Percentage changes induced by treatment with broccoli extract (BE; 10ng/ml) compared with untreated control cells (Con). **(B)** Percentage changes induced by a combined treatment of BE and Tunicamycin (BE+Tun; 10ng/ml, 750ng/ml) compared to Tunicamycin (Tun; 750ng/ml). Green cells represent a significantly decreased expression of ER stress protein in samples treated with either BE or BE+Tun, compared to their respective controls (Con/Tun) ($p<0.05$). Red cells represent a significantly increased expression of the ER stress proteins due to the presence of BE in the sample compared to controls (Con/Tun) ($p < 0.05$). White cells represent no significant change with the presence of BE.

5.4 Discussion

The aim of this study was to determine if a broccoli extract could prevent or reduce ER stress induced by tunicamycin over time to ascertain whether BE may offer a potential protective mechanism over periods of sustained ER stress. These investigations revealed three key findings. Firstly, broccoli extract did not itself exacerbate the normal physiological ER stress protein response within adipocytes. Secondly, broccoli extract significantly reduced tunicamycin-induced ER stress, highlighting the potential role of broccoli in dampening an ER stress response. Finally, the effects of broccoli extract can be sustained over time despite the continued ER stress insult.

Initial studies were carried out in order to identify the effect of BE treatment on the levels of physiological ER stress occurring within adipocytes, to determine that BE could reduce insult driven ER stress without acting as an inhibitor of normal physiological ER stress protein response. mRNA studies indicated that there was very little change in the expression of ER stress markers with the treatment of BE compared with untreated control cells. Similar results were also observed during a subsequent, additional, multiple time series interval analysis study, which revealed that protein expression was mostly unchanged over the multiple time points studied. These findings suggest that BE does not have adverse effects on the physiological ER stress occurring in adipocytes over time.

Further studies were carried out in order to determine whether BE could reduce the level of ER stress that occurs with tunicamycin treatment. Tunicamycin is often used to artificially induce ER stress in cell culture experiments as it blocks the initial step

of glycoprotein biosynthesis, causing an accumulation of unfolded glycoproteins in the ER and leading to ER stress (Oslowski and Urano 2011). As has been observed in many other studies (Bogdanovic, Kraus *et al*. 2015, Wang, Wang *et al*. 2015), tunicamycin did induce ER stress throughout these experiments. Studies using mRNA expression data assessed the impact of BE on tunicamycin-induced ER stress, which revealed that treatment with three different concentrations of BE all prevented the upregulation of ER stress marker genes ATF4, ATF6 and CHOP in a time-dependent manner. The only time point where BE significantly increased the expression of ER stress genes when added to the Tun treatment was with ATF6 at 48hr. If ATF6 is expressed in a cyclic manner, as other UPR components have been demonstrated to in this thesis, it is possible that the addition of BE may alter the expression pattern such that a peak in expression with combined BE+Tun treatments is being compared with a dip in expression with Tun treatment. This highlights the importance of investigating more frequent time points when studying components of the UPR. However, as this was the only time point where BE significantly increased the expression compared to Tun out of all the genes studied, it was considered worthwhile to continue with the study using 10ng/ml for the concentration of BE. It is hard to determine how this concentration may translate to amount of broccoli required in the diet to obtain similar results *in vivo*. The nutritional content of 20g of freeze dried broccoli powder is roughly equivalent to one large head of broccoli, however it is currently unknown how much broccoli would have to be consumed by humans in order to replicate the results seen in these experiments. This is a standard problem encountered with *in vitro* studies, as whilst it provides useful information with regards to cellular processes, extrapolation to *in vivo* can lead to erroneous

conclusions. Future *in vivo* studies would therefore have to be carried out in order to investigate this.

BE demonstrated the most protection with CHOP mRNA, where the protective effect of BE increased over time, culminating in a 62% reduction in the expression induced by tunicamycin at 72hr. This prominent effect with CHOP is most likely due to the fact that it is up-regulated at the end of all three arms of the UPR, resulting in a much more intense expression during ER stress and a more pronounced protective effect of BE (Nishitoh 2012, Li, Guo *et al*. 2015). ATF4 and ATF6, however, both occur earlier in their respective pathways, and are each involved in only one arm of the UPR; consequently, their expression does not increase to the same extent during ER stress and the protective effect of BE is not as prominent. These findings have further implications, as CHOP is a promoter of apoptosis (Li, Guo *et al*. 2015), and has recently been identified as a key mediator of insulin resistance and glucose intolerance during obesity development (Suzuki, Gao *et al*. 2017). As such, these results indicate that BE may reduce the level of apoptosis and insulin resistance that occurs during obesity-mediated ER stress, thus aiding in the survival of the organism.

Protein expression of BiP, P-eIF2α and eIF2α was also assessed to determine the effect of BE at protein level. BiP is a major chaperone located in the ER which is critical for protein quality control, as well as for regulating the activation of ER stress signalling molecules (Gething 1999, Wang, Wey *et al*. 2009). Protein analysis revealed that BiP experienced the least protection by the addition of BE to the tunicamycin treatment: despite BE causing a delay in the initial major increase in expression from 36hr to 46hr, it also significantly increased expression at the final 72hr time point. It

is possible that whilst BE delays the expression of BiP, allowing the cell to function normally for a prolonged period of time, it is unable to counter the ability of tunicamycin to induce ER stress for more than 66hr. This reduced effect of BE protection on BiP expression is most likely due to the important role that BiP has in the detection of ER stress and the subsequent activation of the UPR. As the initial sensor of ER stress, as well as acting as a switch for each of the UPR arms, BiP expression is tightly controlled, with evidence suggesting that it is more tightly regulated at the post-translational level, rather than the transcriptional level (Gülow, Bienert *et al*. 2002, Takayanagi, Fukuda *et al*. 2013). This suggests that the protective effects of BE may occur at the transcriptional level and, as such, BiP is less affected by BE treatment than other UPR proteins.

P-eIF2α and eIF2α were selected for analysis to examine what effect BE has on the translation attenuation system. This system is part of the UPR which reduces protein synthesis rates during ER stress to lessen the load of substrates on the folding machinery in the ER lumen (Harding, Zhang *et al*. 2000). The previous chapters detailed the importance of the translation attenuation system, and illustrated how P-eIF2α and eIF2α undergo oscillation when exposed to tunicamycin in an attempt to reduce stress whilst maintaining a sufficient level of protein production for the cell to survive. When exposed to BE alongside the tunicamycin treatment, both P-eIF2α and eIF2α had a distinct reduction in expression compared to tunicamycin on its own. The maximum expression of P-eIF2α was reduced by 42% in the presence of BE, resulting in a less intense, more stable level of the protein. P-eIF2α is a known transcription factor of ATF4, which in turn is a transcription factor of CHOP, a key component of the apoptosis pathway (Li, Guo *et al*. 2015, Rozpedek, Pytel *et al*.

2016); thus, these results support observations from the mRNA data that reduced expression of P-eIF2α may prevent apoptosis occurring in adipocytes. Similarly, BE reduces the peak expression of eIF2α induced by tunicamycin at 48hr by 55%. These data indicate that the translation attenuation system is less likely to be activated when BE is present alongside inducers of ER stress such as tunicamycin, thus improving the health of adipocytes across these time points.

Analysing the ratio of P-eIF2α to eIF2α to provide information on the rate of eIF2α phosphorylation revealed that BE delays the oscillation cycle that occurs with tunicamycin treatment, with the second major peak occurring at 18hr as opposed to 4hr. Furthermore, the peaks in the phosphorylation rate are much shorter-lived when BE is present. These results are indicative of the adipocytes experiencing a reduced level of ER stress when BE is present, despite an equal dose of tunicamycin being provided. Recent research has revealed that reversal of the translation attenuation system with an inhibitor potently suppresses the expression of PERK-dependent inflammatory genes, without disrupting normal immune function (Guthrie, Abiraman *et al*. 2016). It is also known that the translation attenuation system, whilst blocking general translation, promotes the induction of pro-apoptotic transcriptional factors (Sano and Reed 2013). As such, the delayed, shorter-lived peak rates of eIF2α phosphorylation that occur with BE treatment may reduce both inflammatory and apoptotic cellular signals, preventing further damage to the cell.

5.5 Conclusions

This study has demonstrated that BE is able to mitigate the chronic ER stress response that is induced by tunicamycin, without preventing the routine physiological ER protein response that occurs within adipocytes. Consequently, with the use of BE, damaging cellular processes that result in insulin resistance and apoptosis are less likely to occur. There is therefore the potential that a broccoli supplement in the diet may decrease the level of chronic ER stress that occurs during obesity, thus promoting cellular health and reducing the risk of T2DM. The results in this chapter have contributed to the third aim of this thesis – to investigate the potential protective effects of broccoli against ER stress in adipocytes.

CHAPTER 6:

The Effect of Broccoli on Mitochondria and ROS

6.1 Introduction

As documented previously, ER stress contributes to increased T2DM risk (Ozcan, Cao *et al*. 2004, Eizirik, Cardozo *et al*. 2008, Back and Kaufman 2012). This can arise through the interplay of other associated cellular mechanisms, which ultimately leads to cellular dysfunction and insulin resistance. These associated cellular mechanisms include reactive oxygen species (ROS) production, mitochondrial damage and chronic inflammation. These mechanisms form a complicated signalling network that prepares the cell for a response against the cause of the stress; however this process can increase the risk of developing diseases such as T2DM, as discussed below.

ROS and reactive nitrogen species (RNS) form within cells as a natural by-product of processes such as oxygen metabolism and protein folding (du Plessis, Harlev *et al*. 2017), however excessive production can cause cellular damage (Di Meo, Reed *et al*. 2016). ROS/RNS is a broad term that encompasses many types of reactive species, which each have specific antioxidants to counter them (Di Meo, Reed *et al*. 2016). Catalase, for example, converts hydrogen peroxide (H_2O_2) ROS to water and oxygen, whilst superoxide dismutase is a mitochondrial protein that prevents the build-up of superoxide by-products of oxidative phosphorylation.

In the ER, correct folding of proteins often requires the generation of disulphide bonds which results in the production of hydrogen peroxide (H_2O_2), a form of ROS (Bulleid and van Lith 2014). Similarly, ROS is produced in mitochondria during oxidative phosphorylation as electrons from complex I and complex III from the electron transport chain partially reduce oxygen to form superoxide (Cao and

Kaufman 2014). Under routine circumstances, a balance between ROS and antioxidants that attenuate their damaging effects is maintained, and in some instances ROS can act as protective signalling molecules. However, in cases when overproduction of ROS occurs, or excess ROS is not eliminated, oxidative stress can occur which causes cell and tissue damage (du Plessis, Harlev *et al*.).

During ER stress, the tightly controlled microenvironment of ER protein folding can become compromised, resulting in a futile cycle of disulphide bond formation and reduction which generates large amounts of H_2O_2 ROS (Cao and Kaufman 2014). Production of ROS is exacerbated further through an efflux of Ca^{2+} from the ER to mitochondria which leads to the inhibition of complex III of the electron transport chain (ETC). This increases the production of ROS due to higher levels of the ubisemiquinone radical intermediate being formed (Cao and Kaufman 2014). In addition to this, increased levels of Ca^{2+} in the mitochondria stimulates the Krebs cycle, boosting oxygen consumption and further ROS production. This substantial increase in ROS production outbalances the number of antioxidants, and thus can cause significant damage to the cell.

Whilst low levels of ROS are required for some cellular processes, continuous exposure to ROS can also damage mitochondria. This can lead to oxidative damage to ETC complexes, mitochondrial DNA (mtDNA) and lipids, and cause mitochondrial dysfunction (Besse-Patin and Estall 2014). Mitochondrial dysfunction is characterised by a loss of efficiency in the electron transport chain and reductions in the synthesis of high-energy molecules such as adenosine-5’-triphosphate (ATP) (Nicolson 2014). When this occurs, it requires adaptation through (1) fusion of partially dysfunctional

mitochondria and mixing of their undamaged components to improve overall function, (2) the separation of damaged mitochondria into smaller mitochondria (fission), and (3) the removal and complete degradation of dysfunctional mitochondria (mitophagy) to avoid cellular damage (Nicolson 2014). Impaired mitochondrial function can be a cause of insensitivity towards insulin, arising due to insufficient energy supplies, or defects in the insulin signalling pathway (Abdul-Ghani and DeFronzo 2008, Victor, Rocha *et al*. 2011, Wang, Chi *et al*. 2012). Further to this, ER stress, ROS and mitochondrial dysfunction are all known to induce inflammation, which is a major contributor to insulin resistance and T2DM (Cefalu 2009, Mittal, Siddiqui *et al*. 2014). Mitochondrial function can be assessed by using a Seahorse XF analyser, which provides information on the extracellular acidification rate (ECAR) and oxygen consumption rate (OCR) of cells. ECAR provides an indication of glycolytic rate, as cells undergoing higher rates of glycolysis exhibit higher rates of proton production than cells using oxidative phosphorylation. Higher OCR levels indicate that cells are preferentially producing ATP through oxidative phosphorylation, the more efficient form of energy production. The ratio of OCR to ECAR provides information on the preference of cells for oxidative phosphorylation over glycolysis (Zhang, Nuebel *et al*. 2013).

Studying the OCR relative to the baseline of each treatment also provides information on how the cells respond to particular pharmacological inhibitors as part of a stress test. The sequential addition of oligomycin (an ATP synthase inhibitor), FCCP (carbonyl cyanide p-trifluoromethoxyl-phenylhydrazone, a protonophoric uncoupler), and a combination of rotenone & antimycin A (electron transport inhibitors) allows assessment of key factors of mitochondrial function, such as:

- Proton leak – an indicator of mitochondrial inefficiency: increased proton leak decreases oxidative phosphorylation yield and can be caused by high levels of ROS.
- ATP production – rate of ATP being produced.
- Maximal respiration – maximum rate of ATP being produced in the mitochondria.
- Spare capacity – extra mitochondrial capacity available in a cell to produce energy under stressful conditions. An indicator of long-term cellular survival and function.

An example of how the stress test can provide this information is provided below (Figure 6.1).

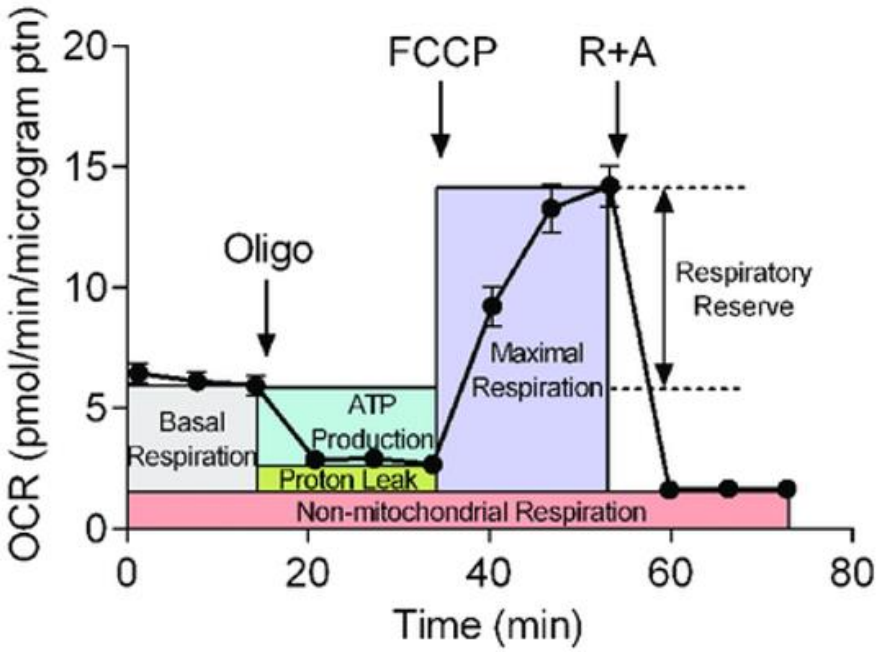

Figure 6.1 Mitochondrial Functions determined by Oxygen Consumption Rate (OCR) Stress Test: Indicators of mitochondrial function such as basal respiration, ATP production, proton leak, maximal respiration, respiratory reserve (also known as spare capacity) and non-mitochondrial respiration, can be compartmentalised by the sequential addition of pharmacological inhibitors, oligomycin (oligo), carbonyl cyanide p-trifluoromethoxy-phenylhydrazone (FCCP) and a combination of rotenone (R) & antimycin A (A). *Figure from (Yang, Chadwick et al. 2017).*

The previous chapter demonstrated the positive influence broccoli extract can have on reducing ER stress; it is therefore plausible that it may also protect against both ROS and mitochondrial dysfunction. Investigating key pathways that may be influenced by the addition of broccoli extract may provide an insight into its mechanism of action, identifying specific cellular components that are involved in its activity.

As such, the aims of this study were to:

1. Determine the effects of tunicamycin on ROS production and mitochondrial health.
2. Assess whether the protective effects of broccoli extend to ROS production and mitochondrial dysfunction.
3. Identify possible pathways through which broccoli extract acts to provide cellular protection.

6.2 Methods

6.2.1 Effect of Broccoli on Mitochondrial Function and ROS

Chub-S7 preadipocyte cells were differentiated over 14 days before being exposed to 10ng/ml broccoli extract (BE), 750ng/ml tunicamycin (Tun), or a combination of the two for 24hr. Those cells treated with both BE and tunicamycin were pre-treated with BE for 24hr prior to the addition of tunicamycin. Vehicle control cells were grown alongside under the same conditions, and are hereafter referred to as control. Following treatment, cells were analysed for ROS, or studied with a Seahorse XF Analyser to determine impact on mitochondrial function.

6.2.2 Investigating Transcriptomic Targets of Broccoli

In order to examine potential pathways through which broccoli extract acts, mRNA samples at the time point where BE had the most impact over the various experiments, 36hr, was studied with transcriptomics. RNA quality was assessed using a bioanalyser, and samples were then converted into libraries of templates that were sequenced and compared to one another to identify any significant changes in expression. Triplicate samples were used for each treatment. Comparing the transcripts that were differentially expressed against Uniprot protein human sequences then allowed pathway information to be obtained.

6.3 Results

6.3.1 Broccoli Extract Prevents Tunicamycin-Induced ROS/RNS

Analysis of different types of ROS revealed that tunicamycin significantly increased ROS/RNS production at 24hr by 28%, whilst BE prevented this increase ($p = 0.005$). There were no significant changes in catalase or SOD specific ROS expression with treatment (Figure 6.3.1).

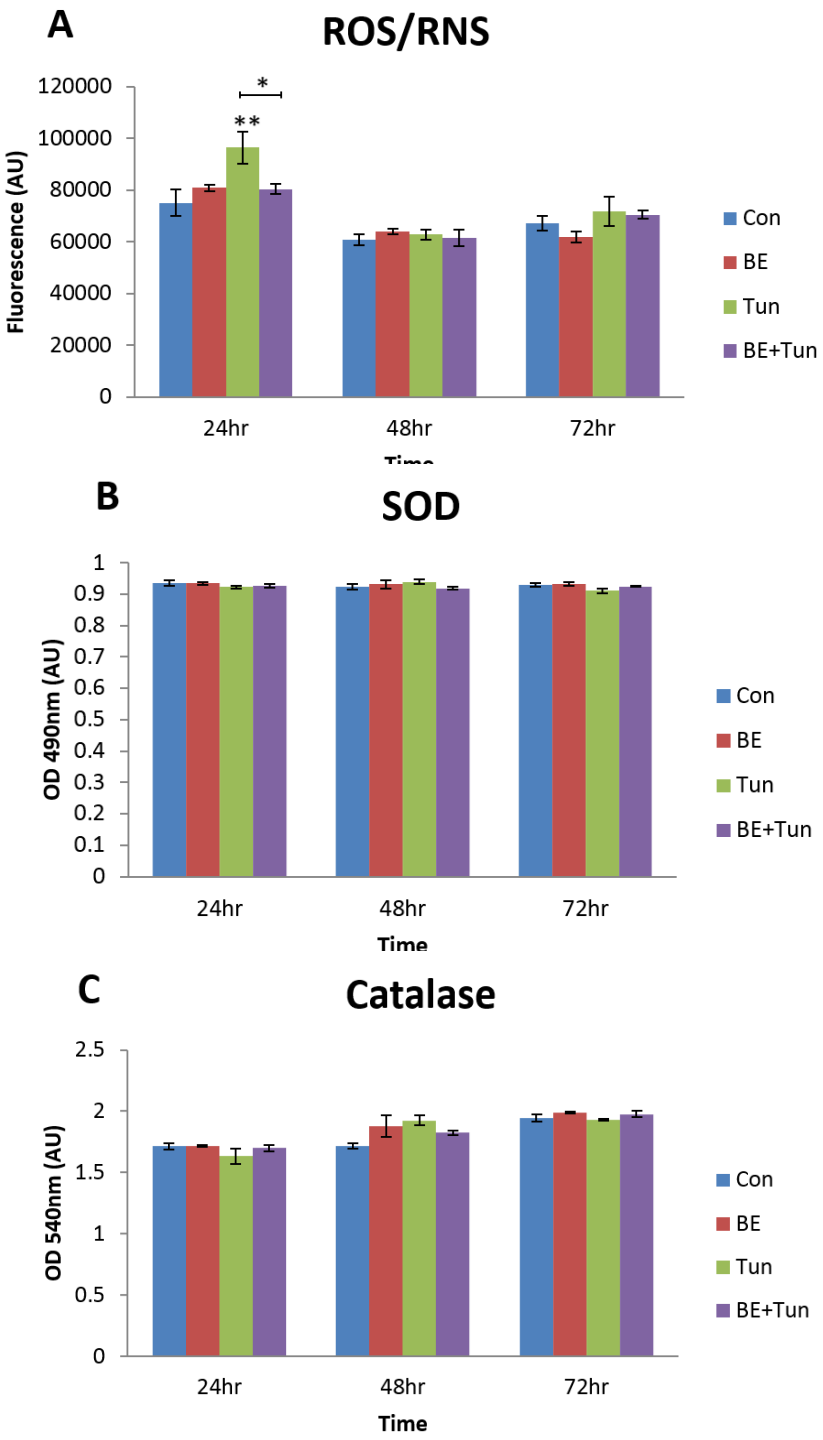

Figure 6.3.1 Effect of Tunicamycin and Broccoli on Reactive Oxygen Species Production: (A) Total reactive oxygen species (ROS) and reactive nitrogen species (RNS), **(B)** superoxide dismutase and **(C)** catalase production were analysed following treatment with 10ng/ml broccoli extract (BE), 750ng/ml tunicamycin (Tun) or a combination of the two (BE+Tun). Statistical analysis was undertaken with control vs. tunicamycin and tunicamycin vs. BE + tunicamycin treatments, p-values: * $p < 0.05$, ** $p < 0.01$, *** $p < 0.001$.

6.3.2 Effect of Tunicamycin and Broccoli on Mitochondrial Function

Key mitochondrial functions were studied in live cells using a Seahorse XF Analyser. Tunicamycin resulted in a 71% increase in overall oxygen consumption rate (OCR), whilst OCR was unaffected by broccoli extract treatment. The combined broccoli extract and tunicamycin treatment (BE+Tun) reduced the 71% increase to only 25%. Conversely, overall ECAR was significantly increased by 24% with BE+Tun treatment ($p < 0.05$), whilst individual BE and tunicamycin treatments resulted in similar levels as control cells (Figure 6.3.2.1).

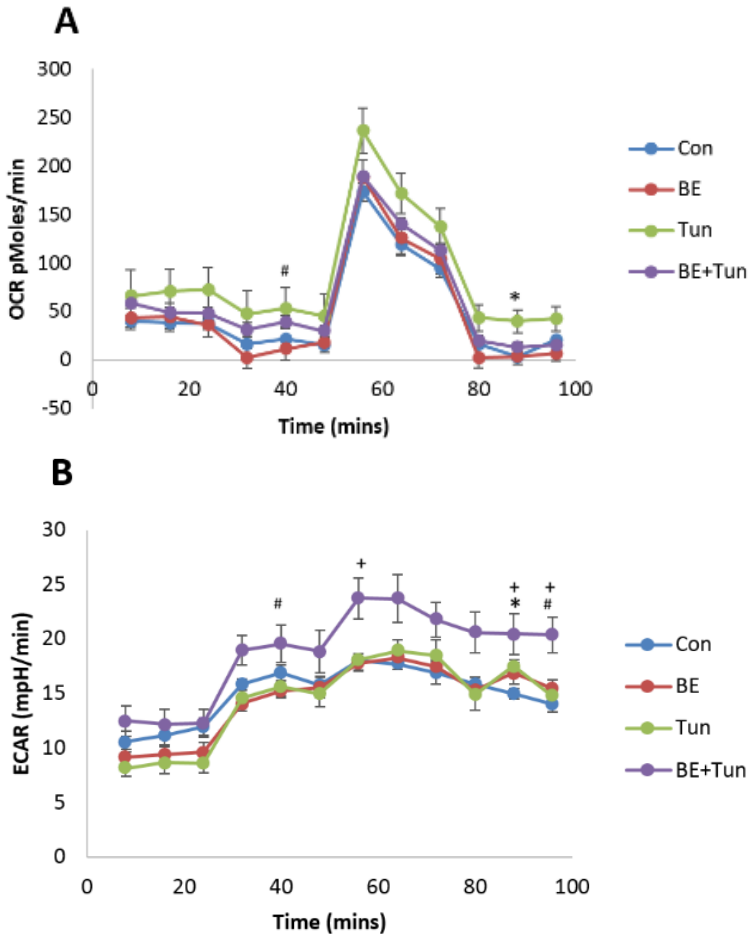

Figure 6.3.2.1 Mitochondrial Function following Broccoli Extract and Tunicamycin Treatment: (A) Oxygen consumption rate (OCR) and **(B)** extracellular acidification rate (ECAR) of adipocytes following treatment with broccoli extract (BE, 10ng/ml), tunicamycin (Tun, 750ng/ml) or a combination of the two (BE+Tun). Statistical analysis was undertaken with control vs. treatment (* = Con vs. Tun, # = Con vs. BE+Tun) and BE+Tun vs. Tun (+), p-values: * $p < 0.05$, ** $p < 0.01$, *** $p < 0.001$.

Analysing OCR results as a percentage of the baseline following application of stress test chemicals provided information on aspects of mitochondrial function, as described in Figure 6.1. Broccoli extract treatment had no detrimental effect on maximal respiration, whilst tunicamycin treatment reduced maximal respiration by 37% relative to control. BE+Tun combined treatment resulted in only an 18% reduction in maximal respiration compared to control. Similar results were also observed with regards to spare capacity, an indicator of long-term cellular survival and function – tunicamycin reduced the spare capacity by 46%, whilst BE+Tun resulted in a smaller reduction of 23% and BE treatment was similar to control (Figure 6.3.2.2).

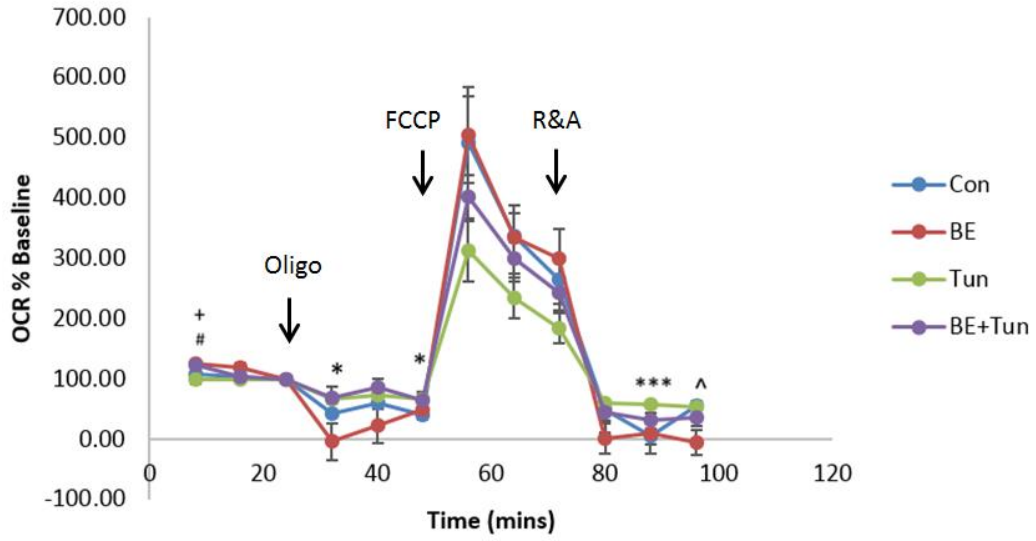

Figure 6.3.2.2 OCR% Baseline following Broccoli Extract and Tunicamycin Treatment: Oxygen consumption rate (OCR) of Chub-S7 adipocytes was measured and calculated as a percentage of the baseline measurement following treatment with broccoli extract (BE, 10ng/ml), tunicamycin (Tun, 750ng/ml) or a combination of the two (BE+Tun). Pharmacological inhibitors oligomycin (oligo), carbonyl cyanide p-trifluoromethoxy-phenylhydrazone (FCCP) and a combination of rotenone (R) & antimycin A (A) were added sequentially, as indicated. Statistical analysis was performed with control vs. treatment (* = Con vs. Tun, # = Con vs. BE+Tun, ^ = Con vs. BE), and Tun vs. BE+Tun (+), p-values: * $p < 0.05$, ** $p < 0.01$, $p < 0.001$.

Studying the ratio of OCR to ECAR revealed that tunicamycin induced a significantly higher rate of OCR at 56 minutes relative to ECAR, and increased the overall ratio by 95%. BE treatment and BE combined with tunicamycin exhibited similar results to control cells (Figure 6.3.2.3).

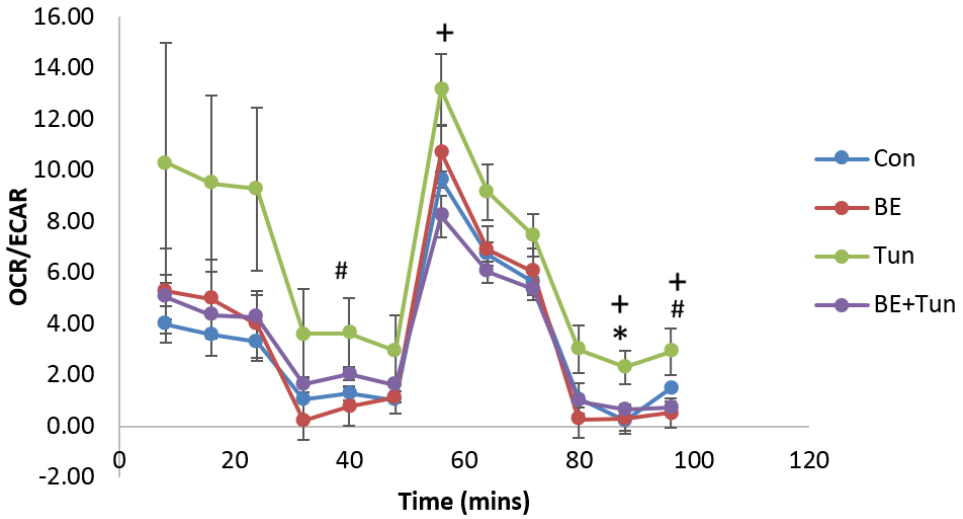

Figure 6.3.2.3 OCR/ECAR Ratio following Broccoli Extract and Tunicamycin Treatment: The ratio of oxygen consumption rate (OCR) to extracellular acidification rate (ECAR) was measured following treatment with broccoli extract (BE, 10ng/ml) Tunicamycin (Tun, 750ng/ml), or a combination of the two (BE+Tun) in order to determine cellular preference for glycolysis or oxidative phosphorylation. Statistical analysis was performed with control vs. treatment (* = Con vs. Tun, # = Con vs. BE+Tun, ^ = Con vs. BE), and Tun vs. BE+Tun (+), p-values: * $p < 0.05$, ** $p < 0.01$, *** $p < 0.001$).

Area under the curve was determined for each factor of mitochondrial function measured. These results are displayed below as a percentage of control values in the form of a heat map (Table 6.3.2.4).

	OCR	ECAR	% OCR Baseline	Max. Respiration	Spare Capacity	OCR/ECAR
Con	100.0	100.0	100.0	100.0	100	100.0
BE	100.4	95.5	97.5	102.6	103.2	105.3
Tun	171.3	96.4	86.4	63.3	54.0	194.9
BE+Tun	125.4	124.0	98.9	81.5	76.8	104.8

Table 6.3.2.4 Effect of Tunicamycin and Broccoli Treatments on Mitochondrial Function: Area under the curve (AUC) of oxygen consumption rate (OCR), extracellular acidification rate (ECAR), OCR as a percentage of baseline measurement (% OCR Baseline), maximal respiration (Max. Respiration), spare capacity and OCR/ECAR ratio was measured following treatment with 10ng/ml broccoli extract (BE), 750ng/ml Tunicamycin (Tun), or a combination of the two (BE+Tun). Results are displayed relative to control values as a heat map where red cells indicate a detrimental change to the mitochondria and green or white cells indicate similar values to control.

A summary of the results obtained on the effect of treatments on mitochondrial dysfunction is provided in Table 6.3.2.5, indicating that BE provides protection against mitochondrial dysfunction induced by tunicamycin.

Function	Description	Result
Oxygen Consumption Rate (OCR)	Indicator of oxidative phosphorylation . A general increase can indicate an influx of Ca^{2+} to the mitochondria, inhibiting the electron transport chain, enhancing ROS and causing apoptosis.	• BE similar to control • 71% increase with Tun • 25% increase with BE + Tun
Extracellular Acidification Rate (ECAR)	Indicator of glycolysis, the less efficient form of ATP production compared to oxidative phosphorylation. Higher values can also indicate the initiation of mechanisms to repair ROS damage.	• BE similar to control • Tun similar to control • 24% increase with BE + Tun
Maximal Respiration	Maximum rate of mitochondrial respiration possible. High values indicate healthy, efficient mitochondria.	• BE similar to control • 37% reduction with Tun • 18% reduction with BE + Tun
Spare Capacity	Extra mitochondrial capacity available in a cell to produce energy under stressful conditions. High values indicate long-term cellular survival and function.	• BE similar to control • 46% reduction with Tun • 23% reduction with BE + Tun
OCR/ECAR Ratio	High values indicate a preference for oxidative phosphorylation, the more efficient form of ATP production compared to glycolysis, but can also indicate an influx of Ca^{2+} to the mitochondria.	• BE similar to control • 95% increase with Tun • BE + Tun similar to control

Table 6.3.2.5 Summary of Mitochondrial Characteristics following Treatment: Oxygen consumption rate (OCR), extracellular acidification rate (ECAR), maximal respiration, spare capacity and OCR/ECAR ratio were all assessed in Chub-S7 adipocytes following treatment with broccoli extract (BE, 10ng/ml), tunicamycin (Tun, 750ng/ml), and a combination of the two (BE + Tun).

6.3.3 Broccoli Extract Upregulates Mevalonate Biosynthesis

Transcriptomics studies revealed a multitude of genes that were altered with treatment. The 20 most up- and down-regulated genes for each treatment are displayed in Figures 6.3.3.1 – 6.3.3.3 below.

A

Gene Name	Protein Name	log2 Fold-Change	p-adj
ATP2B1	Plasma membrane calcium-transporting ATPase 1	7.45769053	2.35E-06
NT5C2	Cytosolic purine 5'-nucleotidase	6.820982557	1.48E-06
RGPD5	RANBP2-like and GRIP domain-containing protein 5/6	6.765929814	3.98E-05
SCARB2	Lysosome membrane protein 2	6.707956477	0.00153344
POLR2B	DNA-directed RNA polymerase II subunit RPB2	6.564641972	0.00789161
DCTN1	Dynactin subunit 1	6.432813332	0.00550352
NBPF14	Neuroblastoma breakpoint family member 14	6.36607457	0.0128438
NIN	Ninein	6.32595554	0.04712363
UTP4	U3 small nucleolar RNA-associated protein 4 homolog	6.190073413	0.00021504
OPA1	Dynamin-like 120 kDa protein, mitochondrial	6.173225554	0.00615833
ADAMTSL1	ADAMTS-like protein 1	6.171191932	0.00550352
RAB30	Ras-related protein Rab-30	6.122487592	0.02394511
RALGAPB	Ral GTPase-activating protein subunit beta	6.095601938	0.00569366
LARP7	La-related protein 7	5.995807078	0.02901011
SMC4	Structural maintenance of chromosomes protein 4	5.948869664	0.00067814
UBE2A	Ubiquitin-conjugating enzyme E2 A	5.692392919	0.07315534
BTAF1	TATA-binding protein-associated factor 172	5.684756789	0.02394511
BROX	BRO1 domain-containing protein	5.553206373	0.00333204
MAPKAP1	Target of rapamycin complex 2 subunit	5.517371387	0.01111222
HMGCR	3-hydroxy-3-methylglutaryl-coenzyme A reductase (HMG-CoA reductase)	5.498152606	0.00569366

B

Gene Name	Protein Name	log2 Fold-Change	p-adj
CSDE1	Cold shock domain-containing protein E1	-5.274622379	4.12E-09
ELF4	ETS-related transcription factor Elf-4	-5.35573139	0.00569366
MAP4K3	Mitogen-activated protein kinase kinase kinase kinase 3	-5.476074479	0.07461185
DMXL1	DmX-like protein 1	-5.477380729	0.00550352
MFAP5	Microfibrillar-associated protein 5	-5.595879597	1.48E-06
NIN	Ninein	-5.639746615	9.28E-08
DSTYK	Dual serine/threonine and tyrosine protein kinase	-5.639847766	0.03548112
PTPN13	Tyrosine-protein	-5.776087327	0.04198158
APC	Adenomatous polyposis coli protein	-5.814977118	0.0756534
RANBP3	Ran-binding protein 3 (RanBP3)	-5.899797668	0.00194747
ERMAP	Erythroid membrane-associated protein	-5.95602615	0.00023557
TSPAN3	Tetraspanin-3	-6.171222702	0.00789161
ST3GAL1	CMP-N-acetylneuraminate-beta-galactosamide-alpha-2,3-sialyltransferase 1	-6.269464732	0.00034818
CST3	Cystatin-C	-6.295050026	0.04775731
PRICKLE2	Prickle-like protein 2	-6.315150042	0.00896279
CEP170B	Centrosomal protein of 170 kDa protein B	-6.390323335	0.00019319
RAB30	Ras-related protein Rab-30	-6.84210161	0.00201531
CLIC4	Chloride intracellular channel protein 4	-7.014960615	0.00588131
PSIP1	PC4 and SFRS1-interacting protein	-7.016060554	0.00569366
SULF1	Extracellular sulfatase Sulf-1	-8.340301921	0.01517533

Table 6.3.3.1 Up- and Down-Regulated Genes following Broccoli Extract Treatment: Chub-S7 cells were treated with 10ng/ml broccoli extract (BE) for 36 hours. The 20 most **(A)** up- and **(B)** down-regulated genes are displayed alongside the associated protein name, log2 fold-change and p-value following adjustment for multiple testing (p-adj).

A

Gene Name	Protein Name	log2 Fold-Change	padj
PMCA1	Plasma membrane calcium-transporting ATPase 1	8.057994037	2.65E-08
NT5C2	Cytosolic purine 5'-nucleotidase	7.309216821	1.91E-08
DCTN1	Dynactin subunit 1	6.470631286	0.00190216
MAGT1	Magnesium transporter protein 1	6.413098687	0.072928409
EIF3L	Eukaryotic translation initiation factor 3 subunit L	6.363290184	0.009001185
TNIP1	TNFAIP3-interacting protein 1	6.208808541	0.001057701
UTP4	U3 small nucleolar RNA-associated protein 4 homolog	6.152278344	4.82E-05
EPS8	Epidermal growth factor receptor kinase substrate 8	6.011588637	0.04776016
USP22	Ubiquitin carboxyl-terminal hydrolase 22	5.975459486	0.025451439
RALGAPB	Ral GTPase-activating protein subunit beta	5.780804269	0.005197465
ADAPT78	Calcipressin-1	5.730274908	0.006683192
NBPF14	Neuroblastoma breakpoint family member 14	5.649026532	0.024560385
XPO4	Exportin-4	5.62139814	0.005629514
OPA1	Dynamin-like 120 kDa protein, mitochondrial	5.596059019	0.010266734
TMEM104	Transmembrane protein 104	5.509045695	0.010667624
TYK2	Non-receptor tyrosine-protein kinase TYK2	5.368493524	0.077638159
GUCD1	Protein GUCD1	5.344252157	0.053626308
IGSF8	Immunoglobulin superfamily member 8	5.269900818	0.001519619
RGPD5	RANBP2-like and GRIP domain-containing protein 5/6	5.262912746	0.002236034
PYCR1	Pyrroline-5-carboxylate reductase 1	5.229171074	0.023089082

B

Gene Name	Protein Name	log2 Fold-Change	padj
DCTN2	Dynactin subunit 2	-4.334385499	0.010080951
MYO9B	Unconventional myosin-IXb	-4.382993654	0.00190216
HUWE1	E3 ubiquitin-protein ligase	-4.594808955	0.005629514
ASH2L	Set1/Ash2 histone methyltransferase complex subunit ASH2	-4.686957465	0.046352222
EIF4E2	Eukaryotic translation initiation factor 4E type 2	-4.993305335	0.074693651
KIAA2026	Uncharacterized protein	-5.15550203	0.025218569
SBNO2	Protein strawberry notch homolog 2	-5.231560762	0.015148849
FLNC	Filamin-C	-5.414391363	0.056592973
KANK1	KN motif and ankyrin repeat domain-containing protein 1	-5.450728325	0.043975334
LEPR	Leptin receptor	-5.529339947	0.004137608
BI1	Bax inhibitor 1	-5.562727417	0.000659027
APC	Adenomatous polyposis coli protein	-5.668527509	0.04749258
PIP5K1A	Phosphatidylinositol 4-	-5.681145291	0.014746137
TMEM104	Transmembrane protein 104	-5.973803056	0.006963264
MAP3K6	Mitogen-activated protein kinase kinase kinase 6	-6.126271368	0.032701083
CST3	Cystatin-C	-6.14691827	0.027898356
ANAPC5	Anaphase-promoting	-6.337020002	0.000371813
GOLGB1	Golgin subfamily B member 1	-6.701450938	0.001727809
NACC2	Nucleus accumbens-associated protein 2	-6.98047649	9.21E-07
FN1	Fibronectin	-7.875169293	0.000298768

Table 6.3.3.2 Up- and Down-Regulated Genes following Tunicamycin Treatment: Chub-S7 cells were treated with 750ng/ml tunicamycin for 36 hours. The 20 most **(A)** up- and **(B)** down-regulated genes are displayed alongside the associated protein name, log2 fold-change and p-value following adjustment for multiple testing (p-adj).

A

Gene Name	Protein Name	log2 Fold-Change	p-adj
PMCA1	Plasma membrane calcium-transporting ATPase 1	7.132037939	2.40E-06
NT5C2	Cytosolic purine 5'-nucleotidase	6.902875542	1.98E-07
DCTN1	Dynactin subunit 1	6.122959117	0.004655936
RALGAPB	Ral GTPase-activating protein subunit beta	6.083819769	0.002594915
BTAF1	TATA-binding protein-associated factor 172	5.970963116	0.006778866
SCARB2	Lysosome membrane protein 2	5.83847228	0.004895152
PYCR1	Pyrroline-5-carboxylate reductase 1	5.834027677	0.006797888
XPO4	Exportin-4	5.468414139	0.008227184
UTP4	U3 small nucleolar RNA-associated protein 4 homolog	5.459179066	0.000734563
ADAPT78	Calcipressin-1	5.449135027	0.012871725
ADAMTSL1	ADAMTS-like protein 1	5.406274178	0.012125871
MRP1	Multidrug resistance-associated protein 1	5.296050203	0.007776599
POLR2B	DNA-directed RNA polymerase II subunit RPB2	5.295421929	0.04603315
NBPF3	Neuroblastoma breakpoint family member 3	5.241283658	0.063542255
GUCD1	Protein GUCD1	5.19011803	0.075285649
IGSF8	Immunoglobulin superfamily member 8	5.108987081	0.002529729
OPA1	Dynamin-like 120 kDa protein, mitochondrial	5.086876371	0.031240596
NBPF14	Neuroblastoma breakpoint family member 14	4.90316789	0.09065089
LARP7	La-related protein 7	4.886471365	0.098721948

B

Gene Name	Protein Name	log2 Fold-Change	p-adj
HUWE1	E3 ubiquitin-protein ligase	-4.056225937	0.019202978
GOLGA2	Golgin subfamily A member 2	-4.062829169	3.03E-05
PLCG2	1-phosphatidylinositol 4,5-bisphosphate phosphodiesterase gamma-2	-4.192416213	0.051130489
TBC1D17	TBC1 domain family member 17	-4.34721013	0.003216294
ANGEL2	Protein angel homolog 2	-4.352906239	0.019617449
TAX1BP1	Tax1-binding protein 1	-4.456893635	0.016202394
ANAPC5	Anaphase-promoting complex subunit 5	-4.457136628	0.077951362
LEPR	Leptin receptor	-4.532184367	0.002752972
DPYSL2	Dihydropyrimidinase-related protein 2	-4.770248232	0.000165729
PPEF2	Serine/threonine-protein phosphatase with EF-hands 2	-4.862954748	0.006890957
PYCR1	Pyrroline-5-carboxylate	-4.9731353	3.14E-06
SNRPD3	Small nuclear ribonucleoprotein Sm D3	-5.005304249	0.020887898
FN1	Fibronectin	-5.025390613	0.074246827
TBC1D2	TBC1 domain family member 2A	-5.308001833	1.93E-06
TBC1D15	TBC1 domain family member 15	-5.336871022	0.042310715
QARS	Glutamine--tRNA ligase	-5.450809695	0.05683344
DIS3L	DIS3-like exonuclease 1	-5.537256774	0.030603748
SELENOW	Selenoprotein W	-6.060864743	0.005885866
NOMO3	Nodal modulator 3	-6.760170864	0.003438845
NFAT5	Nuclear factor of activated T-cells 5	-6.781705194	0.00571724

Table 6.3.3.3 Up- and Down-Regulated Genes following Combined Broccoli Extract + Tunicamycin Treatment: Chub-S7 cells were treated with 10ng/ml broccoli extract (BE) and 750ng/ml tunicamycin (Tun) for 36 hours. The 20 most **(A)** up- and **(B)** down-regulated genes are displayed alongside the associated protein name, log2 fold-change and p-value following adjustment for multiple testing (p-adj).

Transcriptomics studies revealed three results of particular interest:

1. Tunicamycin initiates lipolysis.
2. Carbohydrate degradation is significantly upregulated with tunicamycin treatment, whilst carbohydrate biosynthesis is significantly upregulated with broccoli extract treatment.
3. HMG-CoA reductase (3-hydroxy-3-methyl-glutaryl-coenzyme A reductase), a component of the mevalonate pathway, is significantly upregulated in the two treatments where BE was present (BE and BE+Tun). The BE treatment induced a 45-fold increase ($p = 1.5 \times 10^{-5}$), whilst the BE+Tun treatment resulted in a 21-fold increase ($p = 5.2 \times 10^{-4}$).

Similarities and differences between treatments are represented in Tables 6.3.3.4 and 6.3.3.5.

A.

BE vs Control
Amino-acid biosynthesis; S-adenosyl-L-methionine biosynthesis; S-adenosyl-L-methionine from L-methionine: step 1/1.
Carbohydrate biosynthesis; gluconeogenesis.
Genetic information processing; DNA replication.

B.

Tun vs Control
Carbohydrate degradation; glycolysis; pyruvate from D-glyceraldehyde 3-phosphate: step 2/5.
One-carbon metabolism; tetrahydrofolate interconversion.
Phospholipid metabolism; CDP-diacylglycerol biosynthesis; CDP-diacylglycerol from sn-glycerol 3-phosphate: step 2/3.

C.

BE+Tun vs Control
Amino-acid biosynthesis; L-asparagine biosynthesis; L-asparagine from L-aspartate (L-Gln route): step 1/1.
Protein modification; peptidyl-diphthamide biosynthesis.
Amino-acid biosynthesis; L-proline biosynthesis; L-proline from L-glutamate 5-semialdehyde: step 1/1.

Table 6.3.3.4 Differences in Pathways Activated through Treatment: Unique, significant and important differences in gene expression in pathways activated through treatment with **(A)** broccoli extract (BE, 10ng/ml), **(B)** tunicamycin (Tun, 750ng/ml) and **(C)** BE+Tun, determined through transcriptomics ($p < 0.05$).

A. BE vs Control	B. BE+Tun vs Control	C. Tun vs Control
Metabolic intermediate biosynthesis; (R)-mevalonate biosynthesis; (R)-mevalonate from acetyl-CoA: step 3/3.	Amino-acid biosynthesis; L-cysteine biosynthesis; L-cysteine from L-homocysteine and L-serine: step ½.	Nucleotide-sugar biosynthesis; GDP-alpha-D-mannose biosynthesis; GDP-alpha-D-mannose from alpha-D-mannose 1-phosphate (GTP route): step 1/1.
Protein modification; protein glycosylation.	Amino-acid biosynthesis; L-serine biosynthesis; L-serine from 3-phospho-D-glycerate: step 2/3.; Cofactor biosynthesis; pyridoxine 5'-phosphate biosynthesis; pyridoxine 5'-phosphate from D-erythrose 4-phosphate: step 3/5.	Nucleotide-sugar biosynthesis; UDP-N-acetyl-alpha-D-glucosamine biosynthesis; UDP-N-acetyl-alpha-D-glucosamine from N-acetyl-alpha-D-glucosamine 1-phosphate: step 1/1.
	Sulfur metabolism; glutathione biosynthesis; glutathione from L-cysteine and L-glutamate: step 1/2.	Nucleotide-sugar biosynthesis; UDP-N-acetyl-alpha-D-glucosamine biosynthesis; alpha-D-glucosamine 6-phosphate from D-fructose 6-phosphate: step 1/1.
	Nucleotide-sugar biosynthesis; GDP-alpha-D-mannose biosynthesis; GDP-alpha-D-mannose from alpha-D-mannose 1-phosphate (GTP route): step 1/1.	Amino-acid biosynthesis; L-cysteine biosynthesis; L-cysteine from L-homocysteine and L-serine: step 1/2.
	Nucleotide-sugar biosynthesis; UDP-N-acetyl-alpha-D-glucosamine biosynthesis; UDP-N-acetyl-alpha-D-glucosamine from N-acetyl-alpha-D-glucosamine 1-phosphate: step 1/1.	Amino-acid biosynthesis; L-serine biosynthesis; L-serine from 3-phospho-D-glycerate: step 2/3.; Cofactor biosynthesis; pyridoxine 5'-phosphate biosynthesis; pyridoxine 5'-phosphate from D-erythrose 4-phosphate: step 3/5.
	Nucleotide-sugar biosynthesis; UDP-N-acetyl-alpha-D-glucosamine biosynthesis; alpha-D-glucosamine 6-phosphate from D-fructose 6-phosphate: step 1/1.	Sulfur metabolism; glutathione biosynthesis; glutathione from L-cysteine and L-glutamate: step 1/2.
	Metabolic intermediate biosynthesis; (R)-mevalonate biosynthesis; (R)-mevalonate from acetyl-CoA: step 3/3.	Protein modification; protein glycosylation.
	Protein modification; protein glycosylation.	Protein modification; protein ubiquitination.
	Protein modification; protein ubiquitination.	

	Common between all three treatments
	Common between BE and BE+Tun
	Common between BE+Tun and Tun

Figure 6.3.3.5 Similarities in Pathways Activated through Treatment: Similarities in gene expression in pathways activated through treatment with **(A)** broccoli extract (BE, 10ng/ml), **(B)** tunicamycin (Tun, 750ng/ml) and **(C)** BE+Tun, determined through transcriptomics.

6.4 Discussion

The purpose of this study was to examine the effects of tunicamycin on ROS and mitochondrial dysfunction, as well as to determine whether a broccoli extract could provide protection against the induction of these mechanisms. Using a human adipocyte model, it was revealed that factors such as tunicamycin that induce ER stress also increase cellular ROS and mitochondrial dysfunction. Furthermore, these studies highlighted that broccoli extract provides protection against the impact of tunicamycin treatment on these cellular mechanisms. Examining transcriptomics data at the time point with the largest observed protection by broccoli extract revealed the mevalonate pathway as a potential target through which broccoli extract acts.

Data from ROS assays indicated that treating adipocytes with broccoli extract does not alter the level of ROS present in cells. This is important to establish as studies have shown that although elevated intracellular levels of ROS can cause damage to lipids, proteins and DNA, ROS can also act as signalling molecules in the maintenance of physiological functions (Schieber and Chandel 2014, Kurutas 2016). It is therefore beneficial that the physiological levels of ROS are unchanged with broccoli extract treatment. Further assessment of the data revealed that tunicamycin treatment significantly increased the level of total ROS/RNS at 24hr by 28%. Whilst the specific type of ROS upregulated was undetermined due to no similar increase observed in SOD or catalase assays, the increase in total ROS/RNS was prevented with the addition of broccoli extract to the tunicamycin treatment. This suggests that BE offers metabolic protection by preventing the increase in ROS/RNS that has been

implicated in various disease states, without depleting the level of ROS that may be required for cellular signalling.

Studies into how treatments may impact mitochondria were carried out by assessing data on specific indicators of mitochondrial function. Data obtained on each parameter following treatment suggested that mitochondrial function was not altered from control cells with the addition of broccoli extract. This indicates that broccoli extract treatment does not have a detrimental effect on mitochondria and does not affect their physiological role. Treatment with tunicamycin, however, resulted in an overall 71% increase in OCR, 95% increase in OCR/ECAR ratio, 37% reduction in maximal respiration and a 46% reduction in spare capacity compared with control. The addition of broccoli extract to the tunicamycin treatment prevented such dramatic changes from control values in each of these cases. The exception to this pattern of results is with ECAR data, whereby individual broccoli extract and tunicamycin treatments did not evoke any changes from control, whilst the combined broccoli extract and tunicamycin treatment caused a 24% increase.

The increase in OCR and OCR/ECAR ratio with tunicamycin demonstrated that oxidative phosphorylation is dramatically increased with the treatment, which can be indicative of ER and oxidative stress causing an influx of Ca^{2+} into the mitochondria (Covian, French *et al*. 2014, Du, Amarachintha *et al*. 2016). During ER stress, Ca^{2+} released from the ER is taken up by mitochondria, causing the permeability transition pore to release cytochrome c, enhancing ROS production (Görlach, Bertram *et al*. 2015). Additionally, increased mitochondrial Ca^{2+} levels stimulate Krebs cycle dehydrogenases, which boost oxygen consumption and further ROS production

(Traaseth, Elfering *et al*. 2004). This transfer of Ca^{2+} and subsequent mitochondrial ROS production following ER stress initiates a vicious cycle that leads to impaired cellular homeostasis and can induce apoptosis (Cao and Kaufman 2014). The addition of broccoli extract to the tunicamycin treatment reduced both OCR and OCR/ECAR ratio values compared to the individual tunicamycin treatment. These results demonstrate the protection that broccoli extract provides against cellular dysfunction, preventing the cycle of ER stress, mitochondrial dysfunction and ROS production that often leads to apoptosis. As such, the addition of broccoli extract may prevent macrophage infiltration into adipose tissue, insulin resistance and other obesity-associated metabolic complications that are linked to adipocyte apoptosis, improving cellular health and reducing disease risk (Alkhouri, Gornicka *et al*. 2010).

Conversely to other results, analysing ECAR values showed that both individual broccoli extract and tunicamycin treatments resulted in similar levels to control, whilst the combined broccoli extract and tunicamycin treatment induced a 24% increase. ECAR is a measure of glycolysis, a less efficient form of ATP production than oxidative phosphorylation. Although it appears that the addition of broccoli extract to tunicamycin treatment results in mitochondria relying more on glycolysis for ATP production than with individual tunicamycin treatment, the low level of ECAR in tunicamycin treated cells is likely due to the overuse of oxidative phosphorylation that is caused by Ca^{2+} transfer. Furthermore, there is evidence that stimulation of glycolysis can enhance the repair of DNA damage, and that glycolysis can be utilised as a means to minimise oxidative stress due to the increased production of pyruvate, an effective scavenger of ROS, during the process (Brand 1997, Bhatt, Chauhan *et al*. 2015). As such, studying the results of OCR, ECAR and OCR/ECAR ratio together

indicate that tunicamycin treatment leads to severely unhealthy cells that are prone to apoptosis, whilst the addition of broccoli to the tunicamycin treatment prevents such extensive damage through elevating glycolysis to protect against ROS. This is further evidence that the addition of broccoli extract can lead to the stimulation of protective mechanisms against cellular damage, reducing dysfunction and preventing apoptosis.

Using specific pharmacological inhibitors during the stress test provided further evidence that broccoli extract can reduce the detrimental effects of tunicamycin. Maximal respiration, a measure of the maximum ability of the electron transport chain to generate ATP, was reduced by 37% with tunicamycin treatment, whilst the addition of broccoli extract with tunicamycin resulted in only an 18% reduction. This indicates that tunicamycin has a detrimental impact on mitochondrial health and efficiency of ATP production, whilst the presence of broccoli extract prevents such a pronounced negative effect. In addition to this, spare capacity, which represents the ability of a cell to produce energy under conditions of increased stress, was also reduced by 46% with tunicamycin. This suggests that tunicamycin damages the long-term survival and function of cells by impacting their ability to produce sufficient energy in stressful conditions. The addition of broccoli extract to tunicamycin reduced the reduction in spare capacity to only 23%, improving the long-term function of cells under increased stress. The individual broccoli extract treatment did not impact maximal respiration or spare capacity compared to control, demonstrating that it has no detrimental effect on mitochondrial function, whilst improving many of the parameters affected by tunicamycin treatment.

Whilst time constraints limited the amount of transcriptomics analysis possible, the data identified three key findings relating to the influence of treatments on potential pathway changes. Firstly, the data indicated that tunicamycin increased lipolysis transcripts which affirms current literature that suggests this could be a possible reason for the incapacity of obese white adipocytes to manage lipids effectively, leading to triglyceride breakdown and reduced triglyceride storage in adipose tissue (Picard and Deshaies 2012). The altered dysregulation of triglyceride management in obese adipocytes could therefore contribute to increased triglycerides in the circulation, leading to ectopic fat deposition in other organs and their subsequent dysfunction (Bogdanovic, Kraus *et al*. 2015, Smith 2015). Carbohydrate degradation was also discovered to be significantly upregulated with tunicamycin treatment, whilst carbohydrate biosynthesis was significantly upregulated with the broccoli extract treatment. These two opposing outcomes highlight the differing effects of the treatments and could indicate one possible process through which broccoli reduces the impact of tunicamycin treatment. Finally, and most significantly, activity of the mevalonate pathway (Figure 6.4.1) was increased in cells treated with broccoli extract, either with or without tunicamycin. HMG-CoA reductase (3-hydroxy-3-methyl-glutaryl-coenzyme A reductase), an enzyme involved in this pathway, was significantly upregulated; this is particularly noteworthy as tunicamycin is known to inhibit, or reduce the activity of, HMG-CoA reductase (Volpe and Goldberg 1983, Engstrom, Larsson *et al*. 1989, Larsson and Engström 1989). Statins, which target the mevalonate pathway to reduce cholesterol production, have been shown to promote ER stress (Chen, Wu *et al*. 2008, Mörck, Olsen *et al*. 2009, Lee and Kim 2013). It is therefore possible that as well as the primary mechanism by which tunicamycin

induces ER stress, through inhibiting N-linked glycosylation, tunicamycin may also induce ER stress through inhibiting HMG-CoA reductase and the mevalonate pathway. It should be noted, however, that in some cell types such as cardiac myocytes, statins have been shown to reduce ER stress (Li, Lu et al. 2017) and further insights are therefore required in this area. Inhibition of the mevalonate pathway has also been linked to mitochondrial dysfunction (Tricarico, Crovella *et al*. 2015), which is consistent with present findings in these studies where tunicamycin induces mitochondrial dysfunction whilst broccoli extract protects against it.

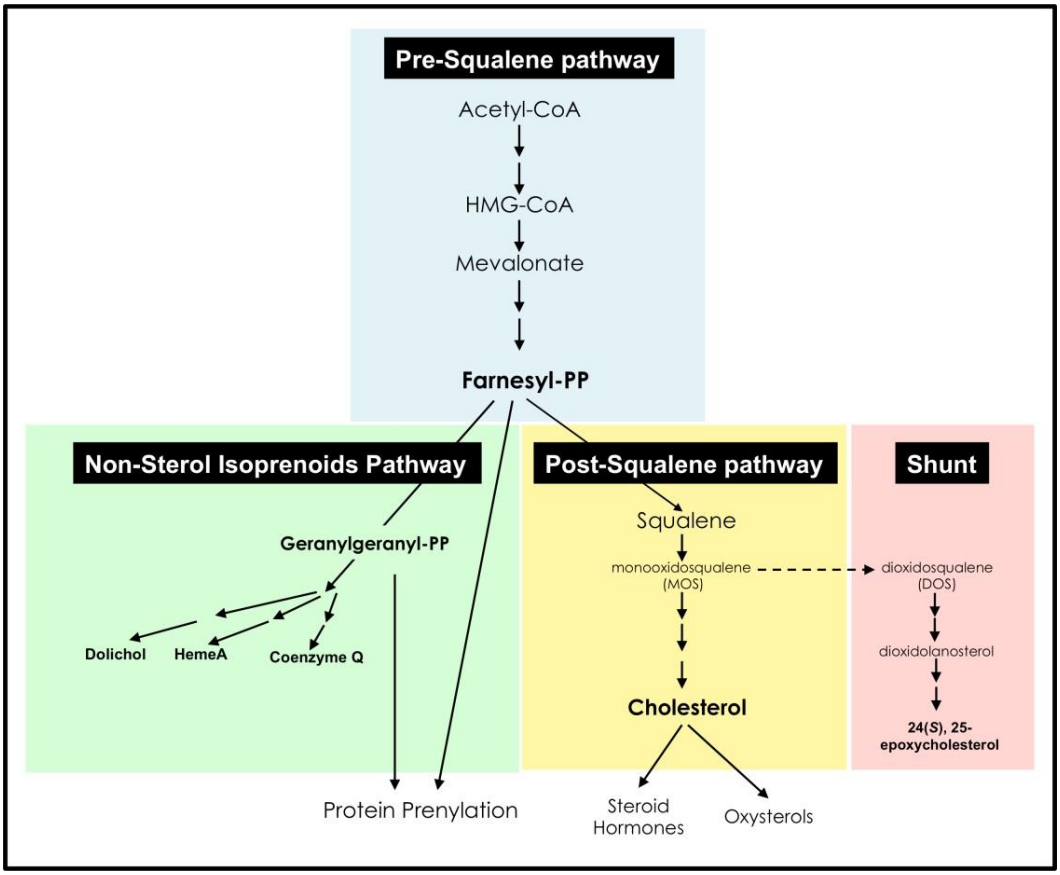

Figure 6.4.1 The Mevalonate Pathway: Broccoli extract (BE) activates the mevanolate pathway by significantly upregulating HMG-CoA reductase. The consequential upregulation of coenzyme Q10 could explain the protection against ER stress, ROS and mitochondrial dysfunction that has been observed with BE in these studies. *Figure from (Mohamed, Smith et al. 2015)*.

Activation of the mevalonate pathway is known to improve mitochondrial function, inhibit oxidative stress and reduce ER stress (Deichmann, Lavie *et al*. 2010, Lee, Lin *et al*. 2012, Yubero-Serrano, Gonzalez-Guardia *et al*. 2012, Alam and Rahman 2014, Xu, Huo *et al*. 2017). It is therefore possible that the protective effect of broccoli extract that has been demonstrated throughout this thesis is due to its activation of the mevalonate pathway. This suggests that broccoli extract may have further impact on cellular metabolism, as upregulation of mevalonate pathway products, such as coenzyme Q10, have been associated with increased antioxidant activity, improving lipid metabolism, ameliorating obesity and suppressing lipid accumulation (Deichmann, Lavie *et al*. 2010, Lee, Lin *et al*. 2012, Yubero-Serrano, Gonzalez-Guardia *et al*. 2012, Alam and Rahman 2014, Xu, Huo *et al*. 2017). Furthermore, coenzyme Q10 is known to decline with age, with diseases such as T2DM, cardiovascular disease, metabolic syndrome and many more associated with this deterioration (Xu, Huo *et al*. 2017), highlighting the potential wider benefits of broccoli extract in preventing these diseases. Additionally, both mice and human studies have begun to examine the use of coenzyme Q10 in the diet as a supplement, with results showing inhibition of weight gain, reduction of white adipose tissue content, enhanced brown adipose tissue function and increased metabolic function amongst other positive effects (Xu, Huo *et al*. 2017). This has demonstrated that dietary coenzyme Q10 can suppress lipid accumulation and mitigate metabolic dysfunction. These present studies indicate that use of broccoli extract could enhance coenzyme Q10, and studies using coenzyme Q10 as a supplement suggest that this could have benefits in patients with T2DM (Shen and Pierce 2015). Therefore, examining the role of broccoli

extract *in vivo* would be of interest to examine its potential as an active cellular component to restore metabolic function.

6.5 Conclusion

In summary, these data have provided an insight into the wider impact of tunicamycin on cellular health and have demonstrated that broccoli extract can protect not only against tunicamycin-induced ER stress, but also against the ROS production and mitochondrial dysfunction that ER stress leads to. This chapter has satisfied the final aim of this thesis, which was to examine the effects of broccoli on other mechanisms that also contribute to metabolic disease, such as ROS and mitochondrial dysfunction. In addition to this, analysis of mRNA through transcriptomics revealed the mevalonate pathway as a potential target through which the protective effects of broccoli are delivered. These data provide further evidence that a broccoli supplement may lead to improved cellular health, and suggest the mevalonate pathway as a potential target through which this may occur.

CHAPTER 7:

Conclusions

This thesis explored how changes in the unfolded protein response (UPR) in human adipocytes varied over time following activation by an inflammatory stimulus, tunicamycin, and a treatment considered to reduce inflammation, broccoli extract. This time series experimental study allowed a mathematical model of the PERK pathway within the UPR to be designed and developed beyond solely using theoretical calculations as in previous studies (Trusina, Papa *et al*. 2008, Erguler, Pieri *et al*. 2013). Further experimental research also highlighted the protective effects of broccoli against ROS and mitochondrial dysfunction, as well as identifying a potential molecular pathway through which the broccoli extract may act.

In order to begin the process of mathematically modelling the UPR, current mathematical models of the system were reviewed in order to gain insight into the ideal complexity of a model for this ER stress response. This also gave an understanding of the challenges associated with developing a model of a biological system of this level of complexity. Evidence for the role of broccoli and other *Brassicas* in the prevention of diseases was also reviewed to design appropriate experiments in order to gain new molecular insights into the stress response, as well as to provide data to support the mathematical modelling process. Following this review, standard cell culture and analytical laboratory practices were carried out in order to collect sufficient experimental data to develop and validate the mathematical model, as well as to investigate the effect of broccoli on various cellular mechanisms. This research identified several novel outcomes that provide new information into how the UPR responds over time. Additionally, these studies revealed that the intensity of ER stress, as well as ROS and mitochondrial dysfunction, is reduced with the addition of a broccoli extract, potentially through activation of

the mevalonate pathway. This current thesis adds to the developing evidence of the health benefits of *Brassicas* on inflammation (Seow, Yuan *et al*. 2002, Hsu, Chow *et al*. 2007, Kirsh, Peters *et al*. 2007, Lam, Ruczinski *et al*. 2010, Youn, Kim *et al*. 2010, Bosetti, Filomeno *et al*. 2012, Hwang and Lim 2014, Jiang, Wu *et al*. 2014) and the potential impact that broccoli could have on cellular health by dissociating the impact of obesity and the subsequent induction of insulin resistance and T2DM.

A literature review into current mathematical models of the UPR revealed two particular models of interest that highlighted the difficulty in selecting an appropriate size and complexity for a model of a biological system. Rutkowski *et al.* created a model that focussed on studying the differences in expression patterns of UPR proteins contributing to cell survival or cell death, and how the outcome subsequently switches from survival to apoptosis (Rutkowski, Arnold *et al*. 2006). This model was relatively small, considering only three proteins and their corresponding mRNAs. Additionally, each ODE only involved one linear synthesis term and one linear degradation term, when in reality the upregulation of proteins and mRNAs is much more complex than this. However, due to the small size of the model, experimental data were sufficient to parameterise it and the subsequent predictions did match the expression profiles of the data, suggesting that there is some accuracy to the model. The second relevant model, by Erguler *et al*., was also designed to study the switch in focus of the UPR from survival to apoptosis (Erguler, Pieri *et al*. 2013). Conversely to Rutkowski's model, however, Erguler's model involved a much wider range of UPR components, which prevented the process of parameter estimation using experimental data, resulting in a model that could only provide responses of a qualitative nature. Despite this, conclusions drawn from this

study identified how the presence of low, intermediate and high activity states of the UPR may determine whether cell survival or cell death becomes the desired outcome. It was also suggested that during the intermediate state, oscillations occur with both translation attenuation and apoptotic signals, which has not been proposed before. However, this was not confirmed in their study due to the lack of experimental data to support this hypothesis.

Following this literature review, an initial mathematical model of the UPR was developed in an attempt to incorporate the benefits of both Rutkowski's and Erguler's models. In order to maintain biological detail without creating a model that was too large to be parameterised and validated with experimental data, only one of the three arms of the UPR was selected to be modelled. This ensured that the reactions controlling the expression of proteins within the pathway could be modelled as in Erguler's *et al.* model, rather than only using one linear synthesis and degradation term per ODE as Rutkowski *et al* did, whilst keeping the model small enough to allow parameterisation with experimental data. This initial model, discussed in Chapter 4, was developed using experimental data over three time points. In order to improve the accuracy of the model, a comprehensive time series study was designed to provide more reliable, granular data. Using information on appropriate model complexity obtained in Chapter 4, an improved model was designed using a biological schematic to develop kinetic equations that were then used to create ODEs in Chapter 5. This is a technique often used when creating mathematical models of biological systems, and resulted in an improved mathematical model that qualitatively matched the biological data. As the mathematical model developed here represents a standard biological process that

occurs in multiple cell types, there is the possibility that the method used throughout this thesis could be generalised to other situations. This could include studying the effect of different BE concentrations on the pathway, or indeed other superfoods entirely, in a multitude of cells. The model could also be extended to include the effects of comparator drugs and inhibitors. However, limitations of the model and software must be acknowledged, such as the relatively low computer power associated with Berkeley Madonna, the dangers of overparameterisation, and the benefits of obtaining more biological data to support the model.

Further to aiding the parameterisation and validation of the new UPR mathematical model, the data collected during this experiment revealed novel results with regards to the expression profiles of UPR proteins over time. As well as exploring the time frame over which proteins are expressed in response to tunicamycin, the expression of proteins involved in the translation attenuation system were discovered to oscillate over time. This was particularly interesting, as it had been predicted through Erguler's *et al.* model of the UPR but had not been previously supported with experimental data. Thus, these data support the proposition of an intermediate UPR state whereby proteins in the translation attenuation system oscillate, as suggested by Erguler *et al.* (Erguler, Pieri *et al*. 2013). Analysis of the ODEs, including linearisation, steady state and asymptotic analyses can provide further information on the system, such as when it may reach an equilibrium state, how stable the equilibria are, and what the limiting behaviours of the system are. This would provide further information and confirmation that the model dynamics match the required known biological responses.

The studies in Chapter 6 were designed following a literature search that highlighted the positive impact that cruciferous vegetables, in particular broccoli, can have on diseases such as cancer and cardiovascular disease (Zhang, Shu *et al*. 2011, Bosetti, Filomeno *et al*. 2012, Tang, Meng *et al*. 2017). Investigating this further revealed that such vegetables can also reduce inflammation and improve damaging lipid profiles of humans (Clarke, Dashwood *et al*. 2008, Bahadoran, Mirmiran *et al*. 2012, Boddupalli, Mein *et al*. 2012, Jiang, Wu *et al*. 2014, Armah, Derdemezis *et al*. 2015). As such, this emphasised the potential of broccoli as a treatment to reduce the impact of ER stress that occurs in obesity and can lead to T2DM. Following the optimisation of a broccoli extract, a comprehensive time series experiment was carried out which revealed that the extract did not exacerbate physiological ER stress that occurs naturally within cells, but appeared to prevent such an intense induction of ER stress following treatment with tunicamycin. This effect was particularly apparent with mRNA and proteins expressed downstream in the UPR, such as CHOP, which is upregulated at the end of all three arms of the UPR. This study demonstrated the tight control over the expression of proteins such as BiP, which is the initial sensor of ER stress and acts as a switch for each of the UPR arms, supporting studies that suggest BiP expression is more tightly regulated at the post-translational level rather than at the transcriptional level (Gülow, Bienert *et al*. 2002, Takayanagi, Fukuda *et al*. 2013). These results established for the first time that broccoli could provide notable protection against the development of insulin resistance in cells exposed to inducers of ER stress, and revealed the potential for a broccoli supplement in the diet that could promote cellular health and reduce T2DM risk. This study did, however, lack a comparator drug known to reduce ER stress to allow comparison with the BE.

Most ER stress inhibitors affect specific proteins within the ER stress pathway, such as ATF6 and P-eIF2α, rather than the whole response. It may not therefore be suitable to compare BE treatment with a known inhibitor, although there is the potential to incorporate this into future experiments if a suitable inhibitor is identified.

Following the results in Chapter 6, further studies were designed to investigate whether the protective effects of broccoli would extend to ROS and mitochondrial dysfunction. Whilst there is little evidence that tunicamycin itself can induce ROS and mitochondrial dysfunction, it is well known that these mechanisms can occur following ER stress (Cao and Kaufman 2014, Park 2014). The aims of the studies in Chapter 7 were therefore to determine firstly whether tunicamycin treatment can induce ROS and mitochondrial dysfunction in adipocytes, and secondly whether BE can protect against these mechanisms. Following cell culture experiments, it was determined that tunicamycin does induce ROS and mitochondrial dysfunction, confirming reports in the literature that ER stress, ROS and mitochondrial dysfunction are interlinked and that induction of ER stress can cause further cellular dysfunction (Tse, Yan *et al*. 2016, Zeeshan, Lee *et al*. 2016, Chen, Zhong *et al*. 2017). Whilst studying the effects of BE on these mechanisms, it was revealed that BE itself did not exacerbate the physiological levels of ROS or mitochondrial characteristics, but reduced the upregulation induced by tunicamycin. As such, it was concluded that BE not only protects against ER stress induced by tunicamycin, but also prevents further cellular dysfunction that occurs with the treatment. In order to gain insight into how BE may have such an effect, transcriptomics was carried out to examine RNA expression at the time point where BE had the most impact. This revealed the

activation of the mevalonate pathway in cells treated with BE, which is known to produce coenzyme Q10, a molecule with numerous cellular health benefits that has also been shown to inhibit weight gain (Deichmann, Lavie *et al*. 2010, Lee, Lin *et al*. 2012, Yubero-Serrano, Gonzalez-Guardia *et al*. 2012, Alam and Rahman 2014, Garrido-Maraver, Cordero *et al*. 2014, Grenier-Larouche, Galinier *et al*. 2015, Xu, Huo *et al*. 2017). This is a novel insight that begins to explain the positive results demonstrated by BE treatment, and highlights the importance of this pathway. Whilst further work is required to confirm these results, the studies carried out in Chapter 7 support those in the current literature that suggest that Tunicamycin inhibits HMG-CoA reductase - the enzyme within the mevalonate pathway that is specifically upregulated by BE (Volpe and Goldberg 1983, Engstrom, Larsson *et al*. 1989, Larsson and Engström 1989). It is therefore possible, as demonstrated in Chapters 6 and 7, that BE provides protection against tunicamycin-induced ER stress, ROS and mitochondrial dysfunction through activation of the mevalonate pathway, which would otherwise be inhibited by tunicamycin treatment. The results in this thesis have therefore fulfilled the aims set out in the Thesis Outline and in section 1.3.

7.1 Limitations

As with all studies, there were certain limitations in this thesis that would need to be accounted for in any future work. For instance, whilst Berkeley Madonna suited the mathematical modelling carried out here, in order to continue studying and expanding the pathway, tests across computer software packages should be undertaken to determine which package may be best to proceed with. This is required to reduce the time taken for the software to solve the ODEs making up the model. The model should also be validated further using data from experiments with different treatments, e.g. the BE, Tun or BE+Tun data, giving increased credibility and reliability to the model. It may also be possible to carry out population studies once enough data have been collected, utilising the biological replicates for each time point in order to do so.

Due to the complexity in the nature of modelling a cellular system with experimental data, a cellular model was used that provided consistency and reproducibility across time and events. In one aspect, this supported the development of a mathematical model, but caused a limitation in another by not utilising different patient based human adipocytes and therefore was not able to view the variability across patients with different BMIs, ages or metabolic conditions. There was the possibility to utilise human samples, but the level of variability in responses, as noted in previous simple measurements of adipokine release (Fain 2010, Lehr, Hartwig *et al*. 2012) (Kusminski, da Silva *et al*. 2007), was considered unfeasible without first defining the model more clearly.

The time series data allowed a much more detailed analysis of change compared to prior studies, however it would have been interesting to follow certain key proteins continuously across time to examine the time series changes in even more subtle detail. The complexity of trying to gain continuous expression data for multiple proteins across time, even using a fluorescent system within confocal microscopy as an example, however, would not have given sufficient quantitative insight into changes. Furthermore, the time frame over which data could be collected would need to be much shorter due to technical limitations with cell viability in such a process.

The optimisation of BE concentration could have been improved by carrying out a full dose-response curve experiment, rather than just looking at three concentrations. Similarly, a better insight into the activity of BE could have been obtained by comparing it to known inhibitors of ER stress. A potential problem with this is that most ER stress inhibitors inhibit specific proteins within the pathway, rather than the whole response, however this could provide information on which part of the pathway is most affected by BE.

Due to a lack of time, the transcriptomics analysis was not as detailed as it could have been. There is a multitude of information that can be obtained from such analysis, and one comparison that would add to these experiments is the direct comparison between Tun and BE+Tun data, rather than comparing them both to control data and subsequently defining the differences between them. Further analysis, including this direct comparison, can be carried out in future work.

7.2 Future Work

The work in this thesis has highlighted several areas which it may be beneficial to study in the future. Firstly, developing mathematical models for the ATF6 and IRE1 arms of the UPR using further experimental data may be beneficial in order to gain a broader perspective of how the response changes over time. Following model parameterisation and validation, it may then be possible to combine and couple the sub-models and form one that represents the whole unfolded protein response that has been parameterised with experimental data. Using a different computational system such as Matlab, as well as collecting more data for the testing and validation processes may be required in order to do this. The lack of accurate parameterisation has been a constant problem in prior mathematical models of the UPR and this work represents the potential to create a validated model of the whole UPR that could be used to aid further experiments.

Secondly, the model in this thesis could be used to compare how dynamics of the PERK pathway are altered when BE treatment is present, both with and without tunicamycin. Comparing the differences in parameter values between treatments could provide information on which protein interactions are altered by the presence of BE. This could further our understanding on how BE specifically affects processes within the UPR.

Additionally, to understand how BE has broader impacts in the cell, the theory proposed in this thesis that BE activates the mevalonate pathway could be examined further. qRT-PCR could be undertaken to investigate the presence of gene transcripts involved in the pathway across treatments to confirm whether genes within the

mevalonate pathway are truly upregulated by BE. Further analysis of the transcriptomics data could also be undertaken to see if there are other genes or pathways specifically altered by BE treatment.

In order to gain more information on the effects of BE across the cell, confocal microscopy work could be used to assess mitochondrial dynamics, both in terms of fusion and fission, and mitochondrial associated membranes (MAMs) between ER and mitochondria. Studying fusion and fission would highlight any mitochondrial elongation and fragmentation occurring which could provide information on mitochondrial dysfunction and cellular health (Westermann 2012). Similarly, the number of MAMs increase when cells experience ER stress (Carreras-Sureda, Pihán *et al*. 2017). As such, investigating MAMs through confocal microscopy could provide further evidence that tunicamycin induces ER stress and has implications on mitochondrial function, and that BE prevents this stress and any subsequent impact on mitochondria. The use of known ER stress inhibitors may aid in these experiments to allow valid comparison with the effects that BE treatment has on the cellular systems.

Finally, there is the potential to explore how the UPR differs between lean and obese cellular adipocyte populations. Using a defined age and BMI would provide consistency that may allow the mathematical model developed here to provide information on which parameters are altered due to the lean or obese cell type. Following this, the impact of using a BE treatment on these cells could be investigated to determine how the lean or obese cell type affects the protection that BE has shown in these studies.

7.3 Final Conclusions

In conclusion, this thesis has researched how the expression profiles of proteins within the UPR vary over time following treatment with tunicamycin, utilising both biological and mathematical modelling techniques, as well as investigating the protective effects of broccoli against ER stress, ROS and mitochondrial dysfunction. The outcomes of this study are as follows:

1. The production of a mathematical model of the PERK pathway of the UPR which qualitatively matches experimental data.
2. Identification of novel oscillating expression profiles of proteins involved in the translation attenuation system that support Erguler's hypothesis of an intermediate stress state.
3. Evidence that broccoli extract reduces the impact of tunicamycin on ER stress, ROS and mitochondrial dysfunction, possibly through activation of the mevalonate pathway.

Collectively, these findings meet the initial thesis aims and suggest that broccoli supplementation may be beneficial in preventing cellular dysfunction in cells exposed to stress. These initial results are promising and may represent the possibility of disconnecting obesity and T2DM, through the manufacturing of a freeze dried broccoli powder that is available to the public. This would have a substantial worldwide impact, with emphasis on healthcare, wellbeing and diet – areas that, with 650 million obese adults and 422 million people suffering from diabetes worldwide (World Health Organisation 2016, World Health Organisation 2017), are vital to improve. In order to confirm these findings, further research would be required to

determine the outcome in specific *in vivo* investigations. If successful, clinical trials would then need to be carried out to analyse the outcomes in humans.

Bibliography

Abdul-Ghani, M. A. and R. A. DeFronzo (2008). "Mitochondrial dysfunction, insulin resistance, and type 2 diabetes mellitus." Current Diabetes Reports **8**(3): 173-178.

Aguirre, V., T. Uchida, L. Yenush, R. Davis and M. F. White (2000). "The c-Jun NH_2-terminal Kinase Promotes Insulin Resistance during Association with Insulin Receptor Substrate-1 and Phosphorylation of Ser^{307}*." Journal of Biological Chemistry **275**(12): 9047-9054.

Ajmera, I., M. Swat, C. Laibe, N. Le Novère and V. Chelliah (2013). "The impact of mathematical modeling on the understanding of diabetes and related complications." CPT Pharmacometrics Syst Pharmacol **2**: e54.

Alam, M. A. and M. M. Rahman (2014). "Mitochondrial dysfunction in obesity: potential benefit and mechanism of Co-enzyme Q10 supplementation in metabolic syndrome." J Diabetes Metab Disord **13**: 60.

Alhusaini, S., K. McGee, B. Schisano, A. Harte, P. McTernan, S. Kumar and G. Tripathi (2010). "Lipopolysaccharide, high glucose and saturated fatty acids induce endoplasmic reticulum stress in cultured primary human adipocytes: Salicylate alleviates this stress." Biochem Biophys Res Commun **397**(3): 472-478.

Alkhouri, N., A. Gornicka, M. P. Berk, S. Thapaliya, L. J. Dixon, S. Kashyap, P. R. Schauer and A. E. Feldstein (2010). "Adipocyte apoptosis, a link between obesity, insulin resistance, and hepatic steatosis." J Biol Chem **285**(5): 3428-3438.

American Association of Clinical Endocrinologists. "Management of Common Comorbidities of Diabetes." Retrieved 28th Sept, 2017, from http://outpatient.aace.com/type-2-diabetes/management-of-common-comorbidities-of-diabetes.

Andrews, S. (2010). "FastQC: A Quality Control Tool for High Throughput Sequence Data." 2018, from http://www.bioinformatics.babraham.ac.uk/projects/fastqc/.

Andruska, N. D., X. Zheng, X. Yang, C. Mao, M. M. Cherian, L. Mahapatra, W. G. Helferich and D. J. Shapiro (2015). "Estrogen receptor α inhibitor activates the unfolded protein response, blocks protein synthesis, and induces tumor regression." Proc Natl Acad Sci U S A **112**(15): 4737-4742.

Antunes, R., V. A. Gonzalez and K. Walsh (2015). Identification of Repetitive Processes at Steady- and Unsteady-State: Transfer Function. 23rd Annual Conference of the International Group for Lean Construction. Perth, Australia**:** 793-802.

Araneta, M. R. and E. Barrett-Connor (2005). "Ethnic differences in visceral adipose tissue and type 2 diabetes: Filipino, African-American, and white women." Obes Res **13**(8): 1458-1465.

Ariyasu, D., H. Yoshida and Y. Hasegawa (2017). "Endoplasmic Reticulum (ER) Stress and Endocrine Disorders." Int J Mol Sci **18**(2): E382.

Armah, C. N., C. Derdemezis, M. H. Traka, J. R. Dainty, J. F. Doleman, S. Saha, W. Leung, J. F. Potter, J. A. Lovegrove and R. F. Mithen (2015). "Diet rich in high glucoraphanin broccoli reduces plasma LDL cholesterol: Evidence from randomised controlled trials." Mol Nutr Food Res **59**(5): 918-926.

Atapattu, P. M. (2015). "Obesity at Menopause: An Expanding Problem." Journal of Patient Care **1**(103): 82-92.

Bach, D., S. Pich, F. X. Soriano, N. Vega, B. Baumgartner, J. Oriola, J. R. Daugaard, J. Lloberas, M. Camps, J. R. Zierath, R. Rabasa-Lhoret, H. Wallberg-Henriksson, M. Laville, M. Palacín, H. Vidal, F. Rivera, M. Brand and A. Zorzano (2003). "Mitofusin-2 determines mitochondrial network architecture and mitochondrial metabolism. A novel regulatory mechanism altered in obesity." J Biol Chem **278**(19): 17190-17197.

Back, S. H. and R. J. Kaufman (2012). "Endoplasmic Reticulum Stress and Type 2 Diabetes." Annual Review of Biochemistry **81**: 767-793.

Bahadoran, Z., P. Mirmiran, F. Hosseinpanah, A. Rajab, G. Asqhari and F. Azizi (2012). "Broccoli sprouts powder could improve serum triglyceride and oxidised LDL/LDL-cholesterol ratio in type 2 diabetic patients: a randomised double-blind placebo-controlled clinical trial." Diabetes Research and Clinical Practice **96**(3): 348-354.
Barbosa, C., I. Peixeiro and L. Romão (2013). "Gene expression regulation by upstream open reading frames and human disease." PLoS Genet **9**(8): e1003529.
Bass, J. J., D. J. Wilkinson, D. Rankin, B. E. Phillips, N. J. Szewczyk, K. Smith and P. J. Atherton (2017). "An overview of technical considerations for Western blotting applications to physiological research." Scand J Med Sci Sports **27**(1): 4-25.
BBMap. (2018). "BBMap short read aligner, and other bioinformatic tools". Retrieved 24th October, 2018, from https://sourceforge.net/projects/bbmap/.
Besse-Patin, A. and J. L. Estall (2014). "An Intimate Relationship between ROS and Insulin Signalling: Implications for Antioxidant Treatment of Fatty Liver Disease." Int J Cell Biol **2014**: 519153.
Bhatt, A. N., A. Chauhan, S. Khanna, Y. Rai, S. Singh, R. Soni, N. Kalra and B. S. Dwarakanath (2015). "Transient elevation of glycolysis confers radio-resistance by facilitating DNA repair in cells." BMC Cancer **15**: 335.
Bjørndal, B., L. Burri, V. Staalesen, J. Skorve and R. K. Berge (2011). "Different adipose depots: their role in the development of metabolic syndrome and mitochondrial response to hypolipidemic agents." J Obes **2011**: 490650.
Boddupalli, S., J. R. Mein, S. Lakkanna and D. R. James (2012). "Induction of phase 2 antioxidant enzymes by broccoli sulforaphane: perspectives in maintaining the antioxidant activity of vitamins a, C, and e." Front Genet **3**: 7.
Boden, G. (1999). "Free fatty acids, insulin resistance, and type 2 diabetes mellitus." Proc Assoc Am Physicians **111**(3): 241-248.
Boden, G., X. Duan, C. Homko, E. J. Molina, W. Song, O. Perez, P. Cheung and S. Merali (2008). "Increase in endoplasmic reticulum stress-related proteins and genes in adipose tissue of obese, insulin-resistant individuals." Diabetes **57**(9): 2438-2444.
Boden, G., X. Duan, C. Homko, E. J. Molina, W. Song, O. Perez, P. Cheung and S. Merali (2008). "Increase in Endoplasmic Reticulum Stress–Related Proteins and Genes in Adipose Tissue of Obese, Insulin-Resistant Individuals." Diabetes **57**(9): 2438-2444.
Boden, G. and S. Merali (2011). "Measurement of the increase in endoplasmic reticulum stress-related proteins and genes in adipose tissue of obese, insulin-resistant individuals." Methods in Enzymology **489**: 67-82.
Bogdanovic, E., N. Kraus, D. Patsouris, L. Diao, V. Wang, A. Abdullahi and M. G. Jeschke (2015). "Endoplasmic reticulum stress in adipose tissue augments lipolysis." J Cell Mol Med **19**(1): 82-91.
Boisvert, S., F. Raymond, E. Godzaridis, F. Laviolette and J. Corbeil (2012). "Ray Meta: scalable de novo metagenome assembly and profiling." Genome Biol **13**(12): R122.
Bolger, A. M., M. Lohse and B. Usadel. (2014). "Trimmomatic: A Flexible Trimmer for Illumina Sequence Data."
Bosetti, C., M. Filomeno, P. Riso, J. Polesel, F. Levi, R. Talamini, M. Montella, E. Negri, S. Franceschi and C. La Vecchia (2012). "Cruciferous vegetables and cancer risk in a network of case-control studies." Ann Oncol **23**(8): 2198-2203.
Brand, K. (1997). "Aerobic glycolysis by proliferating cells: protection against oxidative stress at the expense of energy yield." J Bioenerg Biomembr **29**(4): 355-364.
Bravo, R., T. Gutierrez, F. Paredes, D. Gatica, A. E. Rodriguez, Z. Pedrozo, M. Chiong, V. Parra, A. F. Quest, B. A. Rothermel and S. Lavandero (2012). "Endoplasmic reticulum: ER stress regulates mitochondrial bioenergetics." Int J Biochem Cell Biol **44**(1): 16-20.
Bravo, R., V. Parra, D. Gatica, A. E. Rodriguez, N. Torrealba, F. Paredes, Z. V. Wang, A. Zorzano, J. A. Hill, E. Jaimovich, A. F. Quest and S. Lavandero (2013). "Endoplasmic

reticulum and the unfolded protein response: dynamics and metabolic integration." Int Rev Cell Mol Biol **301**: 215-290.
Bravo, R., V. Parra, D. Gatica, A. E. Rodriguez, N. Torrealba, F. Paredes, Z. V. Wang, A. Zorzano, J. A. Hill, E. Jaimovich, A. F. G. Quest and S. Lavandero (2013). "Endoplasmic Reticulum and the Unfolded Protein Response: Dynamics and Metabolic Integration." International Review of Cell and Molecular Biology **301**: 215-290.
Bulleid, N. J. and M. van Lith (2014). "Redox regulation in the endoplasmic reticulum." Biochemical Society Transactions **42**(4): 905-908.
Cannon, B. and J. A. N. Nedergaard (2004). "Brown Adipose Tissue: Function and Physiological Significance." Physiological Reviews **84**(1): 277-359.
Cantone, M., G. Santos, P. Wentker, X. Lai and J. Vera (2017). "Multiplicity of Mathematical Modeling Strategies to Search for Molecular and Cellular Insights into Bacteria Lung Infection." Front Physiol **8**: 645.
Cao, S. S. and R. J. Kaufman (2014). "Endoplasmic reticulum stress and oxidative stress in cell fate decision and human disease." Antioxid Redox Signal **21**(3): 396-413.
Cao, S. S., K. L. Luo and L. Shi (2016). "Endoplasmic Reticulum Stress Interacts With Inflammation in Human Diseases." J Cell Physiol **231**(2): 288-294.
Carrara, M., F. Prischi and M. M. Ali (2013). "UPR Signal Activation by Luminal Sensor Domains." Int J Mol Sci **14**(3): 6454-6466.
Carreras-Sureda, A., P. Pihán and C. Hetz (2017). "The Unfolded Protein Response: At the Intersection between Endoplasmic Reticulum Function and Mitochondrial Bioenergetics." Front Oncol **7**: 55.
Cefalu, W. T. (2009). "Inflammation, insulin resistance, and type 2 diabetes: back to the future?" Diabetes **58**(2): 307-308.
Cefalu, W. T., G. A. Bray, P. D. Home, W. T. Garvey, S. Klein, F. X. Pi-Sunyer, F. B. Hu, I. Raz, L. Van Gaal, B. M. Wolfe and D. H. Ryan (2015). "Advances in the Science, Treatment, and Prevention of the Disease of Obesity: Reflections From a Diabetes Care Editors' Expert Forum." Diabetes Care **38**(8): 1567-1582.
Chakrabarti, A., L. Aboulmouna and J. D. Varner (2016). "Mechanistic Modeling and Analysis of the Mammalian Unfolded Protein Response." Cold Spring Harbor Laboratory: 28-36.
Chakravarthi, S., C. E. Jessop and N. J. Bulleid (2006). "The role of glutathione in disulphide bond formation and endoplasmic-reticulum-generated oxidative stress." EMBO Rep **7**(3): 271-275.
Chaudhari, N., P. Talwar, A. Parimisetty, C. Lefebvre d'Hellencourt and P. Ravanan (2014). "A molecular web: endoplasmic reticulum stress, inflammation, and oxidative stress." Front Cell Neurosci **8**: 213.
Chen, J. C., M. L. Wu, K. C. Huang and W. W. Lin (2008). "HMG-CoA reductase inhibitors activate the unfolded protein response and induce cytoprotective GRP78 expression." Cardiovasc Res **80**(1): 138-150.
Chen, X., J. Zhong, D. Dong, G. Liu and P. Yang (2017). "Endoplasmic Reticulum Stress-Induced CHOP Inhibits PGC-1α and Causes Mitochondrial Dysfunction in Diabetic Embryopathy." Toxicol Sci **158**(2): 275-285.
Choe, S. S., J. Y. Huh, I. J. Hwang, J. I. Kim and J. B. Kim (2016). "Adipose Tissue Remodeling: Its Role in Energy Metabolism and Metabolic Disorders." Front Endocrinol (Lausanne) **7**: 30.
Chong, W. C., M. D. Shastri and R. Eri (2017). "Endoplasmic Reticulum Stress and Oxidative Stress: A Vicious Nexus Implicated in Bowel Disease Pathophysiology." Int J Mol Sci **18**(4): E771.
Choo, H. J., J. H. Kim, O. B. Kwon, C. S. Lee, J. Y. Mun, S. S. Han, Y. S. Yoon, G. Yoon, K. M. Choi and Y. G. Ko (2006). "Mitochondria are impaired in the adipocytes of type 2 diabetic mice." Diabetologia **49**(4): 784-791.

Clarke, J. D., R. H. Dashwood and E. Ho (2008). "Multi-targeted prevention of cancer by sulforaphane." Cancer Lett **269**(2): 291-304.
Collier, B., L. A. Dossett, A. K. May and J. J. Diaz (2008). "Glucose control and the inflammatory response." Nutrition in Clinical Practice **23**(1): 3-15.
Covian, R., S. French, H. Kusnetz and R. S. Balaban (2014). "Stimulation of oxidative phosphorylation by calcium in cardiac mitochondria is not influenced by cAMP and PKA activity." Biochimica et Biophysica Acta **1837**(12): 1913-1921.
Cui, X. B. and S. Y. Chen (2016). "White adipose tissue browning and obesity." J Biomed Res **31**(1): 1-2.
Cusi, K. (2016). "Treatment of patients with type 2 diabetes and non-alcoholic fatty liver disease: current approaches and future directions." Diabetologia **59**(6): 1112-1120.
Dalwadi, M. P., M. Garavaglia, J. P. Webb, J. R. King and N. P. Minton (2018). "Applying asymptotic methods to synthetic biology: Modelling the reaction kinetics of the mevalonate pathway." J Theor Biol **439**: 39-49.
Dandekar, A., R. Mendez and K. Zhang (2015). "Cross talk between ER stress, oxidative stress, and inflammation in health and disease." Methods Mol Biol **1292**: 205-214.
Darimont, C., I. Zbinden, O. Avanti, P. Leone-Vautravers, V. Giusti, P. Burckhardt, A. M. A. Pfeifer and K. Macé (2003). "Reconstitution of telomerase activity combined with HPV-E7 expression allow human preadipocytes to preserve their differentiation capacity after immortalization." Cell Death And Differentiation **10**: 1025.
de la Cadena, S. G., K. Hernández-Fonseca, I. Camacho-Arroyo and L. Massieu (2014). "Glucose deprivation induces reticulum stress by the PERK pathway and caspase-7- and calpain-mediated caspase-12 activation." Apoptosis **19**(3): 414-427.
De Lorenzo, A., L. Soldati, F. Sarlo, M. Calvani, N. Di Lorenzo and L. Di Renzo (2016). "New obesity classification criteria as a tool for bariatric surgery indication." World J Gastroenterol **22**(2): 681-703.
De Pergola, G. and F. Silvestris (2013). "Obesity as a major risk factor for cancer." J Obes **2013**: 291546.
Deichmann, R., C. Lavie and S. Andrews (2010). "Coenzyme q10 and statin-induced mitochondrial dysfunction." Ochsner J **10**(1): 16-21.
Di Meo, S., T. T. Reed, P. Venditti and V. M. Victor (2016). "Role of ROS and RNS Sources in Physiological and Pathological Conditions." Oxid Med Cell Longev **2016**: 1245049.
Diabetes UK. (2016). "Diabetes Prevalence 2016." Retrieved 14th Nov, 2017, from https://www.diabetes.org.uk/professionals/position-statements-reports/statistics/diabetes-prevalence-2016.
diabetes.co.uk. (2017). "Diabetes.co.uk © 2017 Diabetes Digital Media Ltd." Retrieved April, 2017, from http://www.diabetes.co.uk/diabetes-and-obesity.html.
diabetes.co.uk. (2017). "Treatment for Type 2 Diabetes." Retrieved 29/09/17, 2017, from http://www.diabetes.co.uk/treatment-for-type2-diabetes.html.
Dixon, B. M., S. H. Heath, R. Kim, J. H. Suh and T. M. Hagen (2008). "Assessment of endoplasmic reticulum glutathione redox status is confounded by extensive ex vivo oxidation." Antioxid Redox Signal **10**(5): 963-972.
du Plessis, S. S., A. Harlev, M. I. Mohamed, E. Habib, N. Kothandaraman and Z. Cakar (2017). "Physiological Roles of Reactive Oxygen Species (ROS) in the Reproductive System." Oxidative Stress in Human Reproduction: 47-64.
Du, W., S. Amarachintha, A. F. Wilson and Q. Pang (2016). "SCO2 Mediates Oxidative Stress-Induced Glycolysis to Oxidative Phosphorylation Switch in Hematopoietic Stem Cells." Stem Cells **34**(4): 960-971.
Dufey, E., D. Sepúlveda, D. Rojas-Rivera and C. Hetz (2014). "Cellular mechanisms of endoplasmic reticulum stress signaling in health and disease. 1. An overview." Am J Physiol Cell Physiol **307**(7): C582-594.

Eizirik, D. L., A. K. Cardozo and M. Cnop (2008). "The role for endoplasmic reticulum stress in diabetes mellitus." Endocr Rev **29**(1): 42-61.
Eizirik, D. L., M. Miani and A. K. Cardozo (2013). "Signalling danger: endoplasmic reticulum stress and the unfolded protein response in pancreatic islet inflammation." Diabetologia **56**(2): 234-241.
Ellner, S. P. and J. Guckenheimer (2006). What Are Dynamic Models? Dynamic Models in Biology, Princeton University Press**:** 1-30.
Engstrom, W., O. Larsson and W. Sachsenmaier (1989). "The effects of tunicamycin, mevinolin and mevalonic acid on HMG-CoA reductase activity and nuclear division in the myxomycete Physarum polycephalum." Journal of Cell Science **92**: 341-344.
Erguler, K., M. Pieri and C. Deltas (2013). "A mathematical model of the unfolded protein stress response reveals the decision mechanism for recovery, adaptation and apoptosis." BMC Systems Biology **7**(1): 16.
Espinoza, C., T. Degenkolbe, C. Caldana, E. Zuther, A. Leisse, L. Willmitzer, D. K. Hincha and M. A. Hannah (2010). "Interaction with diurnal and circadian regulation results in dynamic metabolic and transcriptional changes during cold acclimation in Arabidopsis." PLoS One **5**(11): e14101.
Fain, J. N. (2010). "Release of inflammatory mediators by human adipose tissue is enhanced in obesity and primarily by the nonfat cells: a review." Mediators Inflamm **2010**: 513948.
Falconer, C. L., M. H. Park, H. Croker, A. S. Kessel, S. Saxena, R. M. Viner and S. Kinra (2014). "Can the relationship between ethnicity and obesity-related behaviours among school-aged children be explained by deprivation? A cross-sectional study." BMJ Open **4**(1): e003949.
Filadi, R., E. Zampese, T. Pozzan, P. Pizzo and C. Fasolato (2012). Endoplasmic Reticulum-mitochondria connections, calcium cross-talk and cell fate: a closer inspection. Endoplasmic Reticulum Stress in Health and Disease. P. Agostinis and S. Afshin. Dordrecht, Springer Netherlands**:** 75-106.
Fischer, H. P. (2008). "Mathematical modeling of complex biological systems: from parts lists to understanding systems behavior." Alcohol Res Health **31**(1): 49-59.
Flamment, M., E. Hajduch, P. Ferré and F. Foufelle (2012). "New insights into ER stress-induced insulin resistance." Trends Endocrinol Metab **23**(8): 381-390.
Frayn, K. N. and F. Karpe (2014). "Regulation of human subcutaneous adipose tissue blood flow." Int J Obes (Lond) **38**(8): 1019-1026.
Gardner, B. M., D. Pincus, K. Gotthardt, C. M. Gallagher and P. Walter (2013). "Endoplasmic reticulum stress sensing in the unfolded protein response." Cold Spring Harb Perspect Biol **5**(3): a013169.
Gargallo Fernández Manuel, M., I. Breton Lesmes, J. Basulto Marset, J. Quiles Izquierdo, X. Formiguera Sala, J. Salas-Salvadó and F.-S. c. group (2012). "Evidence-based nutritional recommendations for the prevention and treatment of overweight and obesity in adults (FESNAD-SEEDO consensus document). The role of diet in obesity treatment (III/III)." Nutr Hosp **27**(3): 833-864.
Garrido-Maraver, J., M. D. Cordero, M. Oropesa-Ávila, A. Fernández Vega, M. de la Mata, A. Delgado Pavón, M. de Miguel, C. Pérez Calero, M. Villanueva Paz, D. Cotán and J. A. Sánchez-Alcázar (2014). "Coenzyme q10 therapy." Mol Syndromol **5**(3-4): 187-197.
Gathercole, L. L., I. J. Bujalska, P. M. Stewart and J. W. Tomlinson (2007). "Glucocorticoid modulation of insulin signaling in human subcutaneous adipose tissue." J Clin Endocrinol Metab **92**(11): 4332-4339.
Gathercole, L. L., S. A. Morgan, I. J. Bujalska, D. Hauton, P. M. Stewart and J. W. Tomlinson (2011). "Regulation of lipogenesis by glucocorticoids and insulin in human adipose tissue." PLoS One **6**(10): e26223.
Gething, M. J. (1999). "Role and Regulation of the ER Chaperone BiP." Seminars in Cell & Developmental Biology **10**(5): 465-472.

Goldberg, I. J. (2001). "Diabetic Dyslipidemia: Causes and Consequences." The Journal of Clinical Endocrinology & Metabolism **86**(3): 965-971.
Gong, J., X. Z. Wang, T. Wang, J. J. Chen, X. Y. Xie, H. Hu, F. Yu, H. L. Liu, X. Y. Jiang and H. D. Fan (2017). "Molecular signal networks and regulating mechanisms of the unfolded protein response." J Zhejiang Univ Sci B **18**(1): 1-14.
Goossens, G. H. (2008). "The role of adipose tissue dysfunction in the pathogenesis of obesity-related insulin resistance." Physiology and Behaviour **94**(2): 206-218.
Görlach, A., K. Bertram, S. Hudecova and O. Krizanova (2015). "Calcium and ROS: A mutual interplay." Redox Biol **6**: 260-271.
Gray, A. (2000 [Updated 2015]). Nutritional Recommendations for Individuals with Diabetes. L. J. De Groot, G. Chrousos and K. Dungan. Endotext**:** 2000-2015.
Gregor, M. F. and G. S. Hotamisligil (2007). "Thematic review series: Adipocyte Biology. Adipocyte stress: the endoplasmic reticulum and metabolic disease." J Lipid Res **48**(9): 1905-1914.
Gregor, M. F., L. Yang, E. Fabbrini, B. S. Mohammed, J. C. Eagon, G. S. Hotamisligil and S. Klein (2009). "Endoplasmic reticulum stress is reduced in tissues of obese subjects after weight loss." Diabetes **58**(3): 693-700.
Grenier-Larouche, T., A. Galinier, L. Casteilla, A. C. Carpentier and A. Tchernof (2015). "Omental adipocyte hypertrophy relates to coenzyme Q10 redox state and lipid peroxidation in obese women." J Lipid Res **56**(10): 1985-1992.
Grootjans, J., A. Kaser, R. J. Kaufman and R. S. Blumberg (2016). "The unfolded protein response in immunity and inflammation." Nat Rev Immunol **16**(8): 469-484.
Gülow, K., D. Bienert and I. G. Haas (2002). "BiP is feed-back regulated by control of protein translation efficiency." J Cell Sci **115**(Pt 11): 2443-2452.
Guo, B., K. Abdelraouf, K. R. Ledesma, K. T. Chang, M. Nikolaou and V. H. Tam (2011). "Quantitative impact of neutrophils on bacterial clearance in a murine pneumonia model." Antimicrob Agents Chemother **55**(10): 4601-4605.
Guthrie, L. N., K. Abiraman, E. S. Plyler, N. T. Sprenkle, S. A. Gibson, B. C. McFarland, R. Rajbhandari, A. L. Rowse, E. N. Benveniste and G. P. Meares (2016). "Attenuation of PERK signalling selectively controls endoplasmic reticulum stress induced inflammation without compromising immunological responses." The Journal of Biological Chemistry **291**: 15830-15840.
Harding, H. P., Y. Zhang, A. Bertolotti, H. Zeng and D. Ron (2000). "Perk is essential for translational regulation and cell survival during the unfolded protein response." Mol Cell **5**(5): 897-904.
Heavner, B. D., K. Smallbone, B. Barker, P. Mendes and L. P. Walker (2012). "Yeast 5 – an expanded reconstruction of the Saccharomyces cerevisiae metabolic network." BMC Systems Biology **6**(55): 55.
Herr, I. and M. W. Büchler (2010). "Dietary constituents of broccoli and other cruciferous vegetables: implications for prevention and therapy of cancer." Cancer Treat Rev **36**(5): 377-383.
Hetz, C., E. Chevet and S. A. Oakes (2015). "Proteostasis control by the unfolded protein response." Nat Cell Biol **17**(7): 829-838.
Hinrichsen, D. and A. J. Pritchard (2005). Mathematical Systems Theory I: Modelling, State Space Analysis, Stability and Robustness, Springer.
Hotamisligil, G. S. (2006). "Inflammation and metabolic disorders." Nature **444**(7121): 860-867.
Hotamisligil, G. S. (2008). "Inflammation and endoplasmic reticulum stress in obesity and diabetes." Int J Obes (Lond) **32 Suppl 7**: S52-54.
Hou, N. S., A. Gutschmidt, D. Y. Choi, K. Pather, X. Shi, J. L. Watts, T. Hoppe and S. Taubert (2014). "Activation of the endoplasmic reticulum unfolded protein response by lipid

disequilibrium without disturbed proteostasis in vivo." Proc Natl Acad Sci U S A **111**(22): E2271-2280.
Hsu, C. C., W. H. Chow, P. Boffetta, L. Moore, D. Zaridze, A. Moukeria, V. Janout, H. Kollarova, V. Bencko, M. Navratilova, N. Szeszenia-Dabrowska, D. Mates and P. Brennan (2007). "Dietary risk factors for kidney cancer in Eastern and Central Europe." Am J Epidemiol **166**(1): 62-70.
Hummasti, S. and G. S. Hotamisligil (2010). "Endoplasmic reticulum stress and inflammation in obesity and diabetes." Circ Res **107**(5): 579-591.
Hussain, F., C. J. Langmead, Q. Mi, J. Dutta-Moscato, Y. Vodovotz and S. K. Jha (2015). "Automated parameter estimation for biological models using Bayesian statistical model checking." BMC Bioinformatics **16 Suppl 17**: S8.
Hwang, J. H. and S. B. Lim (2014). "Antioxidant and Anti-inflammatory Activities of Broccoli Florets in LPS-stimulated RAW 264.7 Cells." Prev Nutr Food Sci **19**(2): 89-97.
Illumina. (2014). "TruSeq RNA Sample preparation v2 Guide." Retrieved 25.04.18, 2018, from file:///C:/Users/lfulhd/Downloads/truseq-rna-sample-prep-v2-guide-15026495-f%20(1).pdf.
Illumina. (2015). "MiSeq System Guide." Retrieved 25.04.18, 2018, from https://support.illumina.com/content/dam/illumina-support/documents/documentation/system_documentation/miseq/miseq-system-guide-15027617-01.pdf.
Iurlaro, R. and C. Muñoz-Pinedo (2016). "Cell death induced by endoplasmic reticulum stress." FEBS J **283**(14): 2640-2652.
Jeon, S. M., J. E. Kim, S. K. Shin, E. Y. Kwon, U. J. Jung, N. I. Baek, K. T. Lee, T. S. Jeong, H. G. Chung and M. S. Choi (2013). "Randomized double-blind placebo-controlled trial of powdered Brassica rapa ethanol extract on alteration of body composition and plasma lipid and adipocytokine profiles in overweight subjects." J Med Food **16**(2): 133-138.
Jiang, Y., S. H. Wu, X. O. Shu, Y. B. Xiang, B. T. Ji, G. L. Milne, Q. Cai, X. Zhang, Y. T. Gao, W. Zheng and G. Yang (2014). "Cruciferous vegetable intake is inversely correlated with circulating levels of proinflammatory markers in women." J Acad Nutr Diet **114**(5): 700-708.e702.
Jiao, P., J. Ma, B. Feng, H. Zhang, J. A. Diehl, Y. E. Chin, W. Yan and H. Xu (2011). "FFA-induced adipocyte inflammation and insulin resistance: involvement of ER stress and IKKβ pathways." Obesity (Silver Spring) **19**(3): 483-491.
Juge, N., R. F. Mithen and M. Traka (2007). "Molecular basis for chemoprevention by sulforaphane: a comprehensive review." Cell Mol Life Sci **64**(9): 1105-1127.
Kajimoto, K., Y. Minami and H. Harashima (2014). "Cytoprotective role of the fatty acid binding protein 4 against oxidative and endoplasmic reticulum stress in 3T3-L1 adipocytes." FEBS Open Bio **4**: 602-610.
Kajimura, S., B. M. Spiegelman and P. Seale (2015). "Brown and Beige Fat: Physiological Roles beyond Heat Generation." Cell Metab **22**(4): 546-559.
Kamath, A. V., V. Yip, P. Gupta, C. A. Boswell, D. Bumbaca, P. Haughney, J. Castro, S. P. Tsai, G. Pacheco, S. Ross, M. Yan, L. A. Damico-Beyer, L. Khawli and B. Q. Shen (2014). "Dose dependent pharmacokinetics, tissue distribution, and anti-tumor efficacy of a humanized monoclonal antibody against DLL4 in mice." MAbs **6**(6): 1631-1637.
Kaplan, F., J. Kopka, D. W. Haskell, W. Zhao, K. C. Schiller, N. Gatzke, D. Y. Sung and C. L. Guy (2004). "Exploring the temperature-stress metabolome of Arabidopsis." Plant Physiol **136**(4): 4159-4168.
Karvonen-Gutierrez, C. and C. Kim (2016). "Association of Mid-Life Changes in Body Size, Body Composition and Obesity Status with the Menopausal Transition." Healthcare (Basel) **4**(3).

Kaur, G. and J. M. Dufour (2012). "Cell lines: Valuable tools or useless artifacts." Spermatogenesis **2**(1): 1-5.
Kawasaki, N., R. Asada, A. Saito, S. Kanemoto and K. Imaizumi (2012). "Obesity-induced endoplasmic reticulum stress causes chronic inflammation in adipose tissue." Sci Rep **2**: 799.
Kim, J. K., T. Bamba, K. Harada, E. Fukusaki and A. Kobayashi (2007). "Time-course metabolic profiling in Arabidopsis thaliana cell cultures after salt stress treatment." J Exp Bot **58**(3): 415-424.
Kinoshita, A., K. Tsukada, T. Soga, T. Hishiki, Y. Ueno, Y. Nakayama, M. Tomita and M. Suematsu (2007). "Roles of hemoglobin Allostery in hypoxia-induced metabolic alterations in erythrocytes: simulation and its verification by metabolome analysis." J Biol Chem **282**(14): 10731-10741.
Kirsh, V. A., U. Peters, S. T. Mayne, A. F. Subar, N. Chatterjee, C. C. Johnson, R. B. Hayes and L. Prostate, C.lorectal and Ovarian Cancer Screening Trial (2007). "Prospective study of fruit and vegetable intake and risk of prostate cancer." J Natl Cancer Inst **99**(15): 1200-1209.
Klipp, E. and W. Liebermeister (2006). "Mathematical modeling of intracellular signalling pathways." BMC Neuroscience **7**(Suppl 1): S10-S10.
Krebs, M. and M. Roden (2005). "Molecular mechanisms of lipid-induced insulin resistance in muscle, liver and vasculature." Diabetes Obes Metab **7**(6): 621-632.
Kurutas, E. B. (2016). "The importance of antioxidants which play the role in cellular response against oxidative/nitrosative stress: current state." Nutr J **15**(1): 71.
Kusminski, C. M., N. F. da Silva, S. J. Creely, F. M. Fisher, A. L. Harte, A. R. Baker, S. Kumar and P. G. McTernan (2007). "The in vitro effects of resistin on the innate immune signalling pathway in isolated human subcutaneous adipocytes " The Journal of Clinical Endocrinology & Metabolism **92**(1): 270-276.
Lam, T. K., I. Ruczinski, K. J. Helzlsouer, Y. Y. Shugart, L. E. Caulfield and A. J. Alberg (2010). "Cruciferous vegetable intake and lung cancer risk: a nested case-control study matched on cigarette smoking." Cancer Epidemiol Biomarkers Prev **19**(10): 2534-2540.
Larsson, O. and W. Engström (1989). "The role of N-linked glycosylation in the regulation of activity of 3-hydroxy-3-methylglutaryl-coenzyme A reductase and proliferation of SV40-transformed 3T3 cells." Biochem J **260**(2): 597-600.
Lawrence, T. (2009). "The Nuclear Factor NF-κB Pathway in Inflammation." Cold Spring Harbor Perspectives in Biology **1**(6).
Le Novère, N. (2015). "Quantitative and logic modeling of gene and molecular networks." Nature reviews Genetics **16**(3): 146-158.
Ledder, G. (2013). Mathematics for the Life Sciences: Calculus, Modeling, Probability, and Dynamical Systems. Springer Undergraduate Texts in Mathematics and Technology, Springer Sceince+Business Media**:** 83-143.
Lee, A. H., E. F. Scapa, D. E. Cohen and L. H. Glimcher (2008). "Regulation of hepatic lipogenesis by the transcription factor XBP1." Science **320**(5882): 1492-1496.
Lee, B. J., Y. C. Lin, Y. C. Huang, Y. W. Ko, S. Hsia and P. T. Lin (2012). "The relationship between coenzyme Q10, oxidative stress, and antioxidant enzymes activities and coronary artery disease." ScientificWorldJournal **2012**: 792756.
Lee, S. K. and Y. S. Kim (2013). "Phosphorylation of eIF2α attenuates statin-induced apoptosis by inhibiting the stabilization and translocation of p53 to the mitochondria." Int J Oncol **42**(3): 810-816.
Lehr, S., S. Hartwig, D. Lamers, S. Famulla, S. Müller, F. G. Hanisch, C. Cuvelier, J. Ruige, K. Eckardt, D. M. Ouwens, H. Sell and J. Eckel (2012). "Identification and validation of novel adipokines released from primary human adipocytes." Mol Cell Proteomics **11**(1): M111.010504.

Lewerenz, J. and P. Maher (2009). "Basal levels of eIF2alpha phosphorylation determine cellular antioxidant status by regulating ATF4 and xCT expression." J Biol Chem **284**(2): 1106-1115.
Lewy, T. G., J. M. Grabowski and M. E. Bloom (2017). "BiP: Master Regulator of the Unfolded Protein Response and Crucial Factor in Flavivirus Biology." Yale J Biol Med **90**(2): 291-300.
Li, Y., Y. Guo, J. Tang, J. Jiang and Z. Chen (2015). "New insights into the roles of CHOP-induced apoptosis in ER stress." Acta Biochim Biophys Sin (Shanghai) **47**(2): 146-147.
Li, Y., G. Lu, D. Sun, H. Zuo, D. W. Wang and J. Yan (2017). "Inhibition of endoplasmic reticulum stress signaling pathway: A new mechanism of statins to suppress the development of abdominal aortic aneurysm." PLoS One **12**(4): e0174821.
Li, Y., T. J. Soos, X. Li, J. Wu, M. DeGennaro, X. Sun, D. R. Littman, M. J. Birnbaum and R. D. Polakiewicz (2004). "Protein Kinase C θ Inhibits Insulin Signaling by Phosphorylating IRS1 at Ser^{1101}." Journal of Biological Chemistry **279**(44): 45304-45307.
Lindholm, D., L. Korhonen, O. Eriksson and S. Kõks (2017). "Recent Insights into the Role of Unfolded Protein Response in ER Stress in Health and Disease." Front Cell Dev Biol **5**: 48.
Love, M. I., W. Huber and S. Anders (2014). "Moderated estimation of fold change and dispersion for RNA-seq data with DESeq2." Genome Biol **15**(2): 550.
Lowell, B. B. and G. I. Shulman (2005). "Mitochondrial dysfunction and type 2 diabetes." Science **307**(5708): 384-387.
Malhotra, J. D. and R. J. Kaufman (2011). "ER stress and its functional link to mitochondria: role in cell survival and death." Cold Spring Harb Perspect Biol **3**(9): a004424.
Malhotra, J. D., H. Miao, K. Zhang, A. Wolfson, S. Pennathur, S. W. Pipe and R. J. Kaufman (2008). "Antioxidants reduce endoplasmic reticulum stress and improve protein secretion." Proc Natl Acad Sci U S A **105**(47): 18525-18530.
Mao, T., M. Shao, Y. Qiu, J. Huang, Y. Zhang, B. Song, Q. Wang, L. Jiang, Y. Liu, J.-D. J. Han, P. Cao, J. Li, X. Gao, L. Rui, L. Qi, W. Li and Y. Liu (2011). "PKA phosphorylation couples hepatic inositol-requiring enzyme 1alpha to glucagon signalling in glucose metabolism." Proc Natl Acad Sci U S A **108**(38): 15852-15857.
Marchi, S., S. Patergnani and P. Pinton (2014). "The endoplasmic reticulum-mitochondria connection: one touch, multiple functions." Biochim Biophys Acta **1837**(4): 461-469.
Marín-Peñalver, J. J., I. Martín-Timón, C. Sevillano-Collantes and F. J. del Cañizo-Gómez (2016). "Update on the treatment of type 2 diabetes mellitus." World J Diabetes **7**(17): 354-395.
Matassa, D. S., M. R. Amoroso, I. Agliarulo, F. Maddalena, L. Sisinni, S. Paladino, S. Romano, M. F. Romano, V. Sagar, F. Loreni, M. Landriscina and F. Esposito (2013). "Translational control in the stress adaptive response of cancer cells: a novel role for the heat shock protein TRAP1." Cell Death Dis **4**: e851.
Matsuzaki, S., T. Hiratsuka, M. Taniguchi, K. Shingaki, T. Kubo, K. Kiya, T. Fujiwara, S. Kanazawa, R. Kanematsu, T. Maeda, H. Takamura, K. Yamada, K. Miyoshi, K. Hosokawa, M. Tohyama and T. Katayama (2015). "Physiological ER Stress Mediates the Differentiation of Fibroblasts." PLoS One **10**(4): e0123578.
McAdams, H. H. and A. Arkin (1999). "It's a noisy business! Genetic regulation at the nanomolar scale." Trends in Genetics **15**(2): 65-69.
McIntosh, J. E. and R. P. McIntosh (1980). "Mathematical modelling and computers in endocrinology." Monogr Endocrinol **16**: 1-337.
Mingrone, G., S. Panunzi, A. De Gaetano, C. Guidone, A. Iaconelli, G. Nanni, M. Castagneto, S. Bornstein and F. Rubino (2015). "Bariatric-metabolic surgery versus conventional medical treatment in obese patients with type 2 diabetes: 5 year follow-up of an open-label, single-centre, randomised controlled trial." Lancet **386**(9997): 964-973.

Mintz, M., A. Vanderver, K. J. Brown, J. Lin, Z. Wang, C. Kaneski, R. Schiffmann, K. Nagaraju, E. P. Hoffman and Y. Hathout (2008). "Time series proteome profiling to study endoplasmic reticulum stress response." J Proteome Res **7**(6): 2435-2444.
Mirmiran, P., Z. Bahadoran, F. Hosseinpanah, A. Keyzad and F. Azizi (2012). "Effects of broccoli sprout with high sulforaphane concentration on inflammatory markers in type 2 diabetic patients: A randomized double-blind placebo-controlled clinical trial." Journal of Functional Foods **4**(4): 837-841.
Mittal, M., M. R. Siddiqui, K. Tran, S. P. Reddy and A. B. Malik (2014). "Reactive oxygen species in inflammation and tissue injury." Antioxid Redox Signal **20**(7): 1126-1167.
Mochan, E., D. Swigon, G. B. Ermentrout, S. Lukens and G. Clermont (2014). "A mathematical model of intrahost pneumococcal pneumonia infection dynamics in murine strains." J Theor Biol **353**: 44-54.
Mohamed, A., K. Smith and E. P. de Chaves (2015). The Mevalonate Pathway in Alzheimer's Disease — Cholesterol and Non-Sterol Isoprenoids. Understanding Alzheimer's Disease. I. Zerr. IntechOpen**:** 525-573.
Mondal, A. K., S. K. Das, V. Varma, G. T. Nolen, R. E. McGehee, S. C. Elbein, J. Y. Wei and G. Ranganathan (2012). "Effect of endoplasmic reticulum stress on inflammation and adiponectin regulation in human adipocytes." Metab Syndr Relat Disord **10**(4): 297-306.
Montgomery, M. K. and N. Turner (2015). "Mitochondrial dysfunction and insulin resistance: an update." Endocr Connect **4**(1): R1-R15.
Mörck, C., L. Olsen, C. Kurth, A. Persson, N. J. Storm, E. Svensson, J. O. Jansson, M. Hellqvist, A. Enejder, N. J. Faergeman and M. Pilon (2009). "Statins inhibit protein lipidation and induce the unfolded protein response in the non-sterol producing nematode Caenorhabditis elegans." Proc Natl Acad Sci U S A **106**(43): 18285-18290.
Motta, S. and F. Pappalardo (2013). "Mathematical modeling of biological systems." Brief Bioinform **14**(4): 411-422.
Muller, C., R. Salvayre, A. Nègre-Salvayre and C. Vindis (2011). "HDLs inhibit endoplasmic reticulum stress and autophagic response induced by oxidized LDLs." Cell Death Differ **18**(5): 817-828.
Murray, D. B., M. Beckmann and H. Kitano (2007). "Regulation of yeast oscillatory dynamics." Proc Natl Acad Sci U S A **104**(7): 2241-2246.
My Healthy Waist. (2018). "The Influence of Ethnicity on Adipose Tissue Distribution." Retrieved 24th April, 2018, from http://www.myhealthywaist.org/the-concept-of-cmr/intra-abdominal-adipose-tissue-the-culprit/causes-and-correlates-of-intra-abdominal-obesity/influence-of-ethnicity/print.html?printebook=true&cHash=5205fa63b2.
Ndumele, C. E., K. Matsushita, M. Lazo, N. Bello, R. S. Blumenthal, G. Gerstenblith, V. Nambi, C. M. Ballantyne, S. D. Solomon, E. Selvin, A. R. Folsom and J. Coresh (2016). "Obesity and Subtypes of Incident Cardiovascular Disease." J Am Heart Assoc **5**(8): e003921.
Neeland, I. J., C. R. Ayers, A. K. Rohatgi, A. T. Turer, J. D. Berry, S. R. Das, G. L. Vega, A. Khera, D. K. McGuire, S. M. Grundy and J. A. de Lemos (2013). "Associations of visceral and abdominal subcutaneous adipose tissue with markers of cardiac and metabolic risk in obese adults." Obesity (Silver Spring) **21**(9): E439-447.
Nguyen, L. K. (2015). "Computational Network Modelling Laboratory." Retrieved 24.04.18, 2018, from http://www.med.monash.edu.au/biochem/staff/lan-nguyen.html.
Nicolson, G. L. (2014). "Mitochondrial Dysfunction and Chronic Disease: Treatment With Natural Supplements." Integr Med (Encinitas) **13**(4): 35-43.
Niculescu, L. S., G. M. Sanda and A. V. Sima (2013). "HDL inhibits endoplasmic reticulum stress by stimulating apoE and CETP secretion from lipid-loaded macrophages." Biochem Biophys Res Commun **434**(1): 173-178.

Nishitoh, H. (2012). "CHOP is a multifunctional transcription factor in the ER stress response." J Biochem **151**(3): 217-219.
Niu, N. and L. Wang (2015). "In vitro human cell line models to predict clinical response to anticancer drugs." Pharmacogenomics **16**(3): 273-285.
Nuttall, F. Q. (2015). "Body Mass Index: Obesity, BMI, and Health: A Critical Review." Nutr Today **50**(3): 117-128.
O'Hara, L., A. Livigni, T. Theo, B. Boyer, T. Angus, D. Wright, S. H. Chen, S. Raza, M. W. Barnett, P. Digard, L. B. Smith and T. C. Freeman (2016). "Modelling the Structure and Dynamics of Biological Pathways." PLoS Biol **14**(8): e1002530.
Olokoba, A. B., O. A. Obateru and L. B. Olokoba (2012). "Type 2 Diabetes Mellitus: A Review of Current Trends." Oman Medical Journal **27**(4): 269-273.
Oslowski, C. M. and F. Urano (2011). "Measuring ER stress and the unfolded protein response using mammalian tissue culture system." Methods Enzymol **490**: 71-92.
Ozcan, U., Q. Cao, E. Yilmaz, A. H. Lee, N. N. Iwakoshi, E. Ozdelen, G. Tuncman, C. Görgün, L. H. Glimcher and G. S. Hotamisligil (2004). "Endoplasmic reticulum stress links obesity, insulin action, and type 2 diabetes." Science **306**(5695): 457-461.
Ozgur, R., I. Turkan, B. Uzilday and A. H. Sekmen (2014). "Endoplasmic reticulum stress triggers ROS signalling, changes the redox state, and regulates the antioxidant defence of Arabidopsis thaliana." J Exp Bot **65**(5): 1377-1390.
Pacheco, M. M., P. M. Garcia and M. A. P. Diego. (2018). "Atlas of Plant and Animal Histology." Retrieved 28.04.18, 2018, from https://mmegias.webs.uvigo.es/02-english/guiada_a_adiposo.php.
Pagliassotti, M., G. Moran, A. Estrada and M. T. Foster (2014). Endoplasmic Reticulum Stress and Adipose Tissue Function. Adipose Tissue and Adipokines in Health and Disease. G. Fantuzzi and C. Braunschweig, Humana Press, Totowa, NJ**:** 105-114.
Pagliassotti, M. J., P. Y. Kim, A. L. Estrada, C. M. Stewart and C. L. Gentile (2016). "Endoplasmic reticulum stress in obesity and obesity-related disorders: An expanded view." Metabolism **65**(9): 1238-1246.
Park, Y. (2014). "Oxidative stress, mitochondrial dysfunction and endoplasmic reticulum stress." Bio Design **2**(1): 12-20.
Patro, R., G. Duggal, M. Love, R. Irizarry and C. Kingsford. (2013). "Salmon." 5e560835. 2018, from https://salmon.readthedocs.io/en/latest/salmon.html#references.
Picard, F. and Y. Deshaies (2012). "Inflammation, ectopic fat and lipid metabolism: view from the chair." Int J Obes Suppl **2**(Suppl 2): S29-S30.
Qiao, L., P. S. Maclean, J. Schaack, D. J. Orlicky, C. Darimont, M. Pagliassotti, J. E. Friedman and J. Shao (2005). "C/EBPalpha regulates human adiponectin gene transcription through an intronic enhancer." Diabetes **54**(6): 1744-1754.
Quadram Institute Bioscience. (2013). "Beneforté Super Broccoli." Retrieved 05/07/2017, 2017, from http://www.superbroccoli.info/where-buy.
Quinn, T. A. and P. Kohl (2013). "Combining wet and dry research: experience with model development for cardiac mechano-electric structure-function studies." Cardiovasc Res **97**(4): 601-611.
Rahman, M., J. R. Temple, C. R. Breitkopf and A. B. Berenson (2009). "Racial differences in body fat distribution among reproductive-aged women." Metabolism **58**(9): 1329-1337.
Regazzetti, C., P. Peraldi, T. Grémeaux, R. Najem-Lendom, I. Ben-Sahra, M. Cormont, F. Bost, Y. Le Marchand-Brustel, J. F. Tanti and S. Giorgetti-Peraldi (2009). "Hypoxia decreases insulin signaling pathways in adipocytes." Diabetes **58**(1): 95-103.
Ren, W., H. Zhou, H. Xian-Ju and Y. Gao (2014). "Anti-Inflammatory Effects of Bullatine A on LPS-Induced RAW264.7 Cells by Endoplasmic Reticulum Stress." Interdisciplinary Journal of Microinflammation **123**(1).

Richardson, D. K., S. Kashyap, M. Bajaj, K. Cusi, S. J. Mandarino, J. Finlayson, R. A. DeFronzo, C. P. Jenkinson and L. J. Mandarino (2005). "Lipid infusion decreases the expression of nuclear encoded mitochondrial genes and increases the expression of extracellular matrix genes in human skeletal muscle." J Biol Chem **280**(11): 10290-10297.
Rieusset, J. (2018). "The role of endoplasmic reticulum-mitochondria contact sites in the control of glucose homeostasis: an update." Cell Death Dis **9**(3): 388.
Rosiek, A., N. F. Maciejewska, K. Leksowski, A. Rosiek-Kryszewska and Ł. Leksowski (2015). "Effect of Television on Obesity and Excess of Weight and Consequences of Health." Int J Environ Res Public Health **12**(8): 9408-9426.
Rozpedek, W., D. Pytel, B. Mucha, H. Leszczynska, J. A. Diehl and I. Majsterek (2016). "The Role of the PERK/eIF2α/ATF4/CHOP Signaling Pathway in Tumor Progression During Endoplasmic Reticulum Stress." Curr Mol Med **16**(6): 533-544.
Rutkowski, D. T., S. M. Arnold, C. N. Miller, J. Wu, J. Li, K. M. Gunnison, K. Mori, A. A. Sadighi Akha, D. Raden and R. J. Kaufman (2006). "Adaptation to ER stress is mediated by differential stabilities of pro-survival and pro-apoptotic mRNAs and proteins." PLoS Biol **4**(11): e374.
Saely, C. H., K. Geiger and H. Drexel (2012). "Brown versus white adipose tissue: a mini-review." Gerontology **58**(1): 15-23.
Saito, A. and K. Imaizumi (2017). "The broad spectrum of signalling pathways regulated by unfolded protein response in neuronal homeostasis." Neurochemistry International: 130-136.
Sano, R. and J. C. Reed (2013). "ER stress-induced cell death mechanisms." Biochimica et Biophysica Acta **1833**(12): 3460-3470.
Schadt, E. E. (2013). Causal inference and the construction of predictive network models in biology. Handbook of Systems Biology: Concepts and Insights. M. Walhout, M. Vidal and J. Dekker, Elsevier Inc.**:** 499-514.
Schauer, P. R., D. L. Bhatt, J. P. Kirwan, K. Wolski, S. A. Brethauer, S. D. Navaneethan, A. Aminian, C. E. Pothier, E. S. H. Kim, S. E. Nissen and S. R. Kashyap (2014). "Bariatric Surgery versus Intensive Medical Therapy for Diabetes – 3 Year Outcomes." The New England Journal of Medicine **370**: 2002-2013.
Schedlowski, M., H. Engler and J. S. Grigoleit (2014). "Endotoxin-induced experimental systemic inflammation in humans: a model to disentangle immune-to-brain communication." Brain Behav Immun **35**: 1-8.
Schieber, M. and N. S. Chandel (2014). "ROS function in redox signaling and oxidative stress." Curr Biol **24**(10): R453-462.
Schonthal, A. H. (2012). "Endoplasmic Reticulum Stress: Its Role in Disease and Novel Prospects for Therapy." Scientifica **2012**(Article ID 857516): 26.
Scott, I. and R. J. Youle (2010). "Mitochondrial fission and fusion." Essays in Biochemistry **47**: 85-98.
Seino, Y., K. Nanjo, N. Tajima, T. Kadowaki, A. Kashiwagi, E. Araki, C. Ito, N. Inagaki, Y. Iwamoto, M. Kasuga, T. Hanafusa, M. Haneda, K. Ueki and C. o. t. J. D. S. o. t. D. C. o. D. Mellitus (2010). "Report of the committee on the classification and diagnostic criteria of diabetes mellitus." J Diabetes Investig **1**(5): 212-228.
Seo, A. Y., A. M. Joseph, D. Dutta, J. C. Hwang, J. P. Aris and C. Leeuwenburgh (2010). "New insights into the role of mitochondria in aging: mitochondrial dynamics and more." J Cell Sci **123**(Pt 15): 2533-2542.
Seow, A., J. M. Yuan, C. L. Sun, D. Van Den Berg, H. P. Lee and M. C. Yu (2002). "Dietary isothiocyanates, glutathione S-transferase polymorphisms and colorectal cancer risk in the Singapore Chinese Health Study." Carcinogenesis **23**(12): 2055-2061.
Sharma, N. K., S. K. Das, A. K. Mondal, O. G. Hackney, W. S. Chu, P. A. Kern, N. Rasouli, H. J. Spencer, A. Yao-Borengasser and S. C. Elbein (2008). "Endoplasmic reticulum stress markers

are associated with obesity in nondiabetic subjects." J Clin Endocrinol Metab **93**(11): 4532-4541.
Shen, Q. and J. D. Pierce (2015). "Supplementation of Coenzyme Q10 among Patients with Type 2 Diabetes Mellitus." Healthcare (Basel) **3**(2): 296-309.
Sidossis, L. and S. Kajimura (2015). "Brown and beige fat in humans: thermogenic adipocytes that control energy and glucose homeostasis." J Clin Invest **125**(2): 478-486.
Sivitz, W. I. and M. A. Yorek (2010). "Mitochondrial dysfunction in diabetes: from molecular mechanisms to functional significance and therapeutic opportunities." Antioxid Redox Signal **12**(4): 537-577.
Skurk, T., C. Alberti-Huber, C. Herder and H. Hauner (2007). "Relationship between adipocyte size and adipokine expression and secretion." J Clin Endocrinol Metab **92**(3): 1023-1033.
Smith, U. (2015). "Abdominal obesity: a marker of ectopic fat accumulation." J Clin Invest **125**(5): 1790-1792.
Soliman, S. and M. Heiner (2010). "A unique transformation from ordinary differential equations to reaction networks." PLoS One **5**(12): e14284.
Song, G., X. Wu, P. Zhang, Y. Yu, M. Yang, P. Jiao, N. Wang, H. Song, Y. Wu, X. Zhang, H. Liu and S. Qin (2016). "High-density lipoprotein inhibits ox-LDL-induced adipokine secretion by upregulating SR-BI expression and suppressing ER Stress pathway." Sci Rep **6**: 30889.
Sparks, L. M., H. Xie, R. A. Koza, R. Mynatt, M. W. Hulver, G. A. Bray and S. R. Smith (2005). "A high-fat diet coordinately downregulates genes required for mitochondrial oxidative phosphorylation in skeletal muscle." Diabetes **54**(7): 1926-1933.
Sriyudthsak, K., F. Shiraishi and M. Y. Hirai (2016). "Mathematical Modeling and Dynamic Simulation of Metabolic Reaction Systems Using Metabolome Time Series Data." Front Mol Biosci **3**: 15.
Staiano, A. E., S. T. Broyles, A. K. Gupta and P. T. Katzmarzyk (2013). "Ethnic and sex differences in visceral, subcutaneous, and total body fat in children and adolescents." Obesity (Silver Spring) **21**(6): 1251-1255.
Stepien, K. M., R. Heaton, S. Rankin, A. Murphy, J. Bentley, D. Sexton and I. P. Hargreaves (2017). "Evidence of Oxidative Stress and Secondary Mitochondrial Dysfunction in Metabolic and Non-Metabolic Disorders." J Clin Med **6**(7): 6.
Strassburg, K., D. Walther, H. Takahashi, S. Kanaya and J. Kopka (2010). "Dynamic transcriptional and metabolic responses in yeast adapting to temperature stress." OMICS **14**(3): 249-259.
Summers, S. A., L. A. Garza, H. Zhou and M. J. Birnbaum (1998). "Regulation of insulin-stimulated glucose transporter GLUT4 translocation and Akt kinase activity by ceramide." Mol Cell Biol **18**(9): 5457-5464.
Sun, R. Q., H. Wang, X. Y. Zeng, S. M. Chan, S. P. Li, E. Jo, S. L. Leung, J. C. Molero and J. M. Ye (2015). "IRE1 impairs insulin signaling transduction of fructose-fed mice via JNK independent of excess lipid." Biochim Biophys Acta **1852**(1): 156-165.
Suzuki, T., J. Gao, Y. Ishigaki, K. Kondo, S. Sawada, T. Izumi, K. Uno, K. Kaneko, S. Tsukita, K. Takahashi, A. Asao, N. Ishii, J. Imai, T. Yamada, S. Oyadomari and H. Katagiri (2017). "ER Stress Protein CHOP Mediates Insulin Resistance by Modulating Adipose Tissue Macrophage Polarity." Cell Rep **18**(8): 2045-2057.
Swinnen, S. G., J. B. Hoekstra and J. H. DeVries (2009). "Insulin Therapy for Type 2 Diabetes." Diabetes Care **32**(2): 253-259.
Takayanagi, S., R. Fukuda, Y. Takeuchi, S. Tsukada and K. Yoshida (2013). "Gene regulatory network of unfolded protein response genes in endoplasmic reticulum stress." Cell Stress Chaperones **18**(1): 11-23.
Tang, G. Y., X. Meng, Y. Li, C. N. Zhao, Q. Liu and H. B. Li (2017). "Effects of Vegetables on Cardiovascular Diseases and Related Mechanisms." Nutrients **9**(8): 857.

Tangvarasittichai, S. (2015). "Oxidative stress, insulin resistance, dyslipidemia and type 2 diabetes mellitus." World Journal of Diabetes **6**(3): 456-480.
Team, A. i. (2017). "Enzyme Kinetics: A Biochemistry Crash Course." Retrieved 24.04.18, 2018, from https://www.albert.io/blog/enzyme-kinetics-biochemistry-crash-course/.
Torres, N. V. and G. Santos (2015). "The (Mathematical) Modeling Process in Biosciences." Front Genet **6**: 354.
Traaseth, N., S. Elfering, J. Solien, V. Haynes and C. Giulivi (2004). "Role of calcium signalling in the activation of mitochondrial nitric oxide synthase and citric acid cycle." Biochem et Biophysica Acta (BBA) - Bioenergetics **1658**(1-2): 64-71.
Traka, M. H., S. Saha, S. Huseby, S. Kopriva, P. G. Walley, G. C. Barker, J. Moore, G. Mero, F. v. d. Bosch, H. Constant, L. Kelly8, H. Schepers, S. Boddupalli8 and R. F. Mithen (2013). "Genetic regulation of glucoraphanin accumulation in Beneforte broccoli." New Phytologist **198**(4): 1085-1095.
Tran, L., A. Zielinski, A. H. Roach, J. A. Jende, A. M. Householder, E. E. Cole, S. A. Atway, M. Amornyard, M. L. Accursi, S. W. Shieh and E. E. Thompson (2015). "Pharmacologic Treatment of Type 2 Diabetes: Oral Medications." Annals of Pharmacotherapy **49**(5): 540-556.
Trayhurn, P. (2013). "Hypoxia and adipose tissue function and dysfunction in obesity." Physiological Reviews **93**(1): 1-21.
Tricarico, P. M., S. Crovella and F. Celsi (2015). "Mevalonate Pathway Blockade, Mitochondrial Dysfunction and Autophagy: A Possible Link." Int J Mol Sci **16**(7): 16067-16084.
Tripathi, Y. B. and V. Pandey (2012). "Obesity and Endoplasmic Reticulum (ER) Stresses." Frontiers in Immunology **3**: 240.
Trusina, A., F. R. Papa and C. Tang (2008). "Rationalizing translation attenuation in the network architecture of the unfolded protein response." Proc Natl Acad Sci U S A **105**(51): 20280-20285.
Tse, G., B. P. Yan, Y. W. Chan, X. Y. Tian and Y. Huang (2016). "Reactive Oxygen Species, Endoplasmic Reticulum Stress and Mitochondrial Dysfunction: The Link with Cardiac Arrhythmogenesis." Front Physiol **7**: 313.
Tseng, L. N., Y. H. Tseng, Y. D. Jiang, C. H. Chang, C. H. Chung, B. J. Lin, L. M. Chuang, T. Y. Tai and W. H. Sheu (2012). "Prevalence of hypertension and dyslipidemia and their associations with micro- and macrovascular diseases in patients with diabetes in Taiwan: an analysis of nationwide data for 2000-2009." J Formos Med Assoc **111**(11): 625-636.
Tuntland, T., B. Ethell, T. Kosaka, F. Blasco, R. X. Zang, M. Jain, T. Gould and K. Hoffmaster (2014). "Implementation of pharmacokinetic and pharmacodynamic strategies in early research phases of drug discovery and development at Novartis Institute of Biomedical Research." Front Pharmacol **5**: 174.
UniProt. (2018). Retrieved 24th October, 2018, from https://www.uniprot.org/.
Urano, F., X. Wang, A. Bertolotti, Y. Zhang, P. Chung, H. P. Harding and D. Ron (2000). "Coupling of stress in the ER to activation of JNK protein kinases by transmembrane protein kinase IRE1." Science **287**(5453): 664-666.
Urano, K., K. Maruyama, Y. Ogata, Y. Morishita, M. Takeda, N. Sakurai, H. Suzuki, K. Saito, D. Shibata, M. Kobayashi, K. Yamaguchi-Shinozaki and K. Shinozaki (2009). "Characterization of the ABA-regulated global responses to dehydration in Arabidopsis by metabolomics." Plant J **57**(6): 1065-1078.
van Diepen, J. A., J. F. Berbée, L. M. Havekes and P. C. Rensen (2013). "Interactions between inflammation and lipid metabolism: relevance for efficacy of anti-inflammatory drugs in the treatment of atherosclerosis." Atherosclerosis **228**(2): 306-315.
Victor, V. M., M. Rocha, R. Herance and A. Hernandez-Mijares (2011). "Oxidative stress and mitochondrial dysfunction in type 2 diabetes." Curr Pharm Des **17**(36): 3947-3958.

Volpe, J. J. and R. I. Goldberg (1983). "Effect of tunicamycin on 3-hydroxy-3-methylglutaryl coenzyme A reductase in C-6 glial cells." J Biol Chem **258**(15): 9220-9226.
Walder, K., L. Kerr-Bayles, A. Civitarese, J. Jowett, J. Curran, K. Elliott, J. Trevaskis, N. Bishara, P. Zimmet, L. Mandarino, E. Ravussin, J. Blangero, A. Kissebah and G. R. Collier (2005). "The mitochondrial rhomboid protease PSARL is a new candidate gene for type 2 diabetes." Diabetologia **48**(3): 459-468.
Wang, C.-H., K.-T. Chi and Y.-H. Wei (2012). Mitochondrial dysfunction in insulin insensitivity and type 2 diabetes and new insights for their prevention and management. Insulin Resistance. D. S. A. (Ef.), INTECH**:** 55-82.
Wang, G., K. Liu, Y. Li, W. Yi, Y. Yang, D. Zhao, C. Fan, H. Yang, T. Geng, J. Xing, Y. Zhang, S. Tan and D. Yi (2014). "Endoplasmic reticulum stress mediates the anti-inflammatory effect of ethyl pyruvate in endothelial cells." PLoS One **9**(12): e113983.
Wang, H., X. Wang, Z. J. Ke, A. L. Comer, M. Xu, J. A. Frank, Z. Zhang, X. Shi and J. Luo (2015). "Tunicamycin-induced unfolded protein response in the developing mouse brain." Toxicol Appl Pharmacol **283**(3): 157-167.
Wang, M. and R. J. Kaufman (2014). "The impact of the endoplasmic reticulum protein-folding environment on cancer development." Nat Rev Cancer **14**(9): 581-597.
Wang, M., S. Wey, Y. Zhang, R. Ye and A. S. Lee (2009). "Role of the unfolded protein response regulator GRP78/BiP in development, cancer, and neurological disorders." Antioxid Redox Signal **11**(9): 2307-2316.
Westermann, B. (2012). "Bioenergetic role of mitochondrial fusion and fission." Biochim Biophys Acta **1817**(10): 1833-1838.
White, U. A. and Y. D. Tchoukalova (2014). "Sex dimorphism and depot differences in adipose tissue function." Biochim Biophys Acta **1842**(3): 377-392.
Wilkinson, B. and H. F. Gilbert (2004). "Protein disulfide isomerase." Biochemica et Biophysica Acta (BBA) - Proteins and Proteomics **1699**(1-2): 35-44.
Wilkinson, D. J. (2009). "Stochastic modelling for quantitative description of heterogeneous biological systems." Nat Rev Genet **10**(2): 122-133.
Wind, S., D. Schnell, T. Ebner, M. Freiwald and P. Stopfer (2017). "Clinical Pharmacokinetics and Pharmacodynamics of Afatinib." Clin Pharmacokinet **56**(3): 235-250.
Winter, A. D., G. McCormack and A. P. Page (2007). "Protein disulfide isomerase activity is essential for viability and extracellular matrix formation in the nematode Caenorhabditis elegans." Dev Biol **308**(2): 449-461.
Wooley, J. C. and H. S. Lin (2005). Executive Summary. Catalyzing Inquiry at the Interface of Computing and Biology, The National Academies Press (US)**:** 25-33.
World Health Organisation (2011). Use of Glycated Haemoglobin (HbA1c) in the Diagnosis of Diabetes Mellitus: Abbreviated Report of a WHO Consultation.
World Health Organisation (2016). Global Report on Diabetes.
World Health Organisation. (2017). "World Health Organisation Obesity and Overweight Fact Sheet." Retrieved 25th Sept, 2017, from http://www.who.int/mediacentre/factsheets/fs311/en/.
World Health Organisation. (2017). "World Health Organisation: Body Mass Index - BMI." Retrieved 26th Sept, 2017, from http://www.euro.who.int/en/health-topics/disease-prevention/nutrition/a-healthy-lifestyle/body-mass-index-bmi.
World Health Organisation. (2017). "World Health Organisation: Diet." Retrieved 26th Sept, 2017, from http://www.who.int/topics/diet/en/.
World Health Organisation and International Diabetes Federation (2006). Definition and Diagnosis of Diabetes Mellitus and Intermediate Hyperglycaemia.
Wu, J., P. Boström, L. M. Sparks, L. Ye, J. H. Choi, A. H. Giang, M. Khandekar, K. A. Virtanen, P. Nuutila, G. Schaart, K. Huang, H. Tu, W. D. van Marken Lichtenbelt, J. Hoeks, S. Enerbäck,

P. Schrauwen and B. M. Spiegelman (2012). "Beige adipocytes are a distinct type of thermogenic fat cell in mouse and human." Cell **150**(2): 366-376.
Wu, J. and R. J. Kaufman (2006). "From acute ER stress to physiological roles of the Unfolded Protein Response." Cell Death Differ **13**(3): 374-384.
Xu, C., B. Bailly-Maitre and J. C. Reed (2005). "Endoplasmic reticulum stress: cell life and death decisions." The Journal of Clinical Investigation **115**(10): 2656-2664.
Xu, Z., J. Huo, X. Ding, M. Yang, L. Li, J. Dai, K. Hosoe, H. Kubo, M. Mori, K. Higuchi and J. Sawashita (2017). "Coenzyme Q10 Improves Lipid Metabolism and Ameliorates Obesity by Regulating CaMKII-Mediated PDE4 Inhibition." Sci Rep **7**(1): 8253.
Yang, M., A. E. Chadwick, C. Dart, T. Kamishima and J. M. Quayle (2017). "Bioenergetic profile of human coronary artery smooth muscle cells and effect of metabolic intervention." PLoS One **12**(5): e0177951.
Ye, J. (2011). "Adipose tissue vascularization: its role in chronic inflammation." Curr Diab Rep **11**(3): 203-210.
Ye, J. (2014). "Mechanisms of insulin resistance in obesity." Frontiers in Medicine **7**(1): 14-24.
Youn, H. S., Y. S. Kim, Z. Y. Park, S. Y. Kim, N. Y. Choi, S. M. Joung, J. A. Seo, K. M. Lim, M. K. Kwak, D. H. Hwang and J. Y. Lee (2010). "Sulforaphane suppresses oligomerization of TLR4 in a thiol-dependent manner." J Immunol **184**(1): 411-419.
Yubero-Serrano, E. M., L. Gonzalez-Guardia, O. Rangel-Zuñiga, J. Delgado-Lista, F. M. Gutierrez-Mariscal, P. Perez-Martinez, N. Delgado-Casado, C. Cruz-Teno, F. J. Tinahones, J. M. Villalba, F. Perez-Jimenez and J. Lopez-Miranda (2012). "Mediterranean diet supplemented with coenzyme Q10 modifies the expression of proinflammatory and endoplasmic reticulum stress-related genes in elderly men and women." J Gerontol A Biol Sci Med Sci **67**(1): 3-10.
Zeeshan, H. M., G. H. Lee, H. R. Kim and H. J. Chae (2016). "Endoplasmic Reticulum Stress and Associated ROS." Int J Mol Sci **17**(3): 327.
Zhang, H. Q., S. Y. Chen, A. S. Wang, A. J. Yao, J. F. Fu, J. S. Zhao, F. Chen, Z. Q. Zou, X. H. Zhang, Y. J. Shan and Y. P. Bao (2016). "Sulforaphane induces adipocyte browning and promotes glucose and lipid utilization." Mol Nutr Food Res **60**(10): 2185-2197.
Zhang, J., E. Nuebel, D. R. R. Wisidagama, K. Setoguchi, J. S. Hong, C. M. Van Horn, S. S. Imam, L. Vergnes, C. S. Malone, C. M. Koehler and M. A. Teitell (2013). "Measuring energy metabolism in cultured cells, including human pluripotent stem cells and differentiated cells." Nature Protocols **7**(6): 1068-1085.
Zhang, K. and R. J. Kaufman (2008). "From endoplasmic-reticulum stress to the inflammatory response." Nature **454**(7203): 455-462.
Zhang, P., R. Mourad, Y. Xiang, K. Huang, T. Huang, K. Nephew, Y. Liu and L. Li (2012). "A dynamic time order network for time-series gene expression data analysis." BMC Systems Biology **6**(3): S9.
Zhang, X., X. O. Shu, Y. B. Xiang, G. Yang, H. Li, J. Gao, H. Cai, Y. T. Gao and W. Zheng (2011). "Cruciferous vegetable consumption is associated with a reduced risk of total and cardiovascular disease mortality." Am J Clin Nutr **94**(1): 240-246.
Zhao, Y., H. Tang and Y. Ye (2012). "RAPSearch2: a fast and memory-efficient protein similarity search tool for next-generation sequencing data." Bioinformatics **28**(1): 125-126).
Zhu, G. and A. S. Lee (2015). "Role of the unfolded protein response, GRP78 and GRP94 in organ homeostasis." J Cell Physiol **230**(7): 1413-1420.
Zilanawala, A., P. Davis-Kean, J. Nazroo, A. Sacker, S. Simonton and Y. Kelly (2015). "Race/ethnic disparities in early childhood BMI, obesity and overweight in the United Kingdom and United States." Int J Obes (Lond) **39**(3): 520-529.
Zong, Y., S. Feng, J. Cheng, C. Yu and G. Lu (2017). "Up-Regulated ATF4 Expression Increases Cell Sensitivity to Apoptosis in Response to Radiation." Cell Physiol Biochem **41**(2): 784-794.